An investigation of GRP78 expression and inhibition in squamous cell carcinoma of the head and neck

Thesis submitted in accordance with the requirements of the University of Liverpool for the degree of Doctor in Philosophy

by

Mohammed Afeef Aslam

August 2011

Abstract

GRP78 is a known cyto-protective gene which is induced in microenvironments typical of tumours with low glucose and hypoxia. Furthermore up-regulation of GRP78 has been linked to chemo- and radioresistance as well as poor survival outcome.

This study is the first to confirm that GRP78 is up-regulated in tumours of the oropharynx, larynx and hypopharynx compared with matched histologically normal tissue ($p_{(X^2)}<0.001$). Up-regulation of GRP78 may be important for tumour development and therefore we have investigated the consequences of inhibition of GRP78 in cells derived from laryngeal squamous cell carcinomas (LSCC).

EGF-SubA is a novel drug consisting of EGF covalently attached to the A subunit of an E.coli derived AB_5 toxin which can cleave GRP78. EGF-SubA was able to induce EGFR-dependent cytotoxicity in a panel of seven laryngeal SCC cells with an IC_{50} range of between 4-100pM. EGF-SubA treatment induced G1 cell cycle arrest as well as apoptosis. Therefore apoptosis may be the mechanism by which EGF-SubA causes cell death.

In vitro studies demonstrated that EGF-SubA enhances the effects of clinically relevant genotoxic agents. Two Gy survival fractions (SF2) were significantly reduced with EGF-SubA pre-treatment ($p<0.03$). In addition EGF-SubA in combination with the

primary head and neck cancer chemo-therapeutic agent cisplatin, resulted in IC_{50} drug combination indexes (CI) as low as 0.542, which is suggestive of a synergistic effect.

The potency of EGF-SubA appears to be substantially dependent on EGFR membrane expression since cells expressing higher EGFR levels were associated with increased sensitivity to EGF-SubA where Spearman's rank correlation coefficient = 0.919 ($p=0.003$). Furthermore pre-incubation of LSCC cells with sub-toxic doses of cetuximab, a therapeutic monoclonal antibody to EGFR, completely rescued cells from the cytotoxic effects of EGF-SubA ($p_{(t\ test)} \leq 0.005$). This is an important proof of principal for a proposed combined toxin-protectant therapeutic strategy that would permit topical use of EGF-SubA peri- or post-operatively after tumour resection in order to kill any remaining tumour cells, or as an oral rinse in patients who present with pre-malignant lesions of the oral cavity, with any potential systemic toxicity being abrogated by cetuximab.

In summary this study has found that GRP78 is up-regulated in head and neck cancers suggesting that this protein may be important for tumour development and survival. Thus inhibition of GRP78 through EGF-SubA may offer a novel approach to cancer therapy. In addition to suppressing the growth of LSCC cell, EGF-SubA was found to enhance the effects of relevant genotoxic agents *in vitro* of cisplatin and radiation. Further work is now warranted in order to assess the efficacy and toxicity of EGF-SubA, *in vivo,* before phase I clinical trials can commence.

Acknowledgements

I would like to thank the following

My supervisors Dr Mark Boyd and Mr Terry Jones for their guidance throughout the project and the writing up process.

The Wolfson Intercalated Awards Programme for the scholarship which went towards partially funding this research.

Dr Joseph Backer for kindly donating EGF-SubA and Clatterbridge Centre for Oncology NHS Trust for donating cisplatin, 5-Fu, cetuximab and herceptin.

Past and present lab members for all the help and support especially Mrs Rhiannon Hughes for teaching me flow cytometry analysis, immunohistochemistry and western blot analysis.

Most importantly I wish to thank my mother and father my sisters Mona *bajee* and Raheela *bajee* and my brother-in-laws Rehan *bhaiyya* and Hamza *bhaiyya* for always supporting, and guiding me.

Declaration of originality

This thesis is a product of my own work produced during my time at the Department of Molecular and Clinical Cancer Medicine, University of Liverpool, between August 2008 and July 2011. All experiments presented in the results section were performed by myself with the exception of the scoring of the cores from the tissue micro array which was done in parallel with pathologist Dr Mike Wall. The thesis was written by myself with guidance from my supervisors Dr Mark Boyd and Mr Terry Jones. A part of the literature review pages 15-25 has been presented in my Special Study Module 6 but again this was written wholly by myself.

Contents

List of tables and figures

List of abbreviations

18F-FDG	18F-fluorodeoxyglucose
ABC	Avidin biotin complexes
ADH	Alcohol dehydrogenase
AF	Average fluorescence
ALDH	Aldehyde dehydrogenase
APS	Ammonium per sulphate
ATF6	Activating transcription factor 6
BrdU	Bromodeoxyuridine
BSA	Bovine serum albumin
CA9	Carbonic anhydrase 9
CAD	Caspase-activated DNase
CDK	Cyclin dependent kinase
Chk1	Checkpoint kinase 1
CHO	Chinese hamster ovarian
CHOP	C/EBP homologous protein
CI	Combination index
DAB	3,3’-diaminobenzodine
DDR	DNA damage response

DMEM	Dulbecco's modified eagle medium
DMSO	Dimethyl sulfoxide
DNA	Deoxy-ribonucleic acid
DNA-PK	DNA dependent protein kinase
DPX	Depex polystyrene
DSB	Double strand breaks
EDEM1	ER degradation enhancing a mannosidase like protein 1
EGF	Epidermal growth factor
EGFR	Epidermal growth factor receptor
eIF2a	Eukaryotic translation initiation factor-2a
ER	Endoplasmic reticulum
ERAD	Endoplasmic reticulum associated degradation
FBS	Foetal bovine serum
FNAC	Fine needle aspiration cytology
FS	Forward scatter
GAP	GTPase activating protein
GAPDH	Glyceraldehydes 3 phosphate dehydrogenase
GEF	Guanine exchange factor
GRP78	Glucose regulated protein
Gy	Gray
Hepa	Mouse hepatoma cells

1c1c7	
HPV	Human papillomavirus
HRP	Horse radish peroxidase
HSF	Heat shock factor
HSP	Heat shock protein
IC	Inhibitory concentration
ICAD	Inhibitor of caspase-activated DNase
IHC	Immuno histochemistry
IMRT	Intensity modulated radiotherapy
Ire1	Inositol-requiring enzyme 1
mAb	Monoclonal antibody
MEF	Mouse embryonic fibroblast
MTT	3-(4,5-dimethylthiazol-2-yl)-2,5-diphenyl tetrasodium bromide
NCCN	National Comprehensive Cancer Network
NEAA	Non essential amino acids
NER	Nucleotide excision repair
NF-κB	Nuclear factor κB
NICE	National Institute of Clinical Excellence
OD	Optical density
PARP	Poly (ADP-ribose) polymerase

PBS	Phosphate buffered saline
PBST	PBS Tween
PC3	Prostate cancer cells
PDI	Protein disulphide isomerase
PERK	Pancreatic kinase like ER kinase
PET scan	Positron emission tomography scan
PH	Pleckstrin homology
PI	Propidium iodide
PI3K	Phosphatidylinositol 3 kinase
PIP2/3	Phosphatidylinositol-diphosphate/triphosphate
PMSF	Phenyl methane sulfonyl fluoride
PS	Phosphatidylserine
PTEN	Phosphatase and tensin
PyT	Polyoma middle T oncogene
Rb	Retinoblastoma protein
RCF	Relative centrifugal force
rhEGF	Recombinant human epidermal growth factor
RNA	Ribonucleic acid
ROS	Reactive oxygen species
S1P	Site 2 proteases
SAM	S-Adenosyl-L-methionine

SCCHN	Squamous cell carcinoma of the head and neck
SDS	Sodium dodecyl sulphate
SDS-PAGE	Sodium dodecyl sulphate polyacrylamide gel electrophoresis
SF	Survival fraction
SF2	2 Gy survival fraction
SHR	Steroid hormone receptor
siRNA	Small interfering RNA
SRP	Signal recognition particle
SS	Side scatter
SSB	Single strand breaks
TF	Transcription factor
TGF-α	Transforming growth factor
TKI	Tyrosine kinase inhibitor
TMA	Tissue micro array
TRAIL	Tumour necrosis factor related apoptosis inducing ligand
UDP	Uridine diphosphate
UM-SCC	University of Michigan squamous cell carcinoma cell lines
UPR	Unfolded Protein Response
VEGF	Vascular epidermal growth factor
XBP1	X-box-binding protein

1 Introduction

Expression of protein chaperone GRP78 is known to be up-regulated under conditions typical of tumour microenvironments specifically hypoxia and low glucose, possibly acting as a cyto-protective agent under these conditions(1). GRP78 expression has been shown to be up-regulated in a wide variety of cancers including lung, breast and colorectal cancers (1).

Currently there are no published data regarding GRP78 levels in laryngeal tumours, which is the most common of the head and neck sub-sites, or in tumours of the oropharynx or hypopharynx (2). Therefore one of the initial objectives of this research project was to establish whether GRP78 was also up-regulated in these tumours.

Previous studies have shown that up-regulation of GRP78 may contribute to chemo- and radioresistance (3, 4). EGF-SubA is a novel cytotoxic drug that promotes proteolytic cleavage of GRP78 (5) and encompasses a enzymatically active moiety which is a bacterial endotoxin (SubA) covalently bound to EGF to permit targeting of EGFR-expressing cells. We therefore determined whether targeting of GRP78 via EGF-SubA could enhance the effects of clinically relevant genotoxic agents which are currently used in the treatment of head and neck cancers.

Backer and colleagues have suggested that the potency of EGF-SubA may be dependent on EGFR expression and therefore this may allow for the selective targeting of head and neck tumours which are known to over express EGFR (5, 6).

Subtilase A (SubA) is a bacterial toxin, with proteolytic activity, derived from a specific strain of E. coli known as Shiga toxigenic E. Coli (STEC) (7). These strains of E. Coli are known to cause life threatening outbreaks of haemolytic uraemic syndrome (HUS) such as in Australia in 1998 (7) as well as gastrointestinal disease. Therefore we wanted to determine whether cetuximab, a monoclonal antibody (mAb) against EGFR, could inhibit the cytotoxicity of EGF-SubA. This could allow for a combined toxin-protectant approach where topical application of EGF-SubA peri- or post-operatively after tumour resection could be used, with any potential systemic toxicity of EGF-SubA being prevented by cetuximab.

In this literature review an overview of head and neck cancer epidemiology, diagnosis and current management will be discussed. This will be followed by a description of the signalling pathways of EGFR, as well as a review of studies which have analysed expression levels of EGFR in head and neck cancers. Finally the function of GRP78 as a protein chaperone will be discussed as well as a review of current studies that have associated up-regulation of GRP78 with chemo and radioresistance (1, 8).

1.1 Head and neck cancer

1.1.1 Epidemiology, signs and symptoms, diagnosis and current treatment

Head and neck cancer constitutes cancer of the upper aerodigestive tract which incorporates regions of the nasal cavity, oral cavity, larynx, and pharynx. Squamous cell carcinoma of the head and neck (SCCHN) is the 6th most common cancer in the world (9). In 2002 the World Health Organization (WHO) estimated a worldwide incidence of 600,000 new cases and 300,000 deaths each year. Although in national databases oral cavity is typically listed as the most prevalent of the head and neck cancers it consists of several different sub-sites such as the tongue, floor of the mouth, palate and gums as well as the oropharynx. The most prevalent single sub-site is in fact the larynx (10) with approximately 160,000 new cases worldwide each year (2). Similarly within the South East of England of the 8490 newly diagnosed patients with head and neck cancer, between 2000-2004, 2543 (30%) patients had laryngeal cancer (10). The two major risk factors for developing SCCHN are tobacco and alcohol (11). In addition there are site specific risk factors as shown in Table 1.1.1.

This text box is where the original thesis contained the table showing ‘tumour region and associated risk factors’ which was reproduced from reference *(12)*.

Table 1.1.1 Tumour region and associated risk factors.

Table reproduced from reference (12).

Ethanol is oxidised in the liver by alcohol dehydrogenase (ADH) to acetaldehyde, which is a known carcinogen, and then to acetate via aldehyde dehydrogenase (ALDH) (13). If alcohol consumption is high cytochrome P450 2E1 can also oxidise ethanol into acetaldehyde and another carcinogen known as reactive oxygen species (ROS). Acetaldehyde and ROS can induce DNA lesions which if not repaired result in carcinogenesis.

Polymorphisms in genes involved in alcohol metabolism as well as the amount of alcohol consumed can alter the risk of cancer development. For example ADH1B has a polymorphism that enhances alcohol-oxidising capability known as mutant allele

ADH1B*2. Asians who are moderate or heavy drinkers who are heterozygous or homozygous for ADH1B*2 are statistically less likely to develop head and neck cancers compared to those Asians who have wild-type ADH1B genotype with a reduced odds ratio of 0.57 (95% CI 0.36-0.91) (13). Furthermore inactive ALDH2 encoded by the ALDH2*1/2*2 genotype results in increased accumulation of acetaldehyde and is a strong risk factor for head and neck cancers (14).

Acetaldehyde is able to form DNA adducts which may escape cellular repair mechanisms causing miscoding resulting in gene mutations in critical genes such as oncogenes and tumour suppressor genes (14). Ethanol may directly stimulate carcinogenesis by preventing DNA methylation. Methylation is important for suppressing gene transcription. S-Adenosyl-L-methionine (SAM) promotes the transfer of methyl groups however ethanol inhibits synthesis of SAM. Suppression of SAM results in hypomethylation of certain oncogenes, but not of tumour suppressor gene *p53*. This results in up-regulation of oncogenes and down-regulation of p53 (14).

Cigarette smoke contains over 60 known carcinogens (14). These carcinogens are oxygenated by cytochrome P450. However in their intermediate states they are reactive with DNA leading to DNA adducts resulting in mutations and genomic instability. DNA adducts associated with cigarette smoke frequently produce G-to-T transversions (14). Furthermore *in vitro* tests with cigarette carcinogens have induced p53 mutations in a

similar spectrum to that found in lung cancer cells (14).p16 protein inhibits CDK 4 and 6 binding to cyclin D thus preventing pRB phosphorylation and cell cycle progression from G1 into S phase (14). Inactivation of $p16^{INK4a}$ gene, via smoking induced methylation, is another common feature in lung cancer.

Individual susceptibility to cigarette induced cancer is in part dependent on how well potential carcinogenic effects are counteracted. Carcinogenic metabolites may be detoxified by various enzymes such as glutathione-S-transferase and uridine diphosphate (UDP)-glucuronosyl transferases (14). In addition DNA adducts may be eliminated through DNA repair mechanisms such as nucleotide excision repair (14).

A recent rise in oropharyngeal cancer patients have been reported in patients under fifty with no known history of alcohol or smoking. These cancers have been attributed to human papilloma virus (HPV). HPV produces two oncoproteins encoded by E6 and E7 genes (15). E6 can bind onto both p53 and ubiquitin-protein ligase E6 associated protein (E6AP) (16). It is reported that the interaction of E6 between these two proteins subsequently initiates ubiquitin mediated degradation of p53 (16). Normally p53 induces either cell cycle arrest to allow for DNA repair or apoptosis. However E6 expressing cells are deficient in p53 protein resulting in genetic instability (17, 18). p16 is a cyclin dependent kinase inhibitor which prevents pRB phosphorylation thus inhibiting cell cycle progression from G1 to S (19). E7 causes functional inactivation of pRB leading to

unregulated proliferation ‘independent of growth factor signalling’ (19). Functional loss of pRB is an early event in SCCHN which is followed by up-regulation of p16. Thus up-regulation of p16, which can be detected through immunohistochemistry, is used as one of the markers for HPV infection (17).

A meta-analysis by Hobbs and colleagues in 2006, found a strong association between HPV16 and tonsillar cancer (odds ratio (OR): 15.1, 95% CI: 6.8–33.7), a moderate association with oropharyngeal tumours (OR: 4.3, 95% CI: 2.1–8.9) and weak association for oral cancers (OR: 2.0, 95% CI: 1.2–3.4) , and laryngeal tumours (OR: 2.0, 95% CI: 1.0–4.2) (20). SCCHN patients with HPV are more responsive to chemo- and radiation therapy($p \leq 0.05$) compared with HPV negative patients (19). In addition HPV positive patients tend to have a better survival outcome. For example 2 year survival rates of patients with either laryngeal or oropharyngeal grade III or IV tumours were 95% and 62 % ($p=0.005$) in HPV positive versus HPV negative patients, respectively (21).

Patients present with a variety of symptoms depending upon the site of their tumour. For example laryngeal cancers typically present with hoarseness whilst patients with pharyngeal cancers may present with dysphagia and sore throat (2).

Table 1.1.2 provides information on the red flag signs and symptoms of head neck cancer that should warrant urgent two week referral to specialists in Otolaryngology / Head and Neck Surgery.

This text box is where the original thesis contained the table showing 'red flag symptoms and signs of head and neck cancer' which was reproduced from reference *(2).*

Table 1.1.2 Red flag symptoms and signs of head and neck cancer.

Patients should be referred if they have any one of the above signs or symptoms occurring for more than three weeks. Table reproduced from reference (2).

Diagnosis of head and neck cancers, in patients presenting with a palpable neck mass, is confirmed through histological examination of fine needle aspiration cytology (FNAC)

(22). This involves a hollow needle being inserted into the suspected tumour in order to extract cells which will later be visualised by a histopathologist.

Further staging of the extent of tumour load is achieved by radiological imaging (MR or CT scanning of the head and neck and CT scanning of the thorax and upper abdomen) and an examination under anaesthetic. More recently, Positron emission tomography (PET scan) can be combined with 18F-fluorodeoxyglucose (18F-FDG), which is taken up selectively by tumours due to their high glycolytic rates(as observed by Otto Warburg), in order to identify the tumour location, size and to monitor treatment efficacy (2).

Following investigation tumours are staged according to the TNM staging system (22)

Early stage SCCHN tumours are treated with either surgery or radiotherapy (23). The objective of head and neck cancer treatment is to increase locoregional control and survival and to preserve important functions such as swallowing, speech and respiration. Most T1 and T2 tumours of the tongue and oral cavity are treated with surgical resection (24). Exposure to radiotherapy in this area may lead to osteoradionecrosis of the mandible and hence surgery is the preferred choice in tumours of this region (24).

In sites of the larynx, oropharynx and hypopharynx radiotherapy is the preferred option as traditional open surgical intervention often results in swallowing and speech

impairment (24). A recent development is the use of transoral laser microsurgery which permits resection of laryngeal, hypopharyngeal and orophayngeal tumours without significant impairment in function. Furthermore cure rates have been found to be similar to that of radiotherapy and to traditional open methods of surgery (24, 25). The recent trend towards treating stage 1 and 2 tumours with surgery as opposed to radiotherapy may permit the application of topical anti-cancer medication after tumour resection in order to remove any remaining tumour cells around the excised margin.

Both surgery and radiotherapy present with their own complications. Apart from general surgical complications such as infection, head and neck surgery may result in cranial nerve damage (VII, X, XII), spinal accessory nerve damage leading to shoulder dysfunction, impaired swallowing and speech, salivary fistulas, and end stomas from laryngectomy. Complications from radiation include dry mouth due to radiation of the salivary glands (xerostomia), inflammation of the mucosa, and dermatitis. Consequently patients often require enteral nutrition delivered via percutaneous gastrostomy or nasogastic feeding tube (23).

In late stage tumours (grade III and IV) treatment regimes include, induction (neoadjuvant) chemotherapy (ICT) followed by concurrent chemotherapy and radiotherapy (CRT); ICT followed by surgery; CRT alone; surgery followed by post-operative (adjuvant) radiotherapy (PORT) or CRT. Postoperative radiotherapy is

considered when there is high chance of recurrence such as when surgical resection margins are small or when two or more lymph nodes are involved (26). Traditionally, the main drugs used in chemotherapy strategies for SCCHN are cisplatin and 5-FU (22).

1.1.2 Recent advancements in the treatment of head and neck cancer

Current survival rates have reached a plateau as at present only 51% of oral cavity and 61% of laryngeal cancer patients survive past five years since initial diagnosis (23). Therefore there is still a need to develop biomarkers of outcome and/or treatment response as well as methods to allow early detection. In addition, new treatments which improve survival rates and reduce treatment related toxicity are urgently needed.

Over recent years intensity modulated radiotherapy (IMRT) has been increasingly used in the treatment of patients with SCCHN. The technique using data from CT scans, allows the delivery of radiation energy in doses which conform to the 3D shape of the tumour, thereby allowing a much reduced dose to adjacent normal tissue so minimising the collateral damage of external beam RT. IMRT has been shown to preserve the function of salivary glands, optic nerves, the cochlea, pharyngeal constrictor muscles, the brain stem and spinal cord (27). The use of IMRT is now rapidly gaining popularity in the UK (22). One randomized control trial – the PASSPORT trial - compared parotid sparing IMRT to standard radiotherapy and found a 36% ($p=0.004$) reduction in the incidence of xerostomia (27). A separate study by Chen and colleagues in 2009, found

no differences in survival rates or loco- regional control rates between conventional radiotherapy and IMRT and therefore IMRT may provide a means of lowering radiation related morbidity whilst maintaining radiation treatment efficacy (28).

A better understanding of cancer at the molecular level has allowed for the development of drugs which can specifically target proteins responsible for promoting cancer. Of particular relevance in SCCHN has been the Epidermal Growth Factor Receptor (EGFR), which has been at the centre of targeted therapy strategies to date. However, other targets, such as the Unfolded Protein Response and inhibition of HSP90 are the subject of ongoing active research programmes designed to explore their exploitation in the management of SCCHN.

Signals derived from EGFR pathway stimulate cell growth and survival. Overexpression and prolonged activation of EGFR is found in many cancers including head and neck, cervical, bladder, brain, breast, lung stomach, ovary and prostate and is associated with poor clinical outcome (29). In these instances EGFR becomes an oncogene. Several new treatments have been developed in order counteract EGFR oncogenic signalling.

Cetuximab is a monoclonal antibody which competitively binds to EGF receptor blocking EGF induced signalling. (23). In 2008 cetuximab was recommended for locally

advanced head and neck squamous cell carcinoma in combination with radiotherapy once concurrent platinum based therapy had failed (30). Tyrosine kinase inhibitors (TKIs) are ATP competitive inhibitors that prevent trans or autophosphorylation of the tyrosine residues on EGFR therefore blocking signal transduction through these means (31) Current TKI such as lapatinib have undergone phase I trials with chemoradiotherapy for head and neck cancer and are currently undergoing randomised phase II and III evaluation (32). Both cetuximab and TKI will be discussed further in sections 1.2.3 and 1.2.3respectively.

DNA damage response (DDR) which involves coordinating DNA repair and cell cycle arrest may lead to resistance to genotoxic insults caused by a wide variety of chemotherapeutic agents such as cisplatin and radiation (33). Hence interest has recently grown in inhibiting the DDR mechanism. For example poly (ADP-ribose) polymerase (PARP) is responsible for repair of single strand breaks (SSB) in DNA. PARP inhibitors may lead to further double strand breaks (DSB) however these can be repaired by BRCA1/2 which are responsible for coordinating repair of DSB (34). Therefore the use of PARP inhibitors may be more useful in cancers with BRCA1/2 mutations thus leading to irreparable DSB and subsequent apoptosis (34). Since radiation treatment induces DNA damage PARP is being explored as a possible radiosensitising agent. Pre clinical data suggests that PARP inhibitors may potentiate the effects of radiation, which is know to cause SSB and DSB, in a variety of tumours including head and neck cancer

(32). Another protein called Checkpoint kinase 1 (Chk1) is activated upon SSB. As part of the DNA damage response, Chk1 can phosphorylate downstream effectors which are involved in cell cycle arrest, DNA replication checkpoints, as well as proteins involved in DNA repair. Currently both PARP and Chk1 inhibitors are involved in phase I clinical trials (33).

1.2 **EGFR**

1.2.1 EGFR pathway

EGFR is part of the HER/ErbB family of receptor tyrosine kinase proteins (HER/RTK). The family includes EGFR(also known as ErbB1/HER1), ErbB-2/HER2, ErbB-3/HER3, and ErbB-4/HER4 (35).

There are three parts to the EGFR structure as seen in Figure 1.2.1

This text box is where the original thesis contained the diagram showing 'the EGF receptor' which was reproduced from reference *(36)*.

There is a high degree of homology between the tyrosine kinase domains of the HER RTK family members. In contrast, the extracellular domains are less conserved and bind to different ligands. For example only EGFR will bind EGF. Currently there is no known natural ligand for HER2. Ligand binding induces receptor dimerization between

two receptors of the HER RTK family. Dimerization can occur between two identical receptors (homo-dimerization) or betweens two different receptors (hetero-dimerization) (35). Following dimerisation, a process of transphosphorylation then occurs, where the tyrosine kinase domain of one EGFR phosphorylates a variable number of tyrosine residues of the cytoplasmic C terminus of adjacent EGFR molecules as shown in Figure 1.2.2 (36).

This text box is where the original thesis contained the diagram showing 'EGF receptor dimerization after ligand binding' which was reproduced from reference *(36)*.

Figure 1.2.2 EGF receptor dimerization after ligand binding.

In the presence of EGF, EGF receptors dimerize and transphosphorylate tyrosine domains. Figure reproduced from (36).

Various cytoplasmic proteins are then able to bind to specific phosphotyrosine residues. The phosphotyrosine residue to which a given protein binds is governed by the specificity of the SH2 domain of the binding protein. (37).

In addition to the binding of cytoplasmic protein binding, other plasma membrane associated proteins are also able to bind to the phosphotyrosine residues; which once again depends on the specificity of the SH2 domain of the binding protein.

Figure 1.2.3 demonstrates an example of this process. Here EGFR has been activated by EGF. Several phosphotyrosine residues are subsequently formed. The protein Grb2 contains an SH2 domain which facilitates its binding to the RTK phosphotyrosine residues. In addition, Grb2 possesses an SH3 domain which allows binding of Sos. This binding complex ensures that Sos is now in close proximity to the membrane bound Ras, with the result that Sos can activate the Ras signalling pathway. (37). Sos is known as a guanine exchange factor (GEF) which is able to substitute Ras GDP for Ras GTP. Ras signalling is turned off by intrinsic GTPase activity which hydrolyses GTP to GDP. This GTPase activity is enhanced in the presence of GTPase activating proteins (GAPs) (36).

This text box is where the original thesis contained the diagram showing 'intermolecular links between EGFR and RAS' which was reproduced from reference *(37)*.

Figure 1.2.3 Intermolecular links between EGFR and RAS.

Phosphorylation of EGFR tyrosine domains allows binding between the SH2 domain of Grb2 and the cytoplasmic phosphotyrosine residues of EGFR. Simultaneously the SH3 domain of Grb2 facilitates binding of Sos. Sos is now juxtaposed to membrane bound protein Ras which it then activates by phosphorylating Ras bound GDP. Figure reproduced from reference (37).

The two main signalling pathways that are influenced by EGFR binding are:

1. Ras→Raf→Mek→Erk pathway
2. Ras→PI3K→PIP3→Akt/PKB pathway (38)

Ras→Raf→Mek→Erk pathway

Following activation, Ras binds Raf kinase via a domain called an effector loop, resulting in activation of Raf (37). In turn, activated Raf kinase phosphorylates and therefore activates MEK. MEK proceeds to phosphorylate extracellular signal-regulated kinases 1 and 2 (ERK 1 and 2) (37). Following activation ERK moves into the nucleus where it in turn, phosphorylates and activates multiple transcription factors (TFs) such as Ets, Elk-1 and SAP-1 (37). A summary of this pathway is given in Figure 1.2.4.

These TFs in turn coordinate the expression of particular genes (39). By unknown mechanisms TFs facilitate the access of set genes to RNA polymerase(39). Thereby determining which genes are transcribed and ultimately which proteins are produced (39). Proteins produced under the stimulus of the Ras →Raf→Mek→Erk pathway, such as cyclin D1, are needed to drive the cell forward during the G1 phase of the cell cycle (37).

This text box is where the original thesis contained the diagram showing the 'summary of the Ras to Erk pathway' which was reproduced from *reference (37)*

Figure 1.2.4 Summary of the Ras →Raf→Mek→Erk pathway.

This pathway leads to activation of ERK kinase which in turn activates transcription factors, via phosphorylation, such as Ets, Elk-1, and SAP-1. Ets can then activate the expression of genes which regulate growth such as cyclin D1. Erk can also directly activate Mnk1 kinase. Mnk1 kinase then phosphorylates and subsequently activates eurokaryotic initiating factor eIF4E which is essential in order for protein translation. Figure reproduced from reference (37).

pRb regulates cell cycle progression from late G1 to S phase (40). When pRb is not phosphorylated it exerts a restraining effect on transcription factor E2F (40). However, when hyperphosphorylated, pRb detaches from E2F which in turn promotes the transcription of downstream S phase genes leading to cell cycle progression from late G1 into S phase. (40).

Cyclin D1 gene transcription is initiated through the EGFR→Ras→Raf→Mek→Erk pathway. In G1 of the cell cycle, cyclin D combines with cyclin dependent kinases 4 and 6 (CDK4/6) (40). Cyclin D-CDK4/6 complexes initiate phosphorylation of pRb. At this point pRb is only hypophosphorylated and is not deactivated. Phosphorylation of pRb is completed by the action of cyclin E-CDK2 complexes, which results in hyperphosphorylation of pRb and subsequent release of E2F (40). Activated E2Fs can then trigger increased transcription of *cyclin E* genes. Thus this cycle becomes self perpetuating with more cyclin E-CDK2 complexes formed, causing more pRb to become hyperphosphorylated and more activated E2Fs.

Figure 1.2.5 shows that growth factor leads to eventual hyperphosphorylation of pRb. Once the restriction point has been passed, the cell will continue through the cell cycle without the need for further growth factor stimulus.

This text box is where the original thesis contained the diagram showing the 'control of the G1 restriction point and positive feedback loops' which was reproduced from reference *(40)*.

Figure 1.2.5 Control of the G1 restriction point and positive feedback loops.

EGFR signalling leads to increased levels of cyclin D expression. pRB is then phosphorylated by cyclin E/CDK2 and cyclin D/CDK4 complexes. Hyperphosphorylated pRB then releases transcription factor E2F which is required for the transcription of proteins in order for the cell to enter S phase. Figure reproduced from reference (40).

Ras→PI3K→PIP3→Akt/PKB pathway

Ras, once activated through EGFR, can also activate the catalytic domain of phosphatidylinositol 3 kinase (PI3K) (37). PI3K is able to phosphorylate phosphatidylinositol-diphosphate (PIP2) thereby forming phosphatidylinositol-triphosphate (PIP3) (37).

The PH (pleckstrin homology) domain of Akt/PKB is able to bind PIP3 facilitating its biphosphorylation by PDK1 and PDK2 (37). Phosphorylated (active)Akt/PKB then proceeds to phosphorylate a variety of substrates such as GSK-3β (which regulates cell proliferation) and Bad (which regulates cell survival) (37). Figure 1.2.6 shows the activation of the Ras→PI3K→PIP3→Akt/PKB pathway.

This text box is where the original thesis contained the diagram showing 'activation of the Akt/PKB pathway' which was reproduced from reference *(37)*.

Figure 1.2.6 Activation of the Akt/PKB pathway

Ras activates kinase PI3K which then phosphorylate PIP2 to PIP3. An Akt/PKB kinase molecule is then able to dock onto PIP3. This is followed by Akt/PKB complex being phosphorylated by kinases PDK1 and 2. PIP3 is then dephosphorylated via phosphatase PTEN. Figure reproduced from reference (37).

Similar to pRb, $p27^{Kip1}$ and $p21^{Cip1}$ promote cell cycle arrest if damaged DNA remains unrepaired (40). Ordinarily, $p27^{Kip1}$ and $p21^{Cip1}$ inhibit the activity of cyclin CDK complexes in the nucleus. Akt/PKB is able to phosphorylate these two molecules causing their translocation out of the nucleus so that their inhibitory effects on cyclin CDK complexes are lost (40).

Akt/PKB can also suppress apoptosis by inhibiting pro-apoptotic proteins such as Bad and activating anti-apoptotic proteins such as Mdm2 (37).

As outlined in Figure 1.2.6, phosphorylation of PIP2 by PI3K can be reversed by the phosphatase PTEN (37). In many human tumours e.g. breast carcinoma or colon cancer inactivation of PTEN is a common occurrence and leads to unregulated cell cycle progression (37).

1.2.2 EGFR and tumorigenesis

EGFR over expression and prolonged activation of its signalling pathway are characteristic of many solid tumours including that of the head and neck, cervical, bladder, brain, breast, lung stomach, ovary and prostate (29). In these instances EGFR becomes an oncogene. A summary of studies investigating the expression of EGFR in HNSCC is shown in Table 1.2.1.

Study	Main findings
Grandis and colleagues, 1993 (41)	EGFR mRNA levels were elevated by an average of 69 fold in 92% of SCCHN tumours compared to mRNA levels in healthy normal mucosa.
Chung and colleagues, 2006 (42)	58% of HNSCC tissue samples showed *EGFR* gene amplification as determined by FISH.
Ryott and colleagues, 2008 (43)	EGFR protein expression was found to be high in 72% in tumours of the oral tongue squamous cell carcinoma. Furthermore 54% of these tumours had a high *EGFR* gene copy numbers (≥ four gene copy numbers).
Sarkis and colleagues, 2010 (44)	EGFR expression was found in all epithelial layers on oral squamous cell carcinoma specimens where as in normal oral epithelia, EGFR could only be detected in the basal cell layer.

Table 1.2.1 Summary of studies indicating that EGFR is over expressed in HNSCC.

Ryott and colleagues in 2008 showed that EGFR protein was over expressed in 72% of oral tongue squamous cell carcinoma (OTSCC) and that *EGFR* gene amplification was correlated with EGFR over-expression, ($p=0.004$) (43). Figure 1.2.7 shows low and high expression of EGFR protein as detected by IHC and normal and amplified levels of *EGFR* gene as detected by FISH in OTSCC.

This text box is where the original thesis contained the diagram showing 'levels of EGFR protein and gene copy number as determined by IHC and FISH respectively in OTSCC' which was reproduced from reference *(43)*.

Figure 1.2.7 Levels of EGFR protein and gene copy number as determined by IHC and FISH respectively in OTSCC.

(A) EGFR IHC weak staining. (B) EGFR strong staining. (C) EGFR FISH analysis showing normal disomy copy of genes. (D) EGFR gene amplification. Figure reproduced from reference (43).

As well as gene amplification, EGFR protein may be overexpressed in tumours due to reduced rate of ubiquitin mediated proteasomal degradation. Shortly after EGF binding to wild-type EGFR, EGFR is endocytosed, internalized, ubiquitinated and then undergoes proteasomal degradation (45). This process allows for the termination of growth signal and provides a refractory period before the next growth signal is generated. In cells expressing endogenous levels of EGFR (<200,000 receptor molecules per cell), receptor half life is typically between 6-10h, whereas in cells over expressing

EGFR, such as in the epidermoid carcinoma cell line A-431, EGFR half life can exceed 24h (46).

Degradation of EGFR once internalised, is rapid. Following EGFR transphosphorylation, members of the Cbl family of proteins, which contain ring finger E3 ubiquitin ligases, are able to tag EGFR with ubiquitin thereby directing its proteasomal degradation (46). Cbl proteins contain a tyrosine kinase binding domain (TKB) that can bind directly to Tyr1045 of EGFR. In this way EGFR, once phosphorylated, is quickly degraded via Cbl.

EGFR tyrosine kinase domain mutations such as L858R/T790M can impair Cbl-EGFR association and significantly slow endocytosis and degradation compared to cells expressing wild type EGFR (47). Cells expressing these mutant receptors have shown persistently longer mitogenic and antiapoptotic signalling compared to wild type cells (47).

In addition to mutations of the tyrosine kinase domain, EGFRvIII mutants lack the ectodomain (ligand binding portion) of EGFR (29) and are constitutively active, independent of EGF (29). EGFRvIII mutations are commonly found in gliomas, non small cell lung cancer and SCCHN. (29). Furthermore, a study by Sok and colleagues in 2006, found 42% of SCCHN tumours expressing EGFRvIII (48). In addition, EGFRvIII

transfected cells showed reduced rates of apoptosis when treated with cisplatin and decreased growth inhibition with cetuximab treatment when compared to parental cells (48).

Normally growth factors exert their effects via paracrine stimulation (36). However, it has been observed that SCCHN cells may be able to self induce EGFR receptor activation via secretion of such ligands as TGF-α (transforming growth factor) (29). i.e. autocrine stimulation.

Increased *EGFR* gene copy number, over-expression (or reduced degradation) of EGFR and autocrine TGF-α stimulation, have all been correlated with poor survival outcome and increased metastatic potential (29, 49, 50). Grandis and colleagues found 2 year survival rates for SCCHN patients to be 31% for patients with tumours expressing high EGFR levels compared with 90% for those with tumours expressing low EGFR levels.($p=0.001$) (50). In the same study they also observed that the 2 year overall survival for patients with tumours secreting high levels of TGF-α as compared to those with tumours secreting low levels was 50% and 89% ($p=0.001$) respectively (50).

Several studies have suggested that EGFR signalling pathway may be important in causing resistance to radiotherapy treatment. A correlative study was performed, by Ang and colleagues, which examined EGFR levels in patients with advanced head and neck

cancer who had undergone radiotherapy (51). Patients who had tumours expressing relatively low levels of EGFR had significantly greater overall survival, disease free survival, and local regional control rates (51) Thereby inferring that tumours expressing relatively higher levels of EGFR expression are more radioresistant. Similarly, studies involving patients with glioblastoma multiforme or cervical cancer, also demonstrated that EGFR over-expression was a significant predictor for poor response to radiation (52, 53).

1.2.3 Inhibiting EGFR with cetuximab

In 2008 the role of cetuximab in the management of SCCHN was reviewed by the national Institute for Clinical Excellence (NICE). Following this review, the use of cetuximab was permitted for locally advanced head and neck squamous cell carcinoma in combination with radiotherapy in patients for whom concurrent platinum based therapy is unsuitable (30).

Cetuximab is a monoclonal IgG antibody (mAb) which binds to EGFR with a greater affinity than either EGF or TGF-α (54). Binding inhibits the activation of EGFR tyrosine kinases and thus prevents Ras associated downstream signalling pathways that are associated with cell proliferation, prevention of apoptosis, cellular repair and survival as

described in section 1.2.1 (54). Binding of Cetuximab to EGFR promotes receptor internalization but unlike the binding of EGF does not induce proteasomal degradation of EGFR (55).

As mentioned in section 1.2.1 cyclin/CDK complexes, which are formed upon activation of the EGFR pathway, are needed for the phosphorylation of pRB in order for cells to enter the S phase of the cell cycle. Oral squamous cell carcinoma cells were shown to have decreased expression of CDK2 and CDK4 proteins resulting in an associated accumulation of cells in G1 and a corresponding decrease in cells in S phase when treated with cetuximab (56). The authors also demonstrated an increase in expression of G1 cyclin dependent kinase activity inhibitors p15 and p21 (56). To corroborate this, another study found accumulation of the hypophosphorylated pRb protein when squamous carcinoma cells were treated with 30nM of cetuximab for two days as shown in Figure 1.2.8 (57).

As well as G1 arrest, cetuximab is known to induce apoptosis (a summary of the apoptosis pathway is provided in section 1.3.4) by increasing the cellular levels of Bax (a proapoptotic protein) and reducing the levels of Bcl-2 (an anti apoptotic protein), as shown in Figure 1.2.8 . Cetuximab has been shown to down regulate the expression of nuclear factor κB (NF-κB) in pancreatic cell line MDA Panc-28 (58). NF-κB is essential

for the transcription of antiapoptotic protein Bcl-xl – which is an additional mechanism by which cetuximab facilitates apoptosis

Cetuximab may also be involved in the inhibition of angiogenesis. Several studies have shown that upon treatment with cetuximab there were reductions in pro-angiogenic factors such as vascular epidermal growth factor (VEGF) and IL-8 with corresponding decreases in micro-vascular density as compared to controls (59, 60).

This text box is where the original thesis contained the diagram showing 'treatemtn of SCC-13Y cells with 30nM cetuximab (C225)' which was reproduced from reference *(57)*.

Figure 1.2.8 Treatment of SCC-13Y cells with 30nM cetuximab (C225)

SCC-13Y with cetuximab shows that cetuximab modifies cell cycle by increasing p27 expressing and subsequent expression of hypophosphorylated pRB; cetuximab also increases proapoptotic protein levels of Bax. Figure reproduced from reference (57).

As mentioned in section 1.2.2 up-regulation of EGFR in tumours corresponds to radioresistance. A study by Liang and colleagues demonstrated that there was increased radioresistance in clones over expressing EGFR compared to parental lines and that radioresistance was reduced upon the addition of cetuximab (61). The study by Huang found a 2 fold increase in apoptosis, as assessed by the magnitude of the sub-G1 peak, in SCC-13Y cells treated with 6 Gray radiation alone and a 5-6 fold increase in apoptosis when the same cells were treated with 30nM of cetuximab combined with radiation as compared to non irradiated controls (57).

A study by Dittman and colleagues tried to determine the possible mechanism behind cetuximab induced radiosensitisation (62). DNA dependent protein kinase (DNA-PK) is a protein which is found in the nucleus and aids the repair of double strand breaks which occur commonly after ionizing radiation. After radiation the study found large accumulation of EGFR/DNA-PK complexes in the nucleus. When cells were pre-treated with cetuximab there was a significant reduction in EGFR/DNA-PK complexes, a decrease in DNA-PK activity and an increase in residual DNA damage. (62). In addition to this proposed mechanism, it is known that cetuximab causes an increase in the proportion of cells in G1 arrest where cells are known to be more radiosensitive (54).

In contrast to HER2 over-expression, which predicts response to monoclonal antibody trastuzumab (herceptin) against HER2 in breast cancer patients, levels of EGFR have not

correlated with the outcome to cetuximab treatment (63). Clinical studies in metastatic colorectal cancer have shown no correlation between EGFR expression levels and sensitivity to cetuximab (64). Therefore further molecular markers are required to predict the treatment outcome of cetuximab.

Several gene mutations, which fall within the downstream signalling pathway of EGFR, are emerging as indicators of poor response to cetuximab therapy. Once wild-type Ras has been stimulated by EGFR, activated Ras GTP is converted into its inactivated form, Ras GDP, by its own GTPase. KRAS mutations which occur in 40% of colorectal carcinomas have a non functional GTPase site resulting in constitutive signalling and independence from EGFR control (65). Several studies have indicated that KRAS mutations are correlated with poor response to cetuximab in colorectal cancer (65-67). Loss of PTEN and mutant EGFR VIII have also been linked to cetuximab resistance, with one study showing that all patients (n=11) with loss of PTEN, did not receive any additional benefit from cetuximab (68).

Currently the National Comprehensive Cancer Network (NCCN) Clinical Practice Guidelines in Oncology Version 3 2008 recommends *KRAS* genotyping in patients presenting with colorectal carcinoma before the use of EGFR inhibitors (69).

RAS mutations in SCCHN are rare and therefore, similar predictive biomarkers remain elusive.

Apart from inherent resistance to cetuximab, evidence suggests that tumours which initially responded to cetuximab treatment later developed resistance (70). As already explained, EGFR is a member of the HER family of receptor tyrosine kinases which consists of EGFR, HER2, HER3 and HER4. HER family members share several downstream signalling cascades such as the MAPK and PI3K/AKT pathways, which can be initiated upon homo or hetero-dimerization between HER members and therefore one theory is that acquired resistance to cetuximab may be in part due the ability of cells to activate growth signals through other HER RTK members independently thereby bypassing the effect of EGFR blockade (70).

Wheeler and colleagues established cetuximab resistant cell lines following long term exposure to cetuximab. . These include, cell lines derived from non small cell lung cancer (NSCLC; H226) and SCCHN (UMSCC-1). To further clarify the role of the HER family in cetuximab resistant lines, cells in which HER2 was blocked using monoclonal antibody 2C4 or transfected with siRNA against HER3 were treated with and without cetuximab. In both cases loss of either HER2 or HER3 activity resulted in rescue of cetuximab resistance and a consequent reduction of cell proliferation(70). Hence

targeted combination therapy against several members of the HER family may be more efficacious than targeting EGFR alone.

1.2.4 Inhibiting the EGFR pathway with tyrosine kinase inhibitors

Tyrosine kinase inhibitors (TKIs) prevent trans or autophosphorylation of the tyrosine residues of receptor tyrosine kinase (RTK) family members (31). Whilst monoclonal antibodies (mAbs) such as cetuximab are typically specific to one receptor, TKIs may cross react by inhibiting the phosphorylation of tyrosine residues present on other RTK species. (31). Despite this, preferential activity towards one or more RTK species is possible allowing some specificity of action. For example, gefitinib and erlotinib are specific to EGFR whilst lapatinib preferentially inhibits EGFR and HER-2 (31).

Both cetuximab and EGFR targeted TKI gefitinib share similar cytotoxic properties. Both drugs cause G1 arrest, induce proapoptotic protein Bax and reduce expression of antiapoptotic protein Bcl-2, as well as inhibiting the production of VEGF (56, 71, 72). In addition TKIs have been shown to enhance the cytotoxic effects of radiation (57, 73, 74). Similarly, PTEN and Ras mutation have also been linked to TKI resistance (75).

1.3 **GRP78**

1.3.1 Basic functions of the endoplasmic reticulum and the role of chaperones in protein folding

Proteins which are destined to be secreted out of the cell such as immunoglobulins, or which will be incorporated into lysosomes or onto the plasma membrane, require post translational modification in order to become functionally active and are therefore selectively targeted to enter the endoplasmic reticulum (ER) (76).

Chaperones are proteins which facilitate the folding of newly synthesised proteins both in the cytosol and ER. Chaperones do not provide any additional information on how a protein should fold, as this is already pre-determined by the amino acid sequence. However chaperones act as scaffolds, binding to partially folded intermediates and providing structural support to ensure that proteins are folded correctly. Thus they prevent premature folding before all of the nascent peptide chain has been released from the ribosome and thereby avoid the formation of protein aggregates (77). Most chaperones are part of a homologous family known as heat shock proteins: HSP40, HSP60, HSP70, HSP90, HSP100. HSPs are not only involved in folding of proteins but also in: the ubiquitin proteasome system, endoplasmic reticulum associated degradation (ERAD), Unfolded Protein Response (UPR), apoptosis and autophagy (78).

Proteins can enter the ER either during the process of translation (known as cotranslational translocation) or after completion of translation (known as post-translational translocation) as shown in Figure 1.3.1. In cotranslational translocation a 20 amino acid sequence from an elongating polypeptide chain, known as the signal sequence, is recognized and bound by signal recognition particle (SRP) (79). At this point further translation is stopped and the ribosome along with the polypeptide chain move towards the ER. The SRP binds to a receptor on the ER membrane where it is then removed from the signal sequence. The ribosome attaches to a pore in the ER membrane known as a Sec61 protein translocation complex and the polypeptide chain is then able to enter the ER. Translocation then resumes and the ribosome feeds the remainder of the polypeptide chain into the ER (79).

In post-translational translocation the completed unfolded polypeptide chain is supported in the cytosol by chaperones. It is targeted by its signal sequence towards Sec 61and Sec62/63 complexes(79). At this point cytosolic chaperones are released and the peptide passes though the ER pore. GRP78 (also known as Bip) is a chaperone which consists of two functional domains: an N-terminal ATPase domain and a C terminal peptide binding domain (80). Sec 63 is able to catalyse the ATP hydrolysis by GRP78/BiP allowing the chaperone to attach onto hydrophobic parts of the polypeptide chain. When more of the polypeptide chain enters the ER another GRP78/Bip molecule, within the ER lumen, can attach on to it. This attachment prevents retrograde movement of the polypeptide chain

back out into the cytosol. Once the polypeptide chain is completely within the ER lumen, GRP78/Bip can release the polypeptide chain upon exchange of ADP for ATP (79).

This text box is where the original thesis contained the diagram showing 'post-translational translocation' which was reproduced from reference *(79)*.

Figure 1.3.1 Post-translational translocation

(1) Recently translated polypeptide chain is supported by cytosolic chaperones and moves towards the Sec complexes. (2) Cytosolic chaperones dissociate as the polypeptide chain comes into contact with Sec complexes. The J domain of Sec63 causes ATP hydrolysis of GRP78/BiP. GRP78/Bip can now adhere to the polypeptide chain. (3) As more of the polypeptide chain moves into the ER more GRP78/BiP chaperones are able to adhere, thus securing the peptide inside the ER. (4) As all of the peptide is now in the ER GRP78/BiP can now dissociate from nascent peptides. Figure reproduced from reference (79).

After entry into the ER a series of enzymatic post translational modifications of the polypeptide chain occurs. The oxidative environment in the ER and protein disulphide isomerase (PDI) enzymes help catalyse disulphide bond formation between cysteine residues. These bonds form the protein's three dimensional structure (76).

In addition, within the ER, proteins are often cleaved in a process called proteolysis by peptidases. For example insulin is formed in two stages. First the signal sequence is removed from preproinsulin to make prosinsulin (81). Further proteolysis removes a connecting amino acid sequence which becomes unnecessary once disulphide bonds have formed, thus producing insulin (81).

Similarly, lipids may also attach to proteins allowing them to anchor to hydrophobic portions of the cell membrane. Proteins may also undergo glycosylation (attachment of carbohydrates) (81). Once proteins have folded correctly and undergone other post translational modifications their hydrophobic areas are no longer exposed and therefore GRP78 can no longer attach to them.

Proteins which are destined to stay in the ER, such as GRP78, are tagged with a targeting sequence (KDEL or KKXX). Proteins (tagged and untagged) are transported

out of the ER in a non selective manner to the Golgi apparatus. Tagged proteins are then recognized by receptors in the Golgi apparatus and transported back to the ER (76).

1.3.2 The roles of GRP78, PERK, ATF6, and IRE1 in the Unfolded Protein Response

Accumulation of unfolded or incorrectly folded proteins may occur in the ER under certain physiological conditions and can be induced experimentally. Protein folding and maintenance of the ER environment is an energy intensive process. Glucose and ATP in the ER are needed for: binding and unbinding of chaperones, maintenance of Ca^{2+} levels in the ER (which is required for both chaperone function and protein folding), preserving redox homeostasis, for glycosylation, and for ER assisted degradation (ERAD) (82). Furthermore molecular oxygen is essential as an electron acceptor during the formation of disulphide bonds.

The tumour microenvironment is often subject to low oxygen and low glucose levels due to the poor microvasculature and such conditions can lead to increased levels of unfolded proteins in the ER (83). An increased unfolded protein load in the ER may also appear during synthesis of large amounts of secretary proteins such as when B

lymphoblasts begin secreting antibodies upon antigen stimulation or when pancreatic cells secrete insulin (84).

In order to counteract an increase in unfolded or incorrectly folded proteins a mechanism known as the Unfolded Protein Response (UPR) becomes activated. The UPR results in the attenuation of protein translation, and degradation of misfolded protein by a system known as endoplasmic reticulum associated degradation ERAD, thus reducing the protein load in the ER (85). The UPR also induces genes which are involved in the formation of correctly folded proteins such as GRP78 thus increasing the folding capacity of the ER (84). If homeostasis is not resumed then the over stimulation of the UPR, that can ensue, may lead to apoptosis (85).

GRP78 normally binds to and inhibits two ER transmembrane kinase signalling molecules: pancreatic kinase like ER kinase (PERK) and inositol-requiring enzyme 1 (Ire1). As well as these two molecules GRP78 also binds and inhibits to a UPR-specific transcription factor known as activating transcription factor 6 (ATF6) (83). During the accumulation of unfolded proteins, GRP78 preferentially attaches to hydrophobic parts of unfolded proteins thus dissociating from PERK, Ire1 and ATF6. The disassociation of GRP78 from these three molecules enables their activation. (83).

PERK

Upon GRP78 disassociation, PERK is able to dimerize and transphosphorylate its cytosolic kinase domain (83). This kinase domain then phosphorylates eukaryotic translation initiation factor-2α (eIF2α). eIF2 proteins in the GTP state attach to initiator tRNA and bring initiator tRNA towards ribosomes therefore aiding in the start of translation of mRNA (86). Hydrolysis of eIF2-GTP complex results in eIF2-GDP formation and eIF2B (guanine nucleotide exchange factor) must catalyse the removal of GDP for GTP in order for eIF2 to attach to another tRNA and participate once again in translation initiation (86). eIF2α in the phosphorylated state is able to competitively inhibit the function of eIF2B thus reducing translation initiation (86). The inhibition of eIF2B by eIF2α is in equilibrium so there will always be at least some protein translation even if there are high levels of phosphorylated eIF2α (86). Increased levels of phosphorylated eIF2α impedes the translation of most mRNA, therefore reducing the cellular protein load. A direct consequence of translation attenuation is G1 cell-cycle arrest due to the loss of cyclin D1 protein (83).

It has been reported by Paton and colleagues that GRP78 is the only known substrate of E. Coli derived toxin Subtilase (SubA) (7). SubA has proteolytic activity resulting in GRP78 (72 kDa) being cleaved specifically at two leucine residue at positions 416 and 417. This results in two fragments of GRP78 of 28 kDa and 48 kDa (7). A study by Wolfson and colleagues in 2008 (87) measured protein synthesis levels by the [^{3}H]-

Leucine incorporation method in PERK wild-type MEFS and PERK knock out MEFs. When SubA was applied, GRP78 (72kDa) was cleaved into 28kDa and 44kDa moieties in both PERK wild-type MEFs and PERK knock out MEFs, as shown in Figure 1.3.2A. Cleavage of GRP78 lead to the disassociation of GRP78 from PERK, IRE1 and ATF6 and the subsequent activation of the UPR. Upon activation of the UPR there was phosphorylation of eIF2α in the PERK wild-type MEFs but not in the PERK knock out MEFs as shown in Figure 1.3.2B. Figure 1.3.2C shows a subsequent decrease in the amount of protein synthesis in PERK wild-type MEFs compared to the PERK knock out MEFs after the application of SubA.

This text box is where the original thesis contained the diagram showing the 'effects of SubA on GRP78, phosphorylation of eIF2α, and protein synthesis in PERK wild-type MEFs and PERK knock out cells' which was reproduced from reference *(87)*.

Figure 1.3.2 Effects of SubA on GRP78, phosphorylation of eIF2α, and protein synthesis in PERK wild-type MEFs and PERK knock out cells.

A: Western blot of GRP78 showing cleavage of GRP78 after the application of SubA in both wild-type and PERK knock out cells. B: Western blots of eIF2α and its phosphorylated form in wild-type cells (+) and PERK knockout cells (-) after SubA application. C: Percentage protein synthesis as compared to cells prior to the application of SubA in wild-type and PERK knock out cells. Figures reproduced from reference(87).

Paradoxically, a decrease in eIF2 activity favours the translation of activating transcription factor 4 (ATF4) (88). Most mRNA have a cap-structure, consisting of 7-methylguanosine residue, which is linked to the 5' end of the first nucleotide in mRNA sequence (86). This cap-structure is recognised by initiation factor eIF-4F and eIF-4F guides the ribosome towards the start codon of mRNA thus initiating translation. Under high levels of phosphorylated eIF2α translation of those mRNA which contain the cap-structure, decreases. Some mRNA such as that of ATF4 do not contain the cap-structure and are said to be cap-independent mRNA. Although these cap-independent mRNA, are constitutively expressed they are not efficiently translated until there are high levels of phosphorylated eIF2α during for example when the Unfolded Protein Response is activated (86).

ATF4 protein expression in turn, induces transcription factor C/EBP homologous protein (CHOP) (89). A study by Marciniak and colleagues in 2009 (89), demonstrated that CHOP promotes the reactivation of protein synthesis as well as increasing the activity of enzymes involved in protein folding (89). Increased levels of CHOP lead to the expression of target gene *GADD34*. GADD34 contains an eIF2α phosphatase complex which results in eIF2α being dephosphorylated and inactivated thus restarting the translation process. Marciniak and colleagues in 2009 (89), demonstrated that there was increased protein level production in CHOP wild-type mice compared to CHOP

knock-out mice when the mice were given thapsigargin. Thapsigargin is a drug which produces ER stress by depleting calcium resources within the endoplasmic reticulum (90). Marciniak and colleagues also showed that CHOP plays a role in increasing levels ERO1α expression. ERO1α is a protein which oxidises protein disulfide isomerases (PDIs). This then allows PDIs to create disulfide bonds in newly forming proteins in the ER (89). The mechanism of disulphide bond formation is summarised in Figure 1.3.3.

This text box is where the original thesis contained the diagram showing the 'mechanism of disulphide bond formation in proteins by oxidative reaction' which was reproduced from reference *(91)*.

Figure 1.3.3: Mechanism of disulphide bond formation in proteins by oxidative reaction.

ERO1 oxidizes protein disulphide isomerase (PDI) which can then initiate disulphide bonds formation (S-S) on ER proteins. ERO1, once activated by FAD, transfers electrons to molecular oxygen. Figure reproduced from reference (91).

ATF 6

ATF6 is a transcription factor which is also released by GRP78 disassociation upon accumulation of unfolded proteins. Upon release, ATF6 enters the Golgi apparatus where it undergoes partial proteolysis by Site 1 and Site 2 proteases (S1P, S2P). A smaller part of ATF6, at 50kDa, is now free to enter the nucleus where it induces other genes (87). ATF6 increases levels of: GRP78, protein disulphide isomerases, ER degradation enhancing α mannosidase like protein 1 (EDEM1) and transcriptional factors such as CHOP and X-box-binding protein (XBP1) (87). The rise in chaperones as well as proteins which are involved in disulphide bond formation enhances the folding capacity of the ER.

IRE 1

Finally the third UPR protein to be released by GRP78 is IRE1. IRE1 is unusual as it acts as both a serine/threonine kinase and an endoribonuclease (92). After induction of the *XBP1* gene by ATF6, XBP1 mRNA is then spliced by the endoribonuclease part of IRE1 (93). Spliced XBP1 acts as a transcriptional activator that elicits up-regulation of a group of proteins responsible for degrading misfolded proteins. This response is known as the endoplasmic reticulum activated degradation (ERAD) and leads to an overall reduction in misfolded proteins (92). Misfolded proteins are selected by molecular chaperones and targeted for retrotranslocation out of the ER via the Sec61 translocon

complex (94). Currently it is unknown how chaperones are able to distinguish between misfolded and nascent unfolded proteins, in order to target misfolded proteins for degradation. Once outside the ER, misfolded proteins are then ubiquitinated via ubiquitin ligase (94). These targeted proteins then undergo degradation by the proteasome (94). Cells that are deficient in IRE1 or XBP1 are defective at degrading misfolded proteins (93).

Figure 1.3.4 provides a summary of the UPR.

This text box is where the original thesis contained the diagram showing a 'summary of GRP78/Bip and its role in the UPR' which was reproduced from reference *(82).*

Figure 1.3.4: Summary of GRP78/Bip and its role in the UPR

GRP78 otherwise known as Bip disassociates from IRE1, ATF6 and PERK upon binding to either misfolded or unfolded proteins which contain exposed hydrophobic sites. Activated PERK leads to attenuation of protein translation through phosphorylation of eIF2α. Phosphorylation of eIF2α also gives rise to CHOP. CHOP expression results in the reinitiation of protein translation and an increase in proteins which catalyse disulphide bond formation. ATF6 undergoes proteolysis and then enters the nucleus leading to the transcription of chaperones such as GRP78 as well as PDI, CHOP and mXBP1. IRE1 acts as an endoribonuclease removing introns from mXBP1. XBP1 then upregulating proteins which are involved in ER assisted degradation (ERAD). Figure reproduced from reference (82)

1.3.3 Induction of GRP78 in the tissue microenvironment and its role in tumorigenesis

Due to the poor microvasculature, tumours are often subject to conditions of hypoxia and nutritional deprivation. For example normal breast tissue contains typically 10 kPa of oxygen compared to 4 kPa in breast cancer tissue (83). Similarly normal tissue contains glucose levels of 5 mM whilst in many tumours this can range from anywhere between 0-2 mM (83).

Hypoxia and low glucose conditions cause cellular stress and leads to up-regulation of GRP78 as shown by Kakinuma and colleagues in 2008(95). Another study by Sorensen and colleagues 2009 used proteomic techniques to compare protein levels in head and neck cancer cell line $FaDu_{DD}$ under normoxic (21% O_2 for 24h) and hypoxic (1% O_2 for 24h) conditions(96). The study identified over 11 different proteins which were up-regulated under hypoxia. These included GRP78 , protein disulfide isomerase A, as well as glycolytic enzyme glyceraldehydes 3 phosphate dehydrogenase (GAPDH) (96).

GRP78 has been found to be elevated in many tumours such as those of lung, breast, stomach, prostate, colon and liver (1). Up-regulation of GRP78 may be important for tumours to survive and grow in their microenvironment of low oxygen and low glucose.

Below several studies which have investigated the role of GRP78 in tumorigenesis are summarised.

A study by Fu and colleagues in 2008 reported that homozygous deletion of GRP78 in the prostate gland of mice lead to suppression of prostate tumour development and growth (97). All mice in the study had inactive *phosphatase and tensin* gene (*PTEN*). Inactivation of PTEN is a common occurrence in prostate cancers and leads to excessive stimulation and phosphorylation of the PI3K/AKT pathway and subsequent enhanced cell growth and proliferation (see section 1.2.1 for a review of the EGFR signalling pathway). All mice with PTEN inactivation developed tumours within 12-20 weeks of birth. Whilst none of the eight mice with both PTEN inactivation and GRP78 double allele knockout developed any tumours or precancerous lesions (97).

A study by Dong and colleagues in 2009 (98), compared mammary tumour development in GRP78 homozygous +/+ mice to and GRP78 heterozygous +/- mice. All mice expressed the polyoma middle T oncogene (PyT) (98). Tumours were first detectable around 8-10 weeks in the homozygous group but in the heterozygous group tumours were detectable between 10-12 weeks. Furthermore tumour size was reduced by 60% in the heterozygous group as compared to the homozygous group. Hence even partial reduction in GRP78 may be sufficient to impede tumour growth and size (98).

In order to understand whether GRP78 may contribute to human gastric invasion and metastasis GRP78 expression was analysed, by Zhang and colleagues, in patients with N0, N1 and N2/N3 (more than six nodal metastasis) tumours (99). The study found strong association between increased nodal status and high GRP78 expression ($p=0.0037$). Furthermore upon transfection of gastric cancer cells with siRNA against GRP78, in vitro, there was significant inhibition of invasion compared to controls as determined by Matrigel invasion assay ($p<0.001$). These studies indicate that up-regulation of GRP78 may also increase the metastatic potential of tumours (99).

EGF-SubA is a novel drug developed by SibTech® consisting of epidermal growth factor covalently bound to SubA. As mentioned previously SubA is able cleave GRP78 (72 kDa) into 44 kDa and 28 kDa fragments. In the study by Backer and colleagues, human breast and prostate tumours bearing mice underwent a seven day course of intraperitoneal injections of EGF-SubA, resulting in significant reductions in growth in both tumour models. Critically Backer and colleagues observed the treatment was ‘well tolerated in mice without clinical signs of toxicity’ (5). As loss of GRP78 has been shown to suppress tumour development, targeting this protein for example by EGF-SubA may offer a novel way in treating tumours.

1.3.4 Overview of apoptosis

If there is prolonged activation of the UPR, and the issue of unfolded proteins remains unresolved, the UPR mechanism can initiate apoptosis. Before discussing the role of the UPR in apoptosis it is important to review the basic mechanisms involved in apoptosis.

Apoptosis is the active process of cell death. It is executed by a group of proteases collectively known as caspases (100). Effector caspases (such as caspase 3 and 7) are able to cleave more than 100 different proteins which contributes to the emergence of morphological features which are characteristic of apoptosis. These include cleavage of the inhibitor of caspase-activated DNase (ICAD) which leads to activation of CAD and subsequent DNA defragmentation (101). Also proteolysis of several cytoskeletal proteins such as actin results in loss of cell shape (101). Similarly, proteolysis of membrane proteins gives rise to membrane blebbing. The resulting distortion of the cell membrane leads to exposure of phosphatidylserine (PS). PS is recognized by phagocytic cells which then engulf these PS expressing cells (100).

Caspases are synthesised as inactive precursors which require cleavage for activation. Before effector caspases can digest cellular target proteins these caspases need to be activated by the initiator caspases(such as key initiator caspase 9) (100). Caspase 9 is activated by forming a multisubunit complex between Apaf-1 and a protein released by

mitochondria known as cytochrome c (100) This complex collectively is known as an apoptosome.

Cytochrome c release is governed by activation of proapoptotic multidomain proteins Bax and Bak. In healthy cells Bax and Bak are inhibited by interactions with anti apoptotic proteins Bcl-2 and Bcl-x_L (100). Cell death signals can activate a group of proteins known as proapoptotic 'BH3 only proteins', which includes: Bid, Bad, Noxa, Puma and Bim. Upon activation BH3 only proteins can interact with anti apoptotic proteins and cause the release and subsequent activation of Bax and Bak (100).

Caspases are also regulated by a set of proteins known as inhibitors of apoptosis (IAP) which inhibit caspases by binding to them directly or by targeting them for ubiqitinated degradation (100).

In response to DNA damage, the tumour suppressor and transcription factor p53 is up-regulated. Initially ATM and Chk2 protein kinases phosphorylate and stabilize p53 (100). p53 can either induce G1 cell cycle arrest via transcription of Cdk2 inhibitor p21 or cause cell death via transcription of Puma and Noxa (100).

Growth factor signals such as those generated by the epidermal growth factor (EGF) can promote cell survival by activating signal pathways such as PI3 kinase/Akt or Ras/Raf/MEK/ERK (100). Once activated these pathways can phosphorylate and inactivate Bad thereby inhibiting apoptosis (100).

Caspase 3 can also be activated through a mitochondrial independent pathway known as the extrinsic apoptosis pathway. The extrinsic pathway is initiated through the stimulation of death receptors such as CD95 and tumour necrosis factor related apoptosis inducing ligand (TRAIL) (101). Once these receptors are activated through their appropriate ligands, they activate caspase 8 which can then directly control the activity of caspase 3. The extrinsic pathway can be inhibited by FLIP which blocks caspase 8 activation (101). Activated caspase 8 can also enhance the intrinsic pathway by cleaving and stimulating Bid (102).

1.3.5 GRP78 leads to suppression of apoptosis

Several studies as described below have identified GRP78 as a protein which inhibits apoptosis.

As mentioned previously ATF6 up-regulates GRP78 during ER stress (87). Before ATF6 can enter the nucleus and act as a transcription factor it must be split into a smaller fraction by Site 1 protease (S1P). AEBSF is a protease inhibitor which can block S1P and prevent the up-regulation of GRP78 (103).

A study by Shu and colleagues in 2008(103), initiated the ER stress response with thapsigargin and analysed the levels of BAD phosphorylation at Ser75 with and without AEBSF. Ser75 is ordinarily phosphorylated by Raf 1. Phosphorylation of BAD at Ser75 prevents BAD from causing the release of cytochrome c and initiating apoptosis. The study found that the amount of BAD phosphorylation was less, as shown by western blot, when thapsigargin was combined with AEBSF rather than with just thapsigargin alone (103).

The study also found a decrease in mitochondrial membrane potential and an increase in cytochrome c release when thapsigargin was combined with AEBSF, as opposed to

when thapsigargin was used on its own. The study further analysed the contents of a subcellular fraction of mitochondria and found the presence of both GRP78 and Raf 1 by western blot. The study concluded that there may be an interaction between GRP78 and Raf 1that increases phosphorylation of BAD thus inhibiting BAD from initiating apoptosis (103).

As mentioned previously, the study by Reddy and colleagues in 2003(104), found through coimmunoprecipitaion that there may be some interaction between procaspase 7 (35kDa) and GRP78 (104). Confocal microscopy further located both GRP78 and procaspase 7 around the peri nuclear/ER region of the cell. They went on to treat Chinese hamster ovarian (CHO) cells with the topoisomerase inhibitor etoposide. Following treatment, CHO cells that over expressed GRP78 had reduced levels of activated caspase 7 levels (32kDa) when compared to parental CHO cells. Hence GRP78 may be able to suppress caspase 7 activity, via an ATP domain which is able to bind procaspase 7 and prevent caspase 7 activation and subsequent apoptosis (104). When GRP78 was manipulated so that cells expressed a mutant form of GRP78 without the ATP domain there was no interaction between procaspase 7 and GRP78, as determined by immunoprecipitation using anti-caspase 7 antibody. Furthermore, Annexin V labelling and clonogenic survival assay showed increased cell death and reduced cell survival in the mutant GRP78 cell population compared to cells with normal GRP78(104).

1.3.6 UPR and apoptosis.

Primarily the UPR is a prosurvival response; however in the event of prolonged ER stress the UPR initiates the apoptosis cascade. As discussed in section 1.2 CHOP is induced during the activation of both PERK and ATF6 (92). CHOP causes the up-regulation of Bim which is one of the proapoptotic BH3 only proteins (92). CHOP can also induce DR5 which is a TRAIL receptor thus promoting p53 independent apoptosis (102). Not surprisingly activation of caspase 3 can occur during ER stress even in Apaf-$1^{-/-}$ cells (84).

Activation of IRE1 also increases levels of JNK. JNK mediated phosphorylation inhibits the anti-apoptotic activity of BCl-2 whilst activating Bim and inducing BAX (83). A study by Urano and colleagues in 2000(105), showed that following ER stress, IRE1 wild-type fibroblasts increased JNK levels by two fold, whilst JNK expression was impaired in IRE1 knock out fibroblasts(105).

1.3.7 GRP78 and chemo-therapy resistance

A review of the current published data suggests that over expression of GRP78 in tumours may reduce the effectiveness of chemo-therapeutic agents. Cisplatin is the main chemotherapeutic agent used in the treatment of head and neck cancer (106). Cisplatin is able to bind to DNA leading to DNA-DNA inter and more commonly intra-strand crosslinks. Formation of such DNA adducts lead to the suppression of RNA transcription, inhibition of cell division and apoptosis (107).

Lee and colleagues in 2008, transfected glioma cells with GRP78. Subsequent increases in GRP78 expression in these transfected cells resulted in decreased caspase 7 activation and rendered cells resistant to cisplatin induced apoptosis. Upon siRNA treatment against GRP78, decreased cell growth was observed as well as increased sensitisation to both cisplatin and radiation (108).

As explained above, GRP78 is known to inhibit apoptosis through direct interaction with BIK and procaspase 7 (104) (109). Jiang and colleagues in 2009, found that siRNA knockdown of GRP78 increased caspase 4 and 7 activity induced by cisplatin whilst over expression of GRP78 suppressed caspase 4 and 7 activity in melanoma cells(110).

A study by Langer and colleagues in 2008, compared protein expression in patients who responded well to cisplatin/5-FU chemo-therapy to those who were resistant to chemo-therapy (111). All together 34 patients with locally advanced oesophageal adenocarcinomas were treated with neoadjuvant chemo-therapy prior to surgery. Responders to chemo-therapy had a median disease free survival of 16.4 months compared to 8.4 months for nonresponders ($p=0.0015$). Proteomic analysis of primary tumour tissue was used to analyse differences in protein expression of the tumours between responders and non responders and it was found that cellular stress proteins HSP27, HSP60, GRP78 and GRP94 were all up-regulated in the nonresponder group ($p<0.001$) (111).

A study by Scriven and colleagues in 2009 found increased resistance to 5-FU under low glucose conditions in T47D breast cancer cells (112). Cells were grown in normal and low glucose (2 mM) media. Cells grown in low glucose concentration had elevated levels of GRP78 and were significantly more resistant to 5-FU ($p=0.05$) (112). Moreover, Pyrko and colleagues in 2007 found increased sensitivity to 5-FU in knockdown GRP78 glioma cells (113). Furthermore, GRP78 knockdown resulted in reduced cell proliferation, induction of CHOP and increased activated caspase 7 in temozolomide treated cells (113).

A study by Wang and colleagues in 2008(114) wanted to determine whether modifying levels of GRP78 could alter the potency of chemo-therapeutic agent V-16 on lung cancer cells NCI-H446 (114). V-16 is a topoisomerase inhibitor which prevents unravelling of DNA and subsequent DNA copying, and hence targets cells in S phase.

The study involved the up-regulation of GRP78 using the GRP78 inducer A23187 (a calcium ionophore which facilitates the transport of calcium ions into the ER) and reducing GRP78 levels using BAPTA-AM (a calcium chelator which reduces calcium levels in the ER).Cells were either treated with V-16 for 6h and then left to grow in fresh media without drug for a further 48h before analysis, or pre-incubated with either A23187 or BAPTA-AM for 24h followed by V-16. When V-16 was used alone 27.8% ±1.48% of cells underwent apoptosis, as measured by flow cytometry. When the cells were treated with V-16 and A23187 the percentage of cells undergoing apoptosis was significantly reduced at 7% ±1%. With V-16 and GRP78 inhibitor BAPTA-AM the percentage of apoptotic cells was significantly increased relative to the controls at 56.5% ±2.13% ($P < 0.05$) (114).

Cell cycle profile analysis was also performed and it demonstrated that there was a significant decrease in the number of cells in S phase following treatment with A23187 and a corresponding significant increase in the number of cells in S phase with BAPTA-AM cells (114). Hence GRP78 inducers may decrease sensitivity whilst GRP78

inhibitors may increase to chemo-therapeutic agents whose predominant activity occurs during S phase of the cell cycle.

In another study by Pyrko and colleagues in 2007(113), GRP78 was both down regulated using siRNA against GRP78 and up-regulated following transfection with lentivirus expressing human GRP78, in glioma cells U251 (113). Temozolomide is currently a first line chemo-therapeutic agent for patients with malignant gliomas and works by inducing DNA damage and subsequent apoptosis. Upon treatment with temozolomide there were significant decreases in colony survival in cells in which GRP78 had been knocked-down and significant increases in colony survival in cells in which GRP78 expression had been up-regulated as compared to parental cells (113).

BIK is a proapoptotic protein which is up-regulated when breast cancer cells are deprived of oestrogen (109). Many anti-breast cancer agents work by reducing levels of oestrogen available to cancer cells. Tamoxifen is an antiestrogen and fulvestrant is an oestrogen receptor antagonist. BIK is located in the ER and is able to target BAX indirectly which results in release of cytochrome c. However a study by Fu and colleagues in 2007(109), demonstrated by coimmunoprecipitation that GRP78 is able to interact with BIK and prevent it from inducing apoptosis. Oestrogen dependent cells MCF-7/BUS were grown in oestrogen starved growth media which lead to the induction of BIK. (109). BIK is an upstream regulator of BAX. MCF-7/BUS cell which had been

transfected with adenovirus expressing GRP78, resulting in over expression of GRP78, were also cultured in low oestrogen growth media, In this case, BAX activation was reduced in comparison with parental cells. Furthermore cell transfected with siRNA against GRP78 increased levels of apoptosis in oestrogen starved cells. Hence up-regulation of GRP78 may induce resistance to anti-breast cancer agents whose mode of action is to suppress the levels of available oestrogen.

1.3.8 GRP78 and radioresistance

Hypoxic head and neck tumours are highly radioresistant. Oxygen is needed to ensure maximum biological damage from ionizing radiation. A hypoxic environment of less than 3-4 mmHg oxygen leads to hypoxic cells requiring approximately three times as much radiation as normoxic cells in order to achieve the same levels of cytotoxicity (115). Tumour oxygen levels can therefore act as a predictive marker(116). The 'Eppendorf electrode' is widely used in the research setting for detecting oxygen levels in tumours. In the laboratory setting carbonic anhydrase 9 (CA9) proteins can be detected by immunohistochemistry. *CA9* is a gene which is transcribed by hypoxia inducible transcription factor (HIF-α) under hypoxic conditions (116).

A study by Schrijvers and colleagues in 2008(117), classified patient treated with radiotherapy for grade I or II laryngeal tumours into those with high expression of either HIF-α or CA9 or those with low expression(117). Of the 92 patient samples analysed, 59 patients had a hypoxic expression pattern. Out of this subset of patients 32% (19/59) developed recurrence. In the 40 patients classified as having normoxic tumours only 6% (2/32) of patients developed recurrence (117). Similar studies found a significant decrease in local regional control and overall survival in head and neck patients with hypoxic tumours (classed as O_2 concentration of ≤ 2.5 mmHg) treated with radiation therapy (118).

Recent clinical trails have attempted to modify the hypoxic environment in order to improve radiosensitivity. A large Danish clinical trial (DAHANCA) randomly assigned 414 patients with advanced cancer of the supraglottic larynx or pharynx to either radiation and placebo or nimorazole (115). Nimorazole is a hypoxic cell radiosensitizer which mimics oxygen by increasing the concentration of DNA damaging free radicals, but is not metabolized by cells (115). The trial found significant improvements in both local regional tumour control ($p=0.002$) and disease specific survival ($p=0.01$) in patients with high levels of hypoxia as determined by plasma concentrations of osteopontin (a hypoxia marker) but no significant improvements in patients with apparently normoxic tumours (115). Similarly phase II trials are currently taking place which are assessing the potential of ARCON therapy which combines accelerated

radiation therapy with carbogen breathing (95% O2 and 5% CO2) and nicotinamide (119). Nicotinamide prevents the acute closure of blood vessels thus reducing incidences of transient hypoxia (119).

Hypoxic tumours may be more radioresistant not only due to the lack of oxygen but also due to the induction of certain genes under hypoxia such as GRP78 (119).

Several studies have recently associated GRP78 as a radio resistant phenotype. Feng and colleagues in 2010 found GRP78 to be a potential prognostic biomarker with up-regulation of GRP78 in tumours corresponding to radioresistance in patients with nasopharyngeal carcinoma (3). Lee and colleagues in 2008, found that silencing of GRP78 via transfection with siRNA significantly enhanced the sensitivity of glioblastoma cells to radiation (108).

A study by Lin and colleagues in 2010 analysed the expression of proteins between parental and radioresistant cell lines in head and neck cancer (8). This included cells from poorly differentiated tongue squamous cell carcinoma (SAS cell line) and gingival epidermoid carcinoma (OECM1 cell line) (8). These parental cell lines were treated with ionising radiation at sequential 2 Gy intervals. After each treatment, surviving cells were sub-cultured and further exposed to 2 Gy fractions of ionising radiation. This sequence was continued until surviving cells had been subject to a total of 60 Gy. Protein

expression was then compared between parental and radioresistant cell lines. Amongst the proteins that were identified as being up-regulated in the radioresistant lines were three protein chaperones: Gp96, Grp78 and HSP60. Grp78 was up-regulated on average by 2.7 fold (8).

1.3.9 Targeted inhibition of GRP78

GRP78 acts as a protein chaperone, a gatekeeper to the Unfolded Protein Response, and as an anti apoptotic agent by preventing caspase activity.

It is linked to tumorigenesis and is known to be over expressed in a wide variety of cancers such as lung, breast and colorectal cancer. Up-regulation of GRP78 appears to be an adaptive response of tumour cells, enabling these cells to tolerate their typical microenvironment of hypoxia and low glucose availability. Furthermore GRP78 over-expression is implicated in chemo- and radio-resistance and therefore inhibition of GRP78 may aid in the treatment of cancer.

Subtilase A (SubA) is a bacterial toxin, with proteolytic activity, derived from a specific strain of E. coli known as Shiga toxigenic E. Coli (STEC) (7). These strains of E. Coli

are known to cause life threatening outbreaks of haemolytic uraemic syndrome (HUS) such as in Australia in 1998 (7) as well as gastrointestinal disease.

Paton and colleagues identified only GRP78 (a 72kDa protein) to be cleaved by SubA (7). 2D gel electrophoresis showed four spots that were specific to when cells were treated with SubA. Upon matrix assisted laser desorption/ionization-mass spectrometry (MALDI-MS) one of these four spots was identified as GRP78. Furthermore only GRP78 showed 'significant size discrepancy' from ~27kDa on the gel compared to 72 kDa on the database. GRP78, which consists of 654 highly conserved amino acids, is cleaved, by SubA between two leucine residues at position 416-417. In addition, Paton and colleagues demonstrated that a single amino acid substitution at L_{416} ensured that SubA was no longer able to cleave GRP78 into two fragments (7) Although HSP72 shares 7 out of 11 amino acid positions with GRP78, HSP72 does not contain the two leucine cleavage site. As expected Paton and colleagues did not find HSP72 to be cleaved by SubA (7). The protease site of SubA is located at Serine272. Paton et al, mutated SubA at this and this inactive mutant ($SubA_{A272}$) was no longer able to cleave GRP78.

EGF-SubA is a novel drug developed by SibTech® consisting of epidermal growth factor covalently bound to SubA. SubA, as previously discussed, is able to cleave GRP78 (72kDa) into two parts of weight 28kDa and 44kDa which leads to the activation

of the Unfolded Protein Response (UPR). Epidermal growth factor (EGF) is the naturally occurring ligand of the RTK transmembrane protein epidermal growth factor receptor (EGFR). Hence EGF-SubA has the ability to target deliver SubA to EGFR expressing cells. Should the same cells be over-expressing GRP78, it is conceivable that SubA mediated, GRP78 cleavage could result in cell death – a strategy that may be exploitable in the treatment of EGFR expressing tumours which also harbour high levels of GRP78.

2 Aims of this study

Protein chaperone GRP78, a key component of the Unfolded Protein Response which is induced as part of a survival response under certain conditions of stress common in cancer (hypoxia/hypoglycaemia), has been shown to be up-regulated in a wide variety of cancers(1, 4). The up-regulation of GRP78 has been associated with both poor survival outcome as well as increased resistance to current cancer therapies (1, 8, 97, 120). Thus we will examine GRP78 expression in head and neck cancers. In addition to this we will investigate the impact of a novel compound EGF-SubA, which promotes proteolysis of GRP78. EGF-SubA will be tested upon a panel of laryngeal squamous cell carcinoma (LSCC) cells, *in vitro*, alone and in combination with clinically relevant agents.

Although GRP78 is reported as being up-regulated in nasopharyngeal squamous cell carcinoma there are currently no published data regarding GRP78 levels in patients with laryngeal squamous cell carcinoma (LSCC) which constitute the most prevalent sub-group of head and neck patients or in patients with either oropharyngeal or hypopharyngeal SCC (3).

- Therefore we first determined whether GRP78 expression was up-regulated in SCC of oropharynx, larynx and hypopharynx via immunohistochemical

analysis of a tissue micro array of 190 patients. To establish whether GRP78 is a potential prognostic biomarker in head and neck cancer, GRP78 protein expression was correlated with patient survival data.

An increasing body of evidence suggests that up-regulation of GRP78 in tumours may lead to chemo- and radioresistance (1, 8, 97, 120). EGF-SubA is a novel cytotoxic drug that encompasses a bacterial endotoxin (SubA) covalently bound to EGF to permit targeting of EGFR-expressing cells and an enzymatically active moiety SubA which promotes proteolytic cleavage of GRP78 (5).

- Therefore we explored whether EGF-SubA could enhance sensitivity *in vitro* to treatment modalities currently used in the treatment of head and neck cancer, in a panel of LSCC cell lines. Clonogenic assays were used to determine whether EGF-SubA could enhance the effects of ionising radiation. An MTT assay was used to measure any potential antagonistic/synergistic effects between cisplatin and EGF-SubA on cell viability/growth. In addition, flow cytometry-based Annexin V/PI assays were performed in order to determine the effects of combinations of these two drugs on apoptosis.

It has been reported that EGF-SubA cytotoxicity is dependent upon EGFR density and therefore EGF-SubA may, potentially, be more toxic to tumour cells of the head and neck which are known to over-express EGFR, compared to healthy tissue (5).

- EGFR membrane expression will be compared to EGF-SubA sensitivity in our panel of cell lines in order to establish if there is a correlation between these two factors. LSCC membrane expression will be investigated via florescence generated from anti EGFR antibody conjugated PE and flow cytometric analysis.

- Lastly we wanted to determine whether cetuximab, a monoclonal antibody (mAb) against EGFR, can inhibit the cytotoxicity of EGF-SubA (54). This could allow for a combined toxin-protectant approach where topical application of EGF-SubA peri- or post-operatively after tumour resection could be used, or as an oral rinse in patients who present with pre-malignant lesions of the oral cavity, with any potential systemic toxicity of EGF-SubA being abrogated by systemic administration of cetuximab.

Performing the above experiments should allow for a greater understanding of the potential cytotoxic effects of EGF-SubA upon laryngeal squamous cell carcinoma cells, *in vitro*. Furthermore the role of GRP78 as a potential prognostic tumour biomarker will also be clarified.

3 Materials and methods

3.1 Materials and reagents

Materials and reagents were provided by the following suppliers:

Sigma Aldrich: ammonium per sulphate (APS), bovine serum albumin (BSA), bromodeoxyuridine (BrdU), depex polystyrene (DPX), dimethyl sulfoxide (DMSO), Dulbecco's modified eagle medium (DMEM), foetal bovine serum (FBS), L-glutamine solution, MTT, non essential amino acids (NEAA), penicillin, phenyl methane sulfonyl fluoride (PMSF), Phosphate buffered saline (PBS), propidium iodide (PI), RNAse A, RPMI 1640 medium, Spermine, Trypsin-EDTA.

Roche Applied Science: aprotinin, leupeptin, pepstatin, soybean trypsin inhibitor.

Biorad: Bradford protein assay reagent, blotting grade non-fat dry milk powder.

New England Biolabs: broad range protein marker.

Western Lightening Chemiluminescence: enhanced luminal reagent, oxidizing reagent.

Southern Biotech: annexin V conjugated FITC.

Amersham Biosciences: hybond ECL nitrocellulose membrane.

Beckman coulter: isoton solution.

Reagena: reastain quick diff fix, reastain quick diff red, reastain quick diff blue.

Fisher: x-ray film (180mmx240mm)

Vector laboratories: R.T.U vectastain ABC reagent, DAB substrate kit

3.2 **Drugs**

EGF-SubA. Dissolved in 20nM Tris, 0.3M NaCl pH 9.0 (filter sterilized). Kept as stock at 7.5μM at -80^{o}C. Stable at 4^{o}C for one week. Manufactured and generously donated by SibTech Inc. ® USA.

Cetuximab. MW 145781.6. Dissolved in PBS. Kept as stock at 5mg/ml (34.3μM) at 4^{o}C (do not freeze). Supplied by Erbitux®. Generously donated by Clatterbridge Centre for Oncology NHS Trust.

Trastuzumab. MW 145531.5. Dissolved in PBS. Kept as stock at 21mg/ml (144μM) at 4^{o}C (do not freeze). Supplied by Erbitux®. Generously donated by Clatterbridge Centre for Oncology NHS Trust.

AT13387 (HSP90 inhibitor)**.** Dissolved in DMSO. Kept as stock at 10 mM at -80^{o}C. Stable at room temperature for a week. Supplied and generously donated by Astex Therapeutics Ltd. UK.

Cisplatin. MW 300.5. Dissolved in PBS. Kept as stock at 1mg/ml (3.3mM) at room temperature and in the dark. Generously donated by Clatterbridge Centre for Oncology NHS Trust.

Staurosporine. MW 466.53. Dissolved in DMSO. Kept as stock at 1mM at 4^{o}C. Supplied by LC Laboratories USA.

3.3 **Antibodies**

3.3.1 Primary antibodies for western blot

PARP, rabbit polyclonal antibody, final dilution of 3 μg/ml, Abcam (ab6079)

GRP78 (N-20), goat polyclonal antibody, final dilution of 3 μg/ml, Santa Cruz Biotechnology (sc-1050)

GRP78 (H-129), rabbit polyclonal antibody, final dilution 3 μg/ml, Santa Cruz Biotechnology (sc-13968)

Tubulin (DM1A0), mouse monoclonal antibody, final dilution 1:10,000, Santa Cruz Biotechnology (sc-32293)

Actin (C-2), mouse monoclonal antibody, final dilution 3 μg/ml, Santa Cruz Biotechnology (sc-8432)

EGFR (1005), rabbit polyclonal antibody, final dilution 3 μg/ml, Santa Cruz Biotechnology (sc-03)

HSP72 (SPA-810), mouse monoclonal, final dilution 50 ng/ml, Stressgen

3.3.2 Secondary antibodies for western blot

Anti mouse IgG, horse radish peroxidase linked whole antibody, final dilution 1:2,500, Amersham

Anti rabbit IgG, horse radish peroxidase linked whole antibody, final dilution 1:5,000, Amersham

Anti goat IgG, horse radish peroxidase linked whole antibody, final dilution 1:5,000, Zymed

3.3.3 Antibodies used for flow cytometry

Anti EGFR (ICR10) conjugated PE, rat monoclonal antibody, 10 µl of antibody added to 1 ml of cell suspension containing one million cells, Abcam (ab27764-50)

Anti BrdU, mouse monoclonal, 20µl added to cell suspension of 100ul containing one million cells, BD Biosciences (BD347580)

Donkey- anti mouse antibody conjugated FITC, 2.7µl added to cell suspension of 80 µl containing one million cells.

3.4 Cell culture

3.4.1 Cell lines

University of Michigan squamous cell carcinoma cell lines (**UM-SCC**) of head and neck origin were kindly provided by Professor T. Carey at the University of Michigan Medical School, USA. With the exception of UM-SCC 1 which is of oral cavity origin and has mutant p53 status, the rest of the UM-SCC cell lines are of laryngeal origin. UM-SCC 17A and UM-SCC 17AS have p53 wild-type status. UM-SCC 10A and UM-SCC 5 both have a single p53 mutation and retain a wild-type allele (heterozygous G245C and heterozygous V157F respectively). UM-SCC 11B and UM-SCC 81B have no wild-type p53 alleles (mutant C242S and H193R respectively). UM-SCC 12 is p53 null (homozygous Q104X).

Prostate cancer cells (**PC3**) were kindly provided by Mrs Carol Beasley, Department of Pathology, Liverpool University, UK.

Mouse embryonic fibroblasts (**MEF**) used were both null in p53 and MDM2.

Mouse hepatoma cells (**Hepa 1c1c7**) were kindly supplied by the Department of Physiology, Liverpool University UK.

3.4.2 Cell medium and growth environment

All cell lines were grown in a humidified cell incubator at 37^{o}C with 5% CO_2.

All UM-SCC, MEF and Hepa 1c1c7 cells were grown in DMEM, supplemented with 10% (v/v) FBS, 2mM L-glutamine solution, 100 units/ml penicillin with 0.1mg/ml streptomycin solution and 100μM NEAA.

PC3 cells were grown in RPMI 1640, supplemented with 10% (v/v) FBS, 100 units/ml penicillin with 0.1mg/ml streptomycin solution and 100μM NEAA.

3.4.3 Cell culture techniques

At all times aseptic technique was observed in order to avoid contamination. Tissue culture work was carried out in a class II laminar flow tissue culture cabinet.

Cells were grown typically in 175cm^2 tissue culture flasks with 25ml of media solution. Cells were split upon reaching 70-90% confluence. Media was removed and cells were washed once with 5ml of PBS. PBS was removed and 5ml of trypsin-EDTA was added. Adherent cells were then placed in the incubator until they had detached as observed by light microscopy. An equal volume of media as compared to trypsin was added. Cells were then pipetted up and down in order break up any clumps of cells. Cells were then

split according to the cell type. Slow growing cell lines were split typically in a ratio of 1:5 whilst fast growing cell lines were split 1:10.

3.4.4 Cryopreservation and recovery of cryopreserved cell stocks

Cells with high confluence were passaged as described above with the remaining cells used to make up cryopreserved cell stocks as follows. First cells were centrifuged at 300 × RCF, at 4^{o}C for 5 minutes. The supernatant was removed and the pellet of cells was then resuspended in 1ml of freezing media consisting of 90% (v/v) FBS and 10% (v/v) DMSO and placed in a cryo-vial. The cells were kept in a -80^{o}C freezer for 24h in a polystyrene box before being placed into a liquid nitrogen storage tank.

When needed, cells from liquid nitrogen stocks were thawed immediately at 37^{o}C and typically placed into a 75cm^{2} tissue culture flask along with 20ml of media.

3.4.5 Cell grown under hypoxic or low glucose conditions

On occasions UM-SCC cells were grown in low oxygen and low glucose conditions in order to mimic the typical tumour microenvironment.

For cells grown in normal glucose concentrations of 4 g/l, the standard Sigma DMEM media was used (which already contained a glucose concentration of 4 g/l), and supplemented with 10% (v/v) FBS, 2 mM L-glutamine solution, 100 units/ml penicillin with 0.1 mg/ml streptomycin solution and 100 μM NEAA. For the low glucose concentrations a second glucose free media manufactured by GIBCO called 'DMEM (1x) liquid, no glucose' was used in combination with Sigma DMEM. GIBCO DMEM was also supplemented with the above reagents apart from L-glutamine as it already contained this amino acid. Sigma DMEM was subsequently serially diluted in glucose free GIBCO DMEM in order to establish glucose concentrations of 0.4 g/l and 0.04 g/l.

Cells grown in normoxic conditions were simply placed in the humidified cell incubator which contained 5% CO_2 and 95% air. Cells that were to be grown in either 2% or 0% O_2 levels were placed in air tight chambers (Billups Rothenberg inc Modular Incubator Chamber, Patent number 535 2414 box 977 del Mar California 92014). A petri dish containing distilled water was also put inside the air tight chamber in order to humidify the atmosphere. Chambers were initially flushed with a mixture of 5% CO2 and 95% nitrogen and then oxygen content was adjusted with the aid of an oxygen meter (Greisinger humidity meter GOX 100). The air tight chambers were then placed into the incubator.

3.5 **Western blotting**

3.5.1 Reagents and buffers for western blotting

SLIP Buffer (100ml)

50 ml of 0.1 M HEPES (pH 7.5)

10ml of glycerol

0.1ml of Triton X-100

15ml of 150mM NaCl

0.05 g of BSA

Solution made up to 100ml with distilled water

SLIP Buffer was kept for seven days and stored at $4^{o}C$.

PBS/Tween (4 litres)

44.8g $Na_2HPO_4.2H_20$

9.67g $NaH_2PO_4.2H_20$

17.52g NaCl

4ml of Tween 20

Tris-Glycine Electrophoresis Running Buffer (500ml/tank)

25 mM Tris

250 mM glycine

0.1% (w/v) SDS

Tris-Glycine Electrophoresis Transfer Buffer (1L/tank)

25 mM Tris

192 mM glycine

20% (v/v) methanol

4x Sample Buffer (10ml)

0.25 M Tris (pH 6.8)

8% (w/v) SDS

40% (v/v) glycerol

4mg/ml bromophenol blue

1% (v/v) β-mercaptoethanol

Diluted with distilled water to make 2x and 1x samples. Stored at -20^{o}C.

SDS Polyacrylamide Separating Gel (10ml)

	6%	7.5%	10%	12%
H_2O	**5.8ml**	**5.42ml**	**4.8ml**	**4.3ml**
40% Acrylamide mix	**1.5ml**	**1.87ml**	**2.5ml**	**3ml**
1.5 M Tris (pH 8.8)	**2.5ml**	**2.5ml**	**2.5ml**	**2.5ml**
10% SDS	**0.1ml**	**0.1ml**	**0.1ml**	**0.1ml**
10% APS	**0.1ml**	**0.1ml**	**0.1ml**	**0.1ml**
TEMED	**0.008ml**	**0.008ml**	**0.008ml**	**0.008ml**

Table 3.5.1SDS polyacrylamide separating gel formulation

SDS Polyacrylamide Stacking Gel (10ml)

7.225ml H_20

1.275ml of 40% (w/v) acrylamide mix

1.25ml of 1 M Tris (pH 6.8)

0.1ml of 10% (w/v) SDS

0.1ml of 10% (w/v) APS

0.010ml of TEMED

Ponceau Staining Solution (10X stock)

2g Ponceau S

30g sulphosalicyclic acid

30g trichloroacetic acid

H_20 added to make a final volume of 100ml

3.5.2 Cell pellets and protein extraction

Cells were harvested via trypsinisation as described in section 3.4.3. Cells were then centrifuged for five minutes at a speed of 1000 × RPM. The supernatant was removed and the cells were resuspended in 1ml of PBS. The cells were then centrifuged again for five minutes at 1000 × RPM. The supernatant was removed and the pellet was stored at -80^{o}C for at least an hour before beginning protein extraction.

SLIP buffer was placed on ice and combined with the following protease inhibitors: soybean trypsin inhibitor 100ug/ml, aprotinin 2μg/ml, leupeptin 0.5μg/ml, pepstatin A 1μg/ml and phenylmethylsulfonyl fluoride (PMSF) 1mM. Proteases inhibitors prevent endogenous proteases from proteolysis of proteins of interest. Triton X-100 which is present in SLIP buffer permeabilises the cell membrane in order to release proteins.

Cell pellets were resuspended and broken up in 10-50μl of the above solution and left on ice for ten minutes. The samples were then centrifuged at 14000 × RCF for ten minutes at 4^{o}C. The supernatants from each sample was then separated from their pellets and kept on ice.

3.5.3 Calibration of protein samples

Bradford reagent contains a dye called coomassie. When this dye binds to protein it produces a shift in absorbance from 465 nm to 595 nm. Hence this dye can be used as a colorimetric method for total protein quantisation.

Initially a series of protein standards were prepared as follows. Bovine serum albumin (BSA) was serially diluted in the existing SLIP buffer, containing the protease inhibitors, at the following dilutions: 20, 10, 5, 2.5, 1.25, 0.625, 0.3125 and 0 mg/ml. Bradford protein assay reagent was then diluted 1:5 parts with distilled water. 2μl of each of the above concentrations were then placed into separate eppendorfs containing 1 ml of the diluted Bradford reagent. These nine samples were vortexed and then placed in a spectrophotometer in order to establish a standard protein concentration curve. A coefficient of variable of less than 5% was deemed an acceptable level of calibration.

2µl of each of the cellular supernatants were added to 1 ml of diluted Bradford reagent and placed in the spectrophotometer. The volume of supernatant containing 50µg of protein was then calculated. Equal volumes of 2x sample buffer (section 3.5.1) was then added to the supernatant. 1x sample buffer was then added in appropriate volumes so that the final protein concentrations would be 50µg per 20µl.

Sample buffer contains detergent SDS and reducing agent mercaptoethanol. When protein samples are heated SDS is able to disrupt secondary, tertiary, and quaternary structures of proteins producing a linear polypeptide chain which is coated in negatively charged SDS in a ratio of 1.4g of SDS for every 1g of protein (121). Mercaptoethanol is further able to denature the proteins by removing disulphide bonds(121). Proteins now become linear and have a negative charge which is proportional to their weight. During electrophoresis proteins are separated solely on the basis of how much negative charge they carry due to SDS and not on their original shape.

Samples can be either stored at -80^{o}C or heated at 100^{o}C for 5 minutes to denature the proteins and then centrifuged at 14,000 × RCF for 5 minutes at 4^{o}C, prior to being loaded onto the polyacrylamide gel.

3.5.4 SDS polyacrylamide gel electrophoresis (SDS-PAGE)

The percentage polyacrylamide separating gel (Table 3.5.1) was chosen depending upon the molecular weight of the protein to be analysed. High molecular weight proteins such as epidermal growth factor receptor (EGFR) at 135kda required a low percentage gel of around 7.5% whilst low molecular weight proteins such as cyclin D at 35kda required a high percentage gel of around 12%.

Glass plates of 0.75 mm were cleaned with 70% ethanol and placed in their stands. Distilled water was added in between the two plates, for five minutes, to check for leakage and then removed. The appropriate percentage polyacrylamide separating gel (Table 3.5.1) was then added until a level of 1.5 cm below the top of the glass plates was left. The top of the gel was then covered with water and left to set for 30 minutes. Water was then removed and stacking gel (section 3.5.1) was then added with a 0.75 mm 10 well comb. This was left to set for a further 30 minutes.

The plates along with the gel were then placed in a Mini Protean III electrophoresis chamber. 500ml of electrophoresis running buffer (section 3.5.1) was then added to completely fill the central chamber and half of the outside chamber. 15µl of broad range protein marker was added to the first well. 20µl of sample was then loaded into each of the other wells. 20µl of 1x buffer was placed in any remaining wells. The chamber was then subject to 200 v until the loaded samples had reached the bottom of the gel.

Hybond ECL nitrocellulose membrane, two pieces of 3mm Whatman® chromatography paper and two sponges where pre-soaked in transfer buffer (section 3.5.1). Stacking gel was discarded and the separating gel was placed in between the nitrocellulose membrane and chromatography paper. Two sponges were added on the outside and the whole entity was placed in a cassette. The cassette was placed in the chamber in such a way that the membrane faced the positive electrode whilst the gel faced the negative electrode. The negatively charged proteins on the gel would then run in the direction of the nitrocellulose membrane towards the cathode. Transfer buffer (section 3.5.1) was added to the chamber along with an ice pack in order to ensure cooling during transfer. The chamber was left at 100 v for one hour.

3.5.5 Ponceau S Staining

After protein transfer the membrane was removed and stained with Ponceau S (section 3.5.1) to determine whether protein transfer was even. The membrane was cut horizontally at appropriate bands depending upon the molecular weight of the proteins to be studied and then washed in PBS Tween (section 3.5.1) to remove Ponceau S staining.

3.5.6 Incubation of antibodies

The membrane was then incubated in PBS Tween with 5% blotting grade non fat dry milk powder for one hour, with agitation, in order to block antibodies from binding to non specific protein binding sites on the membrane itself.

Primary antibodies (section 3.3.3) were diluted, according to their manufactures' guidelines, in PBS Tween (section 3.5.1). The membrane was then incubated with agitation in its primary antibody for one hour followed by washing in PBS Tween for three cycles of ten minutes. Horse radish conjugated secondary antibodies (section 3.3.2) were diluted in PBS Tween and 5% milk powder. Membranes were then incubated and agitated for an hour with these secondary antibodies (section 3.3.2). This was then followed by three washes with PBS Tween.

Anti bodies against human proteins are created by injecting antigens into animals such as rabbits and mice. During the primary response, when a foreign antigen is initially introduced, IgM antibodies are the first to appear. These lymphocytes do not produce memory cells. Later levels of IgG start to rise as lymphocytes start to produce both memory cells and plasma cells.

When the foreign antibody appears the second time round, during a second injection, there is an immediate increase in IgG levels, as memory B cells differentiate into plasma

cells and produce IgG antibodies. It is these IgG antibodies which are commercially harvested.

Polyclonal antibodies contain a mixture of antibodies which target different epitopes of the same antigen. The mixture of antibodies vary in specificity (whether the anti body recognizes other proteins) and affinity (how well the antibody attaches to the antigen) to one another.

Monoclonal antibodies are a homogenous population of antibodies which recognize a single epitope. The antibodies are generated from a single B cell clone. The specific plasma cell is taken and fused with an immortal cell (myeloma cell line/fusion partner). This is known as a hybridoma. This fusion allows for the production of specific antibodies and indefinite growth in culture (122).

Monoclonal antibodies produce cleaner bands on a western blot as there is less possibility of cross reactivity with other proteins, as there is just one antibody acting against one epitope. However the ability of polyclonal antibodies to recognize several epitopes increases the chance that at least some of the antibodies will bind to the protein of interest especially after possible deleterious effects that sample processing may have upon the protein (122).

3.5.7 Developing

In order to visualize the proteins of interest, after probing with appropriate primary and horse radish conjugated secondary antibodies, the membrane was incubated for 60 seconds with chemiluminescence ECL reagent. This consisted of equal volumes of Enhanced Luminol Reagent and Oxidising Reagent. Horse radish peroxidase is able to catalyse the oxidation of luminol into a chemical which emits light. The location and the amount of horseradish peroxidase corresponds to the position and quantity of protein, and subsequently to the location and amount of light emitted. The luminescence signal can be detected via the Kodak IM4000 image station or on X-ray film, at different exposure times ranging from 10 seconds to 30minutes.

3.5.8 Detecting phosphorylated proteins via western blot

In order to be able to prevent phosphatase enzymes from dephosphorylating phosphorylated proteins such as phospho-EGFR, the following phosphatase inhibitors were added to SLIP buffer (section3.5.1): 5 mM sodium fluoride, 1 mM sodium orthovandate and 10 mM sodium pyrophosphate. SLIP buffer containing phosphatase inhibitors was pre-cooled on ice. Media was removed and the six well tissue culture dishes were placed on ice. Approximately 150 µl of SLIP buffer containing phosphatase inhibitors was placed into one well. Cells were detached using a cell scraper and the cell suspension with SLIP buffer was transferred to the remaining wells. Lysates were then processed for SDS-PAGE and western blot analysis

3.6 **Annexin V apoptosis detection**

3.6.1 General principles of flow cytometry

A flow cytometer passes a laser through individual cells which are flowing in single file. The machine is then able to detect scattered light and fluorescence emissions from these cells. Light emitted in the forward direction from the laser and out of the cell is collected by the forward scatter channel (FSC) and light emitted at 90^{o} is collected by the side scatter channel (SSC).

FSC intensity is related to cell size and can be used to distinguish between cell debris and live cells. SSC is associated with cellular granularity.

Single cells from the same cell line will have similar FS and SS values to each other. In order to analyse the data generated from this group of cells and to exclude data from either cell debris or clumps of cells FS versus SS dot plots are generated and a gate is drawn around the central population of cells.

Detection of fluorochromes by flow cytometry can be used as surrogate indicators for the presence and quantity of various receptors such EGFR via anti EGFR antibody conjugated to fluorochrome PE. Fluorochromes such as PI can bind to DNA and be used in cell cycle analysis. Other fluorochromes can be used for the detection of apoptosis as will be discussed later.

Fluorochromes are compounds which absorb light energy from the laser beam and release this energy in the form of both heat and light energy (fluorescence). The light emitted is always of a longer wave length (lower energy) to that absorbed from the laser and hence the emitted light is of a different colour. The difference between the energy absorbed from the laser and the energy emitted, in the form of fluorescence, is known as Stoke's Shift. For example Argon-ion laser can excite FITC at 488 nm, which is close to FITC's maximal absorbance of 490 nm (or the wave length at which the maximum amount of photons are absorbed). In turn FITC emits a fluorescence at a range of 475-700 nm with maximum emission of photons at 525 nm. With the aid of optical filters various photodetectors (labelled as fl1, fl2, fl3) can then be used to detect appropriate range of wavelengths.

3.6.2 Reagents and buffers used in Annexin V apoptosis detection

- Annexin V conjugated FITC solution (5µl per sample)
- Propidium iodide (PI) was dissolved at a concentration of 100µg/ml in 10 mM potassium phosphate (pH 7.4), 150 mM NaCl. (10µl per sample)
- 10x binding buffer consisting of: 0.1 M Hepes/NaOH (pH 7.4), 1.4 M NaCl, 25 mM $CaCl_2$. For 1X working solution 1 part 10x was diluted in 9 parts distilled water.
- BSA(10mg/ml) in PBS (ice cold)

3.6.3 Protocol for Annexin V apoptosis detection

Apoptosis is structurally characterized by chromatin condensation, reduction in cell volume(reduced FSC signal), and DNA defragmentation via endonucleases (123). During early stages of apoptosis there is loss of phospholipid membrane symmetry which leads to exposure of protein phosphatidyl serine (PS) from the inside to the outside of the cell membrane. PS expression at the cell surface causes identification and removal of apoptosing cells by macrophages *in vivo* (123). Annexin V can bind to PS in the presence of calcium and therefore Annexin V conjugated to fluorochrome FITC can be used to indicate early stages of apoptosis. During late apoptosis there is loss in membrane integrity and PI can now enter cells.

A population of unfixed cells can be stained simultaneously with both PI (red fluorescence) and FITC (green fluorescence) conjugated Annexin V, and analysed by flow cytometry. Four subset populations of cells will appear on a dot plot graph of Annexin V versus PI. Cells which remain unstained are healthy cells. Cells which stain with just Annexin V are undergoing early apoptosis. Cells which stain with just PI are necrotic cells and cells which stain with both Annexin V and PI are cells which have entered late apoptosis. These four subsets can be divided using a quadrant and the percentage of cells in each quadrant can be calculated.

In order to first calibrate the position of the four quadrants, for each of the cell lines, a known healthy population of cells had to be compared to a known apoptotic population of cells.

Staurosporine is a tyrosine kinase inhibitor which is a known potent inducer of apoptosis. Staurosporine was dissolved in its drug vehicle control DMSO and mixed with growth media at a concentration of 2μM. Staurosporine was applied to cells for 24h. This group of cells would therefore help identify the areas of apoptosis in the quadrant. A control group of cells was grown for 24h with growth media mixed with appropriate volumes of DMSO. This group of cells would help to identify the location of healthy cells.

Cells were harvested using trypsin as described previously (section 3.4.3) however the media that the cells were grown in was also collected in order to obtain dead cells that may have detached from the surface. It was important not to over trypsinise cells as this may also lead to damage to the cell membrane. A light microscope was used to determine when 80 to 90% of cells had detached from the surface of the well. Immediately trypsin was neutralised by adding equal amounts of growth media.

Cellular concentrations per ml were determined by Beckman coulter counter and the volume of cells in solution was adjusted so that there would be one million cells per

sample. Cells were spun down at approximately 173 × RCF for five minutes at 4^{o}C. Supernatant was removed and cells were resuspended and washed twice in a solution of ice cold PBS with 1% BSA. Samples were kept on ice.

Cells were centrifuged at approximately 173 × RCF for five minutes at 4^{o}C. The supernatant was removed and the one million cells were resuspended in 1ml of ice cold 1x binding buffer (section 3.6.2). Samples were kept on ice and moved to the flow cytometer. Initially Beckman Coulter Epics XL flow cytometer was used and data was analysed using WIN MDI software (Windows multiple document interface for flow cytometry). However at the start of 2010 the use of a newer machine became available called BD FACSCalibur flow cytometer and the data was analysed on CellQuest Pro Software.

The flow cytometry parameters were as follows: FL1 log to detect FITC Annexin V staining, FL2 log to detect PI, FS linear, SS linear, and 20,000 events.

Sample were stained with 5µl of FITC Annexin V solution and 10µl of PI solution and left on ice and in the dark for exactly ten minutes before being tested. It is critical that sample are tested at exactly ten minutes as any further delay leads to photo bleaching as eventually all cells, if left long enough, will absorb PI.

3.7 Cell cycle analysis

3.7.1 Reagents and buffers used in cell cycle analysis

- 70% ethanol (ice cold)
- RNAse A 10mg/ml in 0.01M sodium acetate
- 1M Tris (pH 7.4)
- PBS Tween (section 3.5.1)
- BSA (10mg/ml) in PBS

3.7.2 Protocol for cell cycle analysis

In cells fixed with 70% ethanol, propidium iodide is able to pass through the membrane and attach to the DNA content. The more the DNA content of a cell the higher the fluorescent signal will be. In G1 the human cell has 23 chromosomes. S phase is the beginning of new DNA synthesis. So cells in S phase will have a higher fluorescent signal then cells in G1. Cells in G2 phase will contain 46 chromosomes thus these cells will give out the greatest amount of fluorescence.

A late stage of apoptosis is DNA degradation. When cells are fixed with 70% ethanol and then subsequently rehydrated some degraded fragments of DNA are able to leach out. This lowers the DNA content of the cell and the fluorescence given out by these apoptotic cells are less than those given out by cells in G1phase. Hence these cells are indicated by a ‘sub-G1’ peak.

In order to identify and distinguish the sub-G1 peak from the G1 peak a group of cells treated with staurosporine 2µM (a known potent inducer of apoptosis) for 24 hours, was used and compared to an untreated healthy population of cells as described in section 3.6.3.

All cells, adherent and non adherent, were harvested as explained in section 3.6.3. Each sample contained a million cells as determined by Beckman coulter counter. Cells were than centrifuged at approximately 173 × RCF for five minutes at 4^{o}C. Supernatant was removed and cells were resuspended and washed twice in a solution of ice cold PBS with 1% BSA. Samples were kept on ice.

The supernatant was removed. 70% ice cold ethanol was added drop wise to the pellet, whilst slowly vortexing, until a total volume of 3 ml of 70% ethanol had been added. Vortexing helps break clumps of cells whilst the ethanol makes the cell membrane permeable to PI. Samples were left on ice for thirty minutes.

Samples were centrifuged at approximately 173 × RCF, for five minutes at 4^{o}C. Supernatant was removed and cells were washed twice and centrifuged in ice cold PBS Tween (section3.5.1) to remove residual ethanol.

As well as DNA, PI is able to bind none specifically to RNA. Therefore specific staining of DNA requires RNAse treatment.

A solution of RNAse was prepared as follows. RNAse was dissolved at a concentration of 10mg/ml in 0.01M sodium acetate (pH 5.2). The solution was boiled for 15 minutes at 100^{o}C to inactivate DNase contaminants. The solution was cooled and nine parts of this solution was added to one part 1 M tris HCl (Ph 7.4). RNAse solution was aliquoted and stored at minus 20^{o}C.

Samples were centrifuges at approximately 173 × RCF, for five minutes at 4^{o}C. Supernatant was removed and cells were mixed with the 100µl of the above RNAse solution. Samples were left on ice for five minutes.

A stock of propidium iodide solution of 1mg/ml dissolved in PBS was kept at 4^{o}C. For each sample 50 µl of this stock solution was added to 850 µl of PBS and then added to the samples already containing the RNAse. Samples were left in the dark for thirty minutes before being analysed by flow cytometer (section 3.6.3).

Occasionally two cells in the G1 phase may adhere together and pass through the laser beam simultaneously. Subsequently these two aggregated cells will produce a similar

nuclear fluorescent signal as a single cell in G2/M phase. This could lead to an over estimation of the G2 population and hence a technique called doublet discrimination needs to be applied.

The emitted fluorescent light signal produces three electronic signals: pulse area/integral, pulse width, and pulse height. Height is the maximum fluorescence, width is the cell transit time, and area is the total fluorescence produced (124). Usually only height signal is recorded for flow cytometry. However for doublet discrimination pulse height is plotted against pulse width in order to distinguish between single cells and aggregates. Single cells in G0/1 or G2/M will have similar transit times (pulse width) whilst aggregated cells have a longer transit time and can easily be gated out (124). Aggregates can be clearly seen to the left of the dot plot in Figure 3.7.1. The region of single cells is then gated and only data produced form this area is analysed.

This text box is where the original thesis contained the diagram showing ‘doublet discrimination’ which was reproduced from reference *(124).*

Figure 3.7.1: Doublet discrimination.

Where pulse width is plotted against pulse area in order to exclude aggregates.(Figure reproduced from reference (124).

The flow cytometry parameters were as follows: Fl2 linear to detect PI, FL2-Width linear, FL2-Area linear, FS linear, SS linear, and 20,000 events.

3.8 DNA synthesis measurement via BrdU assay

3.8.1 Reagents and materials for BrdU assay

- BrdU (1mM stock stored at -20^{o}C)
- Anti BrdU, mouse monoclonal, 20µl added to cell suspension of 100µl containing one million cells
- Donkey- anti mouse antibody conjugated FITC, 2.7µl added to cell suspension of 80µl containing one million cells.
- HCl/Triton X-100 solution = 2 N HCl + 0.5% (v/v) Triton X-100
- PBST = PBS + 0.5% (v/v) Tween-20
- PBSTB = PBS + 0.5% (v/v) Tween-20 + 1% (w/v) BSA
- Citrate phosphate/spermine = 3.4mM, pH 7 citrate phosphate + 0.5mg/ml spermine
- Ethanol 200 proof made to 70% using distilled water. NB do not use ordinary ethanol as it contains metal contaminants
- RNAse A 10mg/ml in 0.01M sodium acetate (section 3.7.1)

3.8.2 Protocol for BrdU assay

In cell cycle profile analysis, of PI staining of fixed permeabilised cells, it is often hard to distinguish clearly between regions of S phase and either late G1 or early G2 phase. In order to identify cells which are specifically in S phase, cells can be pulsed with bromodeoxyuridine (BrdU). BrdU is a thymidine analog which is incorporated during DNA synthesis (S phase). Subsequently the presence of BrdU can be detected via the use of first primary monoclonal antibodies attaching to BrdU and then secondary antibodies conjugated to FITC (FL1). The primary antibody only binds to BrdU in single stranded DNA, therefore before the antibody can be used DNA must be denatured by either heat treatment or strong acids(125).

DNA is also stained with PI (FL2) and then FL2 vs. FL1 dot plots are created in order to see G1, S, and G2/M regions. Only cells which have undergone S phase at the time of BrdU application will be both FITC and PI positive whilst cells in G1 and G2/M will only be PI positive.

Exponentially growing cells were pulsed for 30 minutes at a final concentration of 1µM BrdU (from 1mM stock) in current media at 37^{o}C. Cells were then harvested as explained in section 3.6.3 and then centrifuged at approximately 173 × RCF. Supernatant was removed and the pellet was resuspended in PBS. Again the cells were centrifuged at approximately 173 × RCF, for 5minutes, and the pellet was resuspended

in 3ml spermine-citrate buffer in order for nuclei to be extracted from cells. Cells were left for ten minutes on ice.

Nuclei were then centrifuged at 400 × RCF for 5 minutes, supernatant was removed, and the pellet was resuspended in 3ml PBST. Nuclei were then centrifuged again at 400× RCF and supernatant was removed. Nuclei were then fixed via vortexing and adding drop wise a total of 3ml of 70% ethanol (200 proof, ice cold), in order to make the nuclear membranes permeable to PI. Samples were left on ice for one hour.

Nuclei were then centrifuged at 400 × RCF, for 5 minutes, and resuspended in PBS/Tween-20. Again samples were spun and resuspended in 100µl RNAse A solution as used in section 3.7.2. Samples were left on ice for five minutes.

A total of 3ml of HCl/Triton X-100 solution was added drop wise to the above samples whilst vortexing . This was in order to denature the DNA so that they would become single stranded which would allow for primary antibody binding. Samples were left at room temperature for 30 minutes.

Acid was then neutralised by adding 6 ml of 0.1M sodium borate (using twice the volume of HCl previously used). Samples were incubated for 10 minutes on ice.

Samples were centrifuged at 400 × RCF, supernatant was aspirated, and pellets were resuspended in 1 ml of PBSTB solution. Haemocytometer was used to adjust the concentration of nuclei to one million in 100µl of PBSTB solution.

20µl of the primary antibody against BrdU was added to the above 100ul solution (20µl of the stock primary antibody per million nuclei). Samples were incubated for 30 minutes in the dark at room temperature.

Samples were centrifuged at 400 × RCF, for 5 minute, supernatant was aspirated, and pellets resuspended in 4 ml PBSTB solution. Samples were again centrifuged and resuspended in 80ul of PBSTB solution. 2.7 µl of FITC conjugated secondary antibody was then added. Samples were incubated for 30 minutes in the dark at room temperature.

4 ml of PBSTB solution was then added and samples were centrifuged at 400 × RCF. Supernatant was removed and the pellet was resuspended in 1 ml of 10µg/ml PI in PBS solution. Samples were left in the dark on ice for ten minutes and then taken to the flow cytometer for analysis.

The flow cytometry parameters were as follows: FL1 linear to detect FITC, Fl2 linear to detect PI, FL2-Width linear, FL2-Area linear, FS linear, SS linear, and 20,000 events. Doublet discrimination as described in section 3.7.2 was also performed.

3.9 Detection of EGFR membrane expression via flow cytometry

3.9.1 Reagents and materials

- Anti EGFR (ICR10) antibody conjugated to PE from Abcam (ab27764)

3.9.2 Protocol for detection of EGFR membrane expression

In order to measure the expression of membrane EGFR levels as opposed to total cellular EGFR levels flow cytometric analysis was used. Anti EGFR (ICR10) antibody conjugated to PE from Abcam (ab27764) was used in order to detect membrane EGFR. This antibody was selected as it binds to an extracellular epitope of EGFR.

Cells were grown, trypsinised and then adjusted in order to contain a million cells in 1 ml of growth media, with the aid of a coulter counter. The cells were then incubated with 10 μl of the antibody and left in the dark at room temperature for 30 minutes. After this time cell were washed with 1 % BSA, PBS, pH 7.4 solution and centrifuged at approximately 173 × RCF for five minutes at 4^{o}C. The supernatant was removed and cells were washed again for two more cycles. Washes were to ensure that any unbound antibody was removed from the sample before analysis. Finally the million cells were placed in 1 ml of 1% BSA, PBS, pH 7.4 solution and processed for flow cytometric analysis.

Beckman Coulter Epics XL flow cytometer was used and data was analysed using WIN MDI software (Windows multiple document interface for flow cytometry). FL2 log was used to detect PE average fluorescence (AF) was recorded via the FL2 log channel.

3.10 **Immunohistochemistry**

A tissue micro array (TMA) consisting of tumour samples from 190 patients with head and neck squamous cell carcinoma was analysed via IHC for GRP78 expression. 28 tumours were of hypopharynx origin, 92 were of laryngeal origin, and 70 were of oropharyngeal origin. For each patient, three separate representative tumour cores were included in the TMA. In addition to SCCHN cores taken from patients, histopathologically normal adjacent tissue samples were also acquired from 45 patients. The TMA was obtained from Aintree Hospital.

3.10.1 Reagents and materials for immunohistochemistry

- 10mM citric acid buffer pH 6 (made freshly each time)
- 1% H_2O_2 in methanol
- R.T.U Vectastain ABC reagent
- DAB solution (step1: add 2 drops of buffer stock solution to 5ml distilled H_2O. Step 2: Add 4 drops of DAB and 2 drops of hydrogen peroxide solution and mix well.)
- Acid water = 2ml glacial acetic acid to 98 ml distilled H_20
- Bluing solution = 1.5ml NH_4OH to 89.5ml of 70% (v/v) ethanol
- Haemotoxylin

3.10.2 Protocol for immunohistochemistry

There are two main antibody staining methods called direct and indirect method. The direct method involves the primary antibody being directly conjugated to horse radish peroxidase (122). The procedure is quick but there is not any signal amplification.

In the indirect method the unlabeled primary antibody attaches to the tissue antigen, followed by a secondary antibody which attaches to the primary antibody. The secondary antibody is against the IgG of the animal species in which the primary antibody was raised in. The indirect process produces a higher signal as several secondary polyclonal antibodies can react with various antigen sites on the primary antibody.

The secondary antibody is conjugated to biotin. Tissue samples are then incubated with avidin conjugated to the enzyme horse radish peroxidase. Avidin is a glycoprotein with a high affinity to biotin and therefore avidin biotin complexes (ABC) are formed. 3,3'-diaminobenzodine (DAB) is then placed on the tissue samples along with H_2O_2. Where there is a complex of *antigen-primary antibody-secondary conjugated biotin-avidin conjugated to horse radish peroxidase*, H_2O_2 is able to oxidize DAB into a brown stain. The reaction is catalysed by horse radish peroxidase and H_2O_2 turns into water.

Although formalin fixation is good at preserving the morphology of the cell it may cause alterations in protein structure by forming crosslinks and therefore making the epitopes of interest unavailable to the primary antibody(122). Furthermore formalin may also reduce the overall antigen's negative electrostatic charge therefore reducing the affinity between the epitopes and the positively charged antibodies. In order to reverse these changes, induced by formalin, a process known as antigen retrieval is used in cases where the primary antibody has failed to bind (122).

Below I will discuss the protocol for the indirect ABC method of staining.

Formalin fixed, paraffin embedded immunohistochemistry tissue slides were first dewaxed by placing then in xylene for 10 minutes.

Slides were rehydrated by agitating them for 30 seconds in 100%, 95%, and 70 % ethanol. Slides were then washed in water for 5 minutes whilst agitating.

Endogenous peroxidase activity was blocked by placing slides in 1%(v/v) H_2O_2 in methanol for 12 minutes. Slides were then washed and agitated in PBS Tween (section 3.5.1) for 5 minutes.

For antigen retrieval slides were boiled in the microwave at maximum power for 15 minutes in citric acid buffer solution. Slides were then left to cool in the buffer for 20 minutes. This technique is known as heat induced epitope retrieval (HIER).

Slides were then washed and agitated in PBS Tween (section 3.5.1) for 5 minutes. A PAP pen was used to make a hydrophobic barrier around the border of the tissue samples on the slides.

Tissue samples were incubated for 20 minutes at room temperature in 2.5% (v/v) normal serum in PBS, from species in which secondary antibody was raised. This prevents non specific binding of secondary antibody. During all incubation periods slides were kept in a humidified chamber to prevent tissue samples drying out.

Serum was removed and tissue samples were incubated with primary antibody diluted in the above 2.5% (v/v) serum in PBS. In order to test for the specificity of the secondary antibody the primary antibody was omitted.

Slides were then washed and agitated in PBS Tween (section 3.5.1) for 5 minutes. Slides were then incubated for 30 minutes in 0.5% (v/v) secondary antibody which was diluted in 2.5% (v/v) serum in PBS.

Slides were then washed and agitated in PBS Tween (section 3.5.1) for 5 minutes. Slides were then incubated with RTU Vectastain ABC reagent for 30 minutes.

Slides were then washed and agitated in PBS Tween (section 3.5.1) for 5 minutes. Slides were then incubated in DAB solution in the dark for 10 minutes. Staining intensity was checked every 5 minutes. After use of DAB solution, all DAB solution was bleached for 24h as DAB is a suspected carcinogen.

Slides were then rinsed in normal tap water for 5 minutes. Nuclear staining of tissue samples was performed via incubating slides in haemotoxylin for 1 minute.

Slides were then rinsed under tap water until water turned clear (approximately 10 seconds). Slides were agitated for ten seconds in acid solution and then rinsed in tap water. Slides were then agitated in bluing solution for 1 minute and then rinsed in tap water.

Samples were dehydrated by agitating in 70%, 95%, 100% ethanol and then left in xylene for 10 minutes. Cover slips were then placed onto slides with vectamount glue.

3.11 Clonogenic assay to measure effects of possible drug radiosensitivity

3.11.1 Reagents and materials for clonogenic assay

- Colony fixation staining solution consisting of:

  6% (v/v) glutaraldehyde, 0.5% (w/v) crystal violet, in PBS

3.11.2 Protocol for clonogenic assay

One of the main aims of cancer treatment is to prevent recurrence of tumour growth. Clonogenic assay measures the ability of individual cells to proliferate and form colonies after exposure to ionizing radiation, and this can be achieved in combination with cytotoxic drug treatments if required (126).

Initially T25 flasks were used as these could fit easily into the radiation chamber. A separate T25 flask was used for each drug and radiation dose permutation. Equal number of cells were seeded into each T25 flask so that after 24h their confluence would be around 50%. Cells were then treated with drug or vehicle controls in appropriate media for a further 24h. Pilot studies were performed in order to find the maximum dose of drug that would not lead to a reduction in the number of colonies formed when compared to controls under no radiation exposure.

Cells were then irradiated with 0, 1, 2, or 4 Gy using a ^{137}Cs source which delivers 1Gy in 23 seconds of γ-radiation.

Plating of a sufficient number of cells, without there being an overgrowth of cells, was needed in order to be able to count a reasonable amount of individual colonies (50-150 colonies per well). In order to determine the best concentration of cells for each cell line, cells were plated at a range of concentration from 100 to 10,000 per well of a six well plate and left for two weeks in pilot studies. It was found that the optimum number of cells to seed per well under 0 Gy were: UM-SCC 5 = 1200, UM-SCC 12 = 800, UM-SCC 17A = 7000, UM-SCC 81B = 800.

After radiation cells were then removed from T25 flasks and trypsinised as described in 3.4.3.Cell suspension concentrations were determined by haemocytometer and adjusted so that equal number of cells were seeded into six well plates in set of triplicate samples. Cells were seeded at 1x, 3x and 10x of the above stated concentrations. At low radiation doses 1x cell concentrations would produce a sufficient number of colonies however at higher radiation doses of 6 Gy typically only 10x concentrations would produce enough colonies.

Cells were then left to grow for two weeks to allow for colony formation. Colonies are defined as a focus of 50 or more cells. This allows for five or more cell doublings.

Media was removed and cells were rinsed with PBS. 1 ml of colony fixation solution was placed in each well of the six well plates and left for 30 minutes. The solution was removed and wells were submerged under tap water to remove excess solution. Plates were then left to dry and colonies were counted using a light microscope.

- Plating efficiency (PE) = number of colonies/number of cells seeded under 0 Gy and no drug treatment.
- Survival fraction (SF) = no of colonies formed after treatment/(no of cells seeded × PE)
- Survival (S) data after radiation dose (D) was fitted to the linear quadratic model $S(D)/S(0) = \exp(-(\alpha D+\beta D^2))$. Where linear α and quadratic β values were calculated used SPSS PASW Statistics version 18 as described by Franken and colleagues (126).

3.12 **MTT assay**

3.12.1 Reagents for MTT assay

- MTT 5mg/ml in PBS (filter sterilized and kept as stock at -20^{o}C)
- DMSO

3.12.2 Protocol for MTT

3-(4,5-dimethylthiazol-2-yl)-2,5-diphenyl tetrasodium bromide (MTT) assay is a rapid quantitative colorimetric method for measuring the amount of viable cells. It is often used to measure the cytotoxic effects of drugs *in vitro*. Healthy cells have viable mitochondria which contain mitochondrial dehydrogenase enzymes. These enzymes are capable of reducing yellow MTT into formazan a purple precipitate (127). The more cells that are viable the more MTT will be reduced, resulting in a higher MTT score. Therefore MTT score is a function of viability/growth of cells. DMSO was used to permeabilise cells and to dissolve formazan. The absorbance was measured at an optical density (OD) of 590 nm via a 96 well plate reader.

Cells were harvested as described in section 3.4.3. A haemocytometer was used to count the concentration of cells. Cells were seeded in 96 well plates using a 12 multi channel tip pipette aid. 5000 cells per well were seeded for MEF cell lines; 10,000 cells per well were seeded for UM-SCC 1, 81B and Hepa 1c1c7; 15,000 cells per well were seeded for UM-SCC 5, 12, 17A and 17AS; 20,000 cells were seeded per well for UM-SCC 10A. At

these concentrations cells could proliferate for 7 days without the need for them to be passaged. 200µl of growth media was used per well. Hence for example 200µl of MEF cell solution at a concentration of 25,000 cells/ml was seeded into each well. Cells were then left for 24h for them to adhere to the plates.

After the initial 24h fresh drugs (or drug vehicle control for comparison) and media were replaced daily for a total of 7 days via a multi channel pipette. Cells were seeded in quadruplicates for each of the different concentrations of drug used. Care was taken not to dislodge any cells when either aspirating off media or adding media to wells.

For each of the 7 days a subset of cells were taken for MTT analysis. 20µl of MTT stock was added into each well, in addition to the existing 200µl of media. 96 well plates were then incubated for exactly 3 hours and 30 minutes at 37^{o}C.

190µl of solution was then removed from each well and discarded. 100µl of DMSO was then added to each well. Plates were then left for a further 30 minutes at 37^{o}C. After this time plates were taken to the plate reader and the absorbance was read at an OD of 590 nm.

3.13 **Cell proliferation assay via cell counting**

3.13.1 Reagents and materials for cell counting

- Isoton solution

3.13.2 Protocol for cell counting

Cell counting was performed in order to measure what effects drugs, such as cetuximab and EGF-SubA had upon cell proliferation.

Cells were seeded evenly on 12 well plates at 30-40% confluence. At this confluence cells had room to grow for up to an additional seven days without being passaged. Each well had a surface area of $3cm^2$ and 1ml of growth media was provided in each well. Cells were left for 24h in order to give time for them to adhere to the surface of the well. After 24h, media was replaced with fresh media containing either drug or drug vehicle control. Cells were exposed to the drugs for a total period of five days with fresh drugs and media replaced daily.

Cells were then harvested prior to drug treatment, and 1, 2, 3, 4, 5 days after drug treatment. Media was removed and wells were washed with 0.5ml PBS. PBS was removed and 0.3ml of trypsin was added. Once cells had detached 0.3ml of growth media was used to neutralise the trypsin in each well. The volumes of trypsin and neutralising media were kept constant throughout the experiment.

From the total 0.6ml of cell solution, from each well, 0.1ml was taken and added to 10ml of Isoton solution (Beckman coulter). The concentration of cells per ml was then calculated using a Beckman coulter counter (Z2 coulter® particle count and size analyser). Prior to counting the cells the Beckman coulter was calibrated by flushing it with Isoton solution. Flushing was repeated until the machine gave a cell count of less than 4000 cells/ml from just Isoton solution alone.

3.14 **Statistics**

SPSS PASW statistics package version 18 was used to calculate the following statistics: log-rank test, univariate and multivariate Cox regression analysis, Pearson Chi Square test of independence and Spearman's rank correlation coefficient.

SPSS PASW statistics package version 18 was also used to calculate linear α and quadratic β components of the linear quadratic model $S(D)/S(0) = \exp(-(\alpha D+\beta D^2))$, as described by Franken and colleagues (126).

Student's t test was calculated using Microsoft Excel 2007.

4 Results part 1: investigating GRP78 as a potential prognostic biomarker and inhibiting the activity of this protein with EGF-SubA

4.1 Validation of anti-GRP78 antibody sc-13968 for use in IHC

Hypoxia and glucose deprivation are prominent features in the tumour environment, due to the poorly established microvasculature (128-131). Under such conditions the Unfolded Protein Response is stimulated and a number of genes are induced including GRP78 (128-130). GRP78 has been shown in a number of studies, using proteomics and IHC, to be over-expressed in a variety of tumours including: hepatocellular carcinoma (HCC) (130), pancreatic adenocarcinoma (132), breast cancer (112), melanoma (133), oesophageal adenocarcinoma (120), glioblastoma (108), lung cancer (134) and prostate cancers (129) and in particular in those tumours which had a poorer outcome. This appears not to be a simple bystander effect as GRP78 is implicated in tumorigenesis as mammary tumours are more numerous and grow at a faster rate in wild-type GRP78+/+ mice compared with genetically modified GRP78 -/- or GRP78 +/- mice (see section 1.3.3 for details) (98, 99).

Detection of squamous cell carcinoma of the Head and Neck (SCCHN) is based on clinical examination, tumour tissue biopsy and histopathological assessment. Identification of possible biomarkers that are predictive of early tumour development, or prognosticate response to treatment and/or survival outcome would be of obvious benefit in early diagnosis and for tailoring the best treatment options to individual patients. To date, only one study focusing on nasopharyngeal SCC by Feng et al., 2010, has identified GRP78 as a possible biomarker in head and neck tumours (see section 1.3.8) (3)Hence we investigated GRP78 as a prognostic biomarker of outcome using immunohistochemical analysis of a previously constructed tissue microarray consisting of tissue samples from laryngeal, oropharyngeal and hypopharyngeal tumours.

An anti-GRP78 antibody (sc-1050) - a goat polyclonal antibody from Santa Cruz Biotechnology - has been used in several immunohistochemical studies, including the above mentioned study by Feng et al., in order to analyse the expression of GRP78 between various patient samples (3, 4). Antibodies may cross react with other proteins and therefore it is important to first validate the antibody specificity prior to IHC via other techniques such as western blot analysis. This was particularly important in this instance as we noted a doublet in the 72kDa region during previous experiments using this anti-GRP78 antibody (sc-1050), in which we had used western blotting to quantify the relative presence of GRP78. The most obvious explanation for this finding is that sc-1050 is cross reacting with another protein of similar molecular weight.

An initial BLAST search confirmed that the GRP78 protein shares 65% amino acid identity with HSP72 immediately suggesting its identity as the cross-reacting species.

One of our initial objectives was to find an antibody to use for, IHC, which was specific for GRP78 and did not cross react with other proteins. First the specificity of anti-GRP78 antibody (sc-1050) was tested by western blot. Paton and colleagues identified only GRP78 (a 72kDa protein) to be cleaved by SubA (7). 2D gel electrophoresis showed four spots that were specific to when cells were treated with SubA. Upon matrix assisted laser desorption/ionization-mass spectrometry (MALDI-MS) one of these four spots was identified as GRP78. Furthermore only GRP78 showed 'significant size discrepancy' from ~27kDa on the gel compared to 72 kDa on the database. GRP78, which consists of 654 highly conserved amino acids, is cleaved, by SubA between two leucine residues at position 416-417. In addition, Paton and colleagues demonstrated that a single amino acid substitution at L_{416} ensured that SubA was no longer able to cleave GRP78 into two fragments (7) Although HSP72 shares 7 out of 11 amino acid positions with GRP78, HSP72 does not contain the two leucine cleavage site. As expected Paton and colleagues did not find HSP72 to be cleaved by SubA (7).

Cleavage of GRP78, by SubA, results in two fragments of approximately 44 and 28 kDa. Therefore we used EGF-SubA to test the specificity of anti-GRP78 antibodies since

following treatment with EGF-SubA we would expect a reduction in the intensity of the 72kDa band and the appearance of a band corresponding to one or other of the cleavage products of GRP78, depending on which fragment contains the epitope recognised by the antibody. Therefore UM-SCC cells were treated with either 1nM EGF SubA for 24h or 48h or with drug vehicle control. UM-SCC cells were then processed for western blot analysis as described in section 3.5. The concentration used in our experiment was the same concentration of EGF-SubA as used by Backer and colleagues in their 2009 study on prostate and breast cancer cells (5).

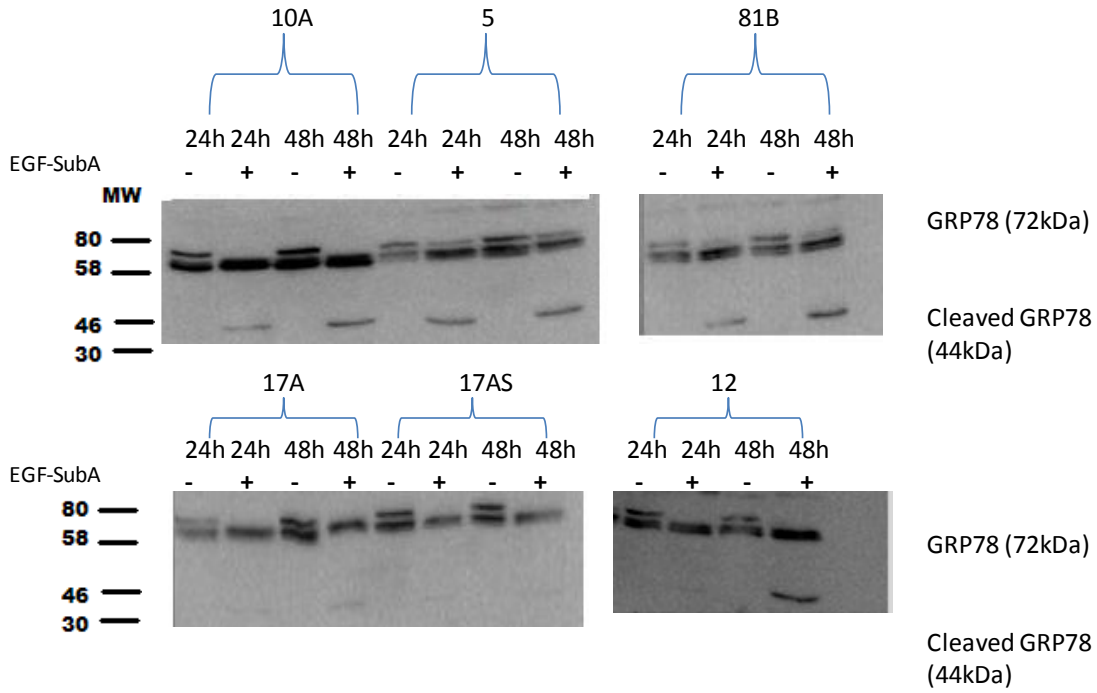

Figure 4.1.1 EGF-SubA promotes cleavage of GRP78 in a panel of LSCC cell lines.

Cells were either treated with EGF-SubA at 1nM or appropriate amount of drug vehicle for controls. 35 μg of protein was loaded into each lane and anti-GRP78 antibody (sc-1050) was used at a concentration of 3 μg/ml. The antibody recognizes the epitope at the N- terminus of GRP78 protein and therefore cleaved GRP78 can be seen between 30 kDa and 46 kDa molecular weight marker bands .In addition, the doublet referred to previously at the 72kDa region can also clearly be seen.

The western blot in Figure 4.1.1 shows two bands between marker weights of 58 kDa and 80 kDa. Upon application of EGF-SubA the slower migrating band disappeared. It was thought that this band was likely to be GRP78 as this was the only protein found to be cleaved by SubA in the study by Paton and colleagues (7). Subsequently a new band appeared between marker weights of 30 kDa and 46 kDa. It was suspected that the new band was the 44 kDa cleaved product of GRP78 which contains the N-terminal fragment recognised by anti-GRP78 antibody (sc-1050).

Anti-GRP78 antibody (sc-1050) appeared to strongly cross react with another unknown protein running just ahead of the un-cleaved GRP78 band. Furthermore the intensity of this band was not altered by the application of EGF-SubA. If this antibody was used as a primary antibody for IHC, it would mean that analysis of GRP78 expression in the TMA would be unreliable as IHC staining from GRP78 to that of the unknown protein would be indistinguishable. Therefore this antibody was deemed unsuitable for use in IHC.

Next the specificity of anti-GRP78 (sc-13968), rabbit polyclonal antibody as a possible alternative was examined by western blot. Gels were loaded with lysates from the same samples as used in the western blots shown in Figure 4.4.1. In order to determine whether anti GRP78 antibody (sc-13968) cross reacted with any other protein whole membranes were blotted with anti-GRP78 antibody (sc-13968). As seen in Figure 4.1.2 anti-GRP78 antibody (sc-13968) revealed a band at a position between marker weights

of 58 kDa and 80 kDa. Upon application of EGF-SubA this band disappeared, and a new band between marker weights of 23 kDa and 30 kDa appeared. The new band appears to be the 28 kDa cleaved carboxy-terminal fragment of GRP78 which contains the epitope recognised by this antibody. There appeared to be considerably less cross reactivity to other proteins with anti-GRP78 antibody sc-13968 than with sc-1050.

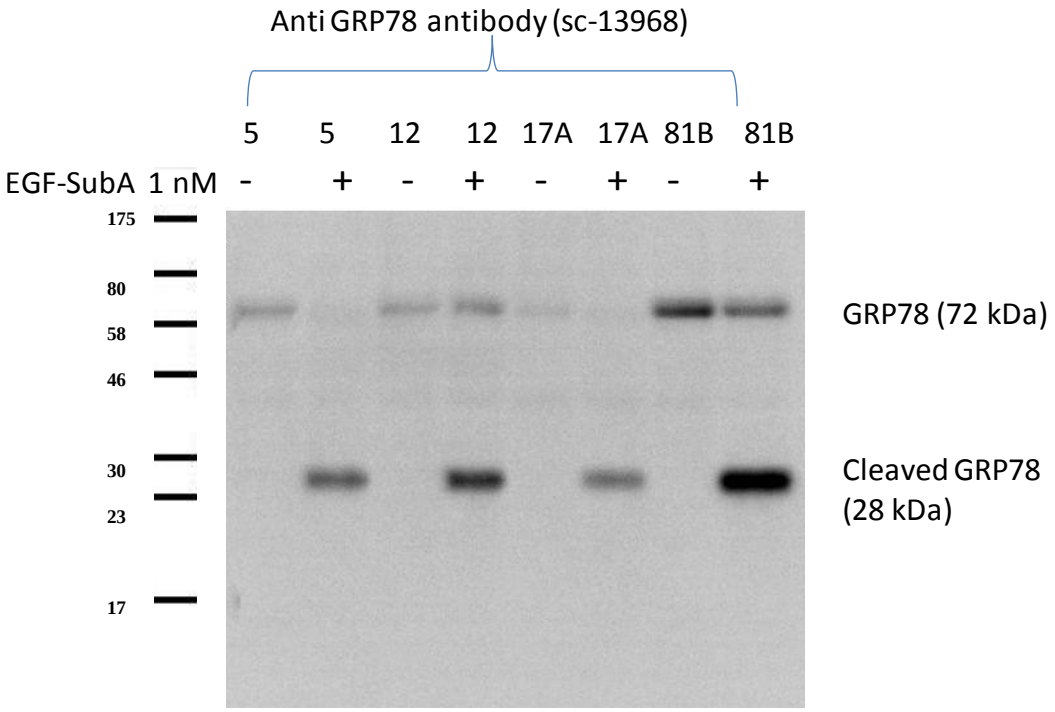

Figure 4.1.2 EGF-SubA promotes cleavage of GRP78 in a panel of LSCC cell lines.

LSCC cells were treated with EGF-SubA at 1nM or appropriate amount of vehicle for controls in order to determine the specificity of anti-GRP78 antibody (sc-13968). 35 μg of protein was loaded into each lane and whole membranes were incubated with anti-GRP78 antibody (sc-13968) at a concentration of 3μg/ml. The antibody recognizes the epitope at the C terminus of GRP78 protein and therefore cleaved GRP78 can be seen between molecular weight marker bands of 23 kDa and 30 kDa.

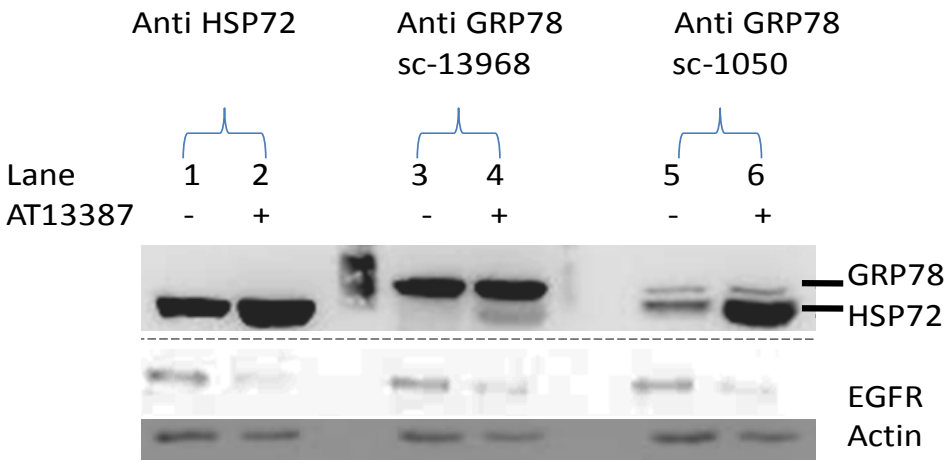

Figure 4.1.3 Anti-GRP78 antibody (sc-1050) cross reacts with HSP72.

UM-SCC 81B cells were treated with either HSP90 inhibitor AT13387 at 1μM for 24h or with drug vehicle control. Membranes were probed with antibodies as indicated: anti-HSP72 antibody at 50 ng/ml (lanes 1 & 2), anti-GRP78 antibody sc-13968 at 3 μg/ml (lanes 3 & 4) and anti-GRP78 antibody sc-1050 at 3 μg/ml (lanes 5 & 6) Anti-EGFR antibody was used at 3 μg/ml. Anti-actin antibody at 3 μg/ml was used as a loading control.

In order to identify whether anti-GRP78 antibody (sc-1050) cross reacted with HSP72 an HSP90 inhibitor was used. The HSP90 inhibitor AT13387 binds and competitively prevents ATP binding to the N-terminus of HSP90 (135). This results in the disruption of the inhibitory interaction of HSP90 with the transcription factor: Heat Shock Factor (HSF) (136). Upon HSP90 inhibition, by AT13387, HSF induces up-regulation of HSP72. Furthermore HSP90 inhibition leads to proteasomal degradation of HSP90 client proteins such as EGFR (137) and thus with HSP90 inhibitor AT13387 an increase in HSP72 levels and a decrease in EGFR levels is observed. See Appendix section 7.2 for a review of HSP90 inhibitors.

UM-SCC 81B cells were treated with HSP90 inhibitor AT13387 at 1μM for 24h(135). SDS-PAGE followed by western blot analysis was used to identify whether or not HSP72 induction could be detectable by anti-GRP78 antibody (sc-1050). As presented in Figure 4.1.3 , when comparing lanes 1 and 2 it is clear that treatment with AT13387 results in HSP72 induction as expected. Furthermore there was a reduction in EGFR levels in lane 2 compared to lane 1, again, as expected.

Using anti-GRP78 antibody (sc-1050) a strong signal was detected, in untreated cells in lane 5, which was located at the same position as HSP72 in lanes 1 and 2. Furthermore this band was induced when cells were treated with AT13387 as shown in lane 6 with a stronger signal being emitted from this band compared to GRP78. This almost certainly

indicates that there is significant cross reaction with anti-GRP78 antibody (sc-1050) with HSP72. Therefore studies which have reported the expression of GRP78 via the use of immunohistochemical staining with anti-GRP78 antibody (sc-1050) may not be reliable.

Using anti-GRP78 antibody (sc-13968), GRP78 was the only protein detected in untreated cells (see lane 3). In cells treated with AT13387 a weak signal was visible running just ahead of GRP78 which was at the same position as HSP72 in lanes 1 and 2. However the majority of the signal was derived from GRP78 protein. Our study indicates that anti-GRP78 antibody (sc-13968) appears to cross-react to a much lesser degree with other proteins and, in our opinion, is therefore a more suitable antibody for GRP78 IHC studies than anti-GRP78 antibody (sc-1050).

4.2 GRP78 is up-regulated in laryngeal squamous cell carcinoma UM-SCC cells *in vitro* in conditions of hypoxia and low glucose

Rapidly growing tumours quickly outgrow their blood supply leading to a typical micro-environment of hypoxia, low pH, and nutrient starvation (138). Under these micro-environmental conditions protein folding is disrupted resulting in the activation of the Unfolded Protein Response and the induction of GRP78 as described in section 1.3.3 (139). Induction of chaperone GRP78 provides a cyto-protective function, under such stress conditions, by allowing for enhanced protein folding capacity, decreased global transcription of cellular proteins and the suppression of pro-apoptotic proteins. Whilst in some cases, the UPR is able to restore cellular homeostasis, should the cellular stresses be of sufficient duration or strength, the UPR is unable to restore cellular function and cell death occurs(140). LSCC cells were exposed to conditions of hypoxia and low glucose to determine whether these stimuli could induce GRP78 expression under conditions typically found in the tumour micro-environment

Tumour hypoxia is commonly defined as an oxygen concentration lower than 3% compared to normal tissue oxygen concentrations which on average contain between 4 and 9% oxygen (140). Tumour hypoxia has been detected in 78% head and neck

squamous cell carcinomas (141).As well as hypoxia, tumours are subject to low glucose levels. Normal tissue typically contains glucose levels of 5 mM whilst in many tumours glucose levels can range from anywhere between 0 and2 mM (83). Previous studies have investigated induction of GRP78 in hypoxic (less than 2% O_2) (142) and low glucose conditions (less than 2 mM glucose) in a number of cell lines (139), however this was the first study to determine whether GRP78 could also be induced in laryngeal squamous cell carcinoma cell lines under typical tumour-microenvironments.

UM-SCC cells were grown in the following conditions for 24 hours:

- Normal conditions of 5% CO_2 + 95% air and 4g/l glucose (20 mM)
- Hypoxic conditions of 2% O_2 with normal glucose levels
- Anoxic condition of 0% O_2 and normal glucose levels
- Low glucose concentrations of either 0.4 g/l (2 mM) or 0.04 g/l (0.2 mM) under normoxia.

All UM-SCC cells were plated on six well plates at a density of 50% and left over night, in normoxic and normal glucose conditions, in order for the cells to adhere. Cells were then grown in the above mentioned conditions for 24 hours as described in Methods section 3.4.5.

After 24 h cells were harvested and processed for western blot analysis (as described in section 3.5). Membranes were incubated with previously validated anti-GRP78 antibody (sc-13968) and luminescent signals produced from GRP78 bands were quantified by densitometry as shown in Figure 4.2.1. All UM-SCC laryngeal squamous cell carcinoma cell lines, that were tested, demonstrated induction of GRP78 in conditions of low oxygen and glucose compared to controls. The only exception to this was in UM-SCC 81B cells which when grown in 2% O_2 showed no increase in GRP78 levels. However GRP78 was induced in UM-SCC cells in anoxic conditions as well as in 0.4g/l glucose. Luminescent signals emitted from the GRP78 bands were increased by at least two fold, as measured by densitometry, in UM-SCC 5, 11B and 12, compared to controls, when these cells were grown either in low glucose media of 0.4g/l glucose or in hypoxic conditions of 2% O_2.

After establishing that GRP78 could be up-regulated in laryngeal squamous cell carcinoma cells, *in vitro*, we wanted to determine whether these tumour cells were capable of proliferating in conditions typical of the tumour micro-environment of hypoxia and low glucose. Cells were seeded into 12 well plates, in triplicate, and left to adhere over night. Cells were grown in conditions of normal glucose concentrations and normoxia, or in low glucose (0.4 g/l), or in hypoxia (2% O_2) for a total of three days (Methods section 3.4.5). Each day, cells were counted as described in Methods section

3.13. Figure 4.2.2 shows the proliferation of UM-SCC cells under these conditions. Not only were all seven UM-SCC cell lines able to survive in conditions of low glucose and hypoxia but they were also able to proliferate. However the rate of proliferation was reduced compared to cells grown in normal glucose concentrations and normoxia.

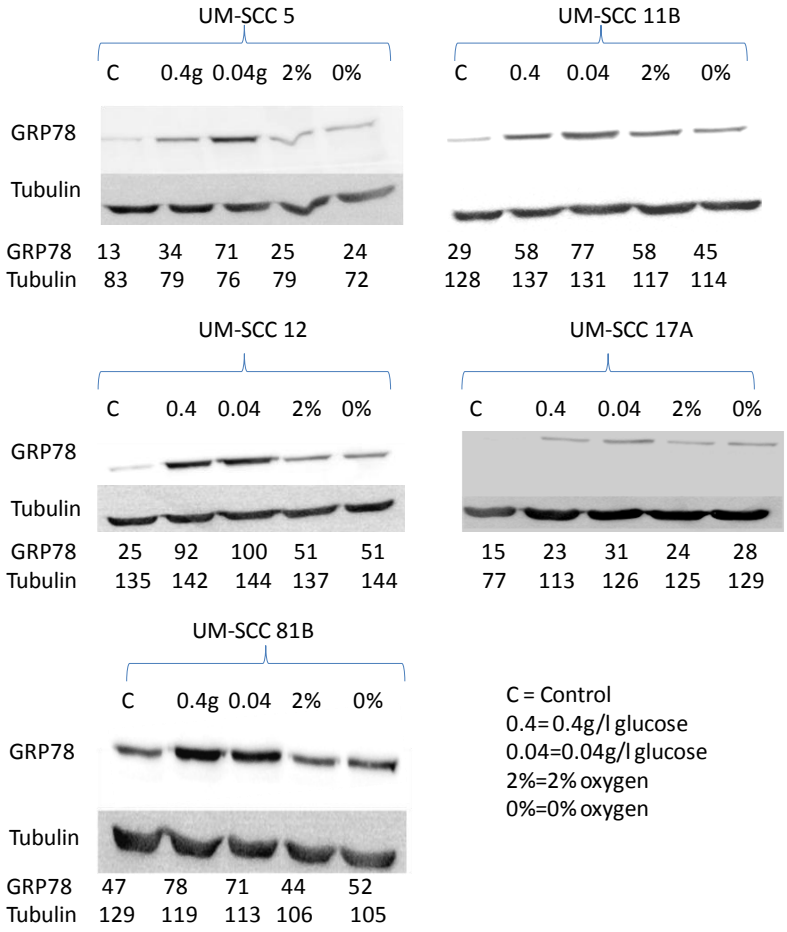

Figure 4.2.1 Induction of GRP78 in conditions of low glucose and hypoxia in a panel of LSCC cells.

Cells were grown in conditions of normoxia and normal glucose concentrations (4g/l)l (control), or low glucose of 0.4g/l glucose, or 0.04g/l glucose, or hypoxic condition of 2% O_2 , or anoxia (0% O_2), as indicated for 24h. GRP78 protein expression was quantified by western blot analysis followed by densitometry. 35 µg of protein loaded into each lane. Membranes were incubated with anti-GRP78 antibody (sc-13968) at 3 µg/ml or with anti-tubulin at 1:10,000 dilution (loading control).

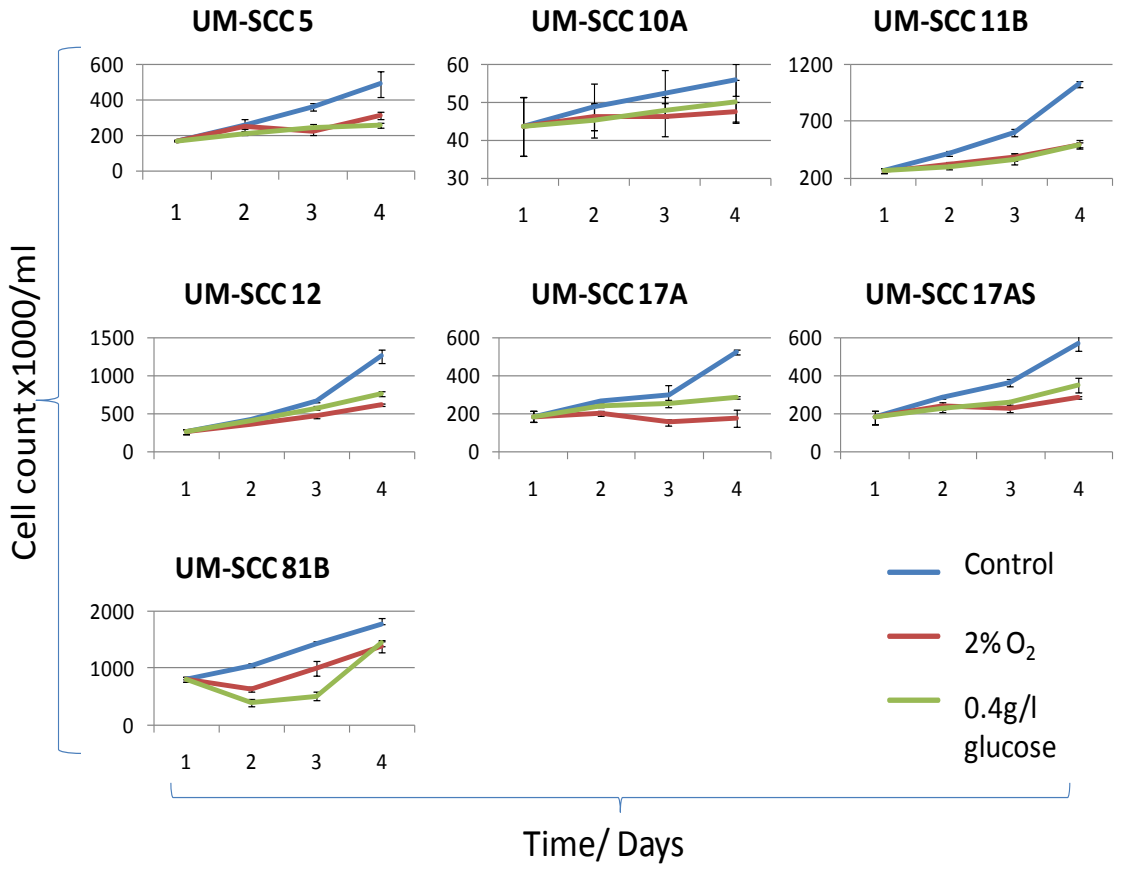

Figure 4.2.2 Growth of LSCC cells under hypoxia and low glucose.

Cells were grown in triplicate in 12 well plates in normal glucose and normoxia, or hypoxia (2% O_2), or low glucose levels (0.4 g/l). Cells were harvested and counted on a daily basis as described in section 3.13. Bars represent s.e.m.

4.3 **GRP78 is up-regulated *in vivo***

Results presented in this thesis have shown that an anti-GRP78 antibody (sc-1050) cross reacts with HSP72 (section 4.1). Studies by Du et al., and Feng et al., which have used this antibody for IHC in order to measure GRP78 expression levels in oesophageal and nasopharyngeal tumours, respectively, therefore probably examined the combined expression levels of GRP78 and HSP72 (3, 4). Our study indicates that anti-GRP78 antibody (sc-13968) appears to be less cross-reactive with other proteins and may therefore be a more suitable antibody for IHC than anti-GRP78 antibody (sc-1050).

Currently there are no published data regarding GRP78 levels in patients with laryngeal, hypopharyngeal and oropharyngeal tumours. By using validated anti-GRP78 antibody (sc-13968) as a primary antibody for IHC we wanted to determine whether or not GRP78 was up-regulated in these tumours and secondly whether GRP78 could be used as a prognostic biomarker for SCCHN.

IHC was performed as described in section 3.10. Prior to performing IHC on the tissue micro array (TMA) the anti-GRP78 antibody (sc-13968) was tested on individual sample sections of SCCHN tissue. It was necessary to perform antigen retrieval as no staining was detected without this pre-treatment. For antigen retrieval, slides were boiled in the

microwave at maximum power for 15 minutes in citric acid buffer solution (see section 3.10).

Anti-GRP78 antibody (sc-13968) was tested at dilutions of 1:100, 1:200, 1:400 and 1:800 on sequential sample sections of SCCHN tissue as well on adjacent histologically normal head and neck squamous epithelium, in order to determine the optimum dilution.

At all dilutions only cytoplasmic staining was observed with no staining within the nucleus which is in accordance with the known localisation of GRP78 in the cell (4). As previously mentioned Du and colleagues observed GRP78 to be up-regulated in tumours compared to histologically normal tissue and therefore we would expect GRP78 staining intensity to be greater in sample sections of SCCHN tissue as compared to histologically normal adjacent tissue (4). At dilutions of 1:100, 1:200 and 1:400 GRP78 staining intensity was greater in SCCHN tissue samples compared to adjacent histologically normal samples as expected. However at 1:800 the staining pattern appeared to be too week and no differences in staining intensity could be observed between histologically normal tissue and SCCHN tissue. Therefore Anti-GRP78 antibody (sc-13968) was used at 1:400 following empirical determination that this was the optimum dilution.

The primary antibody was omitted in order to test the specificity of the secondary antibody as shown in photomicrograph Figure 4.3.1A. Without the primary antibody

there was no DAB staining. A different section from the same tumour block was then incubated with the primary antibody. Figure 4.3.1D shows homogeneous cytoplasmic staining with no staining within the nucleus as expected.

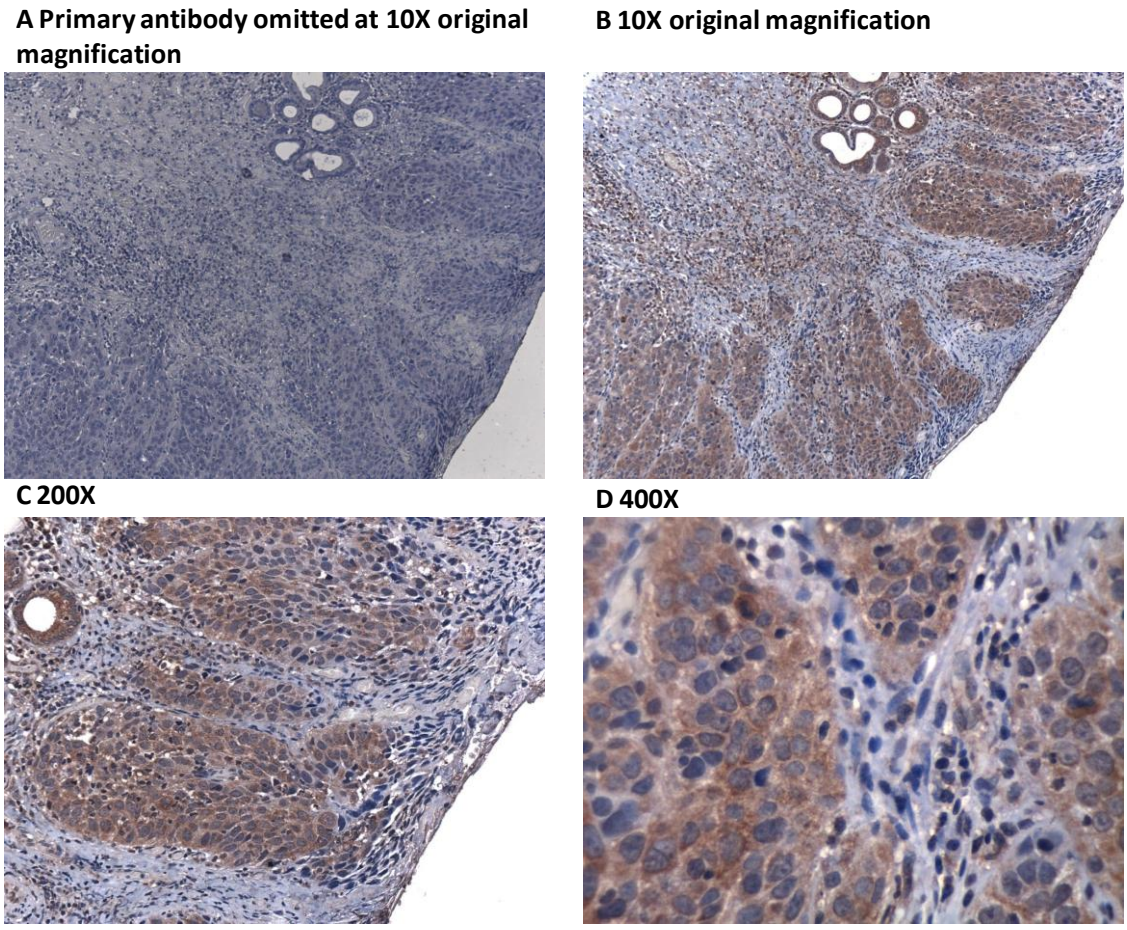

Figure 4.3.1 GRP78 protein detection via IHC on SCCHN sample tissues.

IHC was performed as described in Methods section 3.10. For antigen retrieval, SCCHN tissue samples were boiled in the microwave at maximum power for 15 minutes in citric acid buffer solution. Samples were then incubated with anti-GRP78 primary antibody (sc-13968) at a dilution of 1:400. (A) SCCHN tissue sample with omission of primary antibody at 10X original magnification. (B, C and D) sequential sections of tissue but treated with primary antibody shown at the original magnification of 10X as well as magnifications of 200X and 400X respectively.

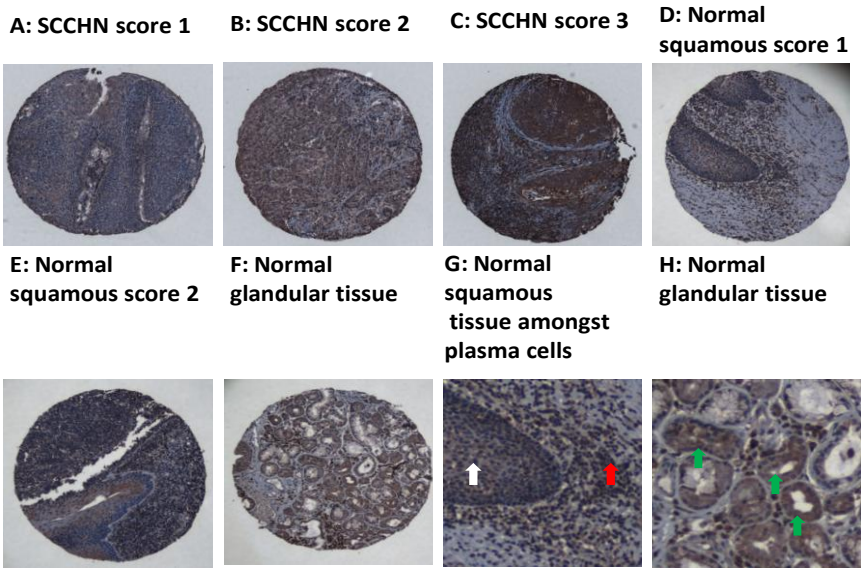

Figure 4.3.2 Immunohistochemical GRP78 staining and scoring of SCCHN.

IHC was performed as described in Methods section 3.10. For antigen retrieval, SCCHN tissue samples were boiled in the microwave at maximum power for 15 minutes in citric acid buffer solution. Samples were then incubated with anti-GRP78 primary antibody (sc-13968) at a dilution of 1:400. TMA cores were scored simultaneously by two observers (the author and specialist registrar pathologist Dr Mike Wall). Score of 1 represents weak GRP78 staining as shown in A and D, 2 for moderate staining as shown in B and E, and 3 for strong staining as shown in C. F shows a tissue micro dot containing mainly glandular tissue. G shows an example of squamous tissue (white arrow) surrounded by plasma cells (red arrow). H shows typical glandular tissue (green arrows). Both plasma cells and glandular tissue stained strongly and were not incorporated into the analysis as this study focused on the pathology of head and neck squamous tissue.

The head and neck tissue micro array (TMA) as described in Methods section 3.10 was analysed via IHC for GRP78 expression. TMA tissue samples were collected at University Hospital Aintree. The TMA was constructed at Liverpool Tissue Bank (LTB) and then returned back to University Hospital Aintree for storage. Scoring of the stained TMA was carried out by both the author and histopathologist, Dr Mike Wall. Statistical analysis of data was performed using StatView V5.0 and SPSS PASW Statistics version 18. GRP78 staining intensity was scored as 1 for weak staining, 2 for moderate staining, and 3 for strong staining as shown in Figure 4.3.2. For each core the area of highest intensity of squamous epithelium was scored providing the area covered more than 10% of the epithelium.

GRP78 staining scores of 45 head and neck tumours were compared to the scores from 45 matched histologically normal tissue. Pearson Chi Square test of independence was used in order to establish whether there were differences in GRP78 expression between tumour tissues and histologically normal tissues. In order to perform Chi Square test, scores of the three tumour cores form each patient were averaged and rounded to the nearest whole number and then compared to scores from histologically normal matched tissue.

GRP78 levels were significantly higher in the tumour tissue samples (n=45) compared with matched histologically normal tissue samples (n=45). 85% of tumour cores versus

24% of histologically normal cores were given a staining score of either 2 (moderate staining) or 3 (strong staining) ($p_{(x}2_{)} < 0.001$). See Table 4.3.1 for more details.

			Scoring Intensity			
			1.00	2.00	3.00	Total
Tissue Type	Normal	Count	34	10	1	45
		Expected Count	20.5	17.5	7.0	45.0
		% within Tissue	75.6%	22.2%	2.2%	100.0%
	Tumour	Count	7	25	13	45
		Expected Count	20.5	17.5	7.0	45.0
		% within Tissue	15.6%	55.6%	28.9%	100.0%
Total		Count	41	35	14	90
		Expected Count	41.0	35.0	14.0	90.0
		% within Tissue	45.6%	38.9%	15.6%	100.0%

Table 4.3.1 Comparison of GRP78 staining score between tumour tissue and matched histologically normal tissue.

GRP78 staining scores of 45 head and neck tumours were compared to the scores from 45 matched histologically normal tissue. There appears to be a strong association between high GRP78 levels and tumour tissue as compared to histologically normal tissue ($p_{(X^2)}<0.001$).

		Low GRP78 expression n=52	High GRP78 expression n=138
Gender	Female	11 (21%)	24 (17%)
	Male	41 (79%)	114 (83%)
Average age		60 ± 12 (stdev)	64 ± 10 (stdev)
Tumour stage	1	9 (17%)	11 (8%)
	2	23 (44%)	47 (34%)
	3	15 (29%)	42 (30%)
	4	5 (10%)	38 (28%)
Nodal involvement	-ve	24 (46%)	49 (36%)
	+ve	28 (54%)	89 (64%)
Recurrence	No	34 (65%)	102 (74%)
	Yes	18 (35%)	36 (26%)
Radiation treatment	No	49 (94%)	124 (90%)
	Yes	3 (6%)	14 (10%)

Table 4.3.2 Demographic information of 190 HNSCC patients who had tissue samples taken for TMA analysis.

Demographic information of patients can be seen in Table 4.3.2. When all tumour tissue samples were analysed on the TMA (n=190) no significant differences in GRP78 expression were observed between stage 1 or 2 (n=90) and stage 3 or 4 (n=100) tumours ($p_{(X^2)}$=0.075) or between node negative (n=72) and node positive (n=118) tumours ($p_{(X^2)}$=0.547). Therefore GRP78 levels may not be a suitable as a diagnostic biomarker.

Survival analysis based on data from 190 SCCHN patients was performed using Kaplan-Meier method and statistical differences between curves were compared using log-rank test. As expected SCCHN patients with stage 1 or stage 2 tumours had a significantly better five year survival compared to patients with stage 3 or 4 tumours ($p_{(\log rank)} < 0.001$), as shown in Figure 4.3.3A. Furthermore patients without nodal involvement survived significantly longer than patients with nodal spread ($p_{(\log rank)}$ = 0.005) (Figure 4.3.3B). These findings are in line with previous studies which have also found high tumour stage and nodal involvement to be associated with poor survival outcome. (143, 144).

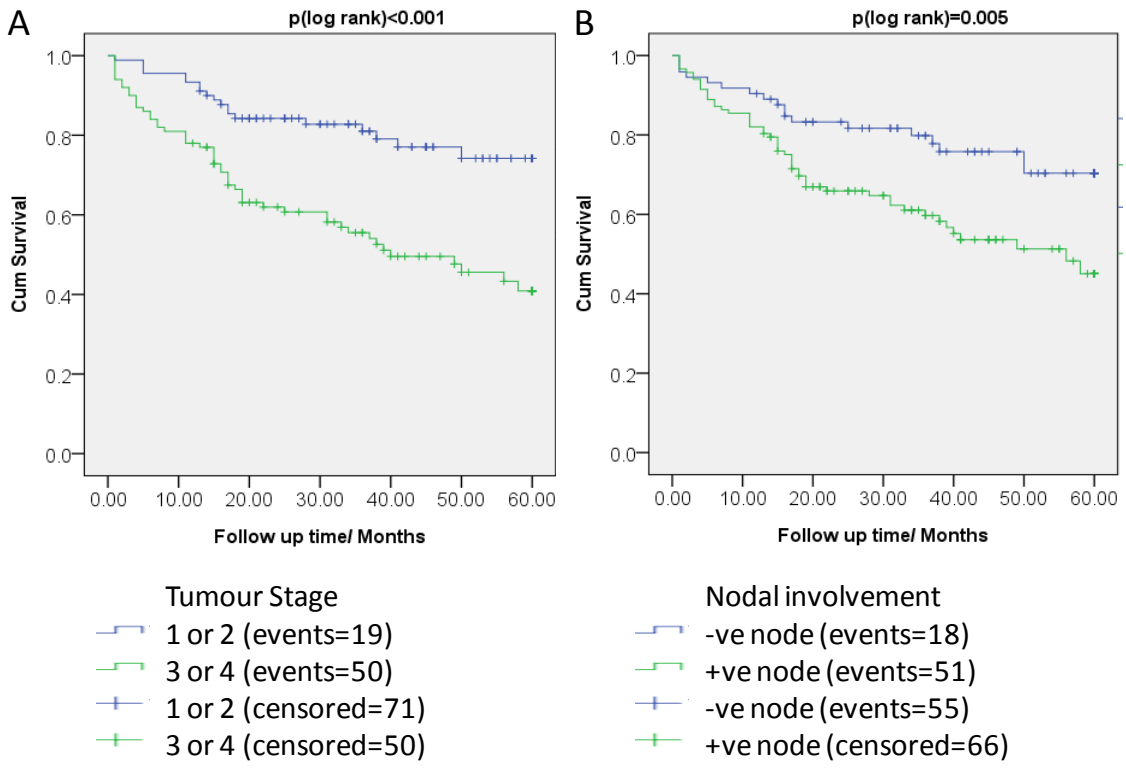

Figure 4.3.3 5 year SCCHN patient survival when compared to tumour stage and nodal status.

(A) Kaplan Meier overall 5 year survival curves for a total of 190 SCCHN patients with stage 1 and 2 tumours compared to stage 3 and 4 tumours. Upon log-rank analysis there was a significantly lower five year survival where p<0.001. (B) Kaplan Meier plot of the same cohort of SCCHN patients dichotomized according to lymph node spread versus no nodal involvement. Log-rank analysis showed patients with nodal involvement having a significant lower five year survival where p=0.005.

Several studies have reported that up-regulation of GRP78 is associated with poor survival in a variety of tumours including: hepatocellular carcinoma (HCC) (130), pancreatic adenocarcinoma (132), breast cancer (112), melanoma (133), oesophageal adenocarcinoma (120), glioblastoma (108), lung cancer (134) and prostate cancers (129).

Here for the first time it was determined whether up-regulation of GRP78 was correlated with poor survival outcome in tumours of the larynx, hypopharynx and oropharynx. Tumours were arbitrarily classed as having high GRP78 expression if their three micro dots produced a mean score of 2 or more, or if the tumour in question had an exceptionally high area of GRP78 expression as indicated by at least one of the three microdots scoring a 3.

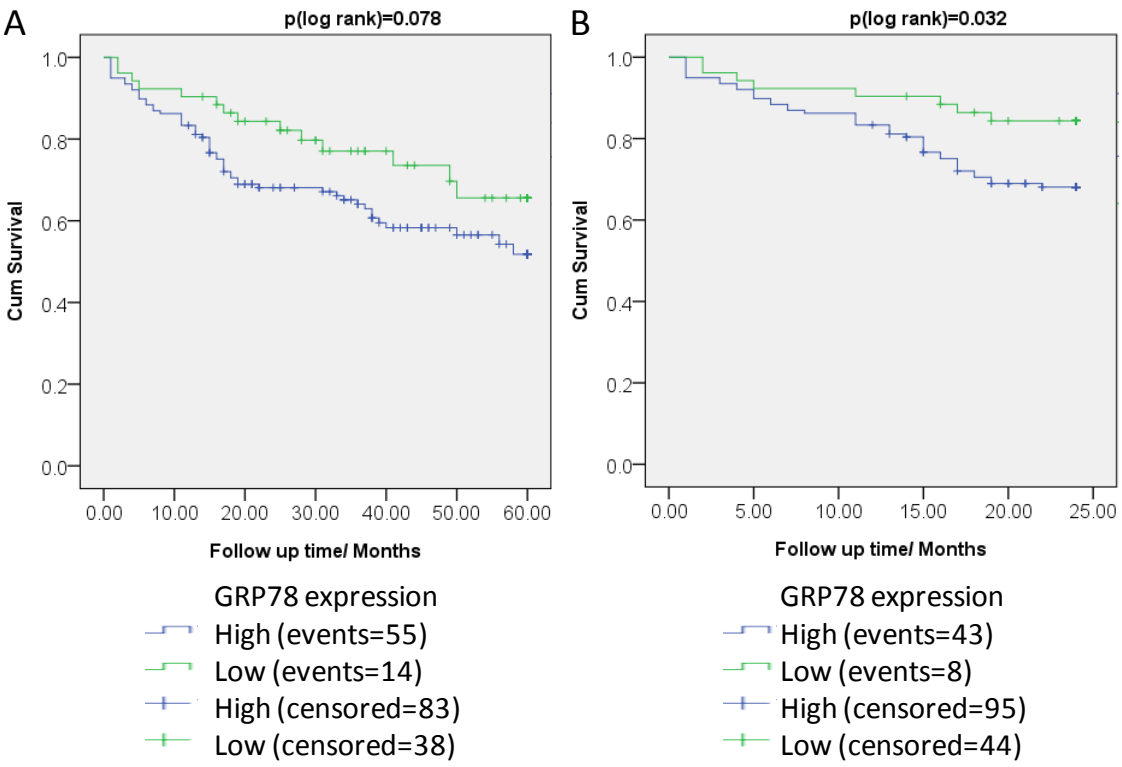

Figure 4.3.4 Association between GRP78 levels in tumours and survival in 190 SCCHN patients.

(A) Kaplan Meier overall 5 year survival curves for 190 SCCHN for patients with high GRP78 levels versus patients with low GRP78 levels. (B) Kaplan Meier overall 2 year survival curves for 190 SCCHN for patients with high GRP78 levels versus patients with low GRP78 levels. Statistical significance was determined by log-rank analysis.

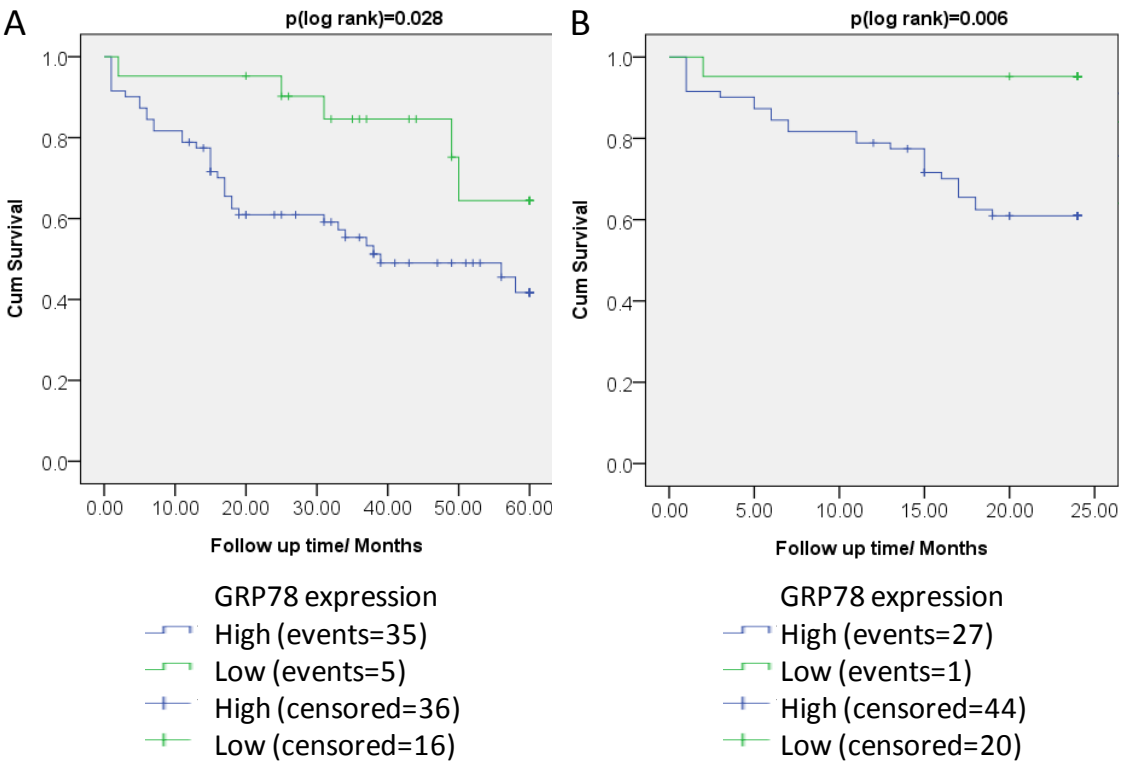

B

Figure 4.3.5 Relationship between GRP78 expression and survival status in patients with LSCC (n=92).

(A) Kaplan Meier overall 5 year survival curves for 92 laryngeal squamous cell carcinoma patients with high GRP78 levels versus patients with low GRP78 levels. (B) Kaplan Meier overall 2 year survival curves for 92 laryngeal squamous cell carcinoma patients with high GRP78 levels versus patients with low GRP78 levels.

The Kaplan Meier 2 year survival analysis of SCCHN patients (n=190) showed that GRP78 up-regulation was significantly associated with lower survival as compared to patients with low GRP78 expressing tumours ($p_{(\log rank)} = 0.032$) (Figure 4.3.4B). Although log-rank is useful in comparing differences in survival in two or more groups on non-parametric censored data, multivariate Cox regression analysis is required to compare the influence of several risk factors on survival at the same time (145).

Initially univariate Cox regression analysis was performed on several factors against two year survival for all head and neck tumours (n=190): gender (p = 0.935), age (p = 0.261), tumour stage (p = 0.001), nodal status (0.018), whether or not patient received radiation therapy (p = 0.523), tumour recurrence (p = 0.004) and GRP78 expression (p =0.038) (as shown in Table 4.3.3). In order to screen for possible significant predictive indicators of survival, covariates were selected for multivariate analysis if their p value was either equal to or less than 0.1. As expected upon multivariate Cox regression analysis tumour stage (p = 0.004), nodal status (p = 0.005) and recurrence (p = 0.001) were found to be significant independent factors in determining two year survival. Patients with high tumour stages of 3 and 4 had an increased hazard ratio of 2.5 compared to patients with stage 1 and 2 tumours. Similarly patients with tumours with nodal involvement had worse prognosis with a hazard ratio of 2.6. Although high GRP78 levels are suggestive of poorer survival outcome with a hazard ratio of 2.04 this finding is not statistically significant (p=0.069).

		Univariate analysis				Multivariate analysis	
Category		**HR**	**P value**	**Category**		**HR**	**P value**
Gender	female	1	0.935				
	male	1.03					
Age	<60	1	0.261				
	≥60	1.413					
Tumour stage	1 or 2	1	0.001	**Tumour stage**	1 or 2	1	0.004
	3 or 4	2.8			3 or 4	2.5	
Nodal status	-ve	1	0.018	**Nodal status**	-ve	1	0.005
	+ve	2.2			+ve	2.6	
Radiation treatment	no	1	0.523				
	yes	1.3					
Tumour recurrence	no	1	0.004	**Tumour recurrence**	no	1	0.002
	yes	2.3			yes	2.5	
GRP78 expression	low	1	0.038	**GRP78 expression**	low	1	0.069
	high	2.2			high	2.044	

Table 4.3.3 Covariates of 190 HNSCC patients from TMA data were analysed in order to assess which factors may help to determine two year survival outcome.

In order to screen for possible predictive indicators of survival, covariates were selected for multivariate analysis if their p value was either equal to or less than 0.1. Upon multivariate analysis only tumour stage, nodal status and tumour recurrence appeared to be significantly independent factors in predicting survival outcome.

As there may be different pathologies involved between the different sub-groups of SCCHN, subsets of this cohort were analysed separately. Upon log rank analysis two year survival was significantly higher for laryngeal patients with low expressing GRP78 tumours (p=0.006) as shown in Figure 4.3.5. Univariate Cox regression analysis was performed against two year survival for laryngeal SCC (n=92) for the following covariates: gender (p = 0.471), age (p = 0.452), tumour stage (p =0.084), nodal status (p=0.005), whether or not patients received radiation therapy (p = 0.69), tumour recurrence (p = 0.741) and GRP78 expression (p =0.026) (as shown in Table 4.3.4). In order to screen for possible significant predictive indicators of survival, covariates were selected for multivariate analysis if their p value was either equal to or less than 0.1. Upon multivariate analysis only nodal status (p = 0.041) was a significantly independent predictor of survival where patients with nodal involvement had an increased hazard ratio of 2.3 compared to patients without nodal involvement. Unexpectedly tumour stage (p = 0.376) was no longer a significant predictor of survival outcome. Although high GRP78 levels are suggestive of poorer survival outcome with a hazard ratio of 7.3 this finding is just below being statistically significant (p=0.052). A larger sample of laryngeal squamous cell carcinoma patients may be needed in order to clarify whether or not GRP78 as well as tumour stage may be suitable prognostic biomarkers.

		Univariate analysis				Multivariate analysis	
Category		**HR**	**P value**	**Category**		**HR**	**P value**
Gender	female	1	0.471				
	male	1.698					
Age	<60	1	0.452				
	≥60	1.4					
Tumour stage	1 or 2	1	0.084	**Tumour stage**	1 or 2	1	0.376
	3 or 4	2.3			3 or 4	1.6	
Nodal status	-ve	1	0.005	**Nodal status**	-ve	1	0.041
	+ve	3			+ve	2.3	
Radiation treatment	no	1	0.69				
	yes	1.2					
Tumour recurrence	no	1	0.741				
	yes	1.3					
GRP78 expression	low	1	0.026	**GRP78 expression**	low	1	0.052
	high	9.684			high	7.311	

Table 4.3.4 Covariates of 92 laryngeal patients from TMA data were analysed in order to assess which factors may help to determine two year survival outcome.

In order to screen for possible predictive indicators of survival, covariates were selected for multivariate analysis if their p value was either equal to or less than 0.1. Upon multivariate analysis only nodal status appeared to be a significantly independent factor in predicting survival outcome.

Prognostic biomarkers predict individual patient outcome, regardless of disease management, ‘distinguishing between good outcome tumours from poor outcome tumours’ (146). In this way prognostic biomarkers may help to decide which patients to treat or what modality to use as well as the aggressiveness of the treatment regime (146). Results presented within this thesis have shown that GRP78, although up-regulated in tumours compared to histologically normal tissue, may not be a significant independent prognostic biomarker. Zhuang et al., also found upon log rank analysis, that patients with high GRP78 expression in melanomas had significantly lower overall survival compared to patients with low GRP78 expression ($p=0.0123$) (133). However, when multivariate analysis was performed by Zhuang et al., GRP78 was no longer a significant independent factor in determining survival ($p=0.178$). It seems likely that the simultaneous use of multiple biomarkers may be more suited in predicting patient outcome as opposed to reliance on one single biomarker. For example multigene expression tests such as MammaPrint (Agendia) can be used to assess whether, after surgery, breast cancer patients, should receive adjuvant therapy or not, in order to avoid relapse (146). A similar ‘multiple biomarker’ approach may be also more applicable for head and neck cancers.

Furthermore there were no significant differences between survival rates of patients with high versus low GRP78 expressing tumours in oropharynx (where 5 and 2 year survival p=0.7 and 0.9 respectively) or hypopharynx (where 5 and 2 year survival p=0.2 and 0.56 respectively) squamous cell carcinoma patients upon log rank analysis. This could be due to different pathologies involved in the various sub-sites. For example it is known that SCCHN patients with HPV are more responsive to chemo- and radiation therapy ($p \leq 0.05$) as compared to HPV negative patients and have better survival outcome (19, 21). Therefore HPV infection which is more prevalent in oropharyngeal tumour compared to laryngeal tumours would be of greater prognostic value in such tumour sub-sites

4.4 Cleavage of GRP78 with EGF-SubA leads to suppression of LSCC cell proliferation

As shown in section 4.3 GRP78 is significantly up-regulated *in vivo* in SCCHN tumours (Figure 4.3.3) as compared to normal histopathological tissue. Furthermore we have demonstrated that GRP78 can be up-regulated in UM-SCC *in vitro* under typical tumour environmental conditions of hypoxia and low glucose (Figure 4.2.1). GRP78 may help protect cancer cells from these adverse conditions therefore making inhibition of this protein potentially important for cancer therapy in SCCHN.A study by Chiu and

colleagues in 2008, used GRP78-siRNA to down regulate the protein in a range of SCCHN cells (1). Growth of cells *in vitro* was suppressed in a range between 18-55% by day five following knockdown of GRP78 by siRNA. As mentioned in section1.3.9, SubA is a protease which is only known to act on GRP78 (72 kDa), cleaving it into 44 and 28 kDa fragments (7). Subsequently the results in this thesis confirm that EGF-SubA is able to cleave GRP78 in UM-SCC cells (Figure 4.1.1and Figure 4.1.2).

Currently only two studies, Backer and colleagues in 2009 and Yahiro and colleagues in 2010, have explored the cytotoxic effects of SubA on prostate, breast, myeloma, rat glioma and cervical cancer cell lines (5, 147). The combination of covalently binding EGF to SubA enhances the toxicity of SubA in EGFR expressing cell lines. The IC_{50} value for SubA in Hela cells has been reported to be 1.43nM (147). The IC_{50} values reported for EGF-SubA were considerably lower with a range between 2pM to 20pM in EGFR expressing cancer cell lines. In EGFR expressing rat glioma cells the IC_{50} was 20pM, whereas in EGFR-null rat glioma cells the IC_{50} value for EGF-SubA was at 6nM (5).

For the first time the effects of EGF-SubA on UM-SCC laryngeal squamous cell carcinoma cell lines were investigated within this thesis. In order to establish what inhibitory effects EGF-SubA had upon the growth of UM-SCC cells a cell counting assay was used where the number of cells per ml in the drug treated group were

compared to the number of cells in the control group. UM-SCC cells were treated with either EGF-SubA, in the same range of drug concentrations as used in the study by Backer and colleagues in 2009 (3pM to 1nM), and compared with drug vehicle control, for a total of five days (5). The experiment was set up as described in section 3.13. Both drugs and media were replaced daily. Number of cells per ml, from three individual wells, were counted using a Beckman Coulter counter, for each individual condition. Typical dose response curves can be seen in Figure 4.4.1 where increasing doses of EGF-SubA lead to a decreasing cell number.

IC_{50} values were calculated from data collected on day five. This was the same time period which Backer and colleagues used to calculate the EGF-SubA IC_{50} for prostate PC3 (IC_{50} = 1pM) and breast cancer cells MDA231luc (IC_{50} = 6pM) (5). IC_{50} curves were plotted as: percentage of cells in the drug treated group as a proportion of cells in the control group (y-axis) against the dose of the drug on a log scale (x-axis). IC_{50} values were within the 6 to 100pM range for UM-SCC cells (Figure 4.4.2).

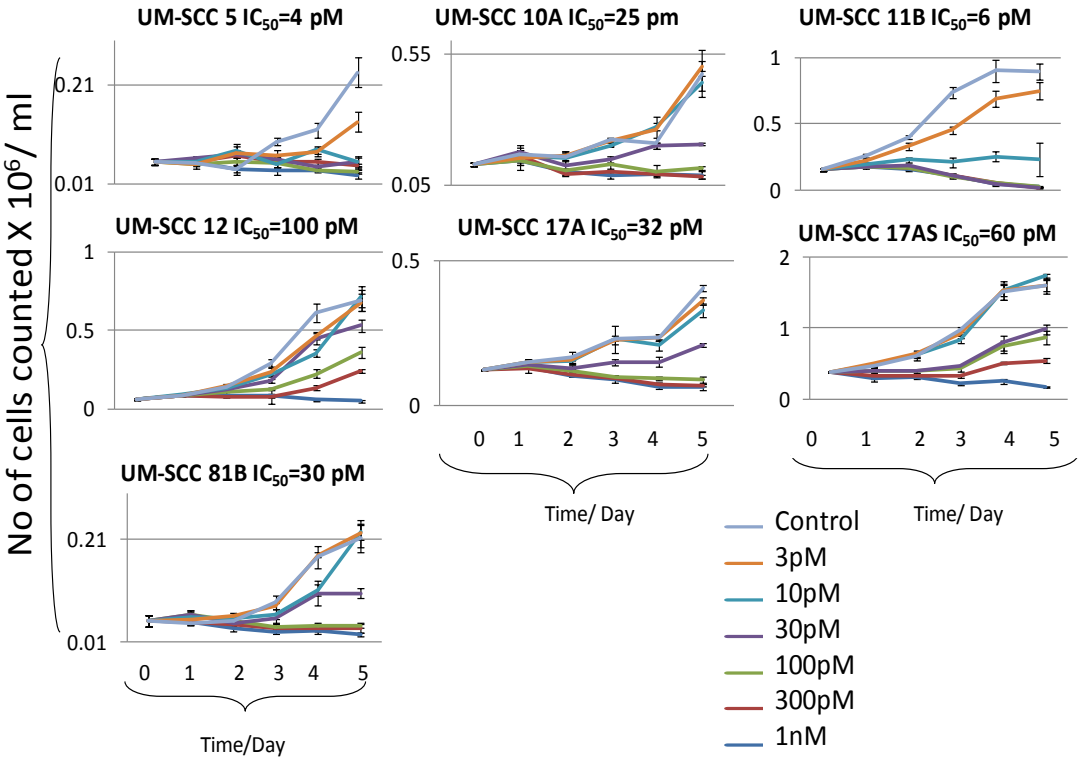

Figure 4.4.1 EGF-SubA is cytotoxic to LSCC cells at pM concentrations.

UM-SCC cells were seeded in 12 well plates and allowed to adhere for 24 hours (day 0). Cells were then treated with either EGF-SubA at ½ log_{10} incremental concentrations of 3pM, 10pM, 30pM, 100pM, 300pM, and 1nM or with vehicle control, for up to five days. Both media and drugs were replaced every 24h. Cells were harvested and counted via a Beckman Coulter counter for each of the days. Error bars represent the s.e.m. from three independent wells.

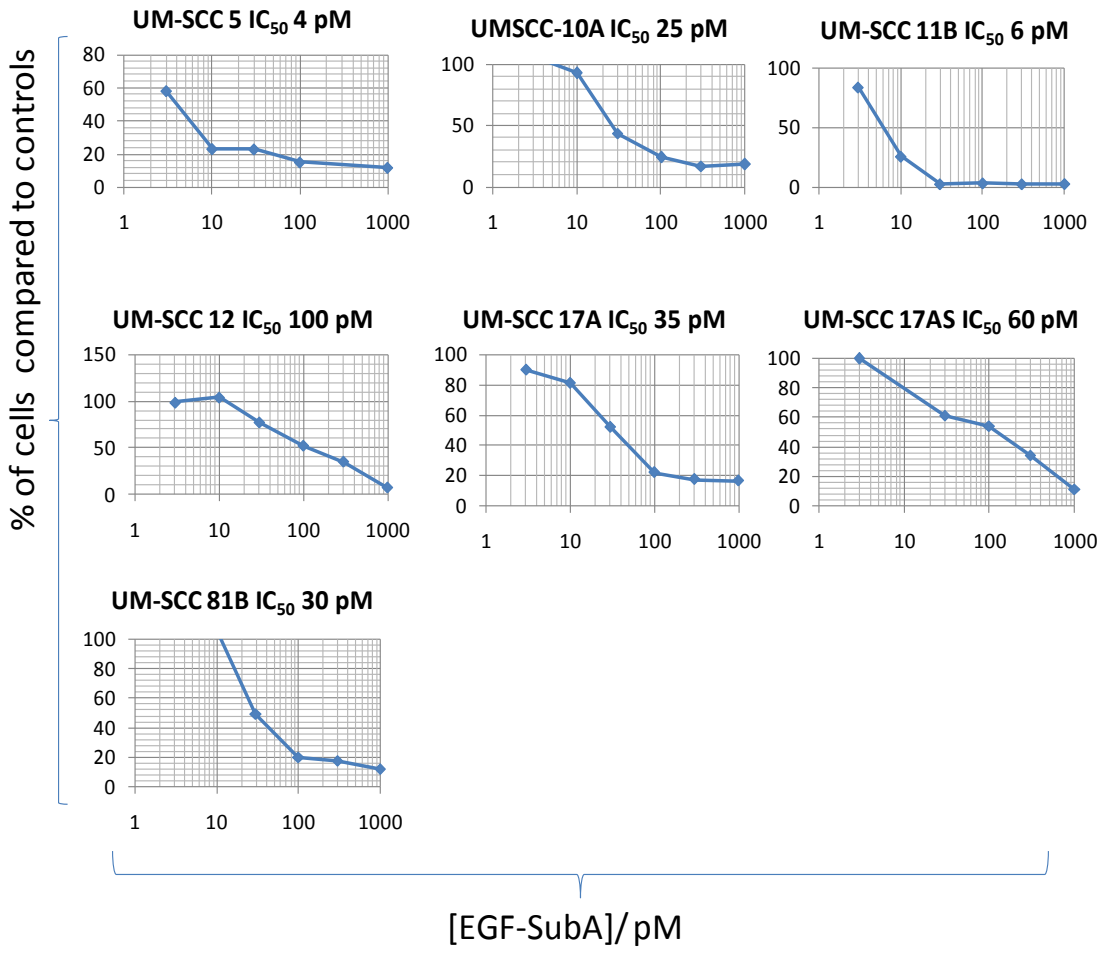

Figure 4.4.2 EGF-SubA IC_{50} plots in a panel of LSCC cells.

IC_{50} data derived from day five of UM-SCC cells being treated with either EGF-SubA at concentrations of 3pM, 10pM, 30pM, 100pM, 300pM, and 1nM or drug vehicle control. IC_{50} curves were plotted as percentage of cells in the drug treated group as a proportion of cells in the control group (y-axis) against the dose of the drug on a log scale (x-axis).

4.5 EGF-SubA induces G1 arrest in LSCC cells

Results in section 4.4 of this thesis have shown that EGF-SubA was able to inhibit the proliferation of UM-SCC cells. Morinaga and colleagues observed a decrease in basal levels of cyclin D1 as well as G1 cell cycle arrest after application of SubA *in vitro* in Hela and Vero cells (148). As cyclin D1 is important in order to allow for cell cycle progression from G1 to S phase it was proposed that loss of cyclin D1 through SubA was the mechanism behind G1 arrest (148).

Phosphorylation of cyclin D1 is required for ubiquitin targeted proteasomal degradation. Upon SubA increased levels of phosphorylated cyclin D1 was observed. Furthermore the use of proteasomal inhibitor MG132 suppressed downregulation of cyclin D1 by SubA. Thus implying that SubA may indirectly induce the proteasomal degradation of cyclin D1.

Flow cytometry was used, in our study, to determine what effects EGF-SubA had upon the cell cycle profile of UM-SCC cells *in vitro.* Conventional analysis of DNA content by staining cells with Propidium Iodide (PI) alone, provides a snapshot of what proportion of cells are in G1, S or G2/M phase at a particular point in time. However because of the overlapping DNA content between G1 with early S phase and mid to late S with G2 and M phases it is hard to accurately distinguish between these.

Bromodeoxyuridine propidium iodide (BrdU)-(PI) double staining easily differentiates between overlapping DNA content of S phase fractions and at the same time provides information on the proportion of cells in G1 and G2. BrdU is a thymidine analogue which is incorporated during DNA synthesis (S phase) into viable cells. Subsequently the presence of BrdU can be detected via the use of monoclonal antibodies that recognise BrdU which are then labelled using secondary antibodies conjugated to FITC (this signal appears in the FL1 channel of the flow cytometer). The primary antibody only binds to BrdU present in single stranded DNA, therefore before the antibody can be used DNA must be denatured by either heat treatment or the use of strong acids(125).

DNA can also be stained with PI once cells have been fixed with ethanol (detected in the FL2 channel of the flow cytometer) and then FL2 vs. FL1 dot plots are created in order to visualise G1, S, and G2/M regions. Only cells which have undergone S phase at the time of BrdU application will be both FITC and PI positive whilst cells in G1 and G2/M will only be PI positive.

Currently there are no studies which have investigated the effect of SubA on cell cycle analysis via BrdU-PI double staining method. Here this method is performed simultaneously alongside the conventional fixed and permeabilised cell staining with PI to produce DNA histograms.

p53 is a tumour suppressor which can act as a transcription factor to promote G1 cell cycle arrest via induction of p21, in response to an array of stimuli such as DNA damage. Therefore, we examined a variety of UM-SCC cells of differing p53 status, to determine whether or not any impact of EGF-SubA upon the cell cycle was independent of p53 status (149). The cell lines studied were UM-SCC 17A which is wild-type for p53, UM-SCC 12 which is p53 null (homozygous Q104X), and UM-SCC 5 which has one p53 wild type allele and a single p53 mutation (heterozygousV157F).

Experiments were performed as described in sections 3.7 and 3.8. UM-SCC cells were first transferred to culture dishes and left to adhere for 24 hours. Cells were then treated with drugs or respective drug vehicles for two days with fresh drugs and media being replaced daily. As this study was the first to perform cell cycle analysis on UM-SCC cell lines with EGF-SubA, a relatively high drug dose (i.e. above the IC_{50} levels) at 300pM was chosen, in order to maximise the chance of detecting any effect. At all times doublet discrimination, as described in section 3.7, was performed in order to discriminate between signals produced from single cells in G2 and doublets of cells in G1.

Regardless of p53 status EGF-SubA was able to induce G1 arrest in all cell lines tested, as shown in Figure 4.5.1 and Figure 4.5.2. The amount of cells in G1 after treatment with EGF-SubA in UM-SCC 17A, 12 and 5 increased by 19%, 7%, and 5%, respectively, as analysed by PI staining of fixed permeabilised cells and 37%, 26% and

6%, as deduced by BrdU-PI double staining. As expected for a G1 arrest, there was a reduction in cells entering S phase. The percentage decreases in the S phase cell fraction after treatment with EGF-SubA as compared to controls in UM-SCC 17A, 12 and 5 were 10%, 9%, and 5% respectively, as analysed by PI staining of fixed permeabilised cells and 46%, 19% and 12%, as deduced by BrdU-PI double staining. This observation may be important since it has been reported by Pawlik and colleagues that cells in G1 are twice as radiosensitive as cells in S phase and therefore EGF-SubA may act as a radiosensitiser (150). The potential for EGF-SubA as a radiosensitiser was explored in Results section 5.4.

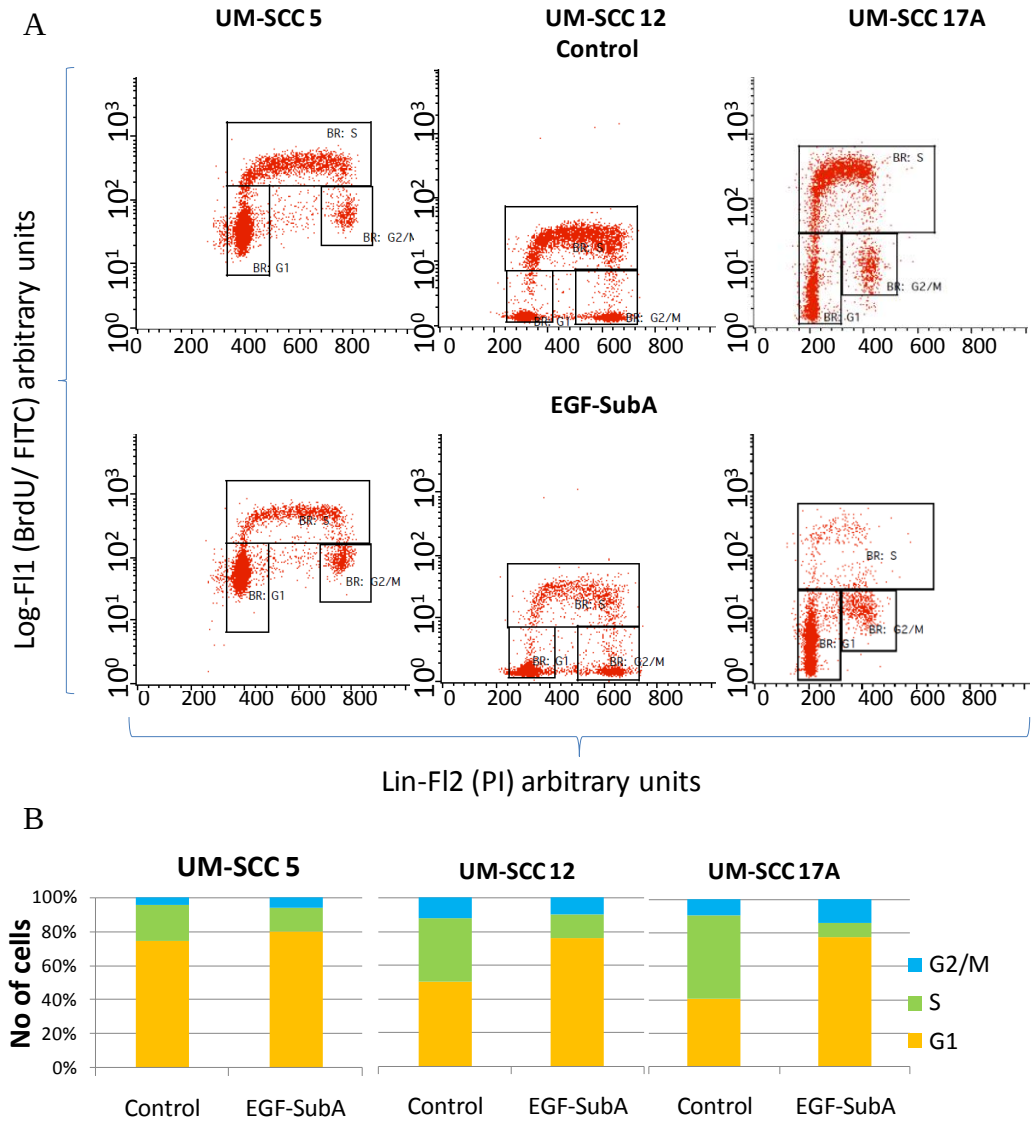

Figure 4.5.1 EGF-SubA induces G1 cell cycle arrest regardless of p53 status.

(A)UM-SCC cells were treated with either EGF-SubA at 300pM, or drug vehicle control for 48h. Cell cycle analysis was performed via BrdU-PI double staining as described in Methods section 3.8. (B) Cells in each phase of the cell cycle in treatment and control groups. Data was analysed on CellQuest Pro Software.

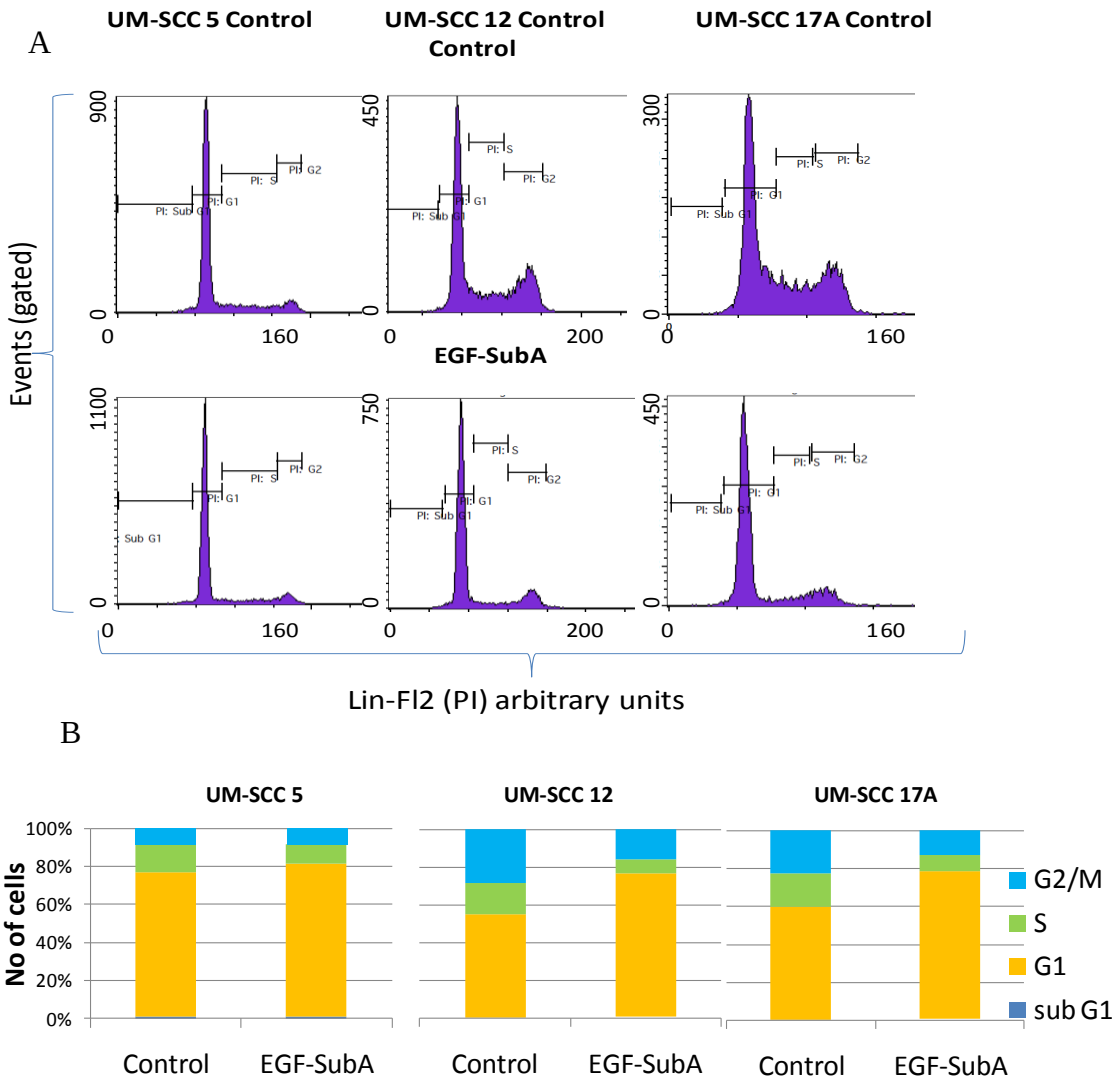

Figure 4.5.2 EGF-SubA induces G1 cell cycle arrest regardless of p53 status.

(A) UM-SCC cells were treated with either EGF-SubA at 300pM or drug vehicle controls for 48h. Cell cycle analysis was performed via staining fixed permeabilised cells with PI (Methods section 3.7). (B) Percentage of cells in each phase of the cell cycle. Data analysed on CellQuest Pro Software. Note that in (A) the axes values are not the same.

4.6 EGF-SubA toxicity is dependent on the presence of the EGFR

Backer and colleagues in 2009, discussed the cytotoxicity of EGF-SubA and that this appeared to be EGFR-dependent with EGFR positive cells having an IC_{50} within the pico molar range and EGFR negative cells having an IC_{50} in the nano molar range(5). For example U266-B1 human myeloma cells which do not express EGFR had an EGF-SubA IC_{50} greater than 6nM compared to EGFR positive human prostate PC3 cells which had an IC_{50} of 1pM (5). Interestingly, the IC_{50} value for SubA tends to be in the nano molar range, regardless of EGFR density, as found in EGFR positive Hela cells which had an IC_{50} of 1.4nM (147). Comparable to the study by Backer and colleagues which focused mainly on prostate, glioma and breast cancer cells, results in this thesis demonstrate that the EGF-SubA IC_{50} of EGFR positive laryngeal squamous carcinoma are also below 1nM with a range of 4pM to 100pM.

Backer and colleagues examined human prostate and breast cancer xenografts in immuno-deficient mice. Following a one week course of intra-peritoneal EGF-SubA injections the study found a 4-10 fold reduction in tumour volume compared to controls, without ‘signs of toxicity being observed in any of the treated groups.’

Currently it is unclear whether such xenograft models provide a reasonable test of toxicity, for pre-clinical studies, since EGF-SubA might not enter mouse cells due to differences in binding of human EGF to murine EGFR. Furthermore we wanted to clarify whether the cytotoxicity of EGF-SubA was, as suggested by Backer and colleagues, dependent on the presence of EGFR. If cytotoxity of EGF-SubA is dependent on EGFR then these effects in theory may be mitigated by cetuximab, which is a mAb against EGFR.

In order to address the question of whether EGF-SubA is toxic to mouse cells at the pico molar level and to confirm simultaneously that EGF-SubA toxicity is dependent on the expression of EGFR, mouse liver HEPA 1c1c7 cells, which express EGFR, and mouse embryonic fibroblasts (MEF) that do not express EGFR were treated with EGF-SubA for a period of five days and a MTT assay was used to measure cell proliferation/viability as described in Materials and method section 3.12.

Initially EGFR expression was confirmed to be present in HEPA 1c1c7 and absent in MEF cells by direct western blot comparison with UM-SCC 12 which is known to express EGFR as shown in Figure 4.6.1A. Secondly Hepa 1c1c7 and MEF cells were treated with EGF-SubA at a range of concentrations between 1pM to 1nM for up to five days as shown in Figure 4.6.1B. As expected the growth of Hepa 1c1c7 EGFR positive cells was inhibited by EGF-SubA, albeit that the IC_{50} was at a relatively high pico molar

concentration of 700pM, whilst no inhibitory effects upon MEF cells were observed, even at an EGF-SubA concentration of 1nM. Thus these results indicate that murine cells which do not express EGFR are not as sensitive to the effects of EGF-SubA compared to murine cells which do express EGFR. Therefore potentially the effects of EGF-SubA may be blocked by cetuximab.

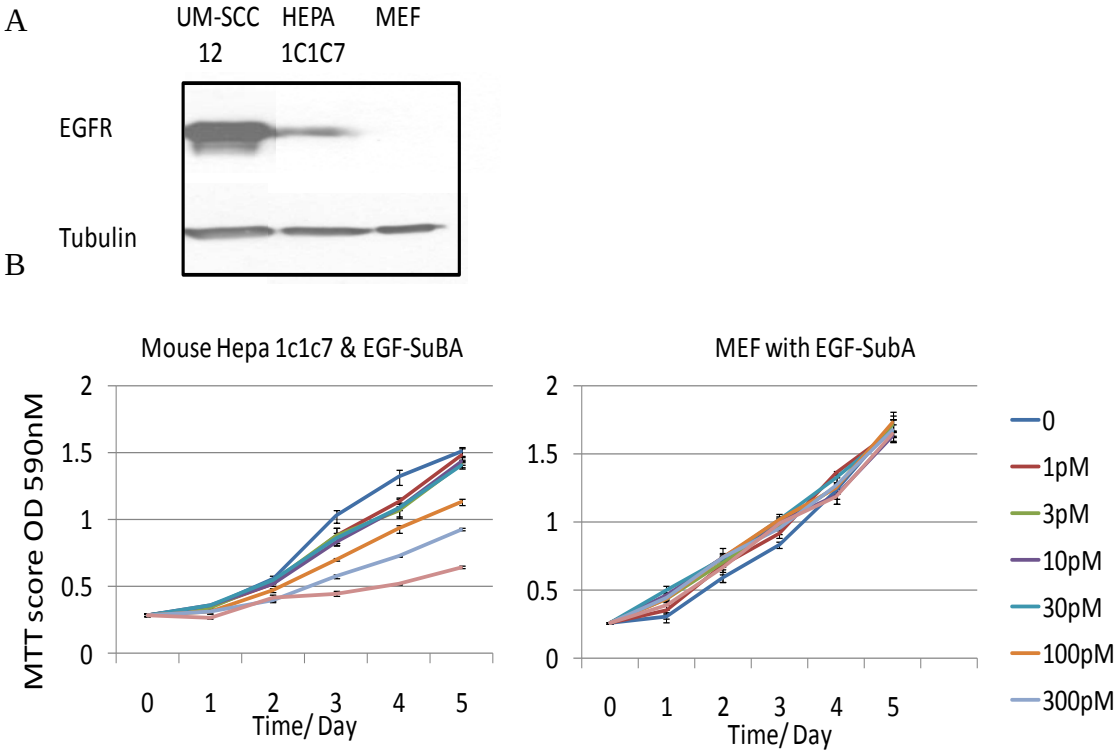

Figure 4.6.1 EGF-SubA is toxic to Hepa 1c1c7 EGFR expressing cells but not to MEF cells which do not express EGFR.

(A) Western blot analysis of UM-SCC 12, Hepa 1c1c7 and MEF. All lanes were loaded with 35 µg protein. Blots were probed with anti EGFR antibody at 3 µg/ml and anti actin antibody at 3µg/ml (protein loading control). (B) Hepa 1c1c7 and MEF cells were treated with either EGF-SubA at concentrations of 1pM, 3pM, 10pM, 30pM, 100pM, 300pM and 1nM or with drug vehicle control, for up to five days. MTT assay was used to assess the quantity/viability of cells. Absorbance was measured at an OD of 590 nm. Error bars represent the s.e.m. from four independent wells.

4.7 EGFR membrane expression is correlated with EGF-SubA sensitivity

Results in section 4.6 indicate that cells that do not express EGFR are not as sensitive to EGF-SubA as EGFR expressing cells. Therefore it was further investigated whether there was a correlation between cell surface EGFR expression and sensitivity to EGF-SubA between cells.

In order to measure membrane EGFR levels as opposed to total cellular EGFR levels, flow cytometric analysis was used. Anti EGFR (ICR10) antibody conjugated to PE from Abcam (ab27764) was used in order to detect membrane EGFR. This antibody was selected as it binds to an extracellular epitope of EGFR.

In pilot western blot experiments it was observed that there were fluctuating amounts of EGFR expression within any one cell line and it seemed likely that this was cell density-dependent. Therefore in order to determine whether EGFR expression changed with cell density, UM-SCC 12 and 81B were grown and harvested at 30%, 60% and 90% confluence as shown in Figure 4.7.1. These cells were chosen on the basis that they were the easiest of the cell lines to grow. It can be seen through western blot analysis that higher total cellular EGFR expression levels were observed at lower cellular density. In

both UM-SCC 12 and 81B EGFR levels were greater at 30% confluence and lower at 90% confluence.

In order to negate the effects of confluence on EGFR expression all cells were harvested at 90% confluence and processed for flow cytometry to determine surface EGFR levels as described in Methods section 3.9.

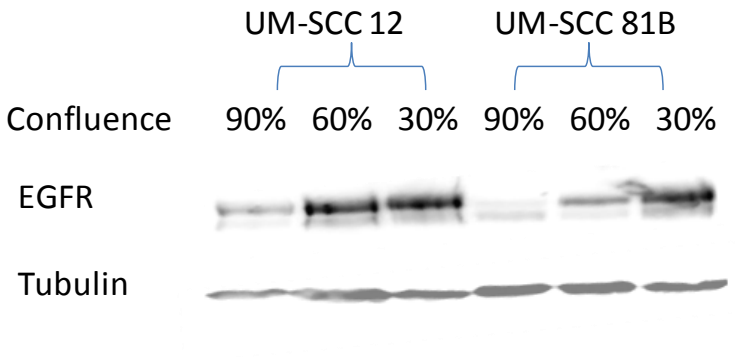

Figure 4.7.1 Higher total cellular EGFR expression was observed at lower cellular confluences.

Western blot analysis of UM-SCC 12 and 81B which were seeded for 24h and then harvested the next day to ensure a confluence of 30%, 60% and 90%. All lanes were loaded with 35 µg protein. Blots were probed for EGFR at 3 µg/ml and tubulin (protein loading control) at a dilution of 1:10,000.

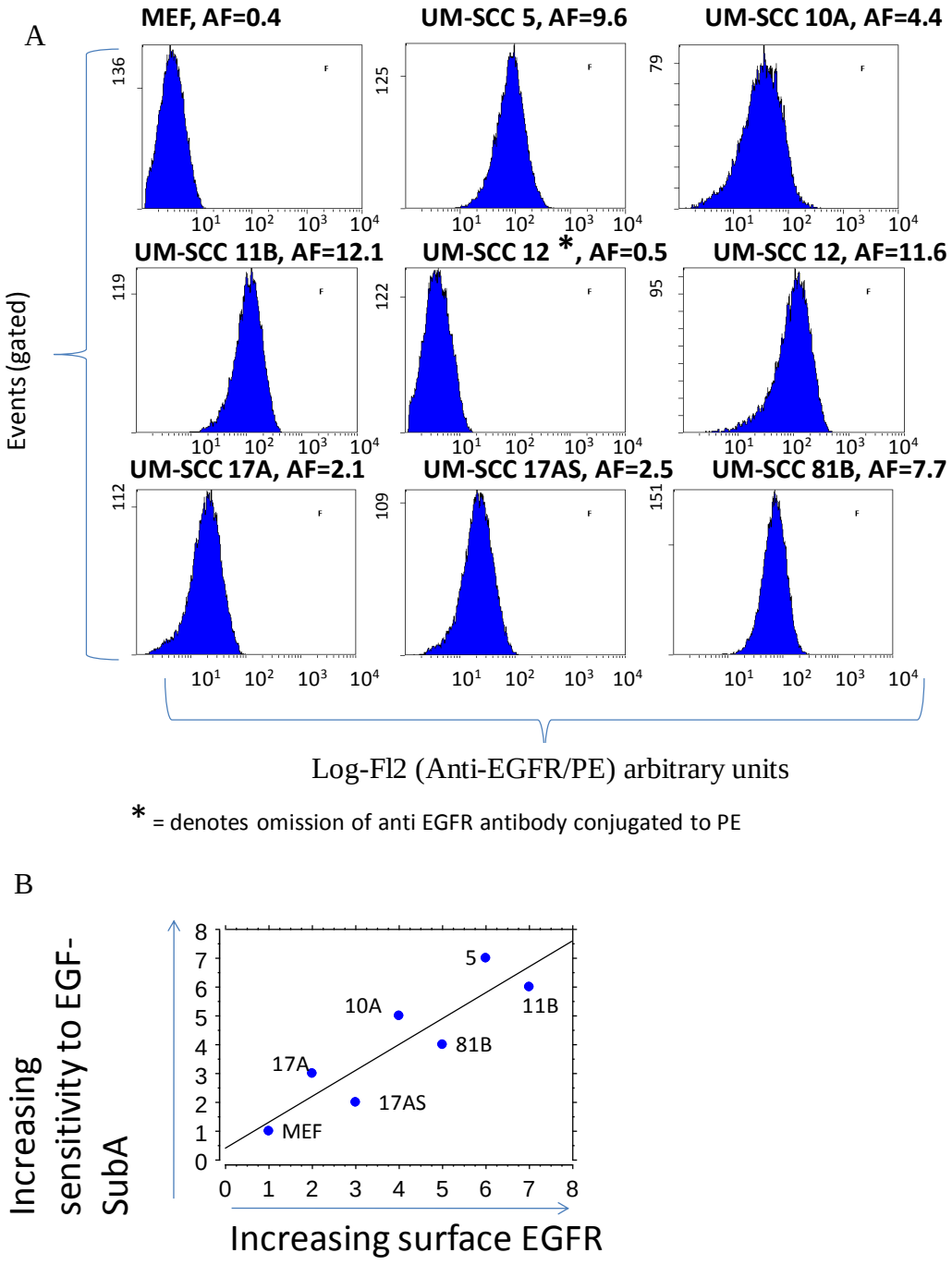

Figure 4.7.2 EGFR membrane expression levels in a panel of LSCC and MEF cells correlates with sensitivity to EGF-SubA.

(A) EGFR expressing UM-SCC 10A, 5, 11B, 12, 17A, 17AS and 81B, as well as MEF cells absent of EGFR were grown for 24h and harvested at 90% confluence. Cells were then incubated with a PE-conjugated anti EGFR antibody (ab27764) and fluorescence detected in the FL2 channel using a log scale to detect mean PE average fluorescence (AF). (B) UM-SCC and MEF membrane EGFR AF levels were plotted against EGF-SubA sensitivity (ranked by IC_{50} values). Cells were ranked from the lowest AF value (MEF=1) to the highest AF value (UM-SCC 11B=7). Cells were also ranked on the sensitivity towards EGF-SubA from the most resistant (MEF=1) to the most sensitive (UM-SCC=7). There was a strong association between high levels of membrane EGFR and increased sensitivity to EGF-SubA with a Spearman's rank correlation coefficient (rs) = 0.919 (p=0.007). UM-SCC 12 was excluded from correlation analysis as it was an outlier with one of the higher AF levels but being the most resistant UM-SCC cell line to EGF-SubA and therefore would have appeared at the furthest point perpendicular to line of best fit.

There appears to be a strong positive association between increasing EGF-SubA sensitivity and high EGFR fluorescence levels, as shown in Figure 4.7.2B where Spearman's rank correlation coefficient (rs) = (0.919) (p=0.007). Therefore it is likely that cytotoxicity of EGF-SubA is, at least partly, dependent on the amount of surface EGFR present on cells. This may be an advantage in selectively targeting tumour cells since EGFR is frequently up-regulated in SCCHN as mentioned in section 1.2.2 (50). EGFR over-expression in head and neck cancer may be due to multiple gene copies and/or to a reduced rate of EGFR targeted ubiquitin degradation (29, 49). UM-SCC 12 appears to be an outlier with the second highest EGFR membrane concentration yet is the most resistant of the cells to EGF-SubA suggesting that EGF-SubA cytotoxicity may in some tumours/cells be dependent on other factors as well.

4.7.1 Cetuximab has little effect on cell proliferation on laryngeal squamous cell carcinoma cells *in vitro*

As seen in sections 4.6 and 4.7 EGF-SubA cytotoxicity appears to be dependent on the presence of membrane bound EGFR. Ultimately therefore it would be interesting to determine if the effects of EGF-SubA could be mitigated by sub-toxic doses of cetuximab. This could potentially mean that EGF-SubA could be used as a topical treatment peri- or post- operatively after resection of a tumour with systemic side effects

of EGF-SubA being blocked with cetuximab, thus widening the therapeutic window of EGF-SubA.

Recently in 2008 the National Institute of Clinical Excellence (NICE) recommended the concurrent use of cetuximab with radiation in patients with locally advanced SCCHN with a Karnofsky performance status score of 90% or above for whom all forms of platinum based chemo-radiotherapy had failed(23).

Efficacy of cetuximab in combination with radiation was analysed by Bonner and colleagues who reported in 2006 on a Phase III clinical trial involving stage III or IV, non-metastatic squamous cell carcinoma of the oropharynx, hypopharynx, or larynx (151). Median local regional control improved collectively for all three tumour sites from 14.9 months for patients treated with radiotherapy alone to 24.4 months for patients treated with radiotherapy and cetuximab (p=0.005). When analyzing the median local regional control for individual sites: oropharynx patients greatly improved from 29 to 49 months, however loco-regional control was marginally improved for laryngeal SCC patients from 11.9 to 12.9 months, and for hypopharynx SCC patients from 10.3 to 12.5 months. As the study was not powered to detect differences in between these subgroups no p values were provided.

Collectively overall survival improved from 29 to 49 months (p=0.03). When analyzing the median overall survival for individual subgroups: oropharynx patients enjoyed improved survival from 30 months to 66 months, however laryngeal patients experienced only marginal improvement in survival outcome, from 31.6 to 32.8 months, whilst the survival of hypopharynx patients improved from 13.5 months to 13.7 months.

In summary when the survival and progression free survival were analysed collectively in all three tumour sites there were statistically significant improvements for patients treated with cetuximab and radiotherapy as opposed to just radiotherapy alone. However when analysing the individual subgroups only patients with oropharyngeal cancers, which formed 60% of the overall number of participants in the trial, appeared to benefit from the combination of cetuximab with radiation therapy whilst and there was little benefit for people with laryngeal cancers. This may be due to different pathologies involved in the various sub-sites. For example it is known that SCCHN patients with HPV are more responsive to chemo- and radiation therapy($p \leq 0.05$) compared with HPV negative patients and have better survival outcome (19, 21). Therefore HPV infection which is more prevalent in oropharyngeal tumour compared to laryngeal may be a determining factor to cetuximab sensitivity.

Amplification of EGFR genes, over expression of EGFR protein, and autocrine TGF-α stimulation which are features present in head and neck cancers, have all been correlated

with poor survival outcome and increased metastatic potential (29, 49, 50) (see section 1.2.2 for more detail). Cetuximab is a monoclonal IgG antibody which binds to EGFR with a greater affinity than either EGF or TGF-α (54). Binding inhibits the activation of EGFR tyrosine kinases and thus prevents Ras associated downstream signalling pathways that are associated with cell proliferation, prevention of apoptosis, cellular repair and survival as described in section 1.2.3(54). Furthermore radiation is known to increase EGFR expression and blockage of EGFR signalling can sensitizes cells to radiation (151)

Although one of the main aims of this thesis was to determine whether cetuximab could act as an antagonist to EGF-SubA, currently there is very little published data on the growth inhibitory effects of cetuximab against laryngeal squamous cell carcinoma both as a single agent and in combination with radiation. Therefore the potency of cetuximab on laryngeal sqaumous cell carcinoma cells was first explored.

In order to establish what inhibitory effects cetuximab had upon the growth of UM-SCC cells an MTT assay was set up as described in section 3.12. The MTT assay is often used to measure the cytotoxic effects of drugs *in vitro*. Healthy cells have viable mitochondria which contain mitochondrial dehydrogenase enzymes. These enzymes are capable of reducing yellow MTT into formazan a purple precipitate (127). The more cells that are viable the more MTT will be reduced, resulting in a higher MTT score. Therefore MTT

score is a function of viability/growth of cells. MTT was found to be less time consuming and more cost effective method as compared to cell counting.

UM-SCC cell lines were seeded into 96 well plates and left for 24h. Cells were then treated with cetuximab at dilutions of 10nM, 100nM and 1μM or with drug vehicle control for a total of seven days. Fresh media and drugs were replaced daily.

As can be seen in Figure 4.7.3 cetuximab had little effect on viability/growth of laryngeal squamous cell carcinoma cell lines, compared to drug vehicle controls, as observed through MTT assay. Maximum effects of cetuximab at reducing viability/growth were reached at 10nM with higher concentrations of cetuximab not leading to any further reduction in MTT score. The most sensitive line was UM-SCC 5 with a 47% decrease in cell viability/proliferation, as compared to controls, after seven days of treatment with 10nM cetuximab. The most resistant cell line was UM-SCC 17AS which showed no response to cetuximab even at 1μM.

As it was observed that cetuximab had little effect on viability/growth on the laryngeal squamous cell carcinoma cells there were concerns as to whether the samples of cetuximab used were functionally active. MTT assay was therefore also performed on a known cetuximab sensitive cell line UM-SCC 1 (derived from an oral tumour). Benavente and colleagues in 2009 had reported an IC_{50} of 5nM for UM-SCC 1 after

three days treatment with cetuximab (152). It was noted that although Benavente and colleagues had shown that UM-SCC 1 was a cetuximab-sensitive cell line, results within this thesis show only a 25% decrease in cell viability/growth after using cetuximab at 1μM for seven days as shown in Figure 4.7.3 (152). Drug assays were repeated on at least one or more occasions, on both laryngeal squamous cell carcinoma cell lines and on UM-SCC 1 cell lines, using more recently obtained vials of cetuximab however no additional toxic effects were observed.

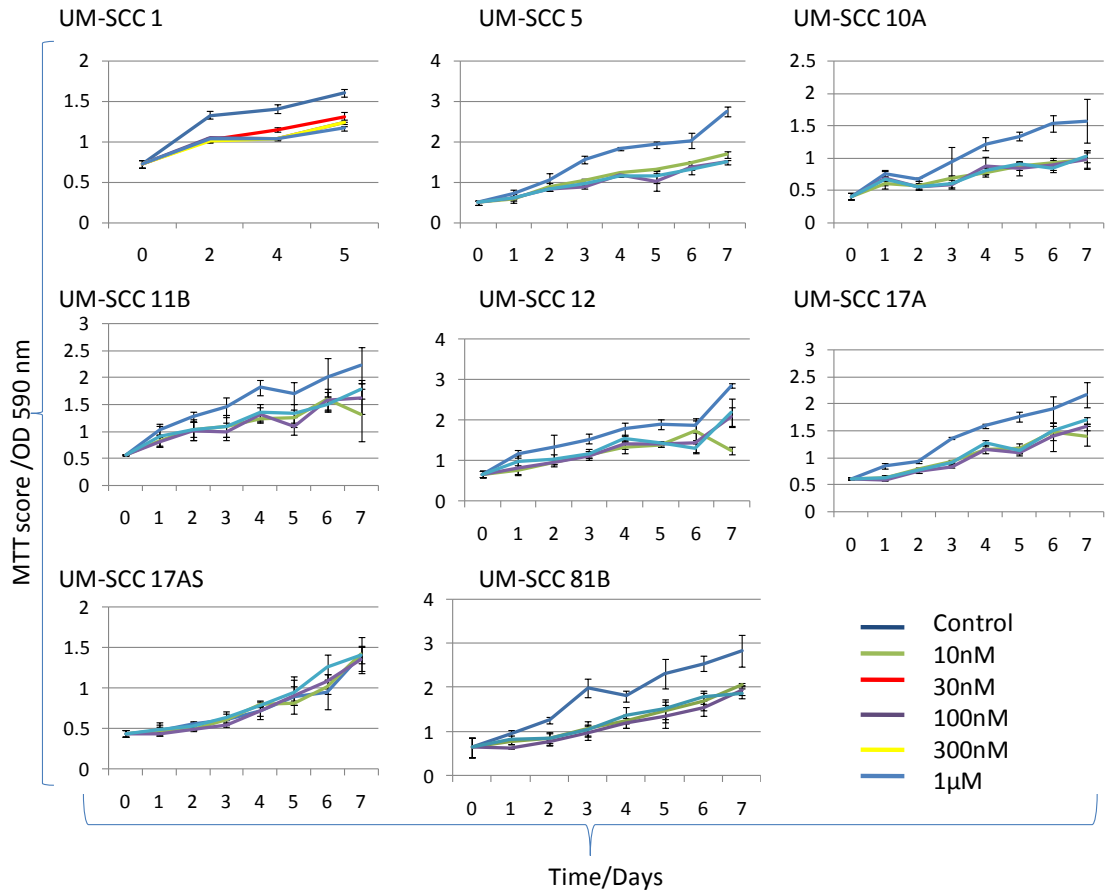

UM-SCC cell line	1	5	10A	11B	12	17A	17AS	81B
Percentage decrease in MTT scores at 1µM cetuximab as a proportion of controls, as recorded on the last day	25%	47%	32%	10%	28%	25%	0%	35%

Figure 4.7.3 Cetuximab has little toxicity even at 1µM on UM-SCC cells.

UM-SCC squamous carcinoma cells were seeded in 96 well plates and allowed to adhere for 24 hours (shown as day 0). Cells were then treated with either cetuximab at dilutions of 10nM, 30nM, 100nM, 300nM and 1μM or with drug vehicle control. As it was observed that cetuximab had little effect on viability/growth on the laryngeal squamous cell carcinoma cells there were concerns as to whether the samples of cetuximab used were functionally active. MTT assay was therefore also performed on a known cetuximab sensitive cell line UM-SCC 1 (derived from an oral tumour). However here it was found that UM-SCC 1 was also not sensitive to cetuximab. Experiments were repeated on at least one or more occasions using more recently obtained vials of cetuximab however no further toxic effects were observed. Table shows the percentage decrease in MTT scores of UM-SCC cells exposed to 1μM of cetuximab as a proportion of controls on day 7 for laryngeal carcinoma cells and day 5 for UM-SCC 1 cells. Both media and drugs were replaced every 24h. MTT assay was used to assess the viability/growth of cells. Absorbance was measured at an OD of 590 nm. Error bars represent the s.e.m. from four independent wells.

4.7.2 Cetuximab is able to inhibit EGF induced phospho EGFR in UM-SCC cells

From previous results shown in this thesis EGF-SubA cytotoxicity appears to be dependent on EGFR (see Results sections 4.6 and 4.7). Therefore one of the objectives of this thesis was to investigate whether cytotoxic effects of EGF-SubA could be inhibited by cetuximab. Benavente and colleagues found that cetuximab was able to block the EGF-stimulated activation of EGFR resulting in reduction in phospho-EGFR levels in UM-SCC 1 cells (152). Cetuximab in a similar fashion may be able to prevent EGF-SubA from binding to EGFR.

From the previous results as shown in Figure 4.7.3 it was seen that cetuximab failed to inhibit the proliferation/viability of UM-SCC cells to an extent where even IC_{50} levels could not be achieved. Therefore it was felt necessary to clarify whether or not cetuximab was at least able to prevent the binding of EGF on EGFR.

The same experiment as performed by Benavente, on UM-SCC 1 cells, was repeated here on range of laryngeal cells including the most sensitive to cetuximab UM-SCC 81B and the most resistant UM-SCC 17AS as well as UM-SCC 5, 12, and 17A, and UM-SCC 1. All cells were harvested once they had reached a confluence of 30%, as it had been previously noted through general observation that EGFR levels fluctuate at

different cell densities (see Figure 4.7.1.). UM-SCC cells were pre-treated with 300nM of cetuximab for two hours followed by addition of EGF at10 μg/ml, or treated with EGF at 10 μg/ml alone, or with drug vehicle control.

In order to prevent phosphatase enzymes from dephosphorylating phospho-EGFR, phosphatase inhibitors were used as well as harvesting cells on ice to further inhibit cellular metabolism (see Methods section 3.5.8 for more details). Lysates were then processed for SDS-PAGE and western blot analysis. Anti phospho-EGFR antibody was used to detect levels of phosphorylated EGFR. Anti EGFR antibody was used to ensure that differences detected in phospho-EGFR expression were not due to fluctuations in EGFR levels. Anti tubulin antibody was used as a loading control. Despite UM-SCC lines showing high resistance to cetuximab in the MTT assay as shown in Figure 4.7.3, Figure 4.7.4 shows that cetuximab was able to adequately reduce EGF binding and prevent subsequent EGFR phosphorylation in all cell lines including UM-SCC 17AS which was the most resistant cell line to cetuximab. Regardless of the fact that cetuximab has little effect on viability/growth of UM-SCC cells, cetuximab may however be able to inhibit cytotoxic effects of EGF-SubA. Furthermore cetuximab resistance has been reported in the literature as being due to mutations downstream the EGFR signalling pathway such as Ras mutations and not on the ability of cetuximab to bind onto EGFR (52). Resistance to cetuximab has been discussed in the literature review (see section 1.2.3).

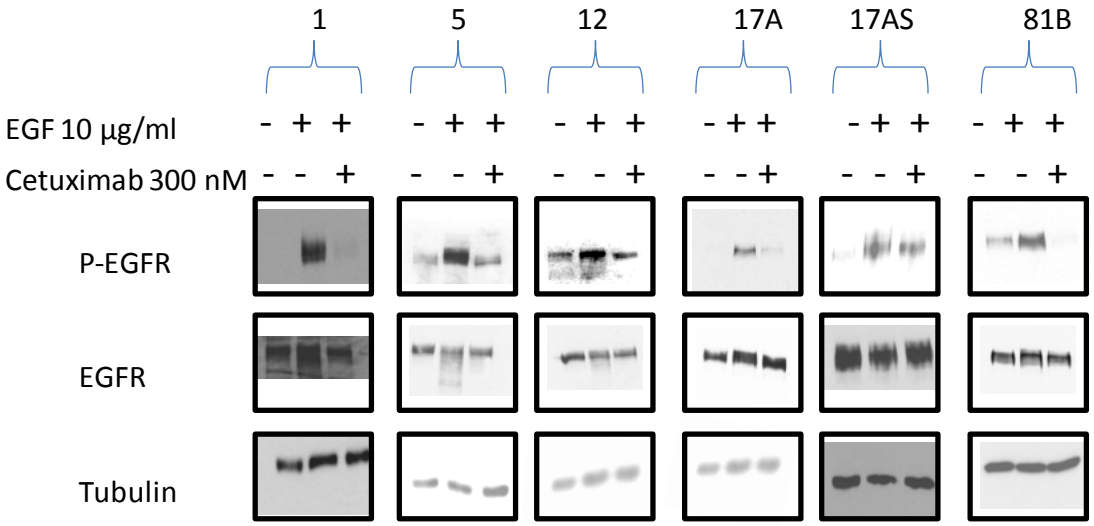

Figure 4.7.4 Cetuximab inhibits EGF mediated phosphorylation of EGFR effectively.

UM-SCC cells were grown and harvested at 30% confluence and either pre-treated with 300nM of cetuximab for two hours followed where indicated by addition of EGF at 10 µg/ml, or treated only with EGF at 10 µg/ml, or with drug vehicle as indicated. Cells were then harvested via cell scraping on ice using SLIP buffer mixed with 5 mM sodium fluoride, 1 mM sodium orthovandate and 10 mM sodium pyrophosphate. All lanes were loaded with 35 µg protein. Membranes were incubated with 3 µg/ml anti p-EGFR antibody, 3 µg/ml anti EGFR antibody and 1:10,000 dilution of anti tubulin antibody (protein loading control) as indicated.

EGF activates EGFR signalling pathway which can then help promote cell proliferation and survival (37). Cetuximab competitively binds to EGFR at a greater affinity than EGF thus preventing cell proliferative and pro-survival effects induced by EGF (54). Growth media of UM-SCC cells consists of in part foetal bovine serum which may not effectively stimulate the EGFR pathway way due to either a lack of EGF or bovine derived EGF which may not be able to interact with human EGFRs. Therefore inadequate stimulation of EGFR in present growth media may explain why the addition of cetuximab may not be effective at inhibiting the proliferation of laryngeal UM-SCC cells *in vitro*, even though it can efficiently block EGF induced phospho-EGFR as shown in Figure 4.7.4.

As activation of EGFR signalling pathway is reported in part to be responsible for the proliferation and enhanced survival of cells, experiments conducted as part of this thesis aimed to determine whether the addition of recombinant human EGF (rhEGF) could enhance cell viability/growth as compared to cells grown without rhEGF (37). Secondly it was investigated whether cetuximab could block this potential rhEGF induced enhancement in cell viability/growth.

A preliminary experiment was used in order to establish dilutions of rhEGF that would achieve maximum phospho-EGFR levels. UM-SCC 81B cells at 30% confluence were incubated with either 0.1 μg/ml, 1 μg/ml or 10 μg/ml EGF for 45 minutes. Cells were

then harvested on ice using phosphatase inhibitors as described in Methods section 3.5.8. and then processed for western blot analysis. Figure 4.7.5 shows that the maximum level of phospho-EGFR was achieved at 1 μg/ml of EGF with no further increases in phospho-EGFR levels being detected at higher concentrations of rhEGF.

One of the most sensitive laryngeal cell lines to cetuximab UM-SCC 81B and the most resistant cell line UM-SCC 17AS were then grown in 96 well plates with fresh media and reagents replaced daily. MTT assay was performed on days 0, 2, 4 and 6. UM-SCC cells were grown under the following conditions:

- with cetuximab at 300nM alone
- or with cetuximab at 300nM for two hours followed by 0.1 μg/ml or 1 μg/ml EGF.
- or with 0.1 μg/ml or 1 μg/ml EGF.
- or with drug vehicle control.

It was predicted that the addition of human rhEGF would increase cell viability/growth in UM-SCC cells, compared to controls, and that cetuximab would be able to inhibit this enhancement in cell viability/growth. However as it can be seen in Figure 4.7.5 there was no increase in cell growth/viability in EGF-treated groups compared to controls in both UM-SCC 17AS and 81B and therefore no additional inhibitory effects of cetuximab were observed as compared to previous experiments as shown in Figure 4.7.3

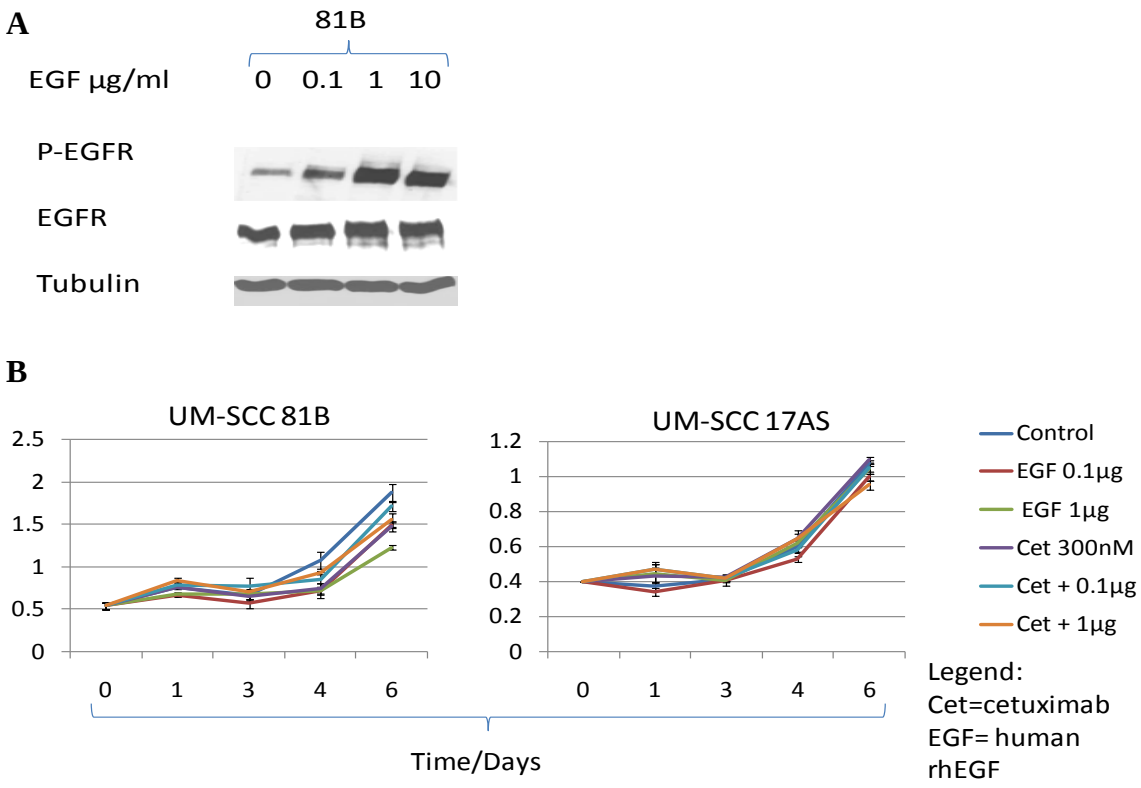

Figure 4.7.5 UM-SCC 17AS and 81B cell viability/growth were not increased with the addition of EGF and there was no change to the inhibitory effect of cetuximab.

(A) Cells were incubated with dilutions of rhEGF for 45 minutes. Cells were harvested via scraping on ice using SLIP buffer mixed phosphatase inhibitors (Methods section 3.5.8) followed by western blot analysis. Membranes were incubated with 3 µg/ml anti p-EGFR antibody, 3 µg/ml anti EGFR antibody and 1:10,000 dilution of anti tubulin antibody (protein loading control) as indicated. (B) UM-SCC 17AS and 81B were pre-treated with cetuximab for 2 h followed by rhEGF, or both agents alone, or with drug vehicle control, for up to 6 days. MTT assay used to assess viability/growth (Methods section 3.12) . Error bars represent the s.e.m. from four independent wells.

4.7.3 Cetuximab does not act as a radiosensitizer in laryngeal squamous cell carcinoma cells.

The above experiments showed that cetuximab has little effect at reducing the proliferation or viability of laryngeal and oral squamous carcinoma cells *in vitro* as determined by MTT assay. Although NICE guidelines in 2008 recommended the use of cetuximab in combination with radiation in locally advanced SCCHN there is currently very little published data which supports the use of cetuximab with radiation for laryngeal squamous cell carcinoma (as reported in section 4.7.1) with Bonner and colleagues phase III trial showing only marginal improvements in disease free and overall survival between patients with laryngeal cancer patients treated with cetuximab with radiotherapy as opposed to radiotherapy alone (151). As radiotherapy is one of the main treatment modalities in SCCHN it was felt necessary to clarify whether or not cetuximab acts as a radiosensitising agent, *in vitro,* to laryngeal squamous cell carcinoma cells. Therefore the radio-enhancing effects of cetuximab were studied on four laryngeal cell lines with varying p53 expression. Loss of p53 function has been associated with chemo- and radioresistance (153). Therefore, we examined a variety of UM-SCC cells of differing p53 status, to determine whether or not any potential radiosensitising effects of cetuximab observed were present regardless of p53 status (149). The cell lines studied were UM-SCC 17A which is wild-type for p53, UM-SCC 12 which is p53 null (homozygous Q104X), UM-SCC 81B which has no p53 wild-type

alleles (mutant H193R), and UM-SCC 5 which has one p53 wild-type allele and a single p53 mutation (heterozygous V157F) in the absence of loss of heterozygosity (i.e. it retains a wild-type allele).

In order to test possible radiosensitisation effects of cetuximab *in vitro,* a clonogenic assay was used. One of the main aims of cancer treatment is to prevent recurrence of tumour growth. A clonogenic assay measures the ability of individual cells to proliferate and form colonies after exposure to ionizing radiation, and this can be achieved in combination with cytotoxic drug treatments if required (126). A colony was defined as more than or equal to 50 cells which allows for an individual cell to have divided more than 5 times. Clonogenic assays were carried out as described in section 3.11.

Pilot studies were performed in order to establish the highest drug concentration that cells could tolerate for 24h without radiation that would provide survival fractions equal to that of drug omitted controls. UM-SCC 12 and 81B were able to tolerate a cetuximab dose of 100nM without differences in survival fraction as compared to controls. Both UM-SCC 5 and UM-SCC 17A when treated with 100nM cetuximab without radiation had survival fractions below the controls and so cells were treated with a lower dose of cetuximab at 10nM. UM-SCC cells were pre-incubated with cetuximab or drug vehicle control for 24h before being irradiated with 0, 1, 2, or 4 Gy. Cells were then seeded in

triplicate into six well plates, in normal growth media without drug and monitored for colony formation for 2-3 weeks.

Colonies were counted using a light microscope. The mean number of colonies were recorded for each set of triplicate samples. Survival fractions were calculated and radiation survival curves were fitted according to the linear-quadratic model $S(D)/S(0)=\exp(-(\alpha D + \beta D^2))$, where D is the irradiation dose in Gy; α is the cell kill per Gy of the initial linear component and β is the cell kill per Gy^2 of the quadratic component of the survival curve. SPSS PASW statistics package version 18 was used to find values of α and β and survival curves were plotted as seen in Figure 4.7.6.

Regardless of p53 status cetuximab did not appear to act as a radiosensitising agent as no significant differences, as determined by unpaired Student's t test, were found in survival fraction at 2 Gy(SF2) between radiated cells pre-treated with cetuximab compared to cells treated only with radiation as shown in Figure 4.7.6.

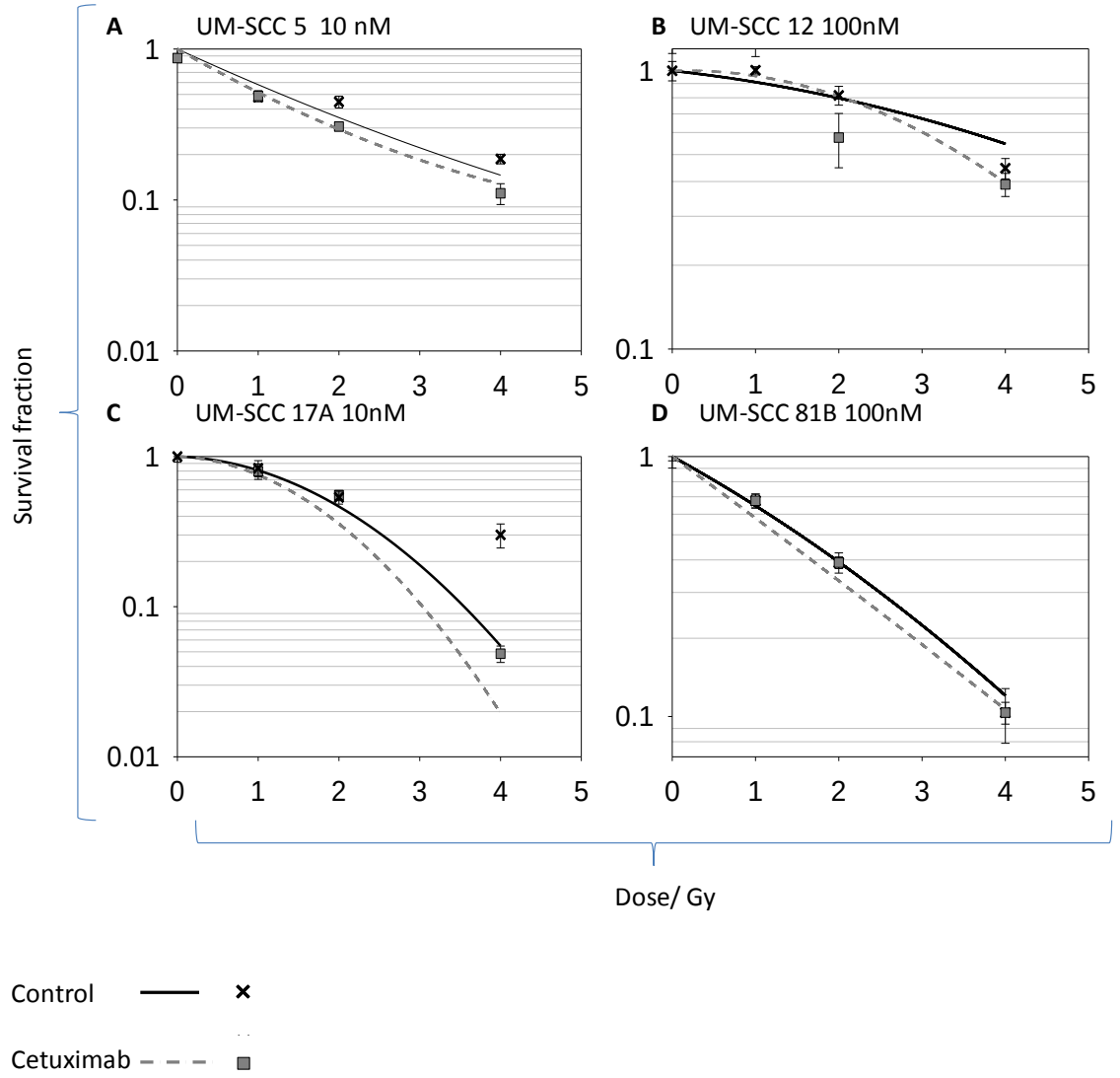

E

Cell	5 Control	5 Cetuximab	12 Control	12 Cetuximab	17A Control	17A Cetuximab	81B Control	81B Cetuximab
SF2	0.4	0.3	0.8	0.6	0.5	0.6	0.4	0.4
P (t test)	0.12		0.17		0.8		0.38	

Figure 4.7.6 Cetuximab does not enhance the effect of radiation in LSCC cells.

(A, B, C, and D) UM-SCC cells were pre-treated for 24h with either 10 or100nM cetuximab or drug vehicle control and then exposed to γ-irradiation at 0, 1, 2, or 4 Gy as indicated. Clonogenic assays were established to allow for colony formation over a time period of two to three weeks. A colony was defined as equal to or more than 50 cells in order to allow for at least five cell doubling times. Crosses and squares indicate means of three survival fractions for each data point with appropriate s.e.m. Cell survival curves were then fitted to the quadratic equation $S(D)/S(0)= \exp(-(\alpha D + \beta D^2))$. *(E) Table showing survival fractions at 2 Gy (SF2) with and without cetuximab. Unpaired Student's t test was used to calculate differences in SF2 between controls and treated cells.*

4.8 **Cetuximab inhibits the cytotoxic effects of EGF-SubA**

Previous experiments conducted for this thesis indicate that the cytotoxicity of EGF-SubA is dependent on the expression of EGFR. For example when EGF-SubA was tested on EGFR expressing mouse liver HEPA 1c1c7 cell lines the IC_{50} was 600pM whilst no cytotoxic effects were observed even at 1nM in mouse embryonic fibroblasts (MEFS) which do not express EGFR (Figure 4.6.1.). In addition there was a strong association between high levels of membrane EGFR and increased sensitivity to EGF-SubA with a Spearman's rank correlation coefficient of (rs) = 0.919 (p=0.007) (Figure 4.7.2).

It was also shown that pre-incubation of cetuximab for two hours was able to efficiently block EGF induced phospho-EGFR in a range of UM-SCC cells as shown Figure 4.7.4.

Based on these previous findings cell counting assays were conducted in order to elucidate whether cetuximab, a mAb against EGFR, could inhibit the cytotoxic effects of EGF-SubA. These experiments were conducted with a view that EGF-SubA could be used as a topically peri or post operatively adjuvant with the aim of enhancing loco-regional control, whilst cetuximab, which is already licensed for use in humans, could be used systematically to prevent any possible organ specific toxicity which might result from the use of EGF-SubA.

UM-SCC 12, 17A and 81B cells were seeded in 12 well plates, in sets of triplicate, and left to adhere for 24 hours. Cells were then treated with either EGF-SubA above and below IC_{50} doses, or pre-incubated with sub-toxic concentrations of cetuximab (10, 30 and 100nM) for two hours prior to the application of EGF-SubA, or treated with drug vehicle control. Fresh drugs and media were replaced daily for a total of four days. Cell concentrations for each condition were determined by cell counting as explained in Methods section 3.13. p-values were calculated between samples exposed to the highest dose of EGF-SubA used with and without cetuximab, in order to establish whether there were statistically significant differences in cell number via the unpaired Student's t test.

In all cases, as shown in Figure 4.8.1, cetuximab even at 10nM was able to dramatically rescue cells from the cytotoxic effects of EGF-SubA. In UM-SCC 12 (Figure 4.8.1) untreated cells reached concentration of 7.3×10^5 cells per ml. Cells treated with cetuximab at 10nM had a similar concentration of 7.4×10^5 cells per ml. Cells treated with 1nM EGF-SubA had a reduced population of 2×10^5 cells per ml whilst cells incubated with 10nM cetuximab prior to EGF-SubA had a significantly higher concentration of 6.8×10^5 cells per ml where $p < 5 \times 10^{-5}$.

In UM-SCC 17A (Figure 4.8.1) untreated cells reached a concentration of 6.3×10^5 cells per ml. Cells treated with cetuximab at 10nM had a similar concentration of 6.8×10^5

cells per ml. Cells treated with 50pM EGF-SubA had a reduced population of 2.1×10^5 cells per ml whilst cells incubated with 10nM cetuximab prior to EGF-SubA had a significantly higher concentration of 5.1×10^5 cell per ml where $p < 0.002$.

In UM-SCC 81B (Figure 4.8.1) untreated cells reached a concentration of 11.1×10^5 cells per ml. Cells treated with cetuximab at 10nM had a similar concentration of 8.4×10^5 cells per ml. Cells treated with 200pM EGF-SubA had a reduced population of 2.2×10^5 cells per ml whilst cells incubated with 10nM cetuximab prior to EGF-SubA had a significantly higher concentration of 10.0×10^5 cell per ml where $p < 9 \times 10^{-6}$.

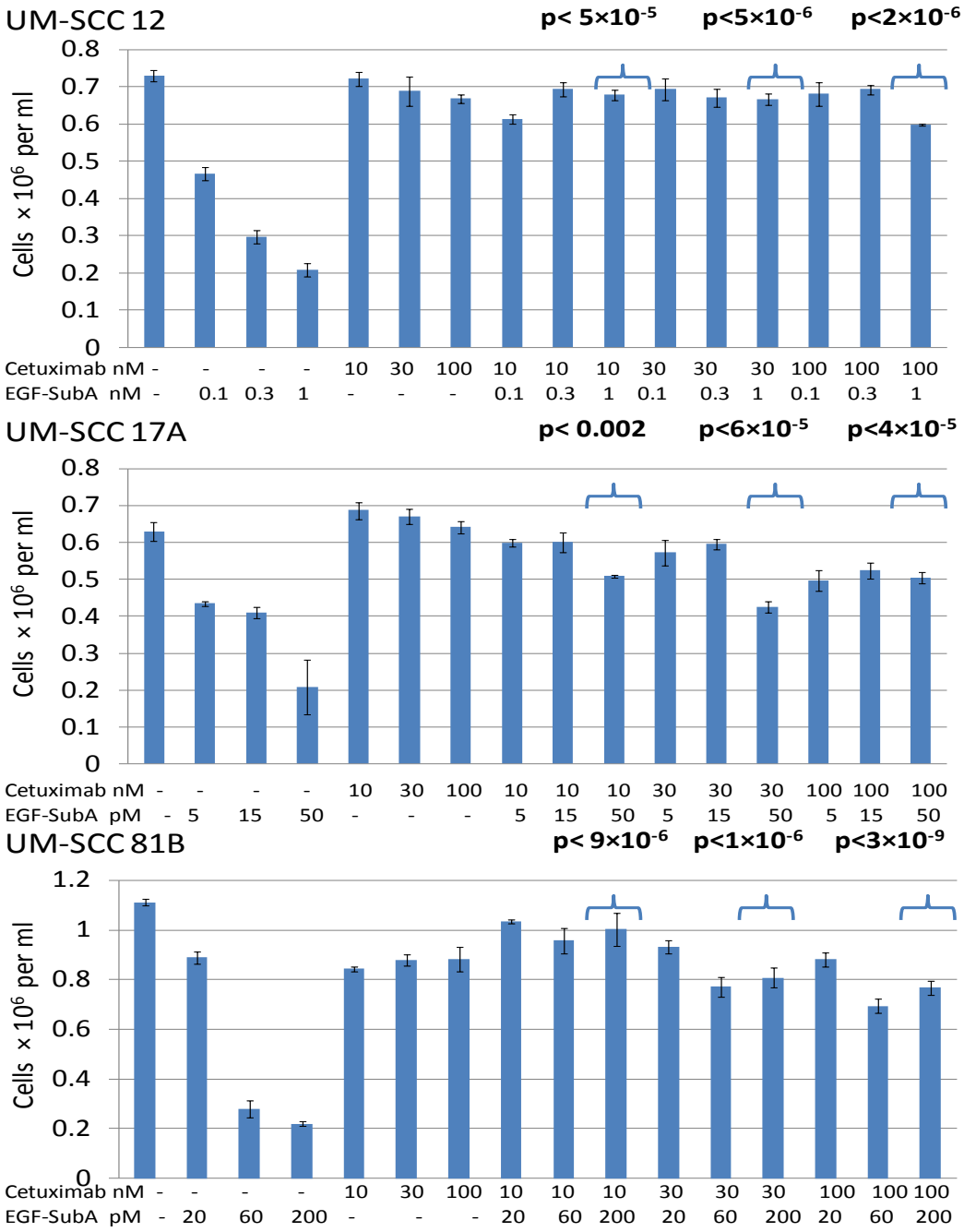

Figure 4.8.1 Pre-incubation with cetuximab is able to rescue cells from the cytotoxic effects of EGF-SubA.

Cells were seeded into 12 well plates and left to adhere for 24h. Cells were then treated with EGF-SubA above and below IC_{50} doses or pre-incubated with sub-toxic concentrations of cetuximab (10, 30 and 100nM) for two hours prior to the application of EGF-SubA, or with drug vehicle control. Fresh drugs and media were replaced daily for a total of four days. Cells were harvested and counted via a Beckman Coulter Counter on the last day. Error bars represent the s.e.m. from three independent wells. p-values were calculated between the highest dose of EGF-SubA used with and without cetuximab, in order to establish whether there were statistically significant differences in cell number via unpaired Student's t test.

5 Results part 2: EGF-SubA enhances the effect of current treatment modalities:

a) by acting synergistically with cisplatin

b) and as a radiosensitising agent.

5.1 EGF-SubA acts synergistically with cisplatin

Cisplatin is one of the main chemotherapeutic agents used in the treatment of head and neck cancer (106). Cisplatin forms DNA adducts by binding to DNA resulting in DNA-DNA inter and more commonly intra-strand crosslinks. These cross links interfere with DNA replication, leading to suppression of RNA transcription and inhibition of cell division (107). DNA damage by intra-strand crosslinks are detected by damage recognizing proteins which coordinate the repair process in a response known as the nucleotide excision repair (NER) (154). DNA damage recognizing proteins also activate several signal transduction pathways including those involving ATR, p53 and MAPK which, in turn can promote cell cycle arrest and cell death – typically via apoptosis (107).

Tumour resistance to cisplatin is a major barrier to effective head and neck cancer therapy. Resistance to cisplatin induced apoptosis has been related to several factors such as: enhanced activity of PI3K/AKT, Ras mutations, hyper-activation of ErbB2, down regulation of proapoptotic proteins such as Bax and Bad, increase in Bcl-2 and Bcl-xL, and loss of p53 function (107).

Recent studies suggest that over expression of GRP78 in tumours may contribute to cisplatin resistance. Lee and colleagues in 2008, transfected glioma cells with GRP78. Subsequent increases in GRP78 expression in these transfected cells lead to decrease in caspase 7 activation and rendered cells resistant to cisplatin induced apoptosis. Upon siRNA treatment against GRP78, decreased cell growth was observed as well as increased sensitisation to both cisplatin and radiation (108). Jiang and colleagues in 2009, demonstrated that cisplatin mediated cytotoxicity of melanoma cells was significantly reduced in cells transfected with siRNA against caspase 4 and 7 siRNA ($p<0.01$) (110). Jiang and colleagues also explored the role of GRP78 in altering cisplatin induced activation of caspase 4 and 7. Upon siRNA knockdown of GRP78 there was increased caspase 4 and 7 activity upon cisplatin treatment, whilst over expression of GRP78 suppressed caspase 4 and 7 activity (110). Hence up-regulation of GRP78 may suppress cisplatin induced cytotoxicity by inhibiting caspase activity.

GRP78 is known to inhibit apoptosis through direct interaction with BIK and procaspase 7 (104), (109). Furthermore continued removal of GRP78 stimulates further the Unfolded Protein Response which activates both intrinsic apoptotic pathways through the induction of such proapoptotic proteins such as Bim and extrinsic apoptotic pathways through the induction of TRAIL ligand DR5 (92, 105). In addition Backer and colleagues in 2009 have shown that 1nM EGF-SubA treatment after 24h resulted in a 3-fold increase in activated caspase 3 levels thus implying that EGF-SubA may induce apoptosis. For further information on how GRP78 and the Unfolded Protein Response regulate apoptosis see sections 1.3.5 and 1.3.6.

Based on the studies by Lee and colleagues in 2008, and Jiang and colleagues in 2009, which point towards up-regulation of GRP78 contributing to cisplatin resistance we investigated, as part of this thesis whether or not EGF-SubA, which cleaves GRP78, could act synergistically with cisplatin. The use of multiple drugs with different mechanisms of action may help to 'improve the efficacy of the therapeutic effect, decrease the dosage but increase or maintain the same efficacy in order to avoid toxicity such as nephrotoxicity and otoxicity which are side effects of cisplatin treatment (155), and minimize or slow down the development of drug resistance' (156).

Initially an MTT growth curves were established in order to measure the effects of cisplatin on the viability/growth of UM-SCC cells, as described in Methods section 3.12.

UM-SCC cells were treated with either cisplatin or with control vehicle for a total of seven day. Cisplatin IC_{50} values were taken on the seventh day of drug treatment as shown in Figure 5.1.1 and Figure 5.1.2. and ranged between 0.6 to 4μM.

Published data regarding cisplatin sensitivity and p53 status is conflicting with some papers suggesting that cisplatin is more sensitive in p53 wild-type cells whilst other studies indicating that p53 mutant cells are more sensitive to cisplatin (107) (157). In order to determine whether EGF-SubA in combination with cisplatin, reduces cell viability/growth, regardless of p53 status a variety of UM-SCC cells were used. The cell lines studied were UM-SCC 17A which is wild-type for p53, UM-SCC 12 which is p53 null (homozygous Q104X), UM-SCC 81B which has no alleles which are p53 wild-type (mutant H193R), and UM-SCC 5 which has one p53 wild-type allele and a single p53 mutation (heterozygous V157F).

Cells were treated with each of the two drugs individually, in combination, or with just control vehicle in quadruplicate sets. Fresh media and drugs were replaced daily for a total of seven days. Cell viability/growth was assed at the end of day seven via MTT assay. A range of values above and below the IC_{50} of both EGF-SubA and cisplatin were combined in order to establish whether there was any synergy, additive or antagonistic effect between these two drugs.

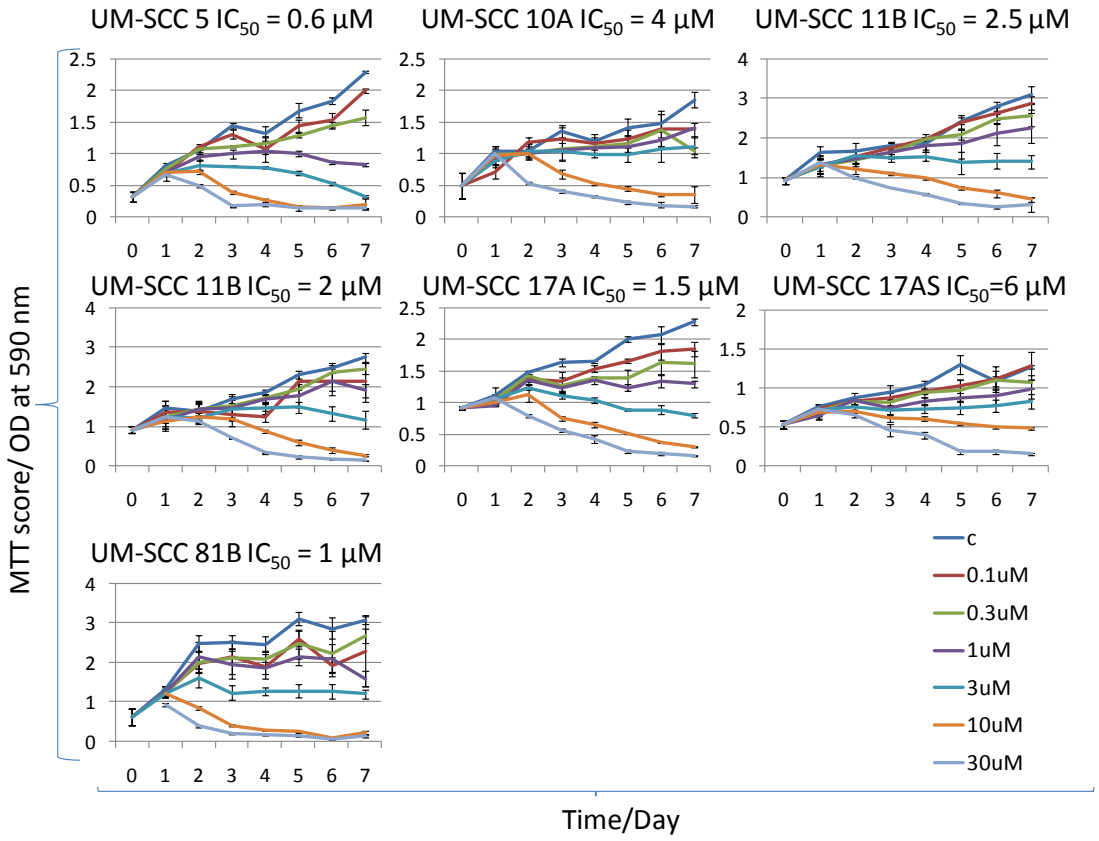

Figure 5.1.1 UM-SCC cells dose response curves with cisplatin.

UM-SCC Cells were seeded in 96 well plates and allowed to adhere for 24 hours (shown as day 0). Cells were then treated with cisplatin at concentrations of 0.1, 0.3, 1, 3,10 and 30µM or with drug vehicle control, for up to seven days. Fresh media and drugs were replaced daily. MTT assay was used to assess the viability/growth of cells. Absorbance was measured at an OD of 590 nm. Error bars represent the s.e.m. from four independent wells.

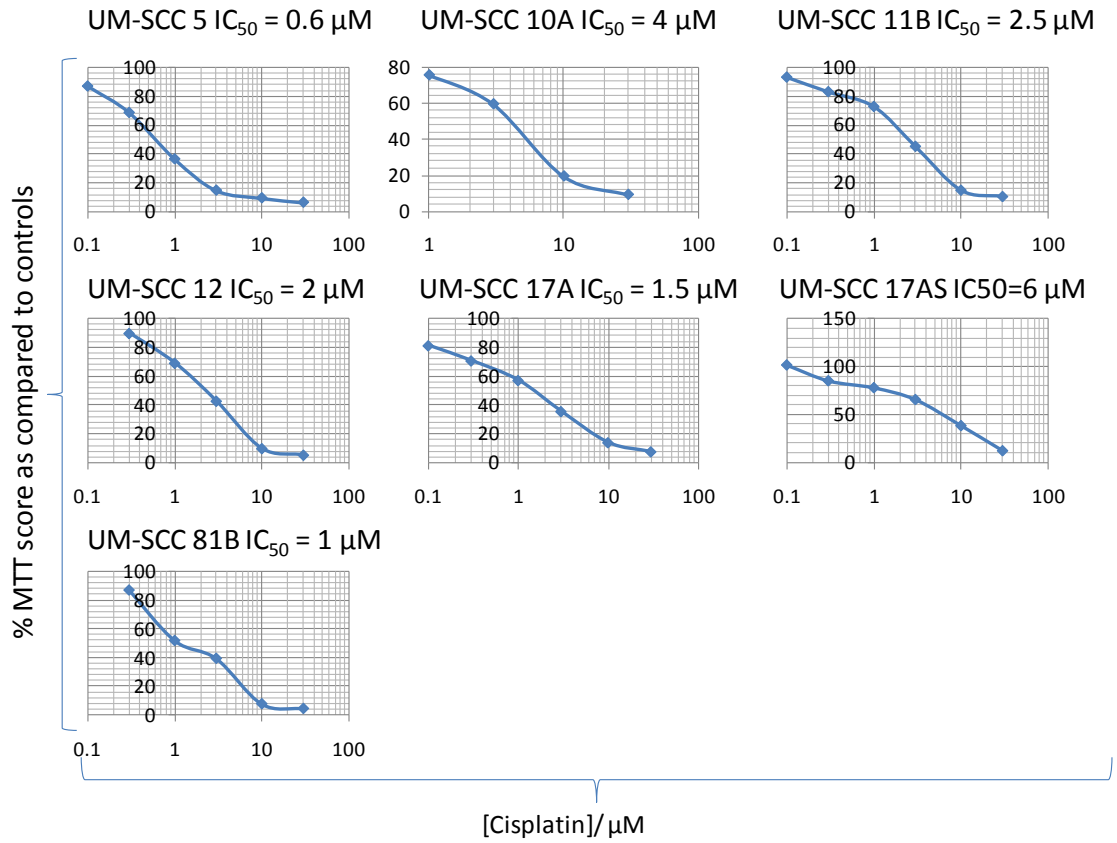

Figure 5.1.2 UM-SCC cell IC_{50} curves with cisplatin.

IC_{50} data derived from day seven of UM-SCC cells being treated with cisplatin at concentrations of 0.1, 0.3, 1, 3, 10 and 30µM or just drug vehicle control. IC_{50} curves were plotted as: percentage MTT scores of UM-SCC cells exposed to drug as a proportion of controls on day 7 (y axis) against the dose of the drug on a log scale (x axis).

For quantification of synergy or antagonism the Combination Index (CI) was used (156). A range between 0.9-1.1 was defined as additive, less than 0.9 indicated synergism and more than 1.1 was described as an antagonistic effect. CI was calculated as $(D)_1/(D_x)_1 + (D)_2/(D_x)_2$. The denominator, $(D_x)_1$ and $(D_x)_2$ is the dose of each of the drugs which, when used alone results in a fixed affect, for example the IC_{50}. The numerators $(D)_1$ and $(D)_2$ are the doses of each drug which when used in combination, to achieve the same fixed effect (156).

An isobologram is a visual representation of the CI. The x and y axis represents the dose of each drugs used. A line is then drawn linking $(D_x)_1$ and $(D_x)_2$ together. Points are then plotted along the graph where combined doses produce the same fixed effect as when both drugs are used individually. Points close to the line represent CI of 1 or an additive effect. Points to the left of the line represent a synergistic effect and points to the right represent an antagonistic effect. The distance away from the line indicates the magnitude of the synergistic or antagonistic effect.

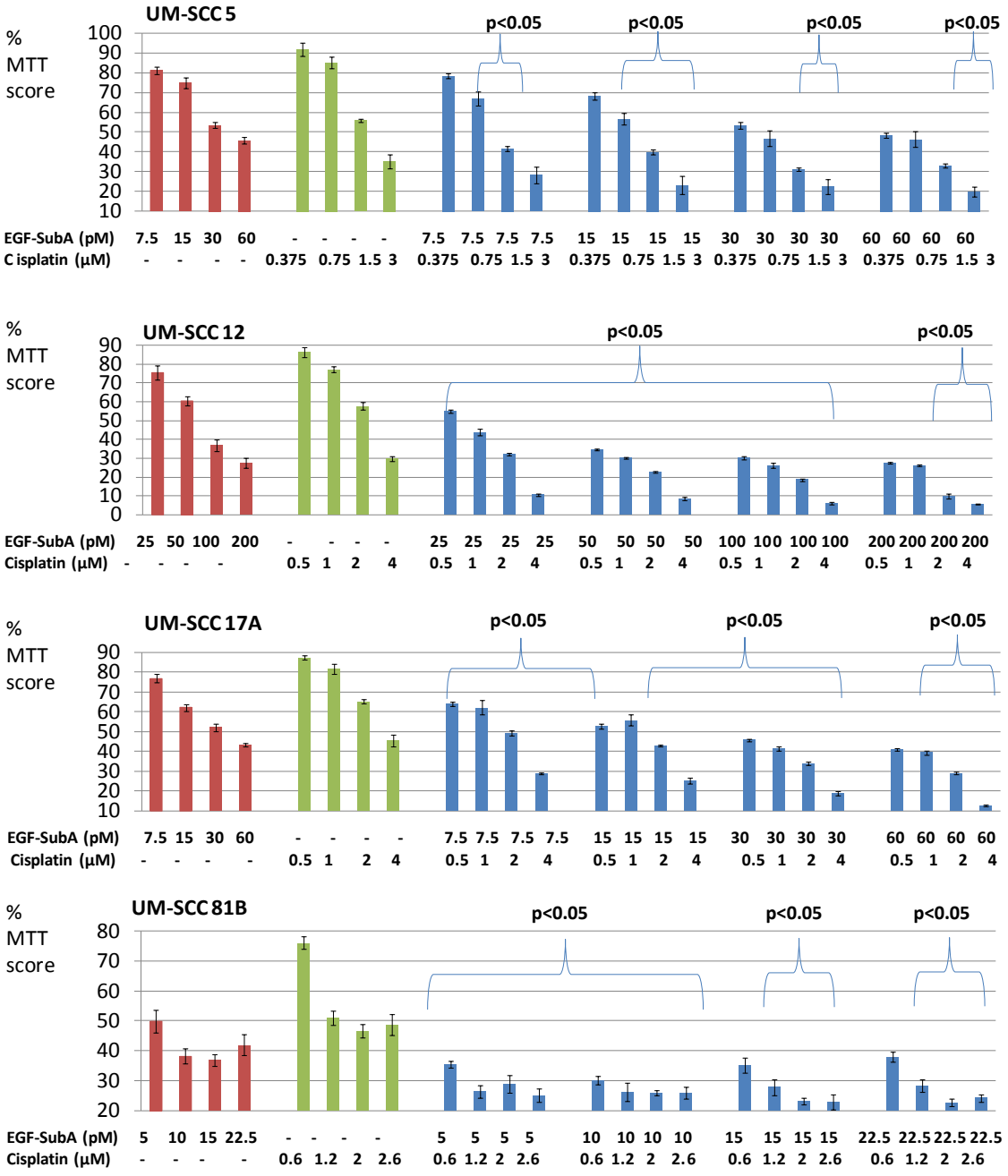

Figure 5.1.3 UM-SCC cells treated with either EGF-SubA, or cisplatin or in combination.

UM-SCC 5,12, 17A and 81B cells were seeded in 96 well plates and allowed to adhere for 24 hours. Cells were then treated with either cisplatin at the stated concentrations or with EGF-SubA at the stated concentrations, or in combination, or with drug vehicle control. Fresh media and drugs were replaced daily for a total of seven days. MTT assay was used to assess the viability/growth of cells after day seven. Absorbance was measured at an. OD of 590 nm. Bars represent the percentage MTT score of treated groups as a proportion of controls. Error bars show the s.e.m. from four independent wells. In the majority of cases there were statistically significant reductions in MTT score when MTT scores from cells treated with single agents were compared to MTT scores of cells treated with both cisplatin and EGF-SubA as deduced by unpaired Student's t test ($p<0.05$).

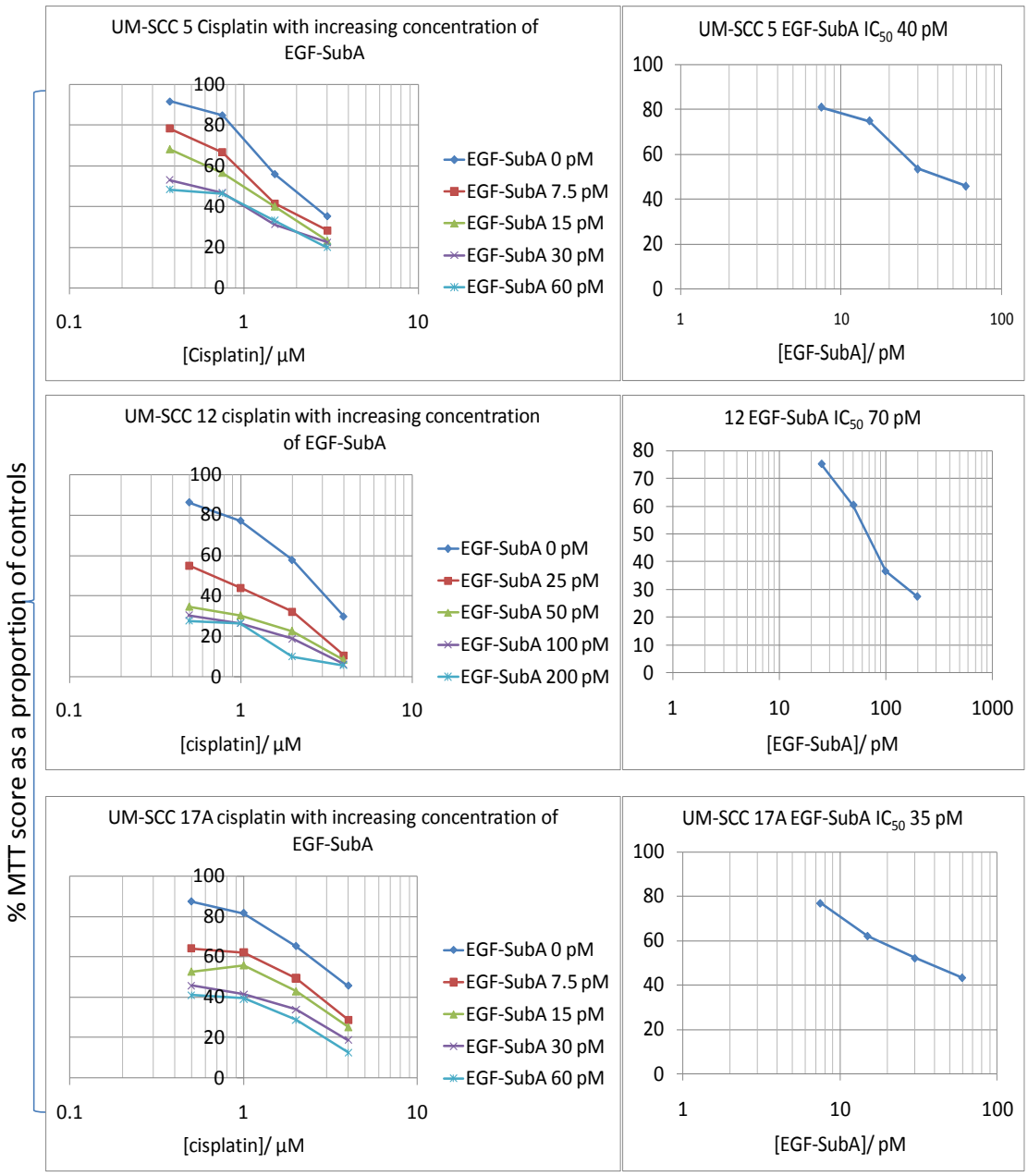

Figure 5.1.4 IC_{50} plots for UM-SCC cells treated with either EGF-SubA, or cisplatin, or in combination.

IC_{50} values were calculated from log plots derived from data as shown in Figure 5.1.3 for either cisplatin on its own, EGF-SubA on its own and any IC_{50} values established when cisplatin and EGF-SubA were used in combination. IC_{50} curves were plotted as: percentage MTT score in the drug treated group as a proportion of the control group (y-axis) against the dose of the drug on a log scale (x-axis).

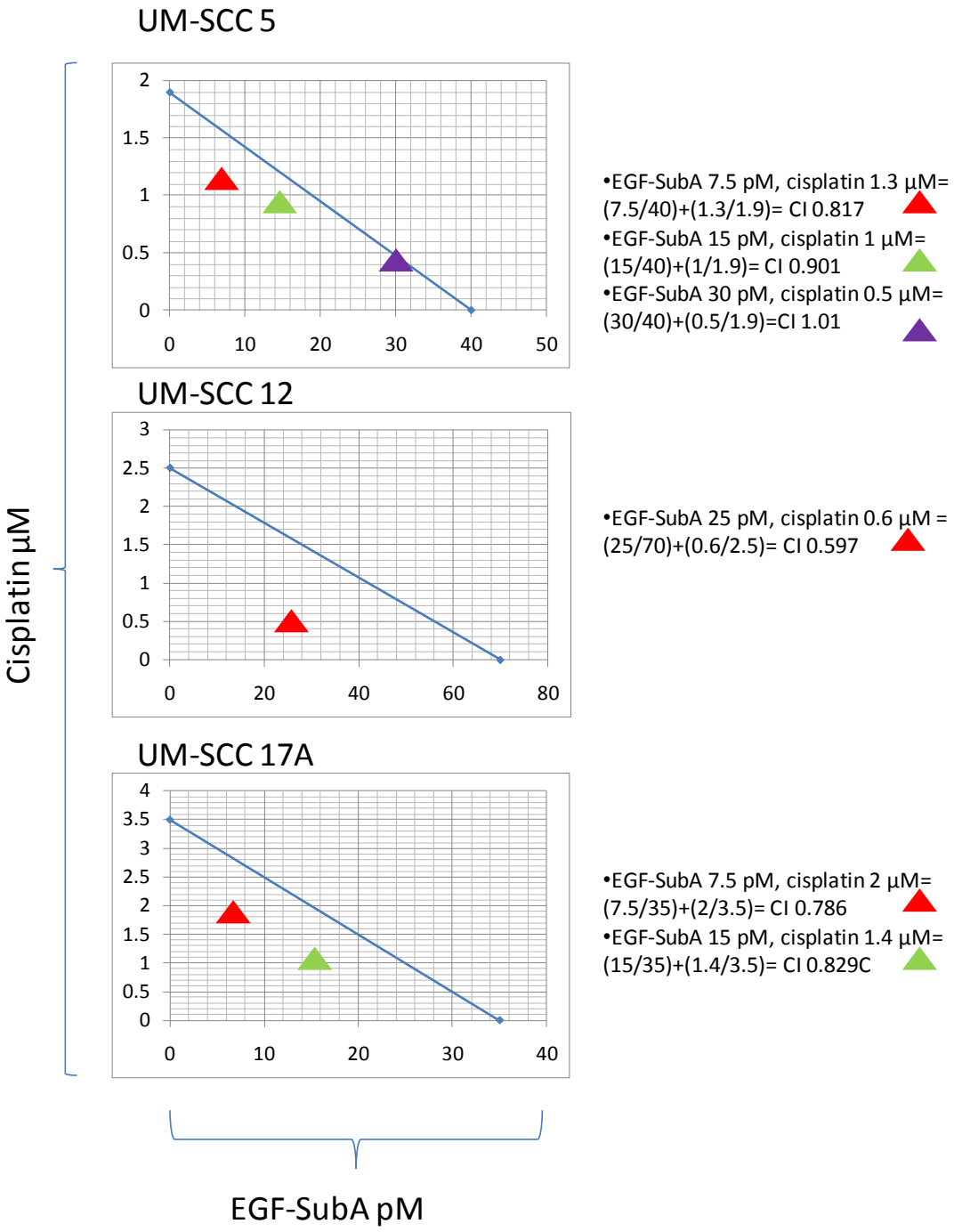

Figure 5.1.5 IC_{50} Isobolograms summarising the combinatorial effect of cisplatin with EGF-SubA

Data derived from Figure 5.1.4 was used to plot isobolograms for UM-SCC cells 5, 12 and 17A. A line joining the IC_{50} value of EGF-SubA and the IC_{50} value of cisplatin for each of the cell lines was plotted. Any IC_{50} values derived form the combination of both EGF-SubA with cisplatin were also plotted as indicated by triangles. Triangles to the left of the isobolar line indicate synergistic effects between cisplatin and EGF-SubA (where combination indexes are 0.9 or less). Triangles plotted on the line indicate additive effects (where combination indexes are close to 1). Triangles plotted to the right indicate antagonistic effects (where combination indexes are greater than 1.1). CI was calculated as $(D)_1/(D_x)_1 + (D)_2/(D_x)_2$. The denominator, $(D_x)_1$ and $(D_x)_2$ is the dose of each of the drugs which, when used alone results in a fixed affect, for example the IC_{50}. The numerators $(D)_1$ and $(D)_2$ are the doses of each drug which when used in combination, to achieve the same fixed effect (156)

EGF-SubA and cisplatin, regardless of p53 status, when used together produced combination index (CI) scores of less than 0.9 in UM-SCC 5, UM-SCC 12 and UM-SCC 17A as seen in Figure 5.1.5 and this is indicative of synergy. Furthermore a statistically significant reduction in MTT score was observed in UM-SCC 81B when MTT scores from cells treated with single agents were compared to MTT scores of cells treated with both cisplatin and EGF-SubA ($p<0.05$) (Figure 5.1.3). An IC_{50} isobologram could not be plotted or CIs calculated in order to quantify whether the effects observed in UM-SCC 81B cells were either additive or synergistic as drug combinatorial MTT scores were greater than the IC_{50} and MTT scores when drugs were used as single agents were less than the IC_{50}.

5.2 Cisplatin in combination with EGF-SubA reduces levels of GRP78.

Cleavage of GRP78 via EGF-SubA induces the Unfolded Protein Response (5). This then results in the activation of transcription factor ATF6 which up-regulates GRP78 (87) (see section 1.3.2 for more detail). From previous results in this thesis (see section 5.1) it has been shown that cisplatin acts synergistically with EGF-SubA. McCollum and colleagues have demonstrated that cisplatin prevents induction of the protein chaperone

HSP72 upon treatment with geldanamycin so here we investigated whether cisplatin may also prevent the induction of GRP78 upon treatment of cells with EGF-SubA.

From Figure 4.1.2 it can be seen that treatment with 1nM EGF-SubA after 24h did not leave any uncleaved GRP78 intact. As one of the aims of this experiment was to determine whether cisplatin could further reduce the level of uncleaved GRP78 in combination with EGF-SubA a lower dose of 100pM EGF-SubA for 24h was chosen which was found to be sufficient to cleave a portion of the GRP78 in the cells but not all. A high dose of cisplatin at 20μM for 24h, which is at least five times the IC_{50} of the UM-SCC cell lines, was chosen in order to exert the maximum effect of cisplatin on levels of GRP78. In summary, cells were treated with either EGF-SubA at 100pM, or cisplatin at 20μM, separately or in combination, or with drug vehicle control, for 24h. Cells were then harvested and processed for SDS-PAGE as explained in section 3.5 and GRP78 levels were analysed via western blot as shown in Figure 5.2.1. EGF-SubA at 100pM was able to cleave GRP78 as. However in all four cell lines there did not appear to be any loss in uncleaved levels of GRP78 upon treatment of EGF-SubA alone, implying that the UPR, via presumably ATF6, was stimulating the up-regulation of additional GRP78. (87). In UM-SCC 5, 12, and 81B cisplatin as a single agent did not alter levels of GRP78. However there was a demonstrable reduction in GRP78 levels in wild-type p53 cell line UM-SCC 17A when cisplatin was used alone. Published data provides conflicting evidence on the effect cisplatin has upon basal levels of GRP78. Some

studies have shown that levels of GRP78 are unaffected by treatment with cisplatin (158), whilst others have demonstrated evidence of increased GRP78 (159) or even decreased GRP78 levels (160).

When EGF-SubA was combined with cisplatin there was a marked loss of uncleaved GRP78 compared to either cisplatin alone, EGF-SubA alone, or drug vehicle control. Just as cisplatin is able to block the binding of HSF-1 to chromatin, upon treatment with geldanamycin leading to inhibition of HSP72 induction (161), it could be hypothesised that cisplatin may also block the interaction of ATF6 with chromatin thus preventing the induction of GRP78. The reduced levels of whole GRP78 when combining EGF-SubA with cisplatin may explain the synergistic effects found in Results section 5.1.

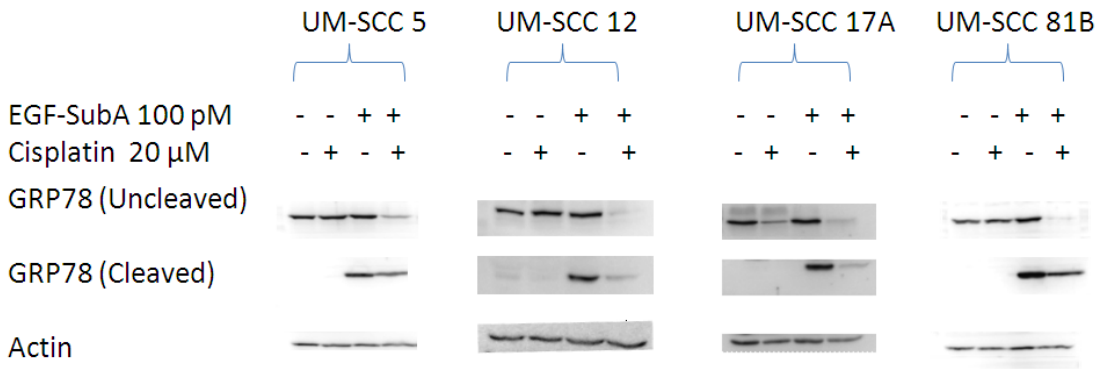

Figure 5.2.1 Cisplatin in combination with EGF-SubA reduces uncleaved GRP78 levels.

Western blot analysis of UM-SCC 5, 12, 17A and 81B treated as indicated with either EGF-SubA at 100pM, or cisplatin at 20µM, or in combination, or with drug vehicle control for 24h. All lanes were loaded with 35 µg protein. Blots were probed for GRP78 (sc-13968) at 3 µg/ml and actin at 3 µg/ml (protein loading control).

5.3 EGF-SubA in combination with cisplatin enhances apoptosis in three out of the four UM-SCC cell lines examined.

GRP78 is known to inhibit apoptosis through direct interaction with BIK and procaspase 7 (104), (109). Furthermore cleavage of GRP78 initiates the UPR which activates both the intrinsic apoptotic pathway through the induction of proapoptotic proteins such as Bim and the extrinsic apoptotic pathway through the induction of TRAIL ligand DR5 (92, 105). For further information on how GRP78 and the Unfolded Protein Response regulate apoptosis see sections 1.3.5 and 1.3.6. In addition Backer and colleagues have shown that 1nM EGF-SubA treatment after 24h increased activated caspase 3 levels by three folds in prostate and breast cancer cells thus suggesting that EGF-SubA may lead to apoptosis.

As previously mentioned Lee and colleagues as well as Jiang and colleagues, demonstrated that up- regulation of GRP78 suppressed caspase 4 and 7 activation in cisplatin treated cells whilst siRNA against GRP78 sensitised cells to cisplatin and increased caspase 4 and 7 activation (108, 110).

Results in this thesis (see section 5.1) have shown that cisplatin in combination with EGF-SubA produces a synergistic effect dramatically reducing cell viability/growth of

laryngeal squamous cell carcinoma cells when compared to cells being treated with either cisplatin or EGF-SubA alone. Although previous studies have reported that cisplatin induces apoptosis in laryngeal cells (162) currently EGF-SubA has only been shown to induce apoptosis in prostate and breast cancer cells (5). Here for the first time it was investigated whether EGF-SubA was able to induce apoptosis in laryngeal squamous carcinoma cells and secondly whether cisplatin in combination with EGF-SubA enhances further apoptosis.

In order to quantify the amount of cell undergoing apoptosis an Annexin V-PI apoptosis assay as described in section 3.6. was used. During the early stages of apoptosis there is loss of phospholipid membrane symmetry which leads to exposure of protein phosphatidyl serine (PS) from the inside to the outside of the cell membrane (123). Annexin V can bind to PS in the presence of calcium and therefore Annexin V conjugated to fluorochrome FITC can be used to indicate early stages of apoptosis. During late apoptosis there is loss in membrane integrity and PI can now enter cells. A population of unfixed cells can therefore be stained simultaneously with both PI (red fluorescence) and FITC (green fluorescence) conjugated Annexin V, and analysed by flow cytometry.

Four subset populations of cells will appear on a dot plot graph of Annexin V versus PI. Cells which remain unstained are healthy cells. Cells which stain with just Annexin V

are undergoing early apoptosis. Cells which stain with just PI are necrotic cells and cells which stain with both Annexin V and PI are cells which have entered late apoptosis. These four subsets can be divided using a quadrant grid and the percentage of cells in each quadrant can be calculated.

In order to first calibrate the position of the four quadrants, for each of the cell lines, a known healthy population of cells had to be compared to an acknowledged apoptotic population of cells. Staurosporine is a tyrosine kinase inhibitor which is a known potent inducer of apoptosis. Cells were treated with 2μM staurosporine or drug vehicle control for 24h. All cells including any cells which were floating in the media, which were most likely dead, were harvested and processed for apoptosis analysis as described in section 3.6. A BD FACSCalibur flow cytometer was used and the data were analysed on CellQuest Pro Software.

As seen in Figure 5.3.1 staurosporine induced apoptosis in UM-SCC 5, 12, 17A and 81B, increasing the amount of cells in the apoptotic state by 82.5%, 71%, 89% and 89% respectively. Following calibration, the defined quadrants were used in order to investigate the level of apoptosis induced in these series of experiments.

Cells were treated for four days with either EGF-SubA at 300pM, or with cisplatin at 2μM, or in combination, or with drug vehicle control. Fresh drugs and media were

replaced daily. As in the calibration experiments, all cells including any cells which were floating in the media, which were most likely dead, were harvested and processed for apoptosis analysis as described in section 3.6. A BD FACSCalibur flow cytometer was used and the data were analysed on CellQuest Pro Software.

EGF-SubA can be seen to induce apoptosis in all four cell lines (Figure 5.3.2). The percentage of apoptotic cells compared to controls increased by: 9% in UM-SCC 5, 21% in UM-SCC 12, 45% in UM-SCC 17A and 12% in UM-SCC 81B.

Similarly cisplatin also induced apoptosis in all four cell lines (Figure 5.3.2). The percentage of apoptotic cells compared to controls increased by: 24% in UM-SCC 5, 23% in UM-SCC 12, 58% in UM-SCC 17A and 28% in UM-SCC 81B.

When EGF-SubA was combined with cisplatin the percentage of apoptotic cells compared to cells treated with either cisplatin alone or EGF-SubA alone increased by at least: 19% in UM-SCC 12, 21% in UM-SCC 17A and 8% in UM-SCC 81B(Figure 5.3.2). However no further increase in the percentage of cells undergoing apoptosis was observed in UM-SCC 5 when EGF-SubA was combined with cisplatin as opposed to cells treated with either cisplatin alone or EGF-SubA alone.

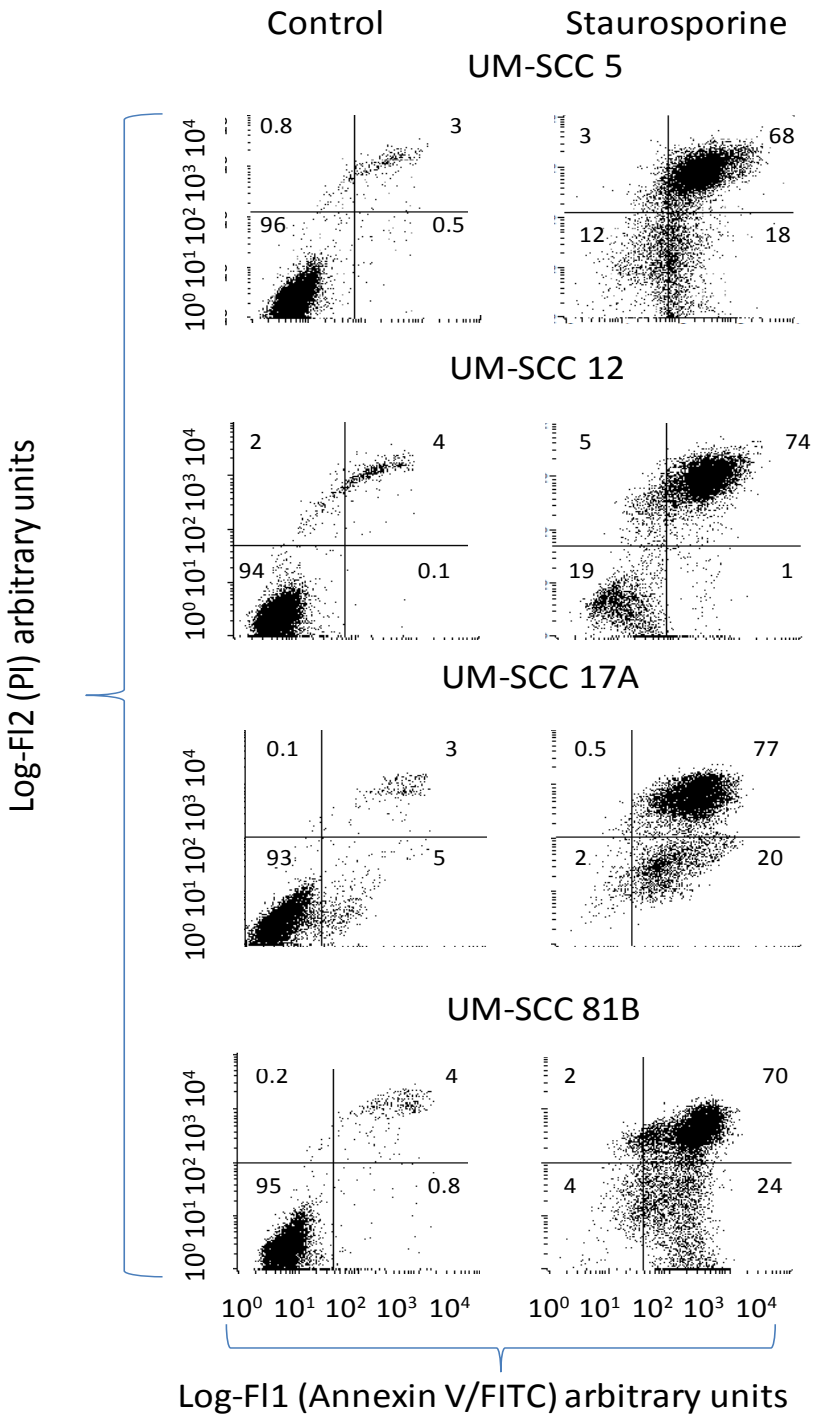

Figure 5.3.1 Staurospine induces apoptosis in UM-SCC cells.

Cells were treated with either 2μM staurosporine, which is a known apoptotic inducing agent, or drug vehicle control for 24h in order to calibrate the quadrants for further apoptosis studies. Cells were analysed for signs of apoptosis using Annexin V/PI staining followed by flow cytometry. Data were processed on CellQuest Pro Software. Upper left quadrant shows necrotic cells (Annexin V –ve/ PI +ve), lower right shows healthy population of cells (Annexin V –ve/ PI –ve), upper right shows cells which have entered late apoptosis (Annexin V +ve/ PI +ve), and lower right quadrant shows cells which are entering early apoptosis (Annexin V +ve/ PI –ve). Numbers represent the percentage of cells in each quadrant.

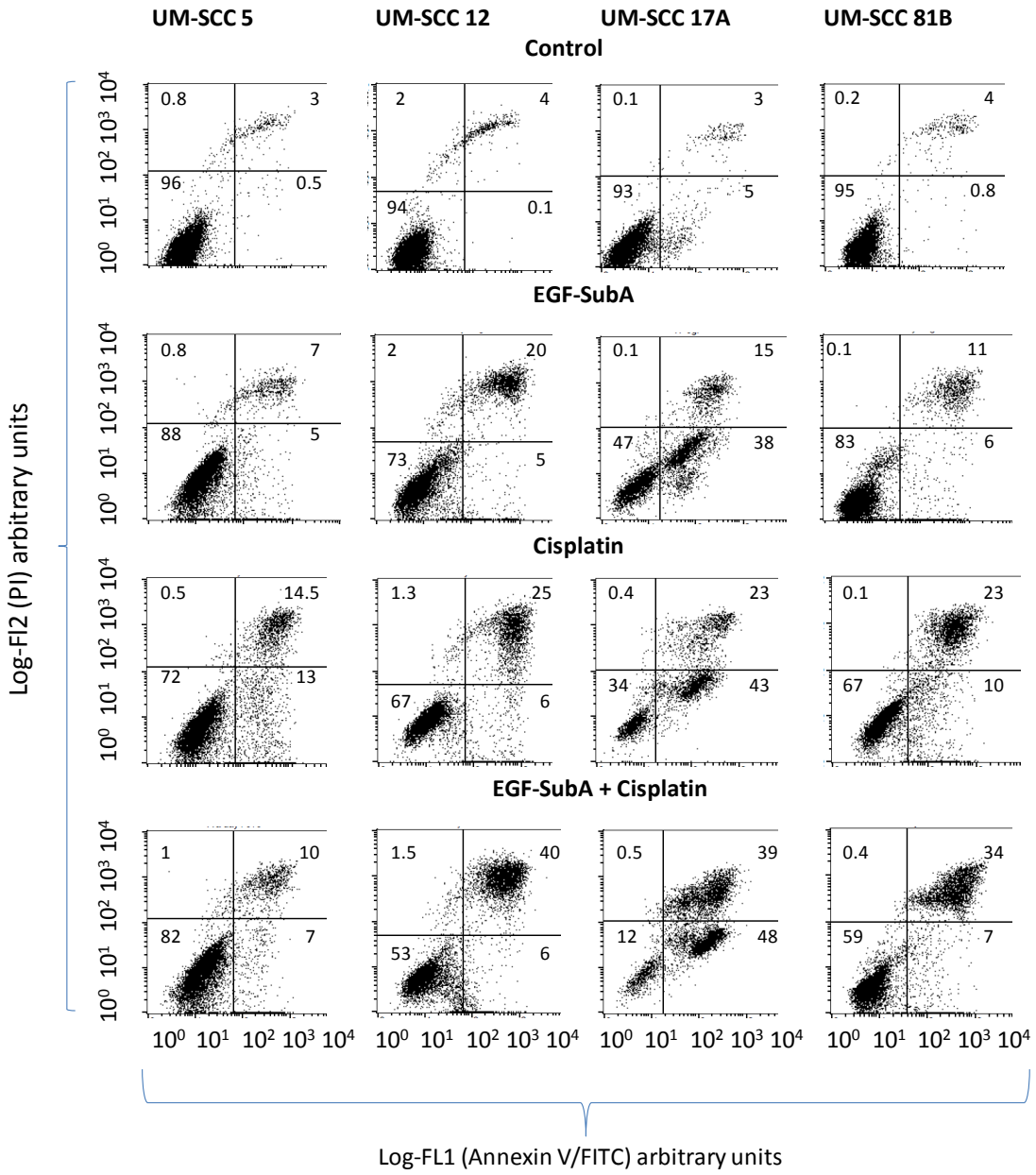

Figure 5.3.2 Apoptosis assays measuring the effects of either EGF-SubA, or cisplatin, or in combination, upon UM-SCC cells.

Cells were treated with either EGF-SubA at 300pM, or with cisplatin at 2μM,or in combination or with drug vehicle control For 4 days. Apoptosis was assessed using Annexin V/PI followed by flow cytometry. Data was processed on CellQuest Pro Software with numbers representing the percentage of cells in each quadrant.

5.4 **EGF-SubA acts as radiosensitising agent.**

Radiation therapy is one of the main treatment modalities for head and neck cancer. Radio-sensitizing agents may help in reducing the known side effect of radiotherapy such as xerostomia, mucositis and dermatitis, by facilitating a decrease in the overall dose of radiation required to achieve a desired effect.

Up-regulation of transmembrane protein EGFR in SCCHN is implicated in radioresistance. A correlative study was performed, by Ang and colleagues, which examined EGFR levels in patients with advanced head and neck cancer who had undergone radiotherapy (51). Patients who had low levels of EGFR had significantly greater overall survival rates, disease frees survival, and local regional control (51). Cetuximab which blocks the EGFR proliferative pathway has been shown to be a radiosensitising agent. A study by Liang and colleagues demonstrated that there was increased radioresistance in clones over expressing EGFR compared to parental lines and that radioresistance was reduced with the addition of cetuximab (61). Therefore other drugs which result in the decrease of EGFR levels may also act to enhance the effects of radiation.

The endoplasmic reticulum (ER) is a site which processes many proteins which are destined for the cell membrane. As GRP78 is a protein chaperone responsible for the correct folding of nascent proteins which enter the ER we investigated whether cleavage

of GRP78 via EGF-SubA could lead to the reduction of the transmembrane protein EGFR. UM-SCC cells were treated with either EGF-SubA at 1nM for 24 h or drug vehicle control. Subsequent western blot analysis revealed that EGF-SubA was able to reduce EGFR protein levels in UM-SCC 10A, 5, 11B, and 12 (Figure 5.4.1).

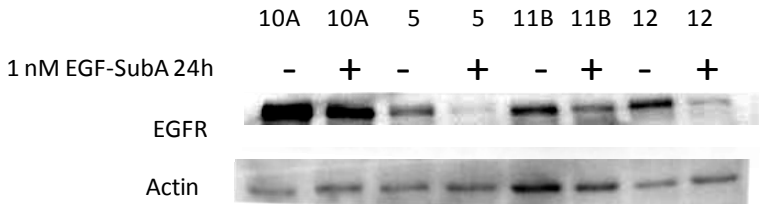

Figure 5.4.1 EGF-SubA reduces EGFR levels.

Western blot analysis of UM-SCC 10A, 5, 11B and 12 treated with either EGF-SubA at 1nM or drug vehicle control for 24h. All lanes were loaded with 35 µg protein. Blots were probed with EGFR at 3 µg/ml and actin 3 µg/ml (protein loading control).

In addition, several studies have associated elevated GRP78 per se with a radio resistant phenotype. Lin and colleagues in 2010, and Feng and colleagues in 2010, found GRP78 to be up-regulated in clones which were able to survive a higher dose of ionising radiation compared to their parental cell lines (3, 8). Feng and colleagues also found up-regulation of GRP78 in radio resistant nasopharyngeal carcinomas thereby implying the possibility that elevated GRP78 could act as a biomarker of radiosensitivity. Lee and colleagues in 2008, found that silencing of GRP78 via transfection with siRNA against GRP78, significantly enhanced the sensitivity of glioblastoma cells to radiation (108).

Several lines of evidence from data presented in this thesis suggest that EGF-SubA may be a radiosensitising agent. As seen in Figure 5.4.1, EGF-SubA is capable of down regulating EGFR as well as cleaving GRP78 (see Figure 4.1.1). High levels of EGFR and GRP78 are implicated in radioresistance and therefore any reduction in their levels may be expected to confer radiosensitivity. We have also shown that EGF-SubA leads to G1 cell cycle arrest (see Figure 4.5.1). Cells in G1 are known to be more sensitive to radiation compared to cells in S phase (150). Following on from these findings we investigated whether pre-treatment with EGF-SubA was able to radiosensitise UM-SCC cells.

In order to test radio sensitisation *in vitro*, a clonogenic assay was used as described in section 3.11. Loss of p53 function has been associated with chemo- and radioresistance (153). Therefore, we examined a variety of UM-SCC cells of differing p53 status, to determine whether or not any potential radiosensitising effects of EGF-SubA observed were present regardless of p53 status (149). As described previously, the cell lines studied were UM-SCC 17A which is wild-type for p53, UM-SCC 12 which is p53 null (homozygous Q104X), UM-SCC 81B which has no alleles which are wild-type p53 (mutant H193R) and UM-SCC 5 which has one wild-type p53 allele and a single p53 mutation (heterozygous V157F).

Pilot studies were performed in order to establish the highest drug concentration applied over 24 hours, which cells could tolerate as measured by survival fractions equal to that of drug omitted controls. UM-SCC 12, 17A and 81B were able to tolerate an EGF-SubA dose of 10pM without differences in survival fraction as compared to controls. UM-SCC 5 treated with 10pM EGF-SubA without radiation had a survival fraction below the control and so cells were treated with a 3pM dose of EGF-SubA. UM-SCC cells were pre-incubated with EGF-subA or appropriate drug vehicle control for 24h before being irradiated with 0, 1, 2, or 4 Gy. Cells were then seeded in triplicate into six well plates, in normal growth media without drug and monitored for colony formation for 2-3 weeks.

Colonies were counted using a light microscope. The mean number of colonies were recorded for each set of triplicate samples. Survival fractions were calculated and radiation survival curves were fitted according to the linear-quadratic model $S(D)/S(0)=\exp(-(\alpha D + \beta D^2))$, where D is the irradiation dose in Gy; α is the cell kill per Gy of the initial linear component and β is the cell kill per Gy^2 of the quadratic component of the survival curve. SPSS PASW statistics package version 18 was used to find values of α and β and survival curves were plotted as seen in

Figure 5.4.2

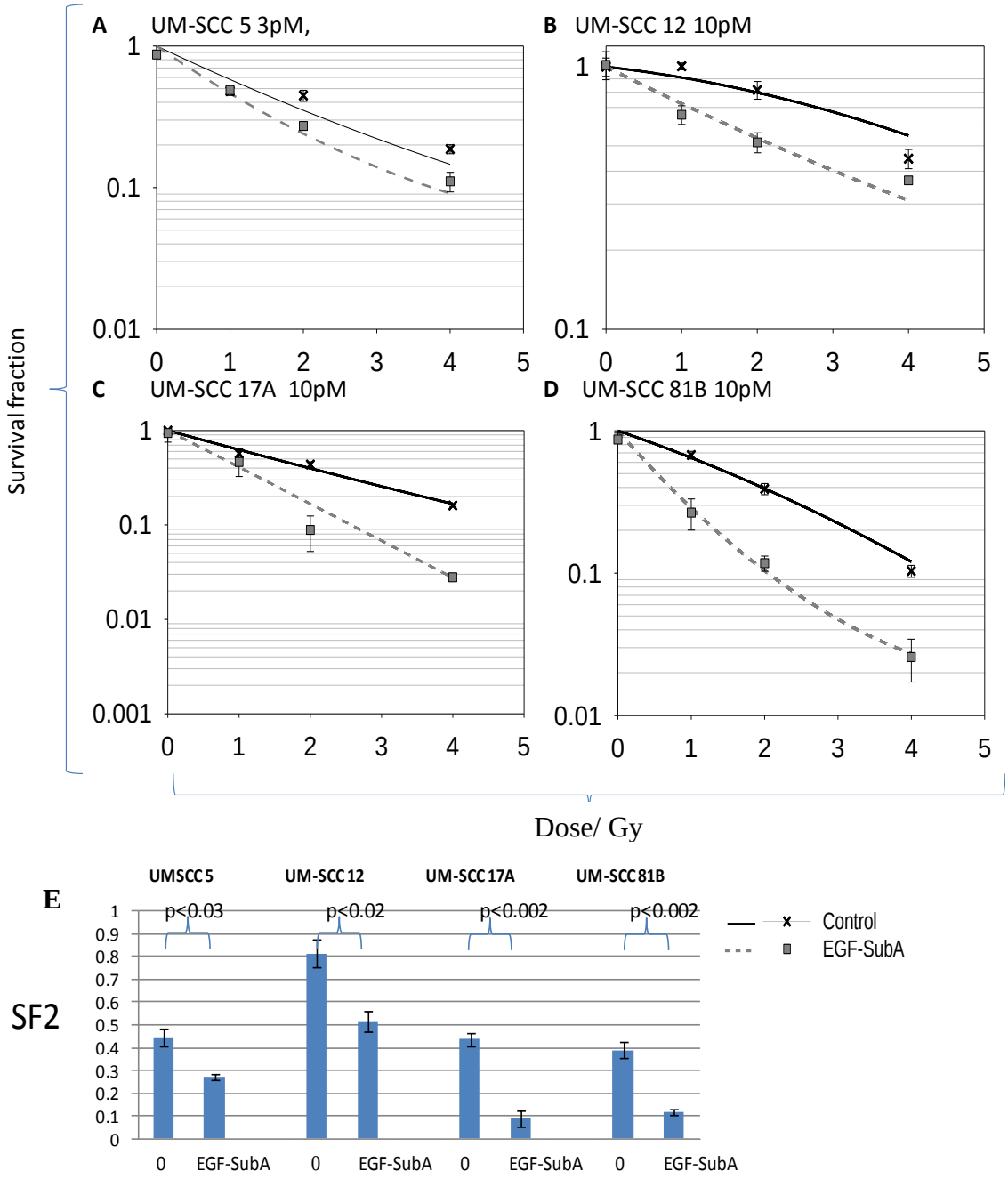

Figure 5.4.2 EGF-SubA is able to radiosensitise UM-SCC cells regardless of p53 status.

UM-SCC cells were pre-treated for 24h with EGF-SubA at either 3 or 10pM or drug vehicle control and then exposed to γ-irradiation at 0, 1, 2, or 4 Gy as indicated. Clonogenic assays were established to allow for colony formation over a time period of two to three weeks. A colony was defined as equal to or more than 50 cells in order to allow for at least five cell doubling times. Crosses and squares indicate means of three survival fractions for each data point with appropriate s.e.m. Survival curves were then fitted to the quadratic equation $S(D)/S(0)= \exp(-(\alpha D + \beta D^2))$*. (E) Bar charts showing survival fractions at 2 Gy with and without EGF-SubA. Unpaired Student's t test was used to calculate differences in SF2 between controls and treated cells.*

EGF-SubA was able to radiosensitise UM-SCC cells, regardless of p53 status as shown in

Figure 5.4.2. At 2 Gy the survival fraction was significantly reduced by 17% ($p<0.03$), 30% ($p<0.02$), 34% ($p<0.002$), 27% ($p<0.002$) in UM-SCC 5, 12, 17A and 81B respectively as compared to controls.

From previous experiments in section 5.1 it was seen that EGF-SubA acted synergistically with cisplatin in reducing cell viability/growth, therefore it was investigated whether EGF-SubA in combination with cisplatin could further enhance the effects of radiation. Pilot studies were performed in order to establish the highest combined drug concentrations that cells could tolerate for 24h without radiation as measured by survival fractions equal to that of drug omitted controls. UM-SCC 5cells were pre-incubated with either EGF-SubA at 3pM alone, or with cisplatin at 1μM alone, or both drugs in combination, or with drug vehicle control for 24h before being irradiated with 0, 1, 2, or 4 Gy. Cells were then seeded in triplicate into six well plates, in normal growth media without drugs and monitored for colony formation for 2-3 weeks.

Clonogenic assays were set up as described in section 3.11. SF2 of EGF-SubA was 17% lower than controls ($p=0.027$), SF2 of cisplatin was 21% lower than controls ($p=0.046$).

When EGF-SubA was combined with cisplatin the SF2 was 24% lower than controls ($p=0.008$) as seen in Figure 5.4.3. Although EGF-SubA combined with cisplatin reduced the survival fraction by a further 3% as compared to when cisplatin was used alone this difference was not significant ($p=0.6$)

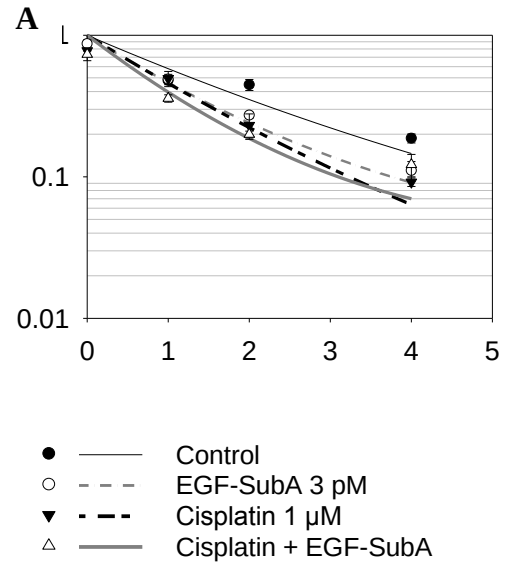

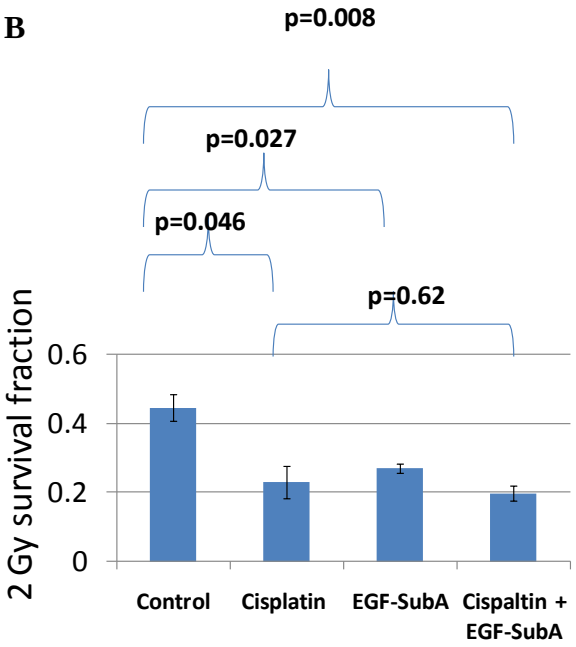

Figure 5.4.3 EGF-SubA in combination with cisplatin does not significantly enhance the effect of radiation any further than when these drugs are used independently.

(A) UM-SCC 5 cells were pre-treated for 24h with either EGF-SubA at 3pM, or cisplatin at 1μM, or in combination, or drug vehicle control and then exposed to γ-irradiation at 0, 1, 2, or 4 Gy as indicated. Clonogenic assays were established to allow for colony formation over a time period of two to three weeks. A colony was defined as equal to or more than 50 cells in order to allow for at least five cell doubling times. Circles and triangles indicate means of three survival fractions for each data point with appropriate s.e.m. Survival curves were then fitted to the quadratic equation $S(D)/S(0)= \exp(-(\alpha D + \beta D^2))$*. (B) Bar charts showing survival fractions at 2 Gy with and without EGF-SubA. Unpaired Student's t test was used to calculate statistical differences in SF2 between various treatment groups.*

6 Discussion

Protein chaperone GRP78, a key component of the Unfolded Protein Response which is induced as part of a survival response under certain conditions of stress common in cancer (hypoxia/hypoglycaemia), has been shown to be up-regulated in a wide variety of cancers(1, 4). The up-regulation of GRP78 in tumours has been associated with poor survival outcome as well as increased resistance to current cancer therapies (1, 8, 97, 120). Thus we examined GRP78 expression in head and neck cancers. In addition to this we investigated the impact of a novel compound EGF-SubA, which promotes proteolysis of GRP78. EGF-SubA was tested upon a panel of LSCC cells, *in vitro*, used alone and in combination with clinically relevant agents.

6.1 Validation of anti-GRP78 antibody for use in IHC

Currently there are no published data regarding GRP78 expression levels in patients with laryngeal cancers which constitute the largest sub group of head and neck patients or in and oropharyngeal and hypopharyngeal tumours (10). Immunohistochemical (IHC) staining of a tissue micro array (TMA) was used in order to determine GRP78 expression levels in laryngeal, oropharyngeal and hypopharyngeal squamous cell carcinoma tissues compared to histologically normal adjacent tissue samples.

The position and intensity of DAB staining in IHC is meant to be representative of the location and quantity, respectively, of the protein of interest, however this is based on the ‘assumption that both the primary and secondary antibodies are selectively bound to their targets’ (163).

Antibodies may cross-react with other proteins and therefore it is important to first validate the antibody specificity prior to IHC via other techniques such as western blot. An initial BLAST search confirmed that the GRP78 protein shares 65% amino acid identity with HSP72. Therefore there is a strong possibility that a specific epitope on GRP78 which is recognised by an antibody will also be present on HSP72.

One of our initial objectives was to find an antibody for IHC, which was specific for GRP78 and did not cross-react with other proteins. First the specificity of anti-GRP78 antibody (sc-1050) was tested via western blot as this antibody had been previously used in the IHC head and neck study by Feng et al.,(3). As mentioned in section 1.3.11, SubA is only known to cleave protein GRP78 (a 72kDa protein) (7). Cleavage of GRP78 by SubA results in 44 and 28 kDa fragments. Therefore we used EGF-SubA to test the specificity of anti-GRP78 antibodies since following treatment with EGF-SubA we would expect a reduction in the intensity of the 72kDa band on a western blot and the appearance of a band corresponding to one or the other cleavage products of GRP78.

The western blot in Figure 4.1.1 shows two bands between marker weights of 58 kDa and 80 kDa. Upon application of EGF-SubA the slower migrating band, which was thought to be GRP78, disappeared and a new band appeared between marker weights of 30 kDa and 46 kDa. It appears likely that the new band was the 44 kDa cleaved product of GRP78, which contains the N-terminus recognised by the anti-GRP78 antibody (sc-1050).

The anti-GRP78 antibody (sc-1050) appeared to strongly cross-react with an unknown protein running just ahead of the uncleaved GRP78 band between marker weights of 58 kDa and 80 kDa. Furthermore, intensity of this band was not altered by the application of EGF-SubA. If this antibody was used as a primary antibody for IHC, it would mean that analysis of GRP78 expression in the TMA would be unreliable, as IHC staining would be indistinguishable between GRP78 and the unknown protein. Therefore this antibody was deemed unsuitable for use in IHC.

Next, the specificity of anti-GRP78 (sc-13968), rabbit polyclonal antibody, as a possible antibody for IHC was examined by western blot. Gels were loaded with the lysates from the same samples as used in the western blots shown in Figure 4.4.1. In order to determine whether anti-GRP78 antibody (sc-13968) cross-reacted with any other

protein, whole membranes were blotted with anti-GRP78 antibody (sc-13968). As seen in Figure 4.1.2, anti-GRP78 antibody (sc-13968) revealed a band which lay between marker weights of 58 kDa and 80 kDa. Upon application of EGF-SubA this band disappeared, therefore it was deduced that this band was GRP78 and a new band between marker weights of 23 kDa and 30 kDa appeared. The new band appears to be the 28 kDa cleaved carboxyl-terminal fragment of GRP78 which contains the epitope recognised by this antibody. Apart from the bands believed to be those of GRP78 and cleaved GRP78 no other bands were visible, therefore it was concluded that there was considerably less cross-reactivity to other proteins with anti-GRP78 antibody (sc-13968) compared to (sc-1050).

As previously mentioned incubating membranes with anti-GRP78 antibody (sc-1050) revealed a non-specific band migrating just ahead of the main GRP78 band, as seen in Figure 4.1.1, which was not affected by EGF-SubA. As HSP72 and GRP78 antibody share 65% identity and are of similar molecular weight, it appears likely that this non-specific band was HSP72. In order to identify whether anti-GRP78 antibody (sc-1050) cross-reacted with HSP72, an HSP90 inhibitor was used. HSP90 inhibitors AT13387 competitively prevents ATP binding to the N-terminus of HSP90 (135). This results in the disruption of the inhibitory interaction of HSP90 with the transcription factor, heat shock factor (HSF) (136). Upon HSP90 inhibition HSF induces up-regulation of HSP72. Furthermore, HSP90 inhibition leads to proteasomal degradation of HSP90 client

proteins such as EGFR (137). Thus with HSP90 inhibitors an increase in HSP72 levels and a decrease in EGFR levels is observed. See Appendix section 7.2 for a review of HSP90 inhibitors.

UM-SCC 81B cells were treated with HSP90 inhibitor AT13387 at 1μM for 24h(135). SDS-PAGE followed by western blot analysis was used to identify whether or not HSP72 induction could be detected by anti-GRP78 antibody (sc-1050). As presented in Figure 4.1.3, HSP72 was detected using anti-HSP72 antibody in lanes 1 and 2. Comparing lanes 1 and 2 it is clear that treatment with AT13387 lead to HSP72 induction as expected. Furthermore, there was a reduction in EGFR levels in lane 2 compared to lane 1, again, as expected.

Using anti-GRP78 antibody (sc-1050) a strong signal was detected in untreated cells in lane 5, which was located at the same position as HSP72 in lanes 1 and 2. Furthermore, this band was induced when cells were treated with AT13387, as shown in lane 6, with a stronger signal being emitted from this band compared to GRP78. This almost certainly indicates that there is significant cross-reaction of the anti-GRP78 antibody (sc-1050) with HSP72. Therefore, studies which have reported the expression of GRP78 via the use of immunohistochemical staining with anti-GRP78 antibody (sc-1050) may not be reliable.

Using anti-GRP78 antibody (sc-13968), GRP78 was the only protein detected in untreated cells present in lane 3. In cells treated with AT13387 a weak signal was visible running just ahead of GRP78, which was at the same position as HSP72 in lanes 1 and 2. However, the majority of the signal was derived from the GRP78 protein. Results presented in this thesis indicate that anti-GRP78 antibody (sc-13968) appears to be less cross-reactive with other proteins and may therefore be a more suitable antibody for IHC than anti-GRP78 antibody (sc-1050). Although there is one commercially available monoclonal antibody to GRP78 sold by Abcam (ab12223), which in theory could be more specific to GRP78 than equivalent polyclonal antibodies, Abcam has shown that it cross-reacts considerably with GRP94 (164). Therefore it was decided to proceed with anti GRP78 antibody sc-13968 for use as the primary antibody for IHC.

Prior to performing IHC on the TMA, the anti-GRP78 antibody (sc-13968) was tested on sections of SCCHN tissue samples as shown in Figure 4.3.1. Omission of the primary antibody was used in order to test the specificity of the secondary antibody as shown in Figure 4.3.1A . Without the primary antibody there was no DAB staining. A different section from the same tumour block was then incubated with the primary antibody. Figure 4.3.1D at 400X original magnification shows homogeneous cytoplasmic staining with no staining within the nucleus, in accordance with expected the localisation of GRP78 in the cell (4).

6.2 GRP78 is significantly up-regulated in SCCHN

GRP78 levels were significantly higher in the tumour tissue samples (n=45) compared with matched histologically normal tissue samples (n=45). 84% of tumour cores versus 24% of histologically normal cores were given a staining score of either 2 (moderate staining) or 3 (strong staining) ($p_{(X^2)}<0.001$). See Table 4.3.1 for more details. These findings are in line with the study by Du et al., where it was found that GRP78 levels were significantly higher in oesophageal squamous cell carcinoma tissue compared to normal histological tissue ($p = 0.047$).

6.3 GRP78 can be induced in typical tumour microenvironmental conditions, *in vitro*

As mentioned in the literature review section, 1.3.2, GRP78 binds to PERK, IREα1,and ATF6 under 'non stress' conditions thus suppressing the Unfolded Protein Response (133). Under 'stressed' conditions such as low ATP availability (due to low availability of both oxygen and glucose which are typical of the tumour microenvironment) or excess protein production, unfolded proteins accumulate. GRP78 preferentially binds to these unfolded proteins resulting in GRP78 disassociating from PERK, IREα1 and ATF6. In turn this causes the activation of the Unfolded Protein Response. Under such UPR-activating conditions ATf6 is now free to act as a transcription factor inducing the up-regulation of GRP78 (133).

Hypoxia has been detected in 78% of head and neck squamous cell carcinoma tumours (141). Hence, this may be one of the reasons why GRP78 is significantly up-regulated in these tumours. Hypoxia is defined as an oxygen concentration lower than 3% compared to normal tissue, which on average has a range between 4 and 9% (140). Normal tissue typically contains glucose levels of 5 mM, whilst in many tumours this can range from anywhere between 0 and 2 mM (83).

In order to determine whether GRP78 is induced in the above typical tumour environment s UM-SCC cells were grown in hypoxic (less than 2% O_2) (142) and low glucose conditions (less than or equal to 2 mM glucose) (139). All UM-SCC laryngeal squamous cell carcinoma cell lines, that were tested, demonstrated induction of GRP78 in conditions of low oxygen and low glucose compared to controls, as seen in Figure 4.2.1. The only exception to this was in UM-SCC 81B which when grown in 2% O_2 showed no further increase in GRP78 levels. However GRP78 was induced in UM-SCC 81B when grown in 0.4g/l glucose. In 0.4g/l glucose and also in 2% O_2, GRP78 expression was increased by a minimum of two fold, as measured by densitometry, in UM-SCC cells 5, 11B, and 12.

6.4 Analysis of whether GRP78 protein levels may be a prognostic indicator for SCCHN

Survival analysis based on data from 190 SCCHN patients was performed using Kaplan-Meier method and statistical differences between curves were compared using log-rank test. As expected SCCHN patients with stage 1 or stage 2 tumours had a significantly better five year survival compared to patients with stage 3 or 4 tumours ($p_{(\log rank)} < 0.001$), as shown in Figure 4.3.3A. Furthermore patients without nodal involvement survived significantly longer than patients with nodal spread ($p_{(\log rank)} = 0.005$) (Figure 4.3.3B). These findings are in line with previous studies which have also found high tumour stage and nodal involvement to be associated with poor survival outcome. (143, 144).

Several studies have reported that up-regulation of GRP78 is associated with poor survival outcome in a variety of tumours including: hepatocellular carcinoma (HCC) (130), pancreatic adenocarcinoma (132), breast cancer (112), melanoma (133), oesophageal adenocarcinoma (120), glioblastoma (108), lung cancer (134) and prostate cancers (129). Here for the first time it was determined whether up-regulation of GRP78 was associated with poor survival outcome in tumours of the larynx, hypopharynx and oropharynx.

The Kaplan Meier 2 year survival analysis of SCCHN patients (n=190) showed that GRP78 up-regulation was significantly associated with lower survival rates ($p_{(log\ rank)}$ = 0.032) (Figure 4.3.4B). Although log-rank is useful in comparing differences in survival in two or more groups on non-parametric censored data, multivariate Cox regression analysis is needed in order to compare the influence of several risk factors upon survival outcome at the same time (145).

As expected upon multivariate Cox regression analysis tumour stage (p = 0.004), nodal status (p = 0.005) and recurrence (p = 0.001) were found to be significant independent factors in determining two year survival. Patients with high tumour stages of 3 and 4 had an increased hazard ratio of 2.5 compared to patients with stage 1 and 2 tumours. Similarly patients with tumours with nodal involvement had worse prognosis with a hazard ratio of 2.6. Although high GRP78 levels are suggestive of poorer survival outcome with a hazard ratio of 2.04 this finding is not statistically significant (p=0.069).

As there may be different pathologies involved between the different sub-groups of SCCHN, subsets of this cohort were analysed separately. Upon log rank analysis both five- and two-year survival were significantly higher for laryngeal patients (n=92) with low-expressing GRP78 tumours (p=0.028 and p=0.006 respectively) as shown in Figure 4.3.5. Upon multivariate analysis only nodal status (p = 0.041) was a significantly independent predictor of survival where patients with nodal involvement had an increased hazard ratio of 2.3 compared to patients without nodal involvement.

Unexpectedly tumour stage (p = 0.376) was no longer a significant predictor of survival outcome. Although high GRP78 levels are suggestive of poorer survival outcome with a hazard ratio of 7.3 this finding is just below being statistically significant (p=0.052). A larger sample of laryngeal squamous cell carcinoma patients may be needed in order to clarify whether or not GRP78 as well as tumour stage may be suitable prognostic biomarkers. Alternatively GRP78 may not, when used in isolation, be a suitable prognostic biomarker for predicting survival outcome.

Prognostic biomarkers predict individual patient outcome, regardless of disease management, 'distinguishing between good outcome tumours from poor outcome tumours' (146). In this way prognostic biomarkers may help to decide which patients to treat or what modality to use as well as the aggressiveness of the treatment regime (146). Results presented within this thesis have shown that GRP78, although up-regulated in tumours compared to histologically normal tissue, may not be a significant independent prognostic biomarker. Zhuang et al., also found upon log rank analysis, that patients with high GRP78 expression in melanomas had significantly lower overall survival compared to patients with low GRP78 expression (p=0.0123) (133). However, when multivariate analysis was performed by Zhuang et al., GRP78 was no longer a significant independent factor in determining survival (p=0.178). It seems likely that the simultaneous use of multiple biomarkers may be more suited in predicting patient outcome as opposed to reliance on one single biomarker. For example multigene

expression tests such as MammaPrint (Agendia) can be used to assess whether, after surgery, breast cancer patients, should receive adjuvant therapy or not, in order to avoid relapse (146). A similar 'multiple biomarker' approach may be also more applicable for head and neck cancers.

Furthermore, there were no significant differences between survival rates of patients with low versus high GRP78 expressing tumours of the oropharynx or hypopharynx upon log rank analysis. This could be due to different pathologies involved in the various sub-sites. For example it is known that SCCHN patients with HPV are more responsive to chemo- and radiation therapy($p \leq 0.05$) compared with HPV negative patients and have better survival outcome (19, 21). Therefore HPV infection which is more prevalent in oropharyngeal tumour compared to laryngeal tumours would be of greater prognostic value in such tumour sub-sites

6.5 EGF-SubA is toxic to laryngeal squamous cell carcinoma cells at pM concentrations, and induces G1 arrest and apoptosis.

A study by Daneshmand and colleagues showed that GRP78 was up-regulated in approximately two thirds of prostate cancer patients and this up-regulation was associated with higher risk of clinical recurrence (relative risk=2 p=0.001) and death (relative risk=1.8 p=0.024) compared to patients with low GRP78 expression (165). Hence there is an indication that GRP78 may have a role in tumour development and treatment resistance. A study by Fu and colleagues in 2008 reported that homozygous deletion of GRP78 in the prostates of mice lead to suppression of prostate tumour development and growth (97). All mice, in the study, had inactive form of the *phosphatase and tensin* gene (*PTEN*). Inactivation of PTEN is a common occurrence in prostate cancers and leads to excessive stimulation and phosphorylation of the PI3K/AKT pathway and subsequent enhanced cell growth and proliferation (see section 1.2.1 for a review of the EGFR signalling pathway). All of mice with PTEN inactivation developed tumours within 12-20 weeks of birth. Whilst none of the eight mice with both PTEN inactivation and GRP78 double allele knockout developed any tumours or precancerous lesions (97).

A study by Dong and colleagues in 2009 (98), compared mammary tumour development in mice that were GRP78 homozygous +/+ to heterozygous GRP78 +/- mice. All mice expressed the polyoma middle T oncogene (PyT) (98). Tumours were first detectable around 8-10 weeks in the homozygous group but in the heterozygous group tumours were detectable between 10-12 weeks . Furthermore tumour size was reduced by 60% in the heterozygous group as compared to the homozygous group ($p<0.001$). Hence even partial reduction in GRP78 may be sufficient to impede tumour growth and size (98).

Results presented in this thesis have shown that GRP78 is both significantly up-regulated in head and neck squamous cell carcinoma patients, as well as being induced *in vitro* under typical tumour micro-environmental conditions of hypoxia and low glucose. Induction of GRP78 may offer tumours a protective role, therefore making GRP78 advantageous for tumorigenesis. Previous studies by Fu and colleagues and Dong and colleagues indicate that loss or reduction of GRP78 expression suppresses tumour development (97, 98). Hence EGF-SubA may offer a novel way, through cleavage of GRP78, of suppressing the growth and development of cancers.

Here we determined whether EGF-SubA was able to impede the growth of laryngeal sqaumous cell carcinoma cells, *in vitro*.

In vitro studies were focused on laryngeal squamous cell carcinoma (LSCC) for two reasons. Firstly, laryngeal carcinoma patients are the largest sub-groups of head and neck patients, and secondly, to avoid the issue of confounding factors caused by the differences in pathogenesis and prognosis, due in part to HPV status, of different anatomical sub-sites (166) .

Cell proliferation assays revealed that EGF-SubA IC_{50} levels were between 4 and 100pM in UM-SCC laryngeal squamous cell carcinomas (Figure 4.4.1). This IC_{50} range is comparable to the results of the study by Backer and colleagues who tested EGF-SubA on prostate PC3 and breast MDA231luc cancer cells and found IC_{50}s of 1 and 30pM, respectively (5).

In order to explore how EGF-SubA may stop the proliferation of UM-SCC cells, cell cycle analysis and apoptosis assays were performed.

The conventional method to perform cell cycle analysis of DNA content is by PI staining of fixed permeabilised cells. However, because of the overlapping DNA content of G1 with early S phase, and late S with G2 and M phases, it is hard to accurately distinguish between these . Bromodeoxyuridine (BrdU) is a thymidine analogue which can be incorporated into DNA during DNA synthesis (S phase). Flow cytometry can then detect the quantity of BrdU via the use of anti BrdU antibodies conjugated with

FITC. BrdU-PI double staining easily differentiates between overlapping DNA content of S phase fractions whilst at the same time quantifying the amount of cells in G1 and G2.

Currently there are no studies which have investigated the effect of SubA on cell cycle analysis via the BrdU-PI double staining method. Here, this method was performed simultaneously alongside the conventional fixed and permeabilised cell staining with PI to produce DNA histograms. We examined a variety of UM-SCC cells of differing p53 status to determine whether or not any impact of EGF-SubA upon the cell cycle was independent of p53 status (149). The cell lines studied were UM-SCC 17A which is wild-type for p53, UM-SCC 12 which is p53 null (homozygous Q104X), and UM-SCC 5 which has one wild-type p53 and a single p53 mutation (heterozygous V157F) .

EGF-SubA was able to induce G1 arrest regardless of p53 status, as shown in Figure 4.5.1 and Figure 4.5.2. The amount of cells in G1 after treatment with EGF-SubA in UM-SCC 17A, 12 and 5 increased by 19%, 7%, and 5%, respectively, as analysed by PI staining of fixed permeabilised cells and 37%, 26% and 6%, as deduced by BrdU-PI double staining. As expected for a G1 arrest, there was a reduction in cells entering S phase. The percentage decreases in the S phase cell fraction after treatment with EGF-SubA as compared to controls in UM-SCC 17A, 12 and 5 were 10%, 9%, and 5% respectively, as analysed by PI staining of fixed permeabilised cells and 46%, 19% and

12%, as deduced by BrdU-PI double staining. This observation may be important since it has been reported by Pawlik and colleagues that cells in G1 are twice as radiosensitive as cells in S phase and therefore EGF-SubA may act as a radiosensitiser (150). The potential for EGF-SubA as a radiosensitiser was explored in Results section 5.4.

Morinaga and colleagues observed a decrease in basal levels of cyclin D1 as well as G1 cell cycle arrest after application of SubA *in vitro* in Hela and Vero cells (141). As cyclin D1 is important in order to allow for cell cycle progression from G1 to S phase it was proposed that loss of cyclin D1 through SubA was the mechanism behind G1 arrest (148).

Phosphorylation of cyclin D1 is required for ubiquitin targeted proteasomal degradation. Upon SubA increased levels of phosphorylated cyclin D1 was observed. Furthermore the use of proteasomal inhibitor MG132 suppressed downregulation of cyclin D1 by SubA. Thus implying that SubA may indirectly induce the proteasomal degradation of cyclin D1.

Our research has shown that cells treated with EGF-SubA have reduced levels of EGFR expression, as shown by western blot analysis in Figure 5.4.1.As part of future investigations it would be interesting to determine whether exposure to EGF-SubA leads to proteasomal degradation of EGFR. This could be in part determined by whether

proteasomal inhibitor MG132 could suppress the down regulation of EGFR upon exposure to EGF-SubA. .

Backer and colleagues observed an increase in activated caspase 3 in prostate carcinoma cells when treated with EGF-SubA, thus suggesting that this drug can induce apoptosis(5). In order to confirm whether EGF-SubA was able to induce apoptosis in LSCC cells the Annexin V-PI apoptosis assay was used. The main advantage of this assay over simply monitoring levels of PARP or caspase 3 is that the fraction of cells which are healthy, undergoing early apoptosis, late apoptosis, or necrosis can be quantified.

p53 is known to be a key regulator of pro-apoptotic proteins such as Puma and Noxa (100). Therefore, we examined a variety of UM-SCC cells of differing p53 status to determine whether or not any impact of EGF-SubA upon induction of apoptosis was independent of p53 status (149). The cell lines studied were UM-SCC 17A which is wild-type for p53, UM-SCC 12 which is p53 null (homozygous Q104X), UM-SCC 81B which is p53 mutant (H193R) and UM-SCC 5 which has one wild type p53 allele and a single p53 mutation (heterozygous V157F).

EGF-SubA can be seen to induce apoptosis in all four cell lines regardless of p53 status (Figure 5.3.2). The percentage of apoptotic cells compared to controls increased by: 9% in UM-SCC 5, 21% in UM-SCC 12, 45% in UM-SCC 17A and 12% in UM-SCC 81B.

Therefore these results are in line with Backer's finding where EGF-SubA was found to induce caspase 3 activity (5).

As mentioned previously, inhibition of GRP78 via SubA cleavage results in the activation of the Unfolded Protein Response (UPR). A study by Yahiro and colleagues (2010) observed that SubA was able to induce the activity caspase 3, 8, and 9 and subsequent PARP cleavage (147). Simultaneous silencing of proapoptotic *Bax* and *Bak* genes resulted in: reduction of cytochrome c release less caspase 3 activation and loss of DNA ladder formation upon treatment of Hela cells with SubA, suggesting that activation of Bax and Bak proteins may contribute towards SubA induced apoptosis. However, the complete mechanism behind how SubA induces Bax and Bak are activity is still not known.

Upon activation of the Unfolded Protein Response, PERK, ATF6 and IRE1 are released by GRP78. Several pathways initiated through the UPR have been implicated in causing apoptosis. As discussed in section 1.1.2, CHOP is induced during the activation of both PERK and ATF6 (92). CHOP causes the up-regulation of Bim, a proapoptotic BH3 only proteins (92).

Activation of IRE1 also increases levels of JNK. JNK-mediated phosphorylation inhibits anti-apoptotic activity of BCl-2 whilst activating Bim and inducing BAX (83). A study

by Urano and colleagues in 2000 (105), showed that upon ER stress, IRE1 wild-type fibroblasts increased JNK levels by two-fold, whilst JNK expression was impaired in IRE1 knockout fibroblasts (105).

In order to confirm whether SubA activated UPR mediates cytochrome c release, Yahiro and colleagues (2010) used siRNA to silence IRE1α, JNK and CHOP. However, there was no decrease in cytochrome c release, suggesting that IRE1α, JNK and CHOP were not necessary for SubA induced apoptosis. Although GRP78 can initiate the UPR, another way in which the cleavage of GRP78 could possibly result in apoptosis is through the loss of direct interaction with proapoptotic proteins. For example, one study observed that the ATP domain of GRP78 was able to bind procaspase 7 and prevent caspase 7 activation and subsequent apoptosis (104). Further co-immunoprecipitation studies may be needed in order to investigate what other proapoptotic proteins GRP78 can interact with and inhibit the function of.

6.6 EGF-SubA is dependent on EGFR for its cytotoxicity, which can be blocked by cetuximab.

EGF-SubA is a novel cytotoxic drug that encompasses a bacterial endotoxin (SubA) covalently bound to EGF to permit targeting of EGFR-expressing cells whilst the enzymatically active moiety, SubA, promotes proteolytic cleavage of GRP78 (5).

Backer and colleagues in 2009 discussed the cytotoxicity of EGF-SubA and that this appeared to be EGFR-dependent, with EGFR expressing cells having an EGF-SubA IC_{50} within the picomolar range and EGFR negative cells having an EGF-SubA IC_{50} in the region of the nanomolar range (5).

In their 2009 study, Backer and colleagues examined the effectiveness of EGF-SubA against human prostate and breast cancer tumour xenografts in immuno-deficient mice. Following a one week course of intra-peritoneal EGF-SubA injections, the study found a 4-10 fold reduction in tumour volume compared to controls, without any 'clinical signs of toxicity observed in any of the treated groups.'

As part of future work members of our research group intend to perform related studies growing human laryngeal tumours in mice and treating them with intra-peritoneal EGF-

SubA injections. Similarly, these studies intend to monitor these mice for evidence of toxicity or other adverse events.

Currently it is unclear whether such xenograft models provide a reasonable test of toxicity, for pre-clinical studies, since EGF-SubA might not enter mouse cells due to differences in binding of human EGF to murine EGFR. Furthermore we wanted to clarify whether the cytotoxicity of EGF-SubA was, as suggest by Backer and colleagues, dependent on the presence of EGFR. If cytotoxity of EGF-SubA is dependent on EGFR then these effects in theory may be mitigated by cetuximab, which is a mAb against EGFR.

In order to address the question of whether EGF-SubA is toxic to mouse cells at the picomolar level and to confirm simultaneously that EGF-SubA toxicity is dependent on the expression of EGFR, mouse liver HEPA 1c1c7 cells, which express EGFR, and mouse embryonic fibroblasts (MEF) that do not express EGFR were treated with EGF-SubA for a period of five days and MTT was used to asses cell proliferation/viability as described in the materials and method section 3.12.

Initially, EGFR expression was confirmed to be present in HEPA 1c1c7 and absent in MEF cells by direct comparison with UM-SCC 12, which is known to express EGFR as shown in Figure 4.6.1A. Secondly, Hepa 1c1c7 and MEF cells were treated with EGF-

SubA at a range of concentrations between 1pM to 1nM for up to five days as shown in Figure 4.6.1B. As expected, growth of Hepa 1c1c7 EGFR positive cells were inhibited by EGF-SubA, albeit that the IC_{50} was at a relatively high picomolar concentration of 700pM, whilst no inhibitory effect in MEF EGFR negative cells was seen, even at an EGF-SubA concentration of 1nM.

Thus these results indicate that murine cells which do not express EGFR are not as sensitive to the effects of EGF-SubA compared to murine cells which do express EGFR. However it is still unclear whether the effects observed in murine cells were indeed EGFR dependent as the EGF-SubA IC_{50} of 700pM for Hepa 1c1c7 cells lies above the EGF-SubA IC_{50} range in human originated cell lines (1-100pM) but is below the IC_{50} range of SubA (>1nM) . In order to addrsss this, further studies could be used which involve comparing SubA IC_{50} levels to EGF-SubA IC_{50} levels in murine cells or the use of cetuximab to try and block the EGF-SubA toxicity.

Results in section 4.6 indicate that EGFR negative cells are not as sensitive to EGF-SubA as EGFR expressing cells. Therefore it was further investigated whether there were correlations between cell surface EGFR expression and sensitivity to EGF-SubA between different cell lines.

In order to measure the expression of membrane EGFR levels as opposed to total cellular EGFR levels, flow cytometric analysis was used. Anti-EGFR (ICR10) antibody conjugated to PE from Abcam (ab27764) was used in order to detect membrane EGFR. This antibody was selected as it binds to an extracellular epitope of EGFR. Average florescence (AF) generated from PE was taken as a surrogate marker for the level of membrane EGFR.

As expected the cytotoxicity of EGF-SubA appears to be substantially dependent on EGFR membrane expression as cells expressing higher EGFR levels were associated with increased sensitivity to EGF-SubA where Spearman's rank correlation coefficient = 0.919 (p=0.003)(see Figure 4.7.2.) Therefore, in conclusion, cytotoxicity of EGF-SubA is in part dependent on the amount of surface EGFR present on cells. As EGFR is often over expressed in tumour cells this may be an advantage in targeting cancer cells specifically and sparing histologically healthy tissue (50).

Based on these findings it was investigated whether cetuximab could inhibit the cytotoxic effects of EGF-SubA. Previously it could be seen that pre-incubation of cetuximab for two hours was able to efficiently block EGF induced phospho-EGFR in a range of UM-SCC cells, as shown in Figure 4.7.4. UM-SCC 12, 17A and 81B (Figure 4.8.1) were treated with EGF-SubA above and below IC_{50} doses or with cetuximab at sub-toxic concentrations of 10, 30 and 100nM, or pre-incubated with cetuximab for two

hours prior to the application of EGF-SubA. In all three cell lines pre-incubation of cetuximab was able to significantly rescue cells from the effects of EGF-SubA even at the lowest concentration of cetuximab ($p<0.05$) (10nM).

SubA is an endotoxin which is produced by Shiga toxigenic Escherichia coli which is known to cause haemorrhagic colitis and haemolytic uremic syndrome, which consists of a triad of: haemolytic anaemia, thrombocytopenia and renal failure (167). EGF-SubA could be used topically peri- or postoperatively around tumours in order kill any remaining cancer cells, whilst cetuximab could be used systematically to prevent any possible organ toxicity, therefore widening the therapeutic window of this drug.

Although one of the main aims of this thesis was to determine whether cetuximab could act as an antagonist to EGF-SubA, currently there is very little published data on the growth inhibitory effects of cetuximab against laryngeal squamous cell carcinoma both as a single agent and in combination with radiation. Therefore the toxicity of cetuximab on laryngeal squamous cell carcinoma cells was also explored.

Even though results presented in this thesis show that cetuximab is able to adequately block EGF induced phosphoylation of EGFR as well as act as an antagonist to EGF-SubA it is unclear why the MTT assay used, was not able to demonstrate that cetuximab was able to significantly suppress the growth of laryngeal squamous cell carcinoma cells

in vitro. Subsequently these experiments were repeated on at least one or more occasions using more recently acquired batches of cetuximab, however no additional toxic effects were observed. Furthermore MTT assays in our study have demonstrated typical dose response curves for EGF-SubA, cisplatin and AT13387 suggesting that there is no apparent problem in performing the technique. One possibility is that these UM-SCC cells may contain mutations downstream the EGFR signalling pathway such as Ras and PTEN mutations (52). Gene mutations may be identified by such techniques as restriction fragment length polymorphism (RFLP) (168).

MTT assay was also performed on a known cetuximab sensitive cell line UM-SCC 1 (derived from an oral tumour). Benavente and colleagues in 2009 had reported an IC_{50} of 5nM for UM-SCC 1 after three days treatment with cetuximab (152). It was noted that although Benavente and colleagues had shown that UM-SCC 1 was a cetuximab-sensitive cell line, results within this thesis show only a 25% decrease in cell viability/growth after using cetuximab at 1μM for seven days as shown in Figure 4.7.3 (152). Benavente and colleagues measured the cytotoxic effects of cetuximab by staining cells with crystal violet and measuring the colour intensity, which acts as a surrogate indicator of how many cells are present, via a plate reader. MTT assay is an indicator of cell viability/proliferation as the change in recorded absorbance is dependent on how many viable mitochondrial dehydrogenase enzymes are present. For future

studies it may be worth comparing whether crystal violet assays produce different levels of IC_{50} compared to MTT assays.

6.7 EGF-SubA acts as a radiosensitiser and synergistically with cisplatin

An increasing body of evidence suggests that up-regulation of GRP78 in tumours may lead to chemo- and radioresistance (1, 8, 97, 120). Therefore we explored whether EGF-SubA could enhance sensitivity *in vitro* to current clinically relevant treatment modalities used for head and neck cancer, such as cisplatin and radiation, in a panel of LSCC cell lines.

Several studies have associated GRP78 as a radioresistant phenotype. Lin and colleagues in 2010 and Feng and colleagues in 2010, found GRP78 to be up-regulated in clones which were able to survive a higher dose of ionising radiation compared to their parental cell lines (3, 8). Feng and colleagues also found GRP78 to be a potential biomarker with up-regulation of GRP78 in tumours corresponding to radioresistance in patients with nasopharyngeal carcinoma. Lee and colleagues in 2008 found that silencing of GRP78 via transfection with siRNA significantly enhanced the sensitivity of glioblastoma cells to radiation (108).

Several lines of evidence from results presented in this thesis suggest that EGF-SubA may be a radiosensitising agent. As seen in Figure 5.4.1, EGF-SubA is capable of down regulating EGFR as well as cleaving GRP78 (see Figure 4.1.1) and both EGFR and GRP78 are implicated in radioresistance. Results in this thesis also demonstrate that EGF-SubA leads to G1 cell cycle arrest (see Figure 4.5.1). Cells in G1 are known to be more sensitive to radiation compared to cells in S phase (150). Based on these findings we investigated whether pre-treatment with EGF-SubA was able to radiosensitise UM-SCC cells.

In order to test radio sensitisation *in vitro*, a clonogenic assay was used as described in section 3.11. One of the main aims of cancer treatment is to prevent recurrence of tumour growth. A clonogenic assay measures the ability of individual cells to proliferate and form colonies after exposure to ionising radiation, and this can be achieved in combination with cytotoxic drug treatments if required (126).

Loss of p53 function has been associated with chemo- and radioresistance (153). Therefore, we examined a variety of UM-SCC cells of differing p53 status to determine whether or not any potential radiosensitising effects of EGF-SubA observed were present regardless of p53 status (149). The cell lines studied were UM-SCC 17A which is wild-type for p53, UM-SCC 12 which is p53 null (homozygous Q104X), UM-SCC

81B were there are no alleles with wild-type p53 (mutant H193R) and UM-SCC 5 which has one wild-type allele and a single p53 mutation (heterozygous V157F)..

EGF-SubA was able to radiosensitise UM-SCC cells, regardless of p53 status, as shown in

Figure 5.4.2. At 2 Gy the survival fraction was significantly reduced by 17% ($p<0.03$), 30% ($p<0.02$), 34% ($p<0.002$), 27% ($p<0.002$) in UM-SCC 5, 12, 17A and 81B, respectively, as compared to controls.

Current studies suggest that over expression of GRP78 in tumours may contribute to cisplatin resistance. Lee and colleagues in 2008 transfected glioma cells with GRP78. Subsequent increases in GRP78 expression in these transfected cells led to a decrease in caspase 7 activation and rendered cells resistant to cisplatin-induced apoptosis. Upon transfection with siRNA against GRP78, decreased cell growth was observed as well as increased sensitisation to both cisplatin and radiation (108). Jiang and colleagues in 2009 found that cisplatin-mediated cytotoxicity of melanoma cells was significantly reduced in cells transfected with caspase 4 and 7 siRNA compared with control siRNA treated cells ($p<0.01$) (110). Jiang and colleagues also explored the role of GRP78 in altering cisplatin induced activation of caspase 4 and 7. siRNA knockdown of GRP78 increased cisplatin induced caspase 4 and 7 activity, whilst over expression of GRP78 suppressed

caspase 4 and 7 activity (110). Hence up-regulation of GRP78 may evoke resistance to cisplatin cytotoxity by inhibiting caspase activity.

Based on the studies by Lee and colleagues in 2008 and Jiang and colleagues in 2009 which demonstrate that up-regulation of GRP78 leads to cisplatin resistance, we investigated, in this thesis, whether or not EGF-SubA, which cleaves GRP78, could act synergistically with cisplatin. The use of multiple drugs with different mechanisms of action may help to 'improve the efficacy of the therapeutic effect, decrease the dosage but increase or maintain the same efficacy in order to avoid toxicity such as nephrotoxicity and otoxicity which are side effects of cisplatin treatment (155), and minimise or slow down the development of drug resistance' (156).

An MTT assay was used to assess the viability/growth of UM-SCC cells treated with cisplatin, EGF-SubA, or in combination.

EGF-SubA and cisplatin when used together produced combination index (CI) scores of less than or equal to 0.9, regardless of p53 status, and this is indicative of synergy. The lowest CI scores in UM-SCC 5 was 0.82, UM-SCC 12 was 0.597, and in UM-SCC 17A was 0.786. (see Figure 5.1.5).

To examine the possible mechanism behind this synergistic interaction between EGF-SubA and cisplatin the effects of both drugs upon GRP78 levels were studied. McCollum and colleagues in 2008 demonstrated that cisplatin was able to block the binding of transcription factor HSF-1 to chromatin upon treatment with geldanamycin, leading to inhibition of HSP72 induction and a synergistic interaction between cisplatin and geldanamycin (161). Our results show that when EGF-SubA was combined with cisplatin there was a marked loss of uncleaved GRP78 compared to all other conditions including controls, cisplatin alone, and EGF-SubA alone as shown in Figure 5.2.1. One hypothesis could be that cisplatin may also block the interaction of transcription factor ATF6 with chromatin, thus preventing the induction of GRP78. The reduced levels of functional GRP78 when combining EGF-SubA with cisplatin may explain the synergistic effects found in section 5.1

In addition, flow cytometry-based Annexin V/PI assays were performed in order to determine what combinatorial effects of these two drugs had upon apoptosis. In UM-SCC 12, 17A and 81B the proportion of cells undergoing apoptosis increased by 19%, 21% and 8%, respectively, when cisplatin was combined with EGF-SubA, as opposed to when cells were treated with either cisplatin or EGF-SubA as single agents (see Figure 5.3.2). However no further increase in apoptosis was detected in UM-SCC 5 cells.

As described above McCollum and colleagues in 2008 demonstrated that cisplatin was able to block the binding of transcription factor HSF-1 to chromatin upon treatment with geldanamycin. In a similar fashion, as part of future investigations it would be interesting to determine if cisplatin could prevent ATF6 interaction with chromatin by performing chromatin immunoprecipitation (ChIP) experiments.

6.8 **Summary of main findings**

For the first time it has been shown that GRP78 is significantly up-regulated in laryngeal, oropharyngeal and hypopharyngeal sqaumous cell carcinomas compared to histologically normal tissue ($p_{(X^2)}<0.001$) and, therefore, up regulation of GRP78 may be important to the development of head and neck cancers. We propose that up-regulation of GRP78 in these tumours may be due to the typical tumour microenvironment of hypoxia and low glucose and have further shown that, *in vitro,* LSCC cells can induce GRP78 under such conditions.

Cleavage of GRP78 through EGF-SubA may provide a potential means of suppressing tumour development. Results in this thesis show EGF-SubA to be cytotoxic to laryngeal squamous cell carcinoma cells in the pM range. It was further demonstrated *in vitro,* that EGF-SubA, was able to enhance the effects of the main treatment modalities of head and

neck cancer - radiation and cisplatin. Xenograft studies are now needed in order to confirm whether or not similar effects can be observed, *in vivo*.

Lastly, the toxicity of EGF-SubA appears to be substantially dependent on EGFR membrane expression since cells expressing higher EGFR levels were more sensitive to EGF-SubA where Spearman's rank correlation coefficient= 0.919 (p=0.003). Furthermore, pre-incubation of LSCC cells with sub-toxic doses of cetuximab, a therapeutic monoclonal antibody to EGFR, completely rescued cells from the cytotoxic effects of EGF-SubA ($p_{(t\ test)} \leq 0.005$). This is an important proof of principal for a combined toxin-protectant approach that would permit topical use of EGF-SubA peri- or postoperatively after tumour resection in order to kill any remaining tumour cells, or as an oral rinse in patients who present with pre-malignant lesions of the oral cavity, with any potential systemic toxicity being abrogated by cetuximab.

In summary our study has found that GRP78 is up-regulated in head and neck cancers suggesting that this protein may be important for tumour development and survival. Thus inhibition of GRP78 through EGF-SubA may offer a novel approach to cancer therapy. In addition to suppressing the growth of LSCC cells, EGF-SubA was found to enhance the effects of relevant genotoxic agents *in vitro* of cisplatin and radiation. Furthermore cetuximab was able to inhibit the toxicity of EGF-SubA thus potentially allowing for a combined toxin-protectant approach.

In order to evaluate whether EGF-SubA can inhibit tumour growth *in vivo,* an athymic nude mice model could be used to grow human head and neck tumour xenografts. Similar to the study by Backer and colleagues which performed xenograft studies of human prostrate and breast tumours, mice could be then given intraperitonial injections of EGF-SubA once tumour cell implantations became palpable (5). Changes in tumour volume could be assessed through direct removal of the tumour or through such techniques as MRI. Furthermore mice could be exposed to combinations of cisplatin or 2 Gy accelerated fractions of radiation with EGF-SubA, in order to establish whether there are either any synergistic interactions between these two drugs or any radio-enhancement effect *in vivo*.

One of the potential uses of EGF-SubA could be as a topical agent to be applied on resected tumour margins in order to remove any remaining tumour cells. Macroscopic excisions of tumour xenografts may be performed on mice with the intent of leaving a small section of tumour behind. These tumour margins could then be exposed to EGF-SubA topically. Core biopsies could then be taken from such treated regions and monitored for any remaining tumour tissue after a suitable time frame.

As previously mentioned Subtilase A toxin is known to cause haemolytic uraemic syndrome therefore it would be important to take full blood counts in mice to assess for

the potential toxicity of EGF-SubA (7). Furthermore toxicity to vital organs such as the liver and kidney should be monitored by assessing levels of alanine transaminase (ALT) and performing creatinine clearance tests, respectively.

The above work would help to assess the efficacy and toxicity of EGF-SubA, *in vivo*, and aid in the progress towards phase I clinical trials.

7 Appendix: Investigating cytotoxicity of HSP90 inhibitor AT13387 in laryngeal squamous cell carcinoma cells, *in vitro*.

7.1 Abstract

HSP90 is required for the stability and development of several oncoproteins including: EGFR, ErbB2, PKB/AKT, HIF-1α and telomerase (137). HSP90 inhibition leads to proteasomal degradation of such client proteins (137). Therefore HSP90 inhibitors provide a means of targeting several oncoproteins at once resulting in attenuation of angiogenesis, cell cycle arrest and apoptosis. Over-expression of the oncoprotein EGFR has been found in more than 50% of head and neck cancer patients and therefore HSP90 inhibitors may be particularly useful in these cancers. Therefore the use of AT13387, which is a novel experimental HSP90 inhibitor, was explored as a potential cytotoxic agent on a panel of laryngeal carcinoma cells.

The IC_{50} range of AT13387 (Astex therapeutics) was found to be between 40nM-1μM on a panel of seven LSCC. Similar to EGF-SubA, AT13387 significantly enhanced the 2 Gy survival fraction in three out of four LSCC cell lines. Furthermore a synergistic effect was found when AT13387 was combined with cisplatin where the IC_{50} drug combination index = 0.875.

In conclusion AT13387 enhances current treatment modalities in head and neck cancer by acting as radiosensitizer and synergistically with cisplatin. *In vivo* work is needed to assess the efficacy and toxicity of this drug before phase I clinical trials can commence.

7.2 Literature review: HSP90 inhibitors in cancer therapy

Heat shock proteins are a highly conserved family of molecular chaperones which are induced under cellular stresses such as high temperature and hypoxia (169). Under such stress, the transcription factor known as heat shock factor (HSF) dissociates from HSP90 and HSP70 and initiates transcription of HSPs (169). HSP90 is known to be overexpressed in cancer and correlates with decreased survival in breast cancer, gastrointestinal stromal tumours (GIST) and non-small cell lung cancer (NSCLC) (170).

Unlike other chaperones, HSP90 is not involved in folding of nascent proteins but is rather engaged in enhancing protein activity and stability. When ATP is bound to HSP90 it induces a conformational change that allows HSP90 to interact with approximately 200 client proteins. The majority of HSP90 client proteins are involved in some aspect of signal transduction including protein kinases, hormone receptors and transcription factors and therefore interest has grown in targeting HSP90 as a means of cancer therapy (170, 171).

Geldanamycin and AT13387 are HSP90 inhibitors which prevent HSP90 interaction with client proteins by competitively occupying the ADP/ATP binding site of HSP90. Inhibition of HSP90 leads to client proteins interacting with ubiquitin ligase CHIP, resulting in the eventual proteasomal degradation of these client proteins(170).

Steroids are responsible for a wide range of functions including glucose metabolism (glucocorticoids), mineral uptake (mineralcorticoids), female development (estrogens) and male development (androgens) (172). For each individual steroid there are steroid hormone receptors (SHR) which become activated transcription factors upon steroid binding. In order for SHRs to be functional an open conformation of the steroid binding cleft is needed. This is created through the interaction between SHRs and HSP90 proteins(172). For instance, the use of HSP90 inhibitors prevent oestrogen receptor –α (ERα) development and ERαs are subsequently degraded. Thus HSP90 inhibitors may prove useful in oestrogen receptor positive breast cancer patients who have developed tamoxifen resistance (169).

HSP90 is also required for the stability and development of several oncoproteins including: EGFR, ErbB2, PKB/AKT, HIF-1α and telomerase (137). HSP90 inhibition leads to proteasomal degradation of such client proteins (137). Therefore HSP90

inhibitors provide a means of degrading several oncoproteins at once resulting in attenuation of angiogenesis, cell cycle arrest and apoptosis.

The importance of EGFR and its downstream signalling pathway in cancer has been reviewed in section 1.2. The process of apoptosis has been reviewed in section 1.3.4. One of the downstream pathways of EGFR, PI3K-AKT acts to suppress apoptosis. PI3K-AKT leads to the inhibition of proapoptotic protein BAD as well as induction of anti apoptotic protein bcl-xl (169). PI3K-AKT pathway can also block the action of cyclin CDK complex inhibitors p27 and p21 thus ensuring the progression of the cell cycle. As AKT is a client protein, PI3K-AKT prosurvival effects can be attenuated with HSP90 inhibitors, even in cases where there is loss of tumour suppressor PTEN (169).

Ras-Raf-ERK pathway is also important in cell survival and proliferation. Mutations in B-Raf and N-Ras lead to subsequent, EGFR independent, autonomous signalling. A derivative of geldanamycin, 17AAG, can also inhibit HSP90 but has the advantage of a wider therapeutic window when compared to geldanamycin which is known to induce liver toxicity. A study by Grbovic and colleagues showed that 17AAG induced the degradation of mutant form V600 B-Raf but not wild-type B-Raf and also wild-type Raf-1, suggesting that HSP90 is required for the stability of mutant but not wild-type B-Raf as shown Figure 7.2.1A (173). 17AAG also induced G1 arrest and reduced levels of pMAPK, and cyclin D in both mutant melanoma B700 B-Raf cell line SK-Mel-28 and

wild-type melanoma cell line SK-Mel-31 as shown in Figure 7.2.1B (173). Hence HSP90 inhibitors may be more potent than cetuximab or TKIs in treating tumours with Ras, Raf mutations or even PTEN loss.

This text box is where the original thesis contained the diagram showing ‘effects of 17AAG on wild-type B-Raf and mutant V600 B-Raf cells’ which was reproduced from reference *(173)*.

Figure 7.2.1Effects of 17AAG on wild-type B-Raf and mutant V600 B-Raf

(A)Degradation of mutant B-Raf (SK-Mel 28) and wild-type Raf-1 but not wild-type B-Raf (SK-Mel 31) upon application of 17AAG. (B) 17AAG induces G1 arrest in both wild-type (SK-Mel 31) and mutant B-Raf (SK-Mel 28) melanoma cells as well as decrease in cyclin D and pMAPK levels. Figures reproduced from reference (173).

Bagatell and colleagues showed that the treatment of neurobalstoma and osteosarcoma cell lines with geldanamycin in combination with cisplatin resulted in greater than additive inhibition of survival and proliferation (174). Normally under HSP90 inhibition, HSF induces transcription of genes such as *HSP72* and *HSP27* (161). However when cells were treated with both geldanamycin and cisplatin there was no further rise in HSP72 levels as compared to controls as shown in Figure 7.2.2 (174).

This text box is where the original thesis contained the diagram showing 'effects of cisplatin and geldanamycin on HSP90 associated proteins AKT and HSP72' which was reproduced from reference *(174)*

Figure 7.2.2 Effects of cisplatin and geldanamycin on HSP90 associated proteins AKT and HSP72.

Osteosarcoma cell lines (Saos-2 cells) were treated with either geldanamycin at 0.5μM (GA),or cisplatin at 50μM (CDDP) or both (G+C). Figure reproduced from reference (174)

A similar study by McCollum and colleagues found synergistic effects, as studied by colony forming assay, when treating A459 and Hela cells in combination with cisplatin and geldanamycin (161). The study showed that cisplatin abrogated the binding of HSF-1, upon treatment with geldanamycin, to chromatin therefore inhibiting the transcriptional activity of HSF-1 and subsequent induction of HSP70(161). Hence the induction of HSP70 may be implicated in the resistance to HSP90 inhibitors and this resistance can be prevented by the use of cisplatin.

Inhibition of EGFR, Raf-1, p53 or NF-κB. has been shown to enhance radiosensitivity in some tumours (171). Russell and colleagues investigated the effects of radiation on glioma (U251 and SF539) and prostate cancer cells (DU145 and PC3) after pre treatment with 17AAG (175). The study showed that client proteins AKT, ErbB2 and Raf-1 were reduced upon exposure of 25-75nM of 17AAG. There was also significant radiosensitisation in all four cell lines with a radiation enhancement ratio ranging between 1.3-1.7 (175) when cells were pre-treated with 75nM 17AAG for 24h. Similar 17AAG radiosensitising results were found in mice with human cervical tumours (176).

7.3 **Aims**

AT13387 and HSP90

Protein chaperone HSP90 enhances the activity and stability of key oncoproteins EGFR, ErbB2, Raf, PKB/AKT and HIF-1α. HSP90 inhibitors lead to the degradation of such HSP90 client proteins (137). Current HSP90 inhibitors such as geldanamycin have been shown to reduce tumour volume, attenuate angiogenesis and act as radiosensitising agents in a variety of tumours including glioma, prostate, pancreas and cervix (137). However they are limited in their clinical use due to poor solubility, extensive metabolism, and hepatic toxicity (177).

Over expression of EGFR has been found in more than 50% of head and neck patients and has been correlated with poor survival outcome, increased metastatic potential and radioresistance and therefore inhibiting the EGFR pathway, through HSP90 inhibitors, may be particularly useful against SCCHN (29, 49, 50). Currently there is no published data regarding the use of HSP90 inhibitors in head and neck cancer possibly due to systemic toxicity of present HSP90 inhibitors. A new smaller synthetic inhibitor of HSP90 AT13387 has been developed which has shown lower toxicity and better bioavailability (177, 178). This study investigates the use of HSP90 inhibitor AT13387 for the first time in UM-SCC laryngeal sqaumous cell carcinomas.

Initially cytotoxicity of AT13387 will be investigated in a panel of LSCC via MTT assay.

Currently there are conflicting results as to whether HSP90 inhibitors can induce G1 or G2 arrest. In order to clarify how AT13387 may stop the proliferation of UM-SCC cells, cell cycle analysis via BrdU-PI flow cytometric analysis will be used.

HSP90 inhibitors have been reported to be radiosensitising agents possibly as they lead to the degradation of EGFR (175). Through western blot analysis it will be seen whether AT13387 can also lead to the loss of EGFR in LSCC. Currently there is no published data demonstrating AT13387 as radiosensitiser. Therefore through clonogenic assay it will be explored whether AT13387 is also a radiosensitising agent

HSP90 inhibitors have also been shown to act synergistically with cisplatin (161). Here it will be investigated whether similar results can be obtained with AT13387 via MTT assay. Furthermore as both AT13387 and EGF-SubA target different protein chaperones it will be seen if combining these two drugs will also lead to synergy.

Performing the above experiments should allow for a greater understanding of the potential for targeting heat shock protein HSP90 as a novel therapeutic target for head and neck cancers.

7.4 Results: Investigating the cytotoxic effects of HSP90 inhibitor AT13387 upon UM-SCC cells.

7.4.1 AT13387 inhibits proliferation of UM-SCC laryngeal carcinoma cells

Currently there are no studies which have reported the use of HSP90 inhibitors such as geldanamycin in head and neck cancers. As mentioned previously in section 7.2 HSP90 is required for the stability and development of several oncoproteins including: EGFR, ErbB2, PKB/AKT, HIF-1α and telomerase (137). HSP90 inhibition leads to proteasomal degradation of such client proteins (137). Therefore HSP90 inhibitors provide a means of degrading several oncoproteins at once resulting in attenuation of angiogenesis, cell cycle arrest and apoptosis. In particular to head and neck cancers, EGFR is commonly over expressed in up to 50% of cases (6) Overexpression of EGFR has been correlated with increased metastatic potential and lower survival rates and because of this HSP90 inhibitors may be an appropriate treatment option for head and neck cancer patients.

Current HSP90 inhibitors such as geldanamycin have been shown to reduce tumour volume, attenuate angiogenesis and act as a radiosensitising agent in a variety of tumours including glioma, prostate, pancreas and cervix (177). However several HSP90

inhibitors such as geldanamycin are limited in their clinical use due to poor solubility, extensive metabolism, and hepatoxicity (177). A new smaller synthetic inhibitor of HSP90, AT13387, by drug company Astex Therapeutics, has been developed which has shown lower toxicity and better bioavailability (177, 178). Here the potential use of HSP90 inhibitor AT13387 on laryngeal squamous cell carcinoma was investigated *in vitro* for the first time.

In order to establish what inhibitory effects AT13387 had upon the growth of UM-SCC cells an MTT assay was set up as described in Methods section 3.12. ATT1387 was first dissolved in DMSO to a concentration of 10 mM. Afterwards ATT1387 was serially diluted in PBS at the required concentrations. It was found in previous experiments that a final dilution of DMSO above 1% was in itself cytotoxic and therefore use of DMSO was limited to below this level. Previously Astex Therapeutics (the manufactures of AT13387) had tested this drug on ovarian, breast, melanoma and non small cell lung cancer cell lines and found the IC_{50} to range from 12 to 55nM (178). The time course of these experiments by Astex Therapeutics allowed for a greater or equal to three cell doubling times. Based on these previous experiments our study used concentrations of between 10nM to 3μM of AT13387. Typically UM-SCC cells double once every two days and therefore the duration of the experiment was for seven days. Fresh drugs and media were replaced daily. Each data point was repeated in quadruplicates. Typical dose

response curves can be seen in Figure 7.4.1 where increasing doses of AT13387 lead to a decreasing cell concentration.

IC_{50} values were calculated from data produced on day seven which allowed for at least three cell doubling times in the UM-SCC lines. IC_{50} curves were plotted as: percentage of MTT score the drug treated group as a proportion of the control group (y-axis) against the dose of the drug used on a log scale (x-axis). IC_{50} curves can be seen in Figure 7.4.2. IC_{50} values were between the 40nM to 1μM range for UM-SCC cells.

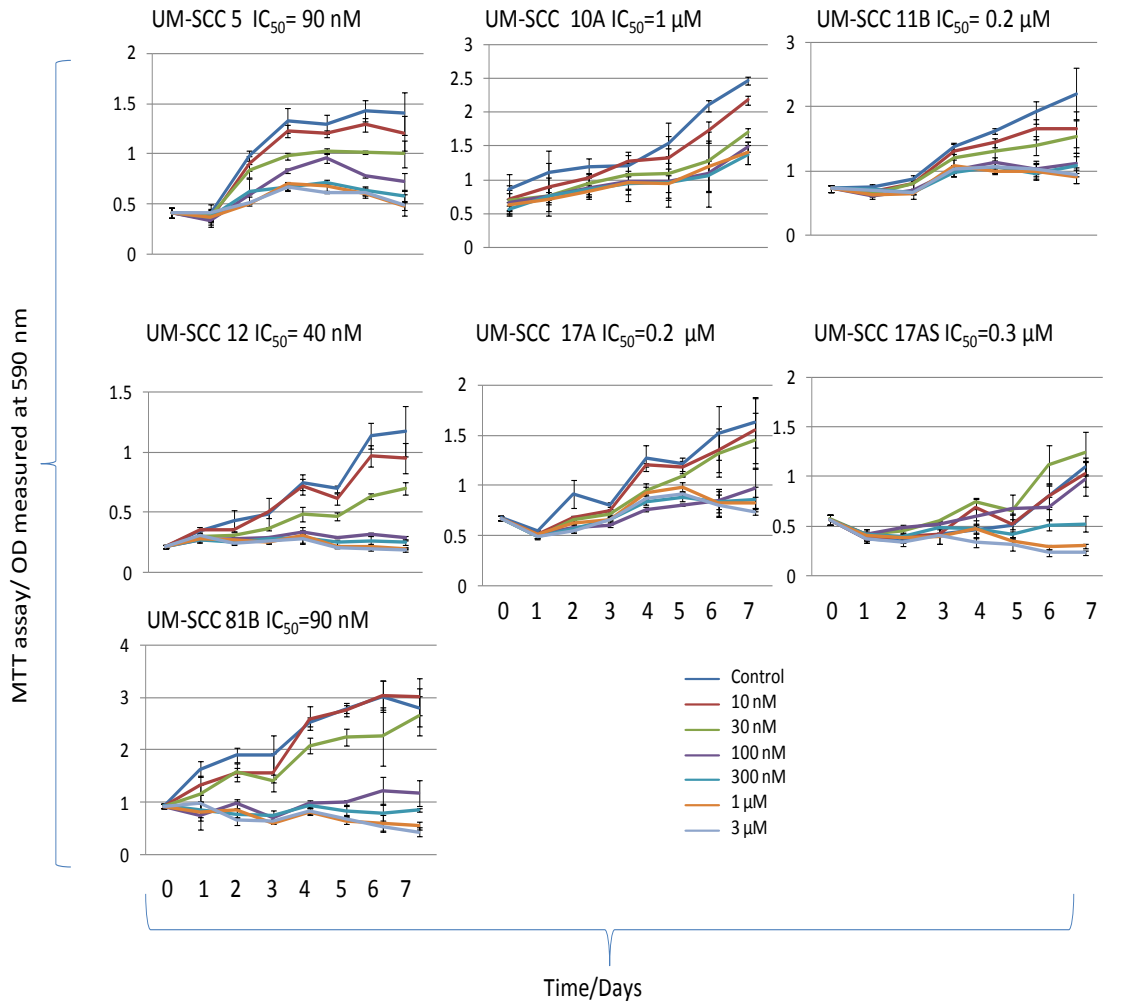

Figure 7.4.1 Dose response curves of LSCC treated with AT13387.

UM-SCC Cells were seeded in 96 well plates and allowed to adhere for 24 hours (shown as day 0). Cells were then treated with either AT13387 at concentrations of 10nM, 30 nM, 100 nM, 300nM, 1µM, and 3µM or with drug vehicle control, for up to seven days. Both media and drugs were replaced every 24h. MTT assay was used to assess the viability/growth of cells. The absorbance was measured at an OD of 590 nm. Error bars represent the s.e.m. from four independent wells.

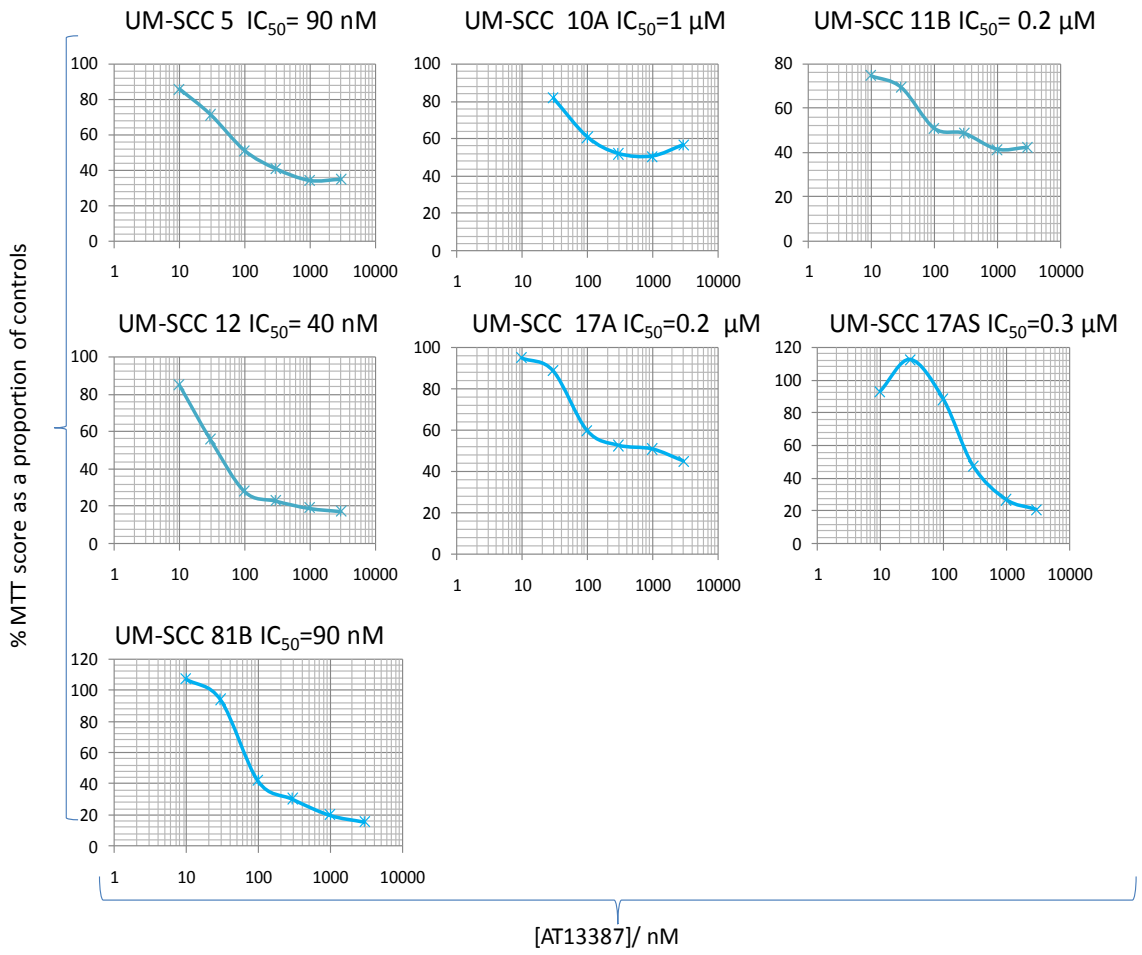

Figure 7.4.2 Figure 4.1.2 LSCC IC_{50} curves treated with AT13387.

IC_{50} data derived from day seven of UM-SCC cells being treated with either AT13387 at concentrations of 10nM, 30nM, 100nM, 300nM, 1µM, and 3µM or just drug vehicle control. IC_{50} curves are plotted as: percentage MTT score in the drug treated group as a proportion of the control group (y-axis) against the dose of the drug on a log scale (x-axis).

7.4.2 AT13387 (HSP90 inhibitor) induces G2 cell cycle arrest.

HSP90 inhibitors lead to the degradation of several HSP90 client protein which are responsible for progression of the cell cycle such as EGFR, Raf, AKT (169, 173). As a result there is suppression of cyclin D through the loss of the Raf pathway. As well as this the removal of AKT means that p21 can suppress the activity of the cyclin D-CDK4/6 complexes. Astex Therapeutics have also shown reduced cyclin D levels upon treatment with AT13387 *in vitro* and reduced levels of AKT after 24h treatment with AT13387 at 1μM (178). Studies have also been performed on 17AAG showing G1 arrest in melanoma cells(173).

At present there is no published data on the use of HSP90 inhibitors in head and neck cancer. In our study flow cytometry analysis is used in order to establish what effect AT13387 has upon the cell cycle of LSCC cell lines.

BrdU-PI double staining was performed simultaneously along side the conventional PI staining of fixed permeabilised cells alone in order to analyse cell cycle profiles. Transcription factor *p53* is a tumour suppressor gene which can cause G1 cell cycle arrest under an array of stimuli such as DNA damage (149). Therefore, we examined a variety of UM-SCC cells of differing p53 status, to determine whether or not any impact

of AT13387 had upon the cell cycle was independent of p53 status (149). The cell lines studied were UM-SCC 17A which is wild-type for p53, UM-SCC 12 which is p53 null (homozygous Q104X), and UM-SCC 5 which has a single p53 mutation (heterozygous V157F) and retains a wild-type allele.

Experiments were set up as explained in Methods sections 3.7 and 3.8. UM-SCC cells were first transferred to culture dishes and left to adhere for 24 hours. Cells were then treated with drugs or respective drug vehicle controls for two days with drugs and media being applied freshly on each day. As this study was the first to perform cell cycle analysis on UM-SCC cell lines with AT13387, relatively high drug doses above the IC_{50} levels at 1μM was chosen, in order to ensure that an effect was observed. BD FACSCalibur flow cytometer machine was used and the data was analysed on CellQuest Pro Software. At all times doublet discrimination, as described in section 3.7, was performed in order to discriminate between signals produced from DNA content of single cells in G2 and doublets in G1.

AT13387 was able to deplete the amount of cells in S phase in all three cell lines as well as cause G2 arrest. This effect appears to be independent of p53. The percentage decrease in S phase cell fraction after treatment with AT13387 as compared to controls in UM-SCC 17A, 12 and 5 were 8%, 4%, and 8% respectively, as analysed by PI staining of fixed permeabilised cells and 70%, 65% and 75% as deduced by BrdU-PI

double staining (see Figure 7.4.3 and Figure 7.4.4). The percentage increase in G2 cell fraction after treatment with AT13387 as compared to controls in UM-SCC 17A, 12 and 5 were 20%, 10%, and 17% respectively, as analysed by PI staining of fixed permeabilised cells and 27%, 24% and 20% as deduced by BrdU-PI double staining.

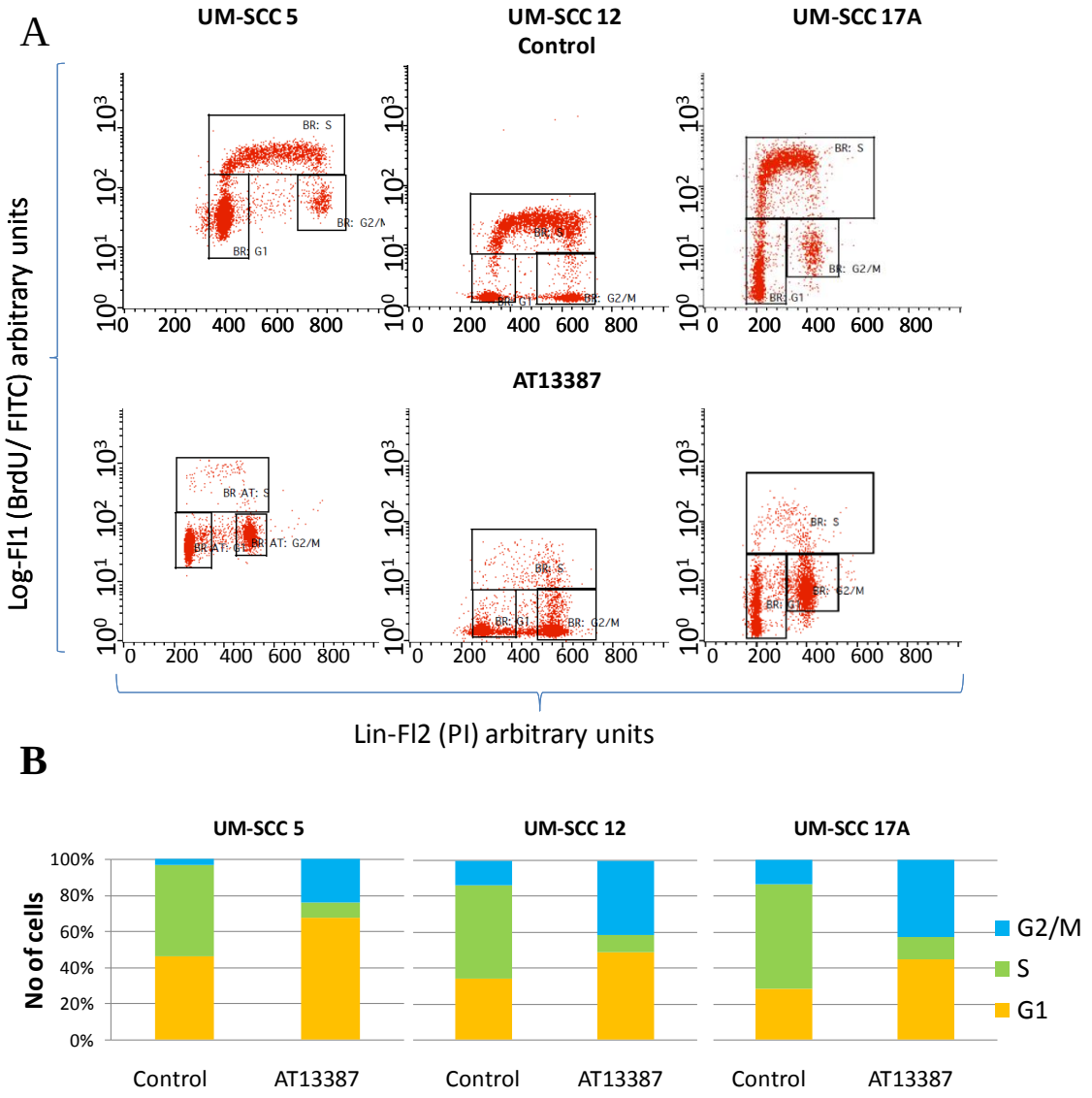

Figure 7.4.3 AT13387 induces G2 cell cycle arrest regardless of p53 status.

(A)UM-SCC cells were treated with either AT13387 at 1μM or drug vehicle control for 48h . Cell cycle analysis was performed via BrdU-PI double staining. (B) Bar charts summarise cell fractions in treatment and control groups. Data was analysed on CellQuest Pro Software.

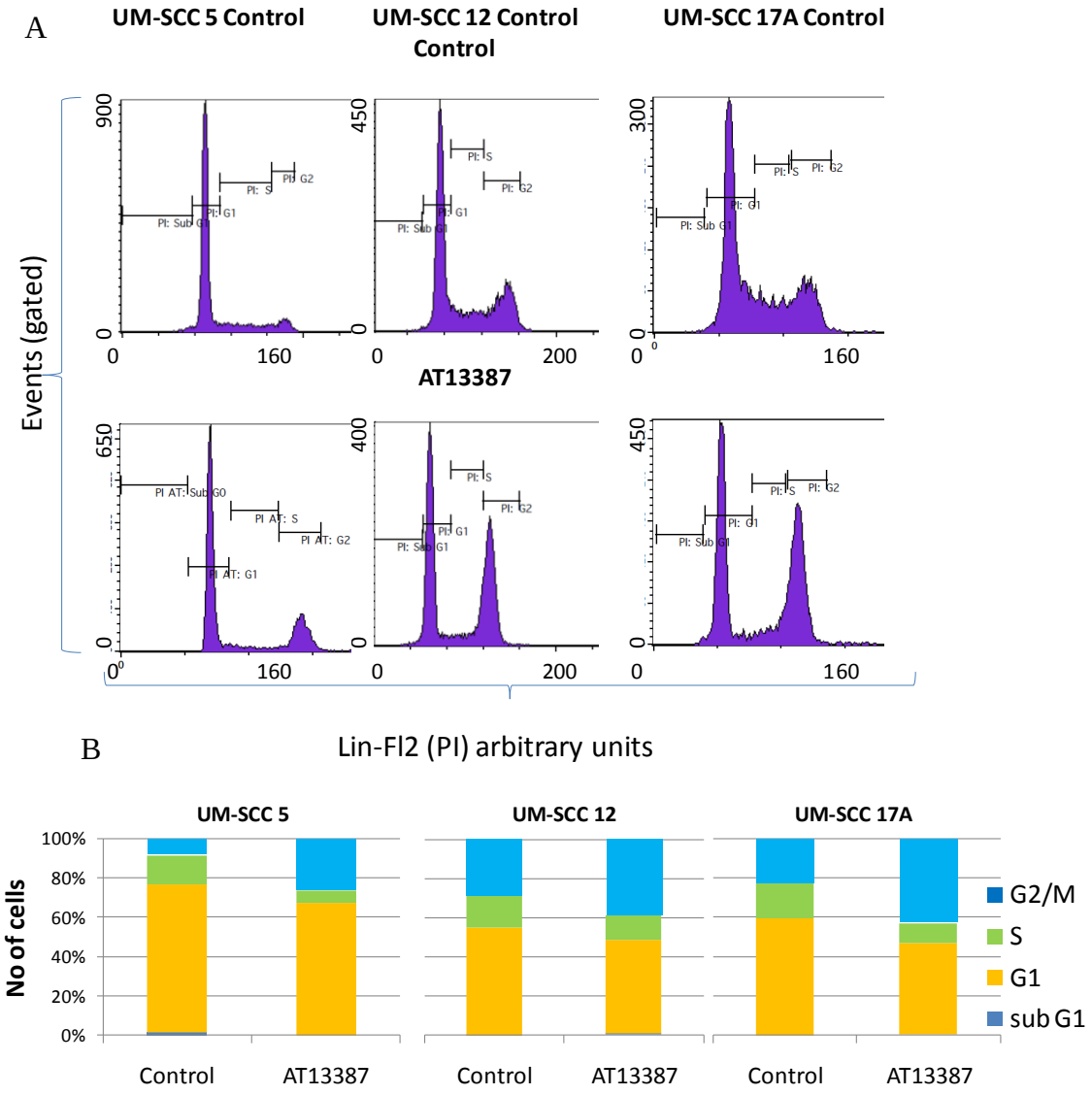

Figure 7.4.4 AT13387 induces G2 cell cycle arrest regardless of p53 status.

(A)UM-SCC cells were treated with either AT13387 at 1μM or drug vehicle control for 48h. Cell cycle analysis was performed via staining of fixed permeabilised cells with PI. (B) Bar charts summarise cell fractions in treatment and control groups. Data was analysed on CellQuest Pro Software. Note that in (A) the axes values are not the same.

7.4.3 AT13387 acts as a radiosensitising agent in three out of the four cell lines tested

It is well known that HSP90 inhibitors lead to the degradation HSP90 client proteins such as EGFR. HSP90 suppresses the activity of transcription factor HSF. Upon HSP90 inhibition there is both a decrease in EGFR levels and a concomitant increase in the transcription of genes such as HSP72 and HSP27 (161). Therefore we investigated whether or not HSP90 inhibitor AT13387 had similar effects on UM-SCC cell lines. A time course was established where cells were treated with AT13387 at 1μM at 4h, 8h, 16h, 24h and 48h, or with drug vehicle control at 24h and 48h. Subsequent western blot analysis was performed on cells treated with AT13387 in order to view EGFR , HSP72 and actin (loading controls) levels as shown in Figure 7.4.5

As can be seen in Figure 7.4.5 there was a gradual increase in HSP72 induction from 4h to 48h and a concomitant decrease in EGFR levels when UM-SCC 17AS and 81B were treated AT13387 at 1μM.

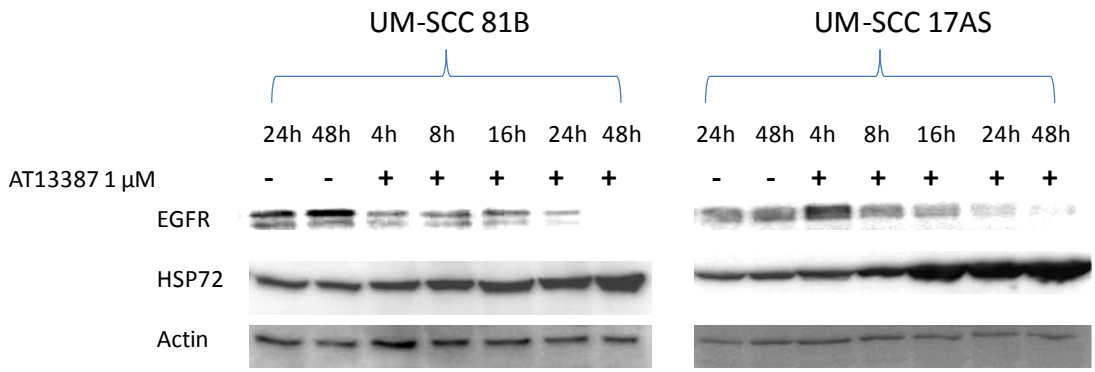

Figure 7.4.5 AT13387 reduces EGFR levels and induces HSP72 on UM-SCC cells.

Western blot analysis of UM-SCC 81B and 17AS treated with AT13387 at 1µM for 4h, 8h, 16h, 24h and 48h or with drug vehicle control for 24 and 48h. All lanes were loaded with 35 µg protein. Blots were probed with anti EGFR antibody at 3 µg/ml, anti HSP72 antibody at 50 ng/ml, and anti actin antibody at 3 µg/ml (protein loading control).

HSP90 inhibitors are known to be radiosensitising agents in a wide variety of tumours however currently there is no published data which has examined the use of HSP90 on head and neck cancers. Inhibition of HSP90 activity allows for a multi-target approach and down regulation of several client proteins that may be responsible for radioresistance. A study by Bull and colleagues found down regulation of ErbB2 and Raf-1, which are proteins which have been implicated in the regulation of radiosensitivity, upon cells pre-treated with 17-DMAG (179). The study also found a significant enhancement in radiosensitivity with 17-DMAG.

As seen in Figure 7.4.5, AT13387 is capable of down regulating EGFR. EGFR and HSP90 client proteins are implicated in radioresistance. Furthermore cells in G2 are considerably more sensitive to radiation compared to cells in S phase (150). Therefore this drug could increase radiosensitisation by synchronising cells into the more radiosensitive phases of the cell cycle. This study therefore investigated whether pre-treatment with AT13387 was able to radio-sensitise UM-SCC cells.

Pilot studies were performed in order to establish the highest drug concentration that cells could tolerate for 24h without exposure to radiation that would provide survival fractions equal to that of drug omitted controls. Both UM-SCC 5 and UM-SCC 17A when treated with 100nM AT13387 without radiation had survival fractions below the controls and so cells were treated with a lower dose of AT13387 at 10nM. UM-SCC 12

and 81B were able to tolerate an AT13387 dose of 100nM without difference in survival fraction as compared to controls. UM-SCC cells were pre-incubated with either 10nM or 100nM At13387, as indicated, or appropriate drug vehicle control for 24h before being irradiated with 0, 1, 2, or 4 Gy. Cells were then seeded in triplicate into six well plates, in normal growth media without drug and monitored for colony formation for 2-3 weeks.

AT13387 was able to radio-sensitise UM-SCC 12, 17A and 81B with significant decrease in SF2 compared to controls of between 13%-38% ($p<0.05$) as seen in Figure 7.4.6. However no significant radiosensitising effect was observed in UM-SCC 5.

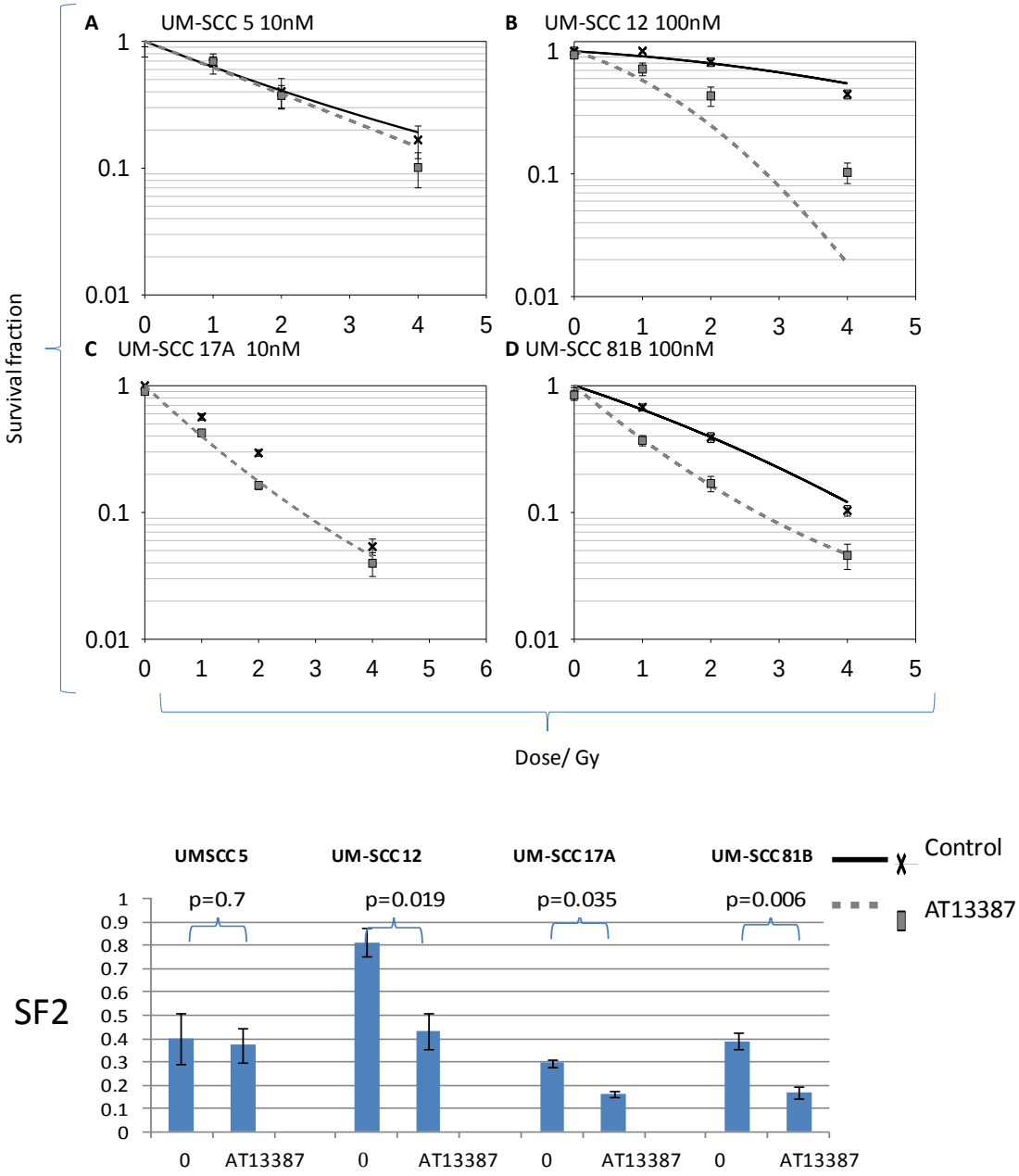

Figure 7.4.6 AT13387 was able to significantly radiosensitise three out four LSCC cell lines.

(A,B,C,D) UM-SCC cells were pre-treated for 24h with AT13387 10-100nM or drug vehicle control and then exposed to γ-irradiation at 0, 1, 2, or 4 Gy as indicated. Clonogenic assays were established to allow for colony formation over a time period of two to three weeks. A colony was defined as equal to or more than 50 cells in order to allow for at least five cell doubling times. Crosses and squares indicate mean of three survival fractions for each data point with appropriate s.e.m. Survival curves were then fitted to the quadratic equation $S(D)/S(0)= \exp(- (\alpha D + \beta D^2))$*. (E) Bar charts showing survival fractions at 2 Gy with and without AT13387. Unpaired Student's t test was used to calculate differences in SF2 between controls and treated cells.*

7.4.4 AT13387 acts synergistic with cisplatin, but antagonistically with EGF-SubA

HSP90 inhibitors such as geldanamycin in combination with cisplatin have been shown to enhance the cytotoxic effects when compared to using either of these drugs on their own. For example Bagatell and colleagues showed that the treatment of neurobalstoma and osteosarcoma cell lines with geldanamycin in combination with cisplatin resulted in greater than additive inhibition of survival and proliferation (174)

HSP90 inhibitors may target the pathways which lead to known cisplatin resistance by the subsequent degradation of HSP90 client proteins such as ErbB2, AKT and mutant Raf (169, 173). Furthermore PI3K-AKT inhibitors have been shown to enhance the effect of cisplatin, in cisplatin resistant lines (180).

HSP72 may also contribute to cisplatin resistance. In one study the use of siRNA against HSP72 made lung cancer cells more sensitive to cisplatin (161). Normally under HSP90 inhibition, HSF induces transcription of genes such as HSP72 and HSP27 (161). However studies have shown that when cells were treated with geldanamycin and cisplatin there was no further rise in HSP72 levels as compared to controls as shown in Figure 7.2.2 (174). In a separate study it was demonstrated how cisplatin abrogated the

binding of HSF-1, upon treatment with geldanamycin, to chromatin therefore inhibiting the transcriptional activity of HSF-1 and subsequent induction of HSP72(161).

Previous results in this thesis have established UM-SCC AT13387 IC_{50} and cisplatin IC_{50} via MTT assay after seven days of drug treatment as seen in Figure 7.4.2. and Figure 5.1.2 respectively. A range of values above and below the IC_{50} of both AT13387 and cisplatin were combined in order to establish whether there was any synergy, additive or antagonistic effect. Cells were treated with each of the two drugs individually, in combination, or with carrying vehicle control in quadruplicate sets. Fresh media and drugs were replaced daily for a total of seven days. Cell viability/growth was assed at the end of day seven via MTT assay. For quantification of synergy or antagonism the combination index (CI) was used (156).

From Figure 7.4.7 it can be seen that AT13387 combined with cisplatin produces a synergistic inhibitory effect against cell viability/growth in UM-SCC 81B where CI=0.875.

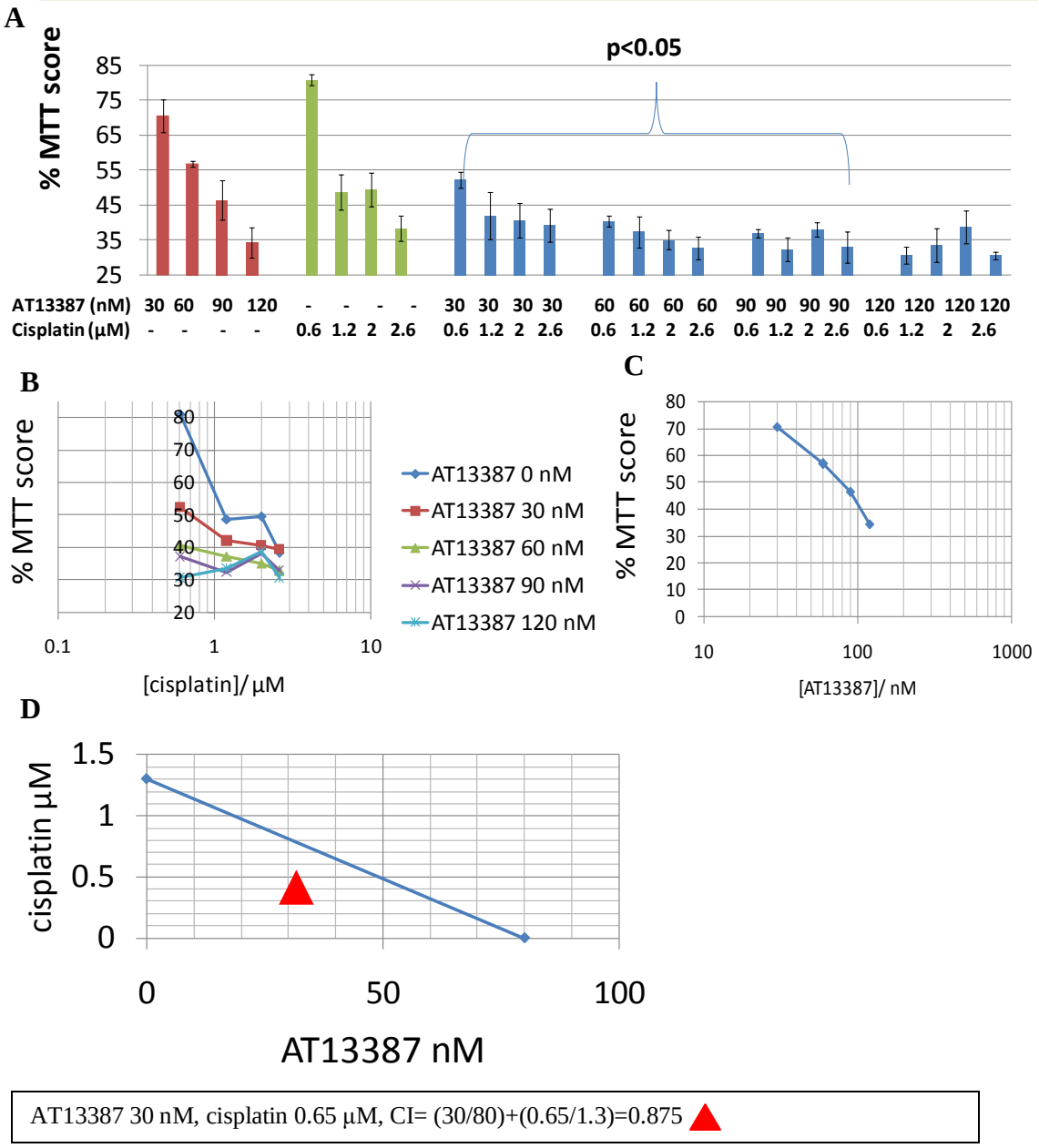

Figure 7.4.7 AT13387 in combination with cisplatin produces a synergistic effect in UM-SCC 81B cells.

(A) UM-SCC 81B were seeded in 96 well plates and allowed to adhere for 24 hours. Cells were then treated at a range concentrations of either cisplatin at 0.6, 1.2, 2, 2.6μM alone or AT13387 at 30, 60, 90, 120nM alone, in combination, or with drug vehicle control. Both media and drugs were replaced every 24h for a total of seven days. MTT assay was used to assess the viability/growth of cells after day seven. The absorbance was measured at an OD of 590 nm. Bars represent the percentage MTT score of treated groups as a proportion of controls. Error bars show the s.e.m. from four independent wells. In the majority of cases there were statistically significant reductions in MTT score when MTT scores from cells treated with single agents were compared to MTT scores of cells treated with both cisplatin and AT13387 as deduced by unpaired Student's t test ($p<0.05$). (B and C) IC_{50} values were calculated from log plots derived from data as shown in A for either cisplatin on its own, AT13387 on its own and any IC_{50} values established when cisplatin and AT13387 were used in combination. IC_{50} curves were plotted as: percentage MTT score in the drug treated group as a proportion of the control group (y-axis) against the dose of the drug on a log scale (x-axis). (D) Isobologram showing a line joining the IC_{50} value of AT13387 at 80nM with the IC_{50} value of cisplatin at 1.3μM. An IC_{50} value can also be seen when AT13387 at 30nM was combine with cisplatin at 0.65μM producing a combination index of 0.875. (CI) at IC_{50}= $(D)_1/(D_x)_1 + (D)_2/(D_x)_2$. $(D_x)_1$ and $(D_x)_2$ is the dose of each of the drugs which, when used alone results in the IC_{50}. $(D)_1$ and $(D)_2$ are the doses of each drug which when in combination result in the IC_{50}.

Both AT13387 and EGF-SubA target different protein chaperones and therefore it was predicted that there might be at least some additive effect if these two drugs were combined together. However when EGF-SubA was combined with AT13387 there was a clear antagonistic effect as shown in Figure 7.4.8 upon UM-SCC 81B. AT13387 and EGF-SubA when used on their own have an IC_{50} value of 120nM and 20μM respectively. When both drugs were used in combination IC_{50} points were reached at: EGF-SubA at 10pM with AT13387 at 80nM producing a CI of 1.17, EGF-SubA at 10pM with AT13387 at 100nM where CI is 1.33, EGF-SubA at 15pM with AT13387 at 50nM resulting in a CI of 1.17, and EGF-SubA at 15pM with AT13387 at 100nM producing a CI of 1.58. One possible explanation for this antagonism may be due to the fact that EGFR is a client protein of HSP90. As shown by Backer and colleagues 2009, EGF-SubA is more potent in EGFR expressing cells compared to EGFR null cells (5). For example rat glioma EGFR +/+ cells had an IC_{50} of 20pM whilst rat glioma EGFR -/- cells had an EGF-SubA IC_{50} of 6nM which is a 30 fold increase. When HSP90 inhibitors are used such as AT13387 there is degradation and subsequent decrease in EGFR levels as shown in Figure 7.4.5, thus possibly reducing the cytoxicity of EGF-SubA.

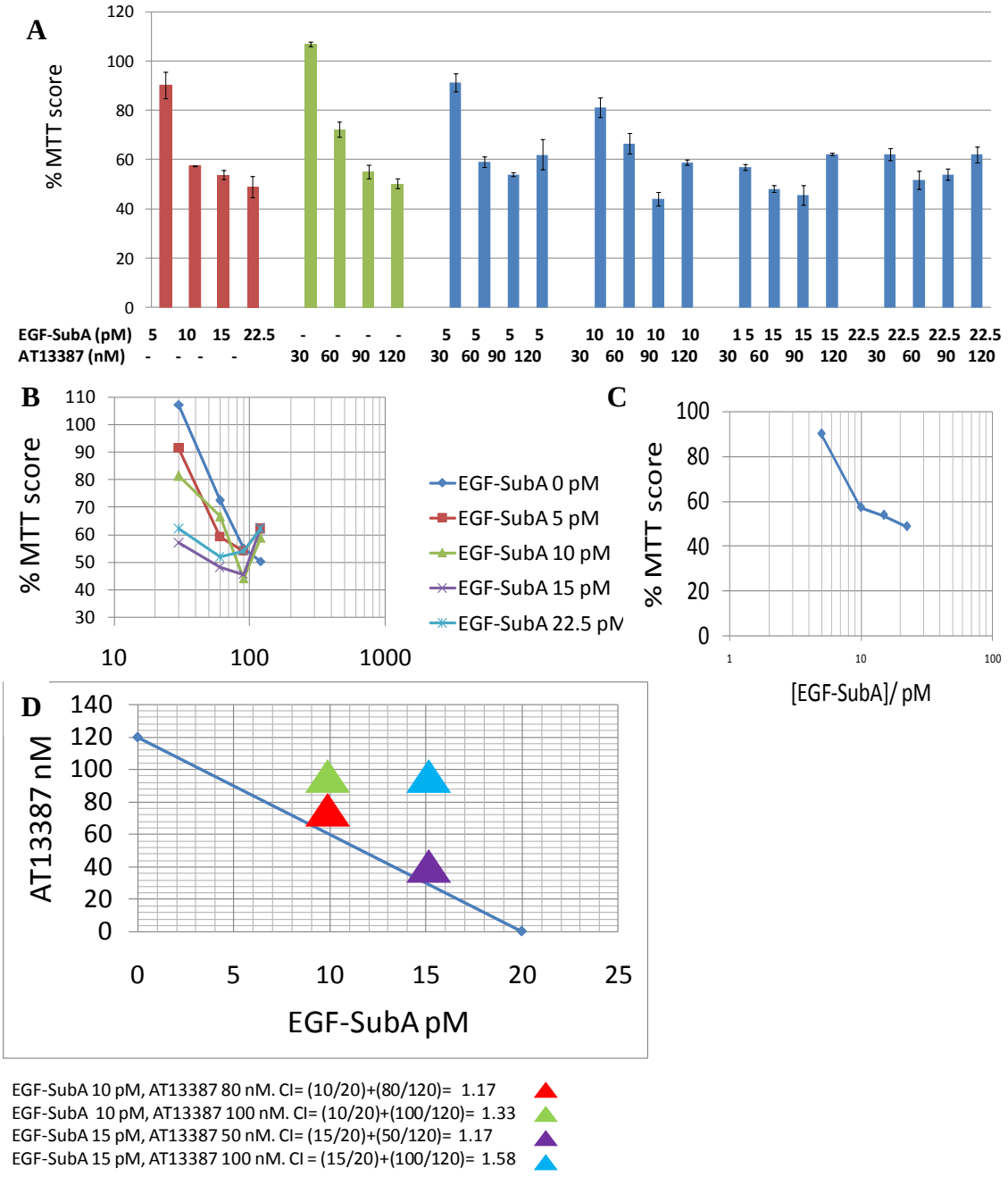

Figure 7.4.8 AT13387 in combination with EGF-SubA produces an antagonistic effect in UM-SCC 81B treated cells.

(A) UM-SCC 81B cells were seeded in 96 well plates and allowed to adhere for 24 hours. Cells were then treated at a range of concentrations of either EGF-SubA at 5, 10, 15, 22.5pM alone or AT13387 at 30, 60, 90, 120nM alone, in combination, or with drug vehicle control. Both media and drugs were replaced every 24h for a total of seven days. MTT assay was used to assess the viability/growth of cells after day seven. The absorbance was measured at an OD of 590 nm. Bars represent the percentage MTT score of treated groups as a proportion of controls. Error bars show the s.e.m. from four independent wells. (B and C) New IC_{50} values were calculated from log plots derived from data as shown in Figure A for either EGF-SubA on its own, AT13387 on its own and any IC_{50} values established when EGF-SubA and AT13387 were used in combination. IC_{50} curves were plotted as: percentage MTT score in the drug treated group as a proportion of the control group (y-axis) against the dose of the drug on a log scale (x-axis). (D) Isobologram showing a line joining the IC_{50} value of AT13387 at 120nM with the IC_{50} value of EGF-SubA at 20pM. When EGF-SubA was combined with AT13387 antagonistic effects were observed with combination (CI) indexes of above 1.1. (CI) at $IC_{50}= (D)_1/(D_x)_1 + (D)_2/(D_x)_2$. $(D_x)_1$ and $(D_x)_2$ is the dose of each of the drugs which, when used alone results in the IC_{50}. $(D)_1$ and $(D)_2$ are the doses of each drug which when in combination result in the IC_{50}.

8 Appendix: Trastuzumab in combination with cetuximab.

8.1 Trastuzumab enhances the cytotoxic effects of cetuximab in UM-SCC 5, 12 and 81B but not in resistant cell line UM-SCC 17AS.

EGFR is a member of the HER family of receptor tyrosine kinases which consists of EGFR, HER2, HER3 and HER4. HER family members share several downstream signalling cascades such as the MAPK and PI3K/AKT pathways, which can be initiated upon homo or hetero-dimerization between HER members (70). For example ligand-EGFR binding stimulates homo-dimerization or hetero-dimerization with other HER family members leading to phosphorylation of tyrosine residues which can then activate downstream pathways. Other HER family members such as HER2 can hetero-dimerize with HER3 activating the same signalling pathways as EGFR. These signalling cascades are responsible for promoting cell proliferation, cell survival, angiogenesis and metastasis (181).

A study by Wheeler and colleagues in 2008 cultured UM-SCC 1 cells in cetuximab for a total of six months thus obtaining a sub group of UM-SCC 1 cells which were resistant

to cetuximab (70). Upon comparison between parental UM-SCC 1 and resistant cells the study found that there were increased levels of phospho-EGFR, phospho-HER2 and phospho-HER3 in the resistant cells. Higher levels of phosphorylated forms of MAPK and AKT were also detected in the cetuximab resistant cells.

It was also demonstrated through co-immunoprecipitation experiments that cetuximab resistant cells displayed increased EGFR binding with HER2 and HER3, thus suggesting that EGFR in cetuximab resistant cells have enhanced ability to hetero-dimerize with and transphosphorylate HER2 and HER3.

To further investigate the role of HER2 and HER3 in cetuximab resistance the study used mAb 2C4 which binds and inhibits HER2 dimerization (70). As well as EGFR, HER2 can also hetero-dimerize with and promote the activity of HER3 (70). Treatment of cetuximab had little effect on HER2, HER3 and AKT activity whereas 2C4 treatment decreased the activity of these tyrosine kinases in the resistant cell lines. When cetuximab and 2C4 were combined together a potent suppression of phospho-HER3 and phospho-AKT was observed suggesting that HER3 activity which is dependent on EGFR and HER2 may promote survival in cetuximab resistant cells. Furthermore the use of siRNA against HER3 resulted in clones overcoming cetuximab resistance. Therefore HER3 through activation via hetero-dimerization with EGFR or HER2 may be a critical signal mediator in promoting cetuximab resistance (70). A similar study by

Kawaguchi and colleagues in 2007 used trastuzumab, a monoclonal antibody against HER2, in combination with cetuximab and found synergistic effects *in vitro* in oesophageal squamous carcinomas (182). Kawaguchi and colleagues used 68nM and 0.68μM dilutions of trastuzumab in combination with cetuximab at 3.4nM and 34nM dilutions (182).

In section 4.7.1 it was seen that cetuximab as a single agent had very little effect on inhibiting the viability/growth of UM-SCC cells. However, as discussed above, it is indicated by the study of Kawaguchi and colleagues that the resistance to cetuximab may be overcome by simultaneously targeting both EGFR and HER2. Therefore, the combined effects of cetuximab with trastuzumab on cell viability/growth in laryngeal and oral squamous cell carcinoma cell lines: UM-SCC 5, 12, 81B and 1 as well as the most resistant cell line which did not show any response to cetuximab alone UM-SCC 17AS, were investigated.

A preliminary MTT proliferation assay was set up in order to monitor the effects of trastuzumab at a high dose of 1μM on the viability/growth of UM-SCC cells. UM-SCC cell lines were seeded into 96 well plates and left for 24h. Cells were then treated with trastuzumab at 1μM or with drug vehicle control for a total of seven days. Due to a shortage of trastuzumab UM-SCC 1 cells were treated with a maximum dilution of

100nM trastuzumab for a period of five days. Fresh media and drugs were replaced daily. MTT analysis was performed as described in materials and methods section 3.12.

As can be seen in Figure 8.1.1, trastuzumab had little effect on the viability/growth of UM-SCC cell lines. In two cases UM-SCC 12 and 81B no decrease in MTT score was observed as compared to controls. UM-SCC 11B was the most sensitive cell line with a decrease of 38% in MTT score after seven days treatment with trastuzumab.

A

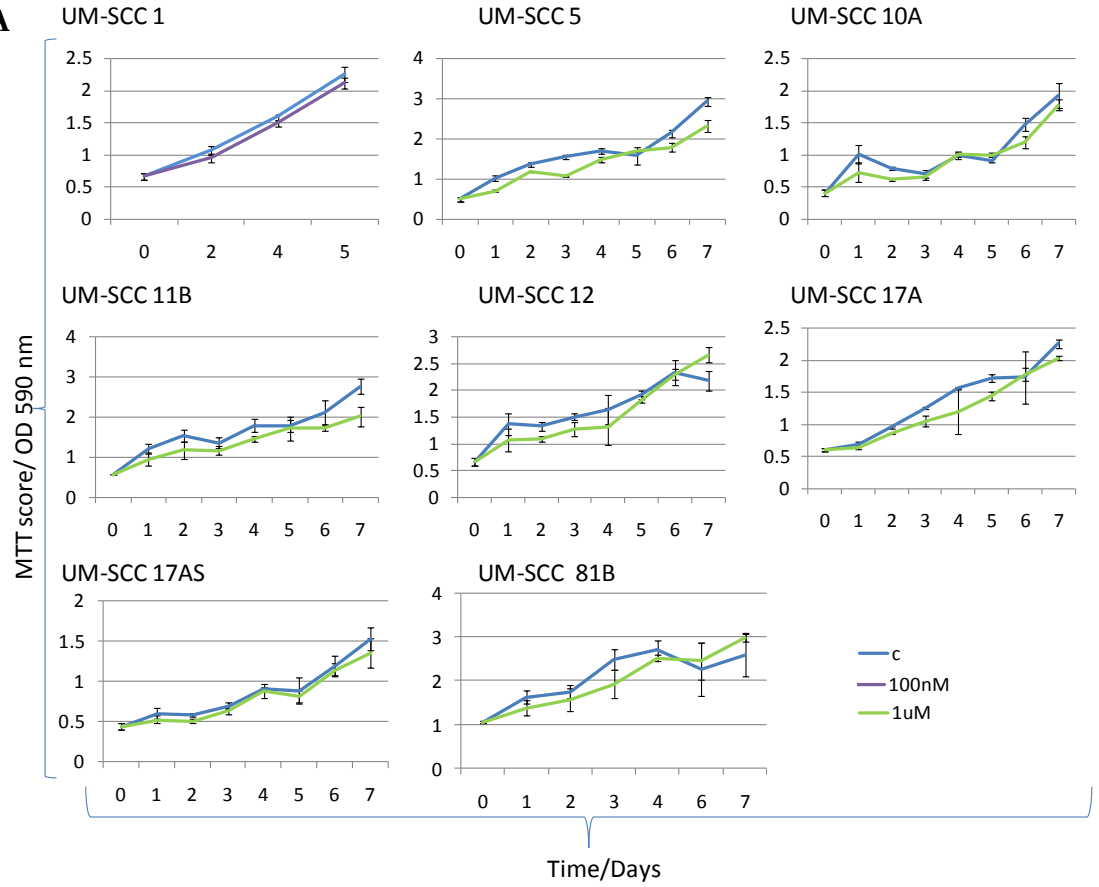

B

UM-SCC	1	5	10A	11B	12	17A	17AS	81B
Percentage decrease in MTT score	5%	21%	11%	38%	0%	9%	13%	0%

Figure 8.1.1 1μM trastuzumab has little effect on the viability/growth of UM-SCC cells.

(A) UM-SCC laryngeal and oral squamous carcinoma cells were seeded in 96 well plates and allowed to adhere for 24 hours (shown as day 0). Laryngeal squamous cell carcinoma cell lines were treated with either trastuzumab at 1μM or with drug vehicle control. Oral squamous cell carcinoma cell line UM-SCC 1 was treated with only 100nM trastuzumab due to a shortage of drug at the time of conducting the experiments. Both media and drugs were replaced every 24h. MTT assay was used to assess the quantity/viability of cells. Absorbance was measured at an OD of 590 nm. Error bars represent the s.e.m. from four independent wells. (B) Percentage decrease in MTT score of treated groups as a proportion of control groups after seven days of 1μM trastuzumab treatment for laryngeal squamous cell carcinoma cell lines or after five days of 100nM trastuzumab treatment for UM-SCC 1.

Next, the inhibitory effects on cell viability/growth of cetuximab in combination with trastuzumab were tested. UM-SCC 1, 5, 12, 17AS and 81B were seeded in 96 well plates and left to adhere for 24h. After which cells were treated with either trastuzumab at 1nM, 10nM and 100nM alone; or cetuximab at 1nM, 10nM, 100nM and 1μM alone, or in combination, or with drug vehicle control. Fresh drugs and media were replaced daily for a total of five days. MTT analysis was performed as described in Methods section 3.12, on the last day. Unpaired Student's t test was used to assess if there was any significant difference in inhibitory effect between drug combination compared to cetuximab and trastuzumab being used as single agents.

The majority of cetuximab and trastuzumab combinations in UM-SCC 1, 5, 12, and 81B produced significantly greater reductions ($p<0.05$) in viability/growth as compared to drugs when used as single agents as seen in Figure 8.1.2. Even at the lowest dilutions of 1nM trastuzumab combined with 1nM cetuximab there were statistically significant ($p<0.05$) decreases in percentage viability/growth as measured by MTT, of 14% in UM-SCC 1, 19% in UM-SCC 5, and 62% in UM-SCC 81B as compared to when cells were treated with single agents. However there was no additional inhibitory effect seen in UM-SCC 17AS when cetuximab at different concentrations were used in combination with trastuzumab at different concentrations. One exception was when 1nM cetuximab was combined with 10nM trastuzumab in UM-SCC 17AS ($p<0.01$) there appeared a

significant inhibitory effect compared to when cetuximab or trastuzumab at these concentrations were used as single agents. However this result may be a possible outlier.

In agreement with Kawaguchi and colleagues in 2007 which found enhanced effects of combining cetuximab with trastuzumab in oesophageal cancer cell lines, results presented in this thesis show that these mAbs produce an enhanced cytotoxic effect against cell viability/growth, when combined together, in laryngeal and oral squamous cell carcinoma cell lines.

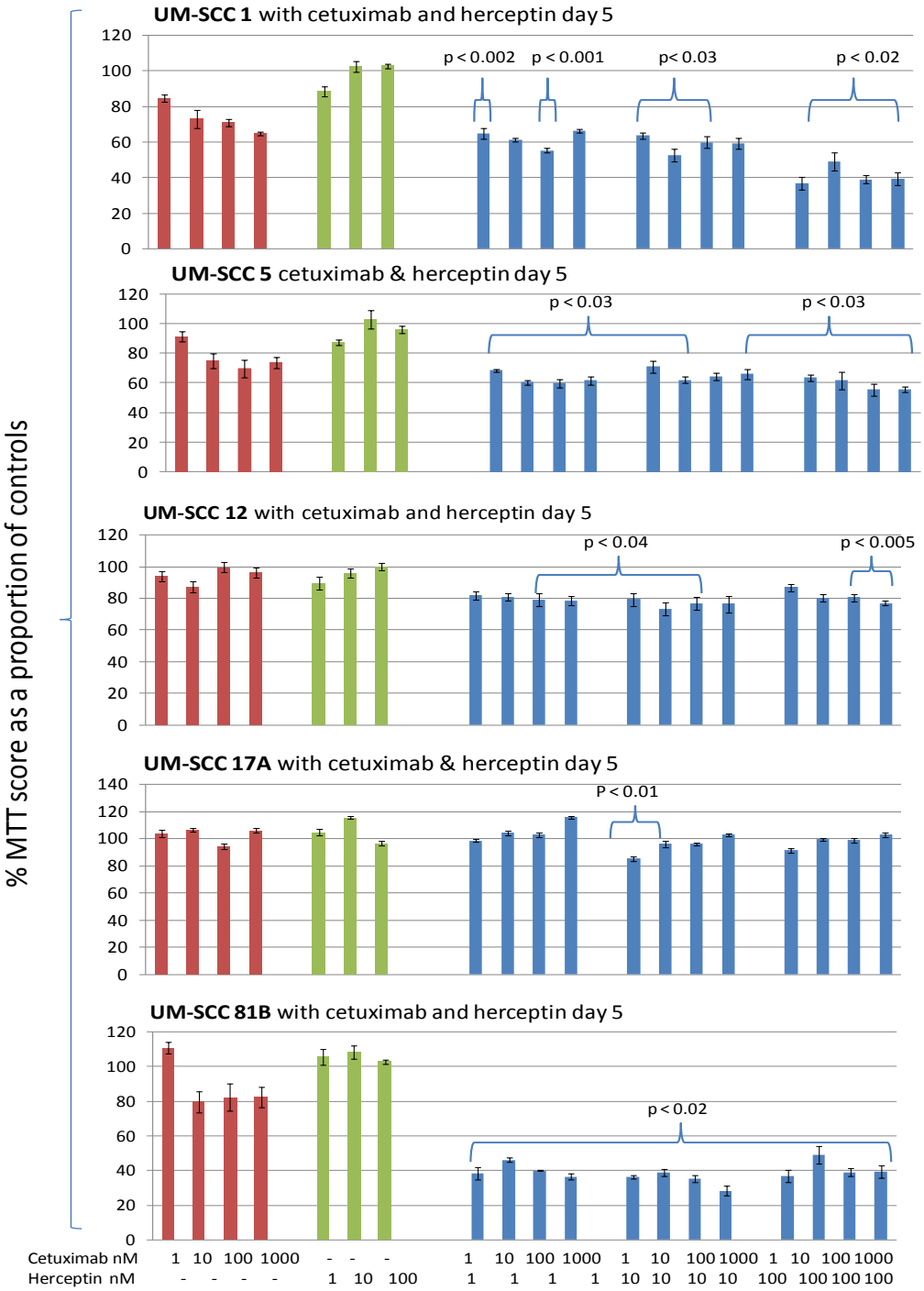

Figure 8.1.2 Cytotoxic effects of either cetuximab alone or trastuzumab alone (herceptin) or in combination on UM-SCC cells.

UM-SCC 5 cells were seeded in 96 well plates and allowed to adhere for 24 hours. Cells were treated with either trastuzumab at 1nM, 10nM and 100nM alone; or cetuximab at 1nM, 10nM, 100nM and 1μM alone, or both drugs in combination, or with drug vehicle control. Both media and drugs were replaced every 24h for a total of five days. MTT assay was used to assess the viability/growth of cells after day five. Absorbance was measured at an OD of 590 nm. Bars represent the percentage MTT score of treated groups compared to controls. Error bars show the s.e.m. from four independent wells. Unpaired Student's t test was used to calculate statistical significance in drug combinations

8.2 Investigating trastuzumab and cetuximab as radiosensitising agents.

Few studies have commented upon the use of trastuzumab as a radiosensitising agent. HER2 inhibition may act as a radiosensitising agent by blocking downstream signalling pathway PI3K/AKT which is known to mediate radioresistance in cancers (181). A study by Linag and colleagues in 2003, which pre-incubated breast cancer cells for 1 hour with 20nM trastuzumab found trastuzumab to act as a radiosensitising agent (181). Furthermore a study by Uno and colleagues in 2001, found trastuzumab to have radiosensitising effects on laryngeal cell line HEp-2. Hep-2 cells were pre-incubated for four days with trastuzumab at concentration of 0.64nM, 6.4nM and 64nM. At all concentrations a significant radiosensitising effect was found.

Previous results in this thesis (see Figure 8.1.2) have shown that cetuximab in combination with trastuzumab was found to have a greater cytotoxic effect than when both drugs were used as single agents, in four out of the five cell lines tested. Therefore it was investigated whether or not cetuximab in combination with trastuzumab could enhance the effects of radiation even further than when trastuzumab and cetuximab were used as single agents.

Pilot studies were performed in order to establish the highest drug combinatorial concentrations that cells could tolerate for 24h without exposure to radiation that would provide survival fractions equal to that of drug omitted controls. UM-SCC cells were pre-incubated with either 1nM trastuzumab alone, 1nM cetuximab alone, or both drugs in combination, or with drug vehicle control for 24h before being irradiated with 0, 1, 2, or 4 Gy. Cells were then seeded in triplicate into six well plates, in normal growth media without drugs and monitored for colony formation for 2-3 weeks.

Colonies were counted using a light microscope. The mean number of colonies were recorded for each set of triplicate samples. Survival fractions were calculated and radiation survival curves were fitted according to the linear-quadratic model $S(D)/S(0)=\exp(-(\alpha D + \beta D^2))$, where D is the irradiation dose in Gy; α is the cell kill per Gy of the initial linear component and β is the cell kill per Gy^2 of the quadratic component of the survival curve. SPSS PASW statistics package version 18 was used to find values of α and β and survival curves were plotted as seen in

Unpaired Student's t test was used to evaluate whether there were significant differences in SF2 between controls and cells pre-treated with trastuzumab at 1nM, or cetuximab at 1nM, or drugs combined together. However no radiosensitising effects were observed as shown in Figure 8.2.1. These results suggest that cetuximab and trastuzumab, *in vitro*, are not effective radiosensitising agents in laryngeal squamous cell carcinoma cell lines. The only exception being when UM-SCC 81B cells were treated with trastuzumab at

1nM there was a significant reduction in survival fraction by 28% as compared to controls (p=0.019).

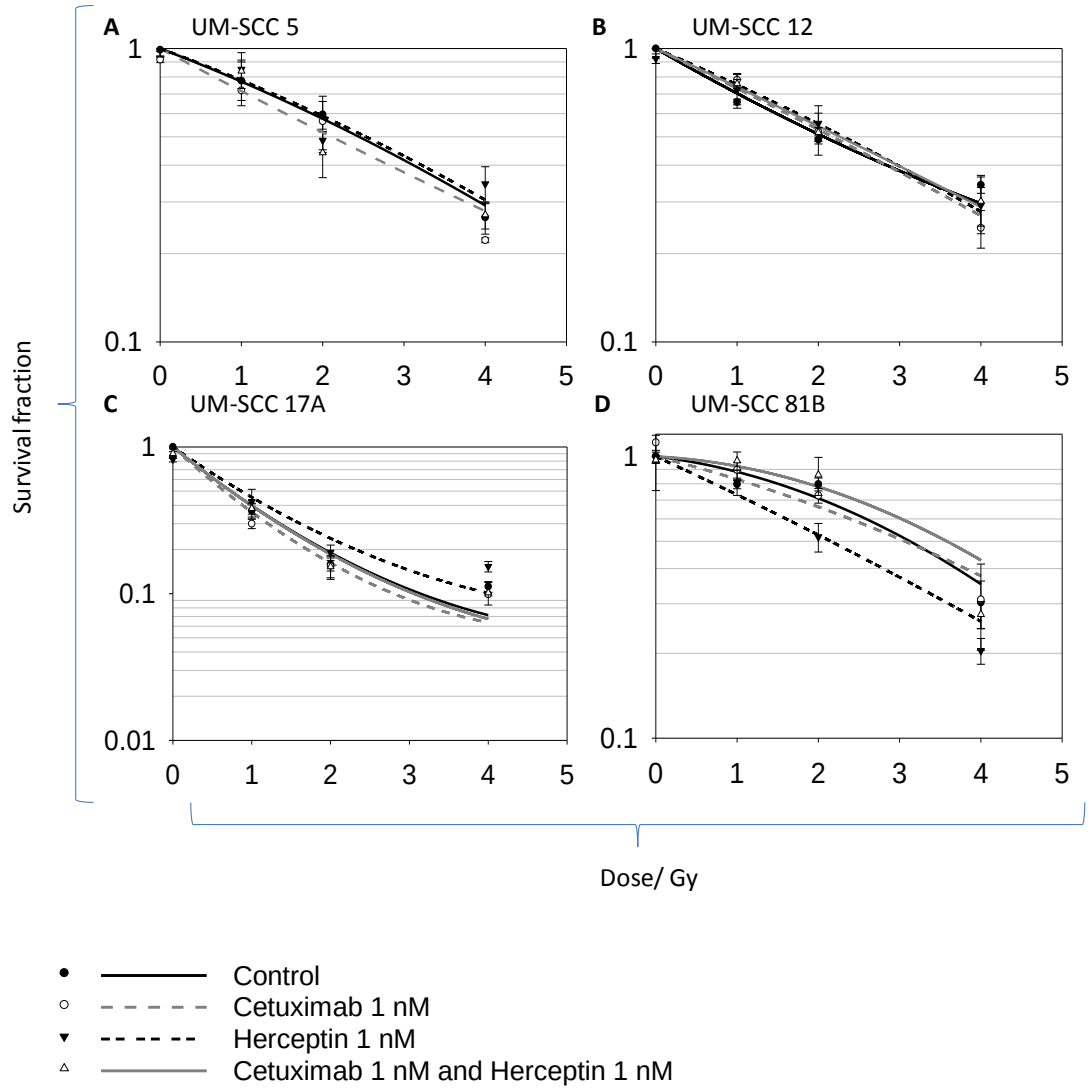

Figure 8.2.1 No enhancement in radiosensitivity was observed at 1nM cetuximab, or 1nM trastuzumab (herceptin), or when both drugs were combined, as compared to controls.

UM-SCC 5, 12, 17A and 81B cells were pre-treated for 24h with 1nM cetuximab, or 1nM trastuzumab, or in combination, or with drug vehicle control and then exposed to γ-irradiation at 0, 1, 2, or 4 Gy as indicated. Clonogenic assays were established to allow for colony formation over a time period of two to three weeks. A colony was defined as equal to or more than 50 cells in order to allow for at least five cell doubling times. Diamonds and triangles indicate mean of three survival fractions for each data point with appropriate s.e.m. Cell survival curves were then fitted to the quadratic equation $S(D)/S(0)= \exp(-(\alpha D + \beta D^2))$*. Unpaired Student's t test was used to evaluate whether there were significant differences in SF2 between controls and treated cells. No significant differences in SF2 between treated and untreated cells were observed with the exception of UM-SCC 81B when cells were treated with trastuzumab 1nM (D) where SF2 decreased by 28% compared to controls (p=0.019).*

9 Appendix: TNM classification for head and neck cancers

9.1 TNM classification

This test box is where the original thesis contained the table showing 'TNM staging for head and neck tumours' which was reproduced from reference *(22)*.

This test box is where the original thesis contained the table showing ‘TNM staging for head and neck tumours’ which was reproduced from reference *(22)*.

This test box is where the original thesis contained the table showing ‘TNM staging for head and neck tumours’ which was reproduced from reference *(22)*.

Figure 9.1.1 Staging of head and neck tumours

Tables reproduced from reference (22)

10 References

1. Chiu C, Lin C, Lee L, Chen Y, Kuo T, Wang H, et al. Glucose regulated protein 78 regulates multiple malignant phenotypes in head and neck cancer and may serve as a molecular target of therapeutic intervention. Molecular cancer therapeutics. 2008;7(9):2788-97.
2. Mehanna H, Paleri V, West CML, Nutting C. Head and neck cancer--Part 1: Epidemiology, presentation, and prevention. BMJ.341:c4684.
3. Feng X-P, Yi H, Li M-Y, Li X-H, Yi B, Zhang P-F, et al. Identification of biomarkers for predicting nasopharyngeal carcinoma response to radiotherapy by proteomics. Cancer Research. May 1;70(9):3450-62.
4. Du X-L, Hu H, Lin D-C, Xia S-H, Shen X-M, Zhang Y, et al. Proteomic profiling of proteins dysregulted in Chinese esophageal squamous cell carcinoma. Journal of Molecular Medicine. 2007 Aug;85(8):863-75.
5. Backer JM, Krivoshein AV, Hamby CV, Pizzonia J, Gilbert KS, Ray YS, et al. Chaperone-targeting cytotoxin and endoplasmic reticulum stress-inducing drug synergize to kill cancer cells. Neoplasia. Nov;11(11):1165-73.
6. Hanawa M, Suzuki S, Dobashi Y, Yamane T, Kono K, Enomoto N, et al. EGFR protein overexpression and gene amplification in squamous cell carcinomas of the esophagus. International Journal of Cancer. 2006 Mar 1;118(5):1173-80.
7. Paton AW, Beddoe T, Thorpe CM, Whisstock JC, Wilce MCJ, Rossjohn J, et al. AB5 subtilase cytotoxin inactivates the endoplasmic reticulum chaperone BiP. Nature. 2006 Oct 5;443(7111):548-52.
8. Lin T-Y, Chang JT-C, Wang H-M, Chan S-H, Chiu C-C, Lin C-Y, et al. Proteomics of the radioresistant phenotype in head-and-neck cancer: Gp96 as a novel prediction marker and sensitizing target for radiotherapy. International Journal of Radiation Oncology, Biology, Physics. Sep 1;78(1):246-56.
9. Parkin DM, Bray F, Ferlay J, Pisani P. Global cancer statistics, 2002. CA: a Cancer Journal for Clinicians. 2005 Mar-Apr;55(2):74-108.
10. Doobaree IU, Landis SH, Linklater KM, El-Hariry I, Moller H, Tyczynski J. Head and neck cancer in South East England between 1995-1999 and 2000-2004: An estimation of incidence and distribution by site, stage and histological type. Oral Oncology. 2009 Sep;45(9):809-14.
11. Mork J, Lie K, Glattre E, Hallmans G, Jellum E, Koskela P, et al. Human papillomavirus infection as a risk factor for squamous cell carcinoma of the head and neck. The New England journal of medicine. 2001;344(15):1125-31.

12. Head and neck cancer: question and answers. National Cancer Institute; 2005 [updated 2005; cited 2011]; Available from: http://www.cancer.gov/cancertopics/factsheet/Sites-Types/head-and-neck.
13. Druesne-Pecollo N, Tehard B, Mallet Y, Gerber M, Norat T, Hercberg S, et al. Alcohol and genetic polymorphisms: effect on risk of alcohol-related cancer. Lancet Oncology. 2009 Feb;10(2):173-80.
14. Toh Y, Oki E, Ohgaki K, Sakamoto Y, Ito S, Egashira A, et al. Alcohol drinking, cigarette smoking, and the development of squamous cell carcinoma of the esophagus: molecular mechanisms of carcinogenesis. International Journal of Clinical Oncology. Apr;15(2):135-44.
15. Braakhuis BJM, Brakenhoff RH, Meijer CJLM, Snijders PJF, Leemans CR. Human papilloma virus in head and neck cancer: the need for a standardised assay to assess the full clinical importance. European Journal of Cancer. 2009 Nov;45(17):2935-9.
16. Ro H-S, Koh BH, Jung SO, Park HK, Shin Y-B, Kim M-G, et al. Surface plasmon resonance imaging protein arrays for analysis of triple protein interactions of HPV, E6, E6AP, and p53. Proteomics. 2006 Apr;6(7):2108-11.
17. Marur S, D'Souza G, Westra WH, Forastiere AA. HPV-associated head and neck cancer: a virus-related cancer epidemic. Lancet Oncology. Aug;11(8):781-9.
18. Mannarini L, Kratochvil V, Calabrese L, Gomes Silva L, Morbini P, Betka J, et al. Human Papilloma Virus (HPV) in head and neck region: review of literature. Acta Otorhinolaryngologica Italica. 2009 Jun;29(3):119-26.
19. Kumar B, Cordell KG, Lee JS, Worden FP, Prince ME, Tran HH, et al. EGFR, p16, HPV Titer, Bcl-xL and p53, sex, and smoking as indicators of response to therapy and survival in oropharyngeal cancer. Journal of Clinical Oncology. 2008 Jul 1;26(19):3128-37.
20. Hobbs CGL, Sterne JAC, Bailey M, Heyderman RS, Birchall MA, Thomas SJ. Human papillomavirus and head and neck cancer: a systematic review and meta-analysis. Clinical Otolaryngology. 2006 Aug;31(4):259-66.
21. Vu HL, Sikora AG, Fu S, Kao J. HPV-induced oropharyngeal cancer, immune response and response to therapy. Cancer Lett. Feb 28;288(2):149-55.
22. Junor E, See K, Brown E, Carroll D, Cohen L, Collie D, et al. Diagnosis and management of head and neck cancer. A national clinical guideline. In: Network SIG, editor.; 2006.
23. Mehanna H, West CML, Nutting C, Paleri V. Head and neck cancer--Part 2: Treatment and prognostic factors. BMJ.341:c4690.
24. Yao M, Epstein JB, Modi BJ, Pytynia KB, Mundt AJ, Feldman LE. Current surgical treatment of squamous cell carcinoma of the head and neck. Oral Oncology. [Review].43(3):213-23.
25. Liu JC, Shah JP. Surgical technique refinements in head and neck oncologic surgery. Journal of Surgical Oncology. [Research Support, N.I.H., Extramural Review].101(8):661-8.

26. Langendijk JA, Ferlito A, Takes RP, Rodrigo JP, Suarez C, Strojan P, et al. Postoperative strategies after primary surgery for squamous cell carcinoma of the head and neck. Oral Oncology. [Review].46(8):577-85.
27. Bhide SA, Nutting CM. Recent advances in radiotherapy. BMC Medicine.8:25.
28. Chen AM, Farwell DG, Luu Q, Chen LM, Vijayakumar S, Purdy JA. Misses and near-misses after postoperative radiation therapy for head and neck cancer: Comparison of IMRT and non-IMRT techniques in the CT-simulation era. Head & Neck. Nov;32(11):1452-9.
29. Kim S, Grandis JR, Rinaldo A, Takes RP, Ferlito A. Emerging perspectives in epidermal growth factor receptor targeting in head and neck cancer. Head & Neck. 2008 May;30(5):667-74.
30. NICE. Cetuximab for the treatment of locally advanced squamous cell cancer of the head and neck. 2008.
31. Dassonville O, Bozec A, Fischel JL, Milano G. EGFR targeting therapies: monoclonal antibodies versus tyrosine kinase inhibitors. Similarities and differences. Critical Reviews in Oncology-Hematology. 2007 Apr;62(1):53-61.
32. Powell C, Mikropoulos C, Kaye SB, Nutting CM, Bhide SA, Newbold K, et al. Pre-clinical and clinical evaluation of PARP inhibitors as tumour-specific radiosensitisers. Cancer Treatment Reviews. Nov;36(7):566-75.
33. Dai Y, Grant S. New insights into checkpoint kinase 1 in the DNA damage response signaling network. Clinical Cancer Research. Jan 15;16(2):376-83.
34. Yap TA, Sandhu SK, Carden CP, de Bono JS. Poly(ADP-ribose) polymerase (PARP) inhibitors: Exploiting a synthetic lethal strategy in the clinic. CA: a Cancer Journal for Clinicians. Jan-Feb;61(1):31-49.
35. Normanno N, Maiello MR, De Luca A. Epidermal growth factor receptor tyrosine kinase inhibitors (EGFR-TKIs): simple drugs with a complex mechanism of action? Journal of Cellular Physiology. 2003 Jan;194(1):13-9.
36. Weinberg RA. Growth factors and their receptors. The biology of cancer: Garland Science, Taylor & Francis Group, LLC; 2007. p. 119-58.
37. Weinberg RA. Cytoplasmic signalling circuitary programs many of the traits of cancer. The biology of cancer: Garland Science, Taylor & Francis Group, LLC; 2007. p. 159-208.
38. Spano JP, Milano G, x00E, rard, Vignot S, phane, et al. Potential predictive markers of response to EGFR-targeted therapies in colorectal cancer. Critical Reviews in Oncology-Hematology. 2008 Apr;66(1):21-30.
39. Weinberg RA. The biology and genetics of cells and organisms. The biology of cancer: Garland Science, Taylor & Francis Group, LLC; 2007. p. 1-24.
40. Weinberg RA. PRb and the control of the cell cycle clock. The biology of cancer; 2007. p. 255-306.
41. Grandis JR, Tweardy DJ. Elevated levels of transforming growth factor alpha and epidermal growth factor receptor messenger RNA are early markers of carcinogenesis in head and neck cancer. Cancer Research. [Research Support, Non-U.S. Gov't].53(15):3579-84.

42. Chung CH, Ely K, McGavran L, Varella-Garcia M, Parker J, Parker N, et al. Increased epidermal growth factor receptor gene copy number is associated with poor prognosis in head and neck squamous cell carcinomas. Journal of Clinical Oncology. [Research Support, Non-U.S. Gov't].24(25):4170-6.
43. Ryott M, Wangsa D, Heselmeyer-Haddad K, Lindholm J, Elmberger G, Auer G, et al. EGFR protein overexpression and gene copy number increases in oral tongue squamous cell carcinoma. European Journal of Cancer. [Research Support, N.I.H., Intramural
Research Support, Non-U.S. Gov't].45(9):1700-8.
44. Sarkis SA, Abdullah BH, Abdul Majeed BA, Talabani NG. Immunohistochemical expression of epidermal growth factor receptor (EGFR) in oral squamous cell carcinoma in relation to proliferation, apoptosis, angiogenesis and lymphangiogenesis. Head & neck oncology.2:13.
45. Dikic I, Giordano S. Negative receptor signalling. Current Opinion in Cell Biology. 2003 Apr;15(2):128-35.
46. Sorkin A, Goh LK. Endocytosis and intracellular trafficking of ErbBs. Experimental Cell Research. 2009 Feb 15;315(4):683-96.
47. Shtiegman K, Kochupurakkal BS, Zwang Y, Pines G, Starr A, Vexler A, et al. Defective ubiquitinylation of EGFR mutants of lung cancer confers prolonged signaling. Oncogene. 2007 Oct 25;26(49):6968-78.
48. Sok JC, Coppelli FM, Thomas SM, Lango MN, Xi S, Hunt JL, et al. Mutant epidermal growth factor receptor (EGFRvIII) contributes to head and neck cancer growth and resistance to EGFR targeting. Clinical Cancer Research. 2006 Sep 1;12(17):5064-73.
49. Temam S, Kawaguchi H, El-Naggar AK, Jelinek J, Tang H, Liu DD, et al. Epidermal growth factor receptor copy number alterations correlate with poor clinical outcome in patients with head and neck squamous cancer. Journal of Clinical Oncology. 2007 Jun 1;25(16):2164-70.
50. Grandis JR, Melhem MF, Gooding WE, Day R, Holst VA, MM W. Levels of TGF-α and EGFR protein in head and neck squamous cell carcinoma and patient survival. Journal of the National Cancer Institute. 1998;90(11):824-32.
51. Ang KK, Berkey BA, Tu X, Zhang H-Z, Katz R, Hammond EH, et al. Impact of epidermal growth factor receptor expression on survival and pattern of relapse in patients with advanced head and neck carcinoma. Cancer Research. 2002 Dec 15;62(24):7350-6.
52. Barker FG, 2nd, Simmons ML, Chang SM, Prados MD, Larson DA, Sneed PK, et al. EGFR overexpression and radiation response in glioblastoma multiforme. International Journal of Radiation Oncology, Biology, Physics. 2001 Oct 1;51(2):410-8.
53. Noordhuis MG, Eijsink JJH, Ten Hoor KA, Roossink F, Hollema H, Arts H, et al. Expression of epidermal growth factor receptor (EGFR) and activated EGFR predict poor response to (chemo)radiation and survival in cervical cancer. Clinical Cancer Research. 2009 Dec 1;15(23):7389-97.

54. Vincenzi B, Schiavon G, Silletta M, Santini D, Tonini G. The biological properties of cetuximab. Critical Reviews in Oncology-Hematology. 2008 Nov;68(2):93-106.
55. Jaramillo ML, Leon Z, Grothe S, Paul-Roc B, Abulrob A, O'Connor McCourt M. Effect of the anti-receptor ligand-blocking 225 monoclonal antibody on EGF receptor endocytosis and sorting. Experimental Cell Research. 2006 Sep 10;312(15):2778-90.
56. Kiyota A, Shintani S, Mihara M, Nakahara Y, Ueyama Y, Matsumura T, et al. Anti-epidermal growth factor receptor monoclonal antibody 225 upregulates p27(KIP1) and p15(INK4B) and induces G1 arrest in oral squamous carcinoma cell lines. Oncology. 2002;63(1):92-8.
57. Huang SM, Bock JM, Harari PM. Epidermal growth factor receptor blockade with C225 modulates proliferation, apoptosis, and radiosensitivity in squamous cell carcinomas of the head and neck. Cancer Research. 1999 Apr 15;59(8):1935-40.
58. Sclabas GM, Fujioka S, Schmidt C, Fan Z, Evans DB, Chiao PJ. Restoring apoptosis in pancreatic cancer cells by targeting the nuclear factor-kappaB signaling pathway with the anti-epidermal growth factor antibody IMC-C225. Journal of Gastrointestinal Surgery. 2003 Jan;7(1):37-43; discussion
59. Perrotte P, Matsumoto T, Inoue K, Kuniyasu H, Eve BY, Hicklin DJ, et al. Anti-epidermal growth factor receptor antibody C225 inhibits angiogenesis in human transitional cell carcinoma growing orthotopically in nude mice. Clinical Cancer Research. 1999 Feb;5(2):257-65.
60. Petit AM, Rak J, Hung MC, Rockwell P, Goldstein N, Fendly B, et al. Neutralizing antibodies against epidermal growth factor and ErbB-2/neu receptor tyrosine kinases down-regulate vascular endothelial growth factor production by tumor cells in vitro and in vivo: angiogenic implications for signal transduction therapy of solid tumors. American Journal of Pathology. 1997 Dec;151(6):1523-30.
61. Liang K, Ang KK, Milas L, Hunter N, Fan Z. The epidermal growth factor receptor mediates radioresistance. International Journal of Radiation Oncology, Biology, Physics. 2003 Sep 1;57(1):246-54.
62. Dittmann K, Mayer C, Rodemann H-P. Inhibition of radiation-induced EGFR nuclear import by C225 (Cetuximab) suppresses DNA-PK activity. Radiotherapy & Oncology. 2005 Aug;76(2):157-61.
63. Huang S, Armstrong EA, Benavente S, Chinnaiyan P, Harari PM. Dual-agent molecular targeting of the epidermal growth factor receptor (EGFR): combining anti-EGFR antibody with tyrosine kinase inhibitor. Cancer Research. 2004 Aug 1;64(15):5355-62.
64. Saltz LB, Meropol NJ, Loehrer PJ, Sr., Needle MN, Kopit J, Mayer RJ. Phase II trial of cetuximab in patients with refractory colorectal cancer that expresses the epidermal growth factor receptor. Journal of Clinical Oncology. 2004 Apr 1;22(7):1201-8.
65. De Roock W, Claes B, Bernasconi D, De Schutter J, Biesmans B, Fountzilas G, et al. Effects of KRAS, BRAF, NRAS, and PIK3CA mutations on the efficacy of

cetuximab plus chemotherapy in chemotherapy-refractory metastatic colorectal cancer: a retrospective consortium analysis. Lancet Oncology. Aug;11(8):753-62.
66. Yen L-C, Uen Y-H, Wu D-C, Lu C-Y, Yu F-J, Wu IC, et al. Activating KRAS mutations and overexpression of epidermal growth factor receptor as independent predictors in metastatic colorectal cancer patients treated with cetuximab. Annals of Surgery. Feb;251(2):254-60.
67. Loupakis F, Ruzzo A, Cremolini C, Vincenzi B, Salvatore L, Santini D, et al. KRAS codon 61, 146 and BRAF mutations predict resistance to cetuximab plus irinotecan in KRAS codon 12 and 13 wild-type metastatic colorectal cancer. British Journal of Cancer. 2009 Aug 18;101(4):715-21.
68. Frattini M, Saletti P, Romagnani E, Martin V, Molinari F, Ghisletta M, et al. PTEN loss of expression predicts cetuximab efficacy in metastatic colorectal cancer patients. British Journal of Cancer. 2007 Oct 22;97(8):1139-45.
69. Yen L-C, Yeh Y-S, Chen C-W, Wang H-M, Tsai H-L, Lu C-Y, et al. Detection of KRAS oncogene in peripheral blood as a predictor of the response to cetuximab plus chemotherapy in patients with metastatic colorectal cancer. Clinical Cancer Research. 2009 Jul 1;15(13):4508-13.
70. Wheeler DL, Huang S, Kruser TJ, Nechrebecki MM, Armstrong EA, Benavente S, et al. Mechanisms of acquired resistance to cetuximab: role of HER (ErbB) family members. Oncogene. 2008 Jun 26;27(28):3944-56.
71. Huang S-M, Li J, Armstrong EA, Harari PM. Modulation of radiation response and tumor-induced angiogenesis after epidermal growth factor receptor inhibition by ZD1839 (Iressa). Cancer Research. 2002 Aug 1;62(15):4300-6.
72. Ciardiello F, Bianco R, Damiano V, Fontanini G, Caputo R, Pomatico G, et al. Antiangiogenic and antitumor activity of anti-epidermal growth factor receptor C225 monoclonal antibody in combination with vascular endothelial growth factor antisense oligonucleotide in human GEO colon cancer cells. Clinical Cancer Research. 2000 Sep;6(9):3739-47.
73. Ciardiello F, Caputo R, Bianco R, Damiano V, Pomatico G, De Placido S, et al. Antitumor effect and potentiation of cytotoxic drugs activity in human cancer cells by ZD-1839 (Iressa), an epidermal growth factor receptor-selective tyrosine kinase inhibitor. Clinical Cancer Research. 2000 May;6(5):2053-63.
74. Magn, x00E, N., Fischel JL, Dubreuil A, Formento P, et al. Sequence-dependent effects of ZD1839 ('Iressa') in combination with cytotoxic treatment in human head and neck cancer. British Journal of Cancer. 2002 Mar 4;86(5):819-27.
75. Mellinghoff IK, Wang MY, Vivanco I, Haas-Kogan DA, Zhu S, Dia EQ, et al. Molecular determinants of the response of glioblastomas to EGFR kinase inhibitors.[Erratum appears in N Engl J Med. 2006 Feb 23;354(8):884]. New England Journal of Medicine. 2005 Nov 10;353(19):2012-24.
76. Cooper GM. Protein sorting and transport. The cell: Sinauer; 1997. p. 347-87.
77. Wegrzyn RD, Deuerling E. Molecular guardians for newborn proteins: ribosome-associated chaperones and their role in protein folding. Cellular & Molecular Life Sciences. 2005 Dec;62(23):2727-38.

78. Gestwicki JE. Special series: Molecular chaperones in protein folding and disease. Biopolymers. Mar;93(3):209-10.
79. Osborne AR, Rapoport TA, van den Berg B. Protein translocation by the Sec61/SecY channel. Annual Review of Cell & Developmental Biology. 2005;21:529-50.
80. Walter S, Buchner J. Molecular chaperones--cellular machines for protein folding. Angewandte Chemie-International Edition. 2002 Apr 2;41(7):1098-113.
81. Cooper GM. Protein synthesis, processing, and regulation. The cell: Sinauer; 1997. p. 273-310.
82. Malhotra JD, Kaufman RJ. The endoplasmic reticulum and the unfolded protein response. Seminars in Cell & Developmental Biology. 2007 Dec;18(6):716-31.
83. Scriven P, Brown NJ, Pockley AG, Wyld L. The unfolded protein response and cancer: a brighter future unfolding? Journal of Molecular Medicine. 2007 Apr;85(4):331-41.
84. Rutkowski DT, Kaufman RJ. A trip to the ER: coping with stress. Trends in Cell Biology. 2004 Jan;14(1):20-8.
85. Racek T, x00E, Buhlmann S, x00Fc, st F, Knoll S, et al. Transcriptional repression of the prosurvival endoplasmic reticulum chaperone GRP78/BIP by E2F1. Journal of Biological Chemistry. 2008 Dec 5;283(49):34305-14.
86. DeGracia DJ, Kumar R, Owen CR, Krause GS, White BC. Molecular pathways of protein synthesis inhibition during brain reperfusion: implications for neuronal survival or death. Journal of Cerebral Blood Flow & Metabolism. 2002 Feb;22(2):127-41.
87. Wolfson J, May K, Thorpe C, Jandhyala D, Paton J, Paton A. Subtilase cytotoxin activates PERK, IRE1 and ATF6 endoplasmic reticulum stress signalling pathways. Cellular microbiology. 2008;10(9):1775-86.
88. Harding H, Novoal I, Zhang Y, Zeng H, Wek R, Schapira M, et al. Regulated translation initiation controls stress-induced gene expression in mammalian cells. Molecular cell. 2000;6(1099-1108).
89. Marciniak S, Yun C, Oyadomari S. CHOP induces death by promoting protein synthesis and oxidation in the stressed endoplasmic reticulum. Genes & development. 2004;18:3066-77.
90. Lei K, Davis R. JNK phosphorylation of bim related members of the Bcl2 family induces Bax dependent apoptosis. PNAS. 2004;100(5):2432-7.
91. Tu B, Weissman J. Oxidative protein folding in eukaryotes: mechanism and consequences. The journal of cell biology. 2004;164(3):341-6.
92. Healy SJM, Gorman AM, Mousavi-Shafaei P, Gupta S, Samali A. Targeting the endoplasmic reticulum-stress response as an anticancer strategy. European Journal of Pharmacology. 2009;625(1-3):234-46.
93. Malhotra J, Kaufman R. The endoplasmic reticulum and the unfolded protein response. Seminars in cell & developmental biology. 2007;18(716-731).

94. Hosokawa N, Tremblay LO, Sleno B, Kamiya Y, Wada I, Nagata K, et al. EDEM1 accelerates the trimming of alpha1,2-linked mannose on the C branch of N-glycans. Glycobiology. May;20(5):567-75.
95. Kakinuma Y, Katare RG, Arikawa M, Muramoto K, Yamasaki F, Sato T. A HIF-1alpha-related gene involved in cell protection from hypoxia by suppression of mitochondrial function. FEBS Letters. 2008 Jan 23;582(2):332-40.
96. Sorensen BS, Horsman MR, Vorum H, Honore B, Overgaard J, Alsner J. Proteins upregulated by mild and severe hypoxia in squamous cell carcinomas in vitro identified by proteomics. Radiotherapy & Oncology. 2009 Sep;92(3):443-9.
97. Fu Y, Wey S, Wang M, Ye R, Liao C-P, Roy-Burman P, et al. Pten null prostate tumorigenesis and AKT activation are blocked by targeted knockout of ER chaperone GRP78/BiP in prostate epithelium. Proceedings of the National Academy of Sciences of the United States of America. 2008 Dec 9;105(49):19444-9.
98. Dong D, Ni M, Li J, Xiong S, Ye W, Virrey JJ, et al. Critical role of the stress chaperone GRP78/BiP in tumor proliferation, survival, and tumor angiogenesis in transgene-induced mammary tumor development. Cancer Res. 2008 Jan 15;68(2):498-505.
99. Zhang J, Jiang Y, Jia Z, Li Q, Gong W, Wang L, et al. Association of elevated GRP78 expression with increased lymph node metastasis and poor prognosis in patients with gastric cancer. Clinical & Experimental Metastasis. 2006;23(7-8):401-10.
100. Cooper GM, Hausman RE. Cell death and cell renewal. The cell 5th edition: Sinauer Associates Inc; 2009. p. 693-723.
101. Fulda S, Debatin KM. Extrinsic versus intrinsic apoptosis pathways in anticancer chemotherapy. Oncogene. 2006 Aug 7;25(34):4798-811.
102. Yamaguchi H, Wang H-G. CHOP is involved in endoplasmic reticulum stress-induced apoptosis by enhancing DR5 expression in human carcinoma cells. Journal of Biological Chemistry. 2004 Oct 29;279(44):45495-502.
103. Shu C-W, Sun F-C, Cho J-H, Lin C-C, Liu P-F, Chen P-Y, et al. GRP78 and Raf-1 cooperatively confer resistance to endoplasmic reticulum stress-induced apoptosis. J Cell Physiol. 2008 Jun;215(3):627-35.
104. Reddy RK, Mao C, Baumeister P, Austin RC, Kaufman RJ, Lee AS. Endoplasmic reticulum chaperone protein GRP78 protects cells from apoptosis induced by topoisomerase inhibitors: role of ATP binding site in suppression of caspase-7 activation. J Biol Chem. 2003 Jun 6;278(23):20915-24.
105. Urano F, Wang X, Bertolotti A, Zhang Y, Chung P, Harding HP, et al. Coupling of stress in the ER to activation of JNK protein kinases by transmembrane protein kinase IRE1. Science. 2000 Jan 28;287(5453):664-6.
106. Marcu LG. The role of amifostine in the treatment of head and neck cancer with cisplatin-radiotherapy. European Journal of Cancer Care. 2009 Mar;18(2):116-23.
107. Siddik ZH. Cisplatin: mode of cytotoxic action and molecular basis of resistance. Oncogene. 2003 Oct 20;22(47):7265-79.

108. Lee HK, Xiang C, Cazacu S, Finniss S, Kazimirsky G, Lemke N, et al. GRP78 is overexpressed in glioblastomas and regulates glioma cell growth and apoptosis. Neuro-Oncology. 2008 Jun;10(3):236-43.
109. Fu Y, Li J, Lee AS. GRP78/BiP inhibits endoplasmic reticulum BIK and protects human breast cancer cells against estrogen starvation-induced apoptosis. Cancer Res. 2007 Apr 15;67(8):3734-40.
110. Jiang CC, Mao ZG, Avery-Kiejda KA, Wade M, Hersey P, Zhang XD. Glucose-regulated protein 78 antagonizes cisplatin and adriamycin in human melanoma cells. Carcinogenesis. 2009 Feb;30(2):197-204.
111. Langer R, Ott K, Specht K, Becker K, Lordick F, Burian M, et al. Protein expression profiling in esophageal adenocarcinoma patients indicates association of heat-shock protein 27 expression and chemotherapy response. Clinical Cancer Research. 2008 Dec 15;14(24):8279-87.
112. Scriven P, Coulson S, Haines R, Balasubramanian S, Cross S, Wyld L. Activation and clinical significance of the unfolded protein response in breast cancer. British Journal of Cancer. 2009 Nov 17;101(10):1692-8.
113. Pyrko P, Schonthal AH, Hofman FM, Chen TC, Lee AS. The unfolded protein response regulator GRP78/BiP as a novel target for increasing chemosensitivity in malignant gliomas. Cancer Research. 2007 Oct 15;67(20):9809-16.
114. Wang Y, Wang W, Wang S, Wang J, Shao S, Wang Q. Down-regulation of GRP78 is associated with the sensitivity of chemotherapy to VP-16 in small cell lung cancer NCI-H446 cells. BMC Cancer. 2008;8:372.
115. Overgaard J, Eriksen JG, Nordsmark M, Alsner J, Horsman MR, Danish H, et al. Plasma osteopontin, hypoxia, and response to the hypoxia sensitiser nimorazole in radiotherapy of head and neck cancer: results from the DAHANCA 5 randomised double-blind placebo-controlled trial. Lancet Oncology. 2005 Oct;6(10):757-64.
116. Brown JM, Le Q-T. Tumor hypoxia is important in radiotherapy, but how should we measure it?[comment]. Int J Radiat Oncol Biol Phys. 2002 Dec 1;54(5):1299-301.
117. Schrijvers ML, van der Laan BFAM, de Bock GH, Pattje WJ, Mastik MF, Menkema L, et al. Overexpression of intrinsic hypoxia markers HIF1alpha and CA-IX predict for local recurrence in stage T1-T2 glottic laryngeal carcinoma treated with radiotherapy. Int J Radiat Oncol Biol Phys. 2008 Sep 1;72(1):161-9.
118. Silva P, Homer JJ, Slevin NJ, Musgrove BT, Sloan P, Price P, et al. Clinical and biological factors affecting response to radiotherapy in patients with head and neck cancer: a review. Clinical Otolaryngology. 2007 Oct;32(5):337-45.
119. Kaanders JHAM, Pop LAM, Marres HAM, Bruaset I, van den Hoogen FJA, Merkx MAW, et al. ARCON: experience in 215 patients with advanced head-and-neck cancer. International Journal of Radiation Oncology, Biology, Physics. 2002 Mar 1;52(3):769-78.
120. Langer R, Feith M, Siewert JR, x00Fc, diger, Wester H-J, et al. Expression and clinical significance of glucose regulated proteins GRP78 (BiP) and GRP94 (GP96) in human adenocarcinomas of the esophagus. BMC Cancer. 2008;8:70.

121. Osborne C, Brooks SA. SDS-PAGE and Western blotting to detect proteins and glycoproteins of interest in breast cancer research. Methods in Molecular Medicine. 2006;120:217-29.
122. Kumar GL, Rudbeck L. Immunohistochemistry Staining methods. Dako; 2010 [updated 2010; cited 2010]; Fifth:[Available from: http://www.dako.com/uk/08002_ihc_staining_methods_5ed.pdf.
123. Koopman G, Reutelingsperger CP, Kuijten GA, Keehnen RM, Pals ST, van Oers MH. Annexin V for flow cytometric detection of phosphatidylserine expression on B cells undergoing apoptosis. Blood. 1994 September 1, 1994;84(5):1415-20.
124. UCL. Cell cycle basics. 2010 [updated 2010; cited]; Available from: http://www.ucl.ac.uk/wibr/services/docs/cellcyc.pdf.
125. Shapiro H. Detection of BrUdR incorpoporation with anti-BrUdR antibody. Practical flow cytometry. 4th ed: Wiley-Lis; 2003. p. 455.
126. Franken NAP, Rodermond HM, Stap J, Haveman J, van Bree C. Clonogenic assay of cells in vitro. Nature Protocols. 2006;1(5):2315-9.
127. Ulukaya E, Ozdikicioglu F, Oral AY, Demirci M. The MTT assay yields a relatively lower result of growth inhibition than the ATP assay depending on the chemotherapeutic drugs tested. Toxicology in Vitro. 2008;22(1):232-9.
128. Pan Y-X, Lin L, Ren A-J, Pan X-J, Chen H, Tang C-S, et al. HSP70 and GRP78 induced by endothelin-1 pretreatment enhance tolerance to hypoxia in cultured neonatal rat cardiomyocytes. Journal of Cardiovascular Pharmacology. 2004 Nov;44 Suppl 1:S117-20.
129. Glen A, Gan CS, Hamdy FC, Eaton CL, Cross SS, Catto JWF, et al. iTRAQ-facilitated proteomic analysis of human prostate cancer cells identifies proteins associated with progression. Journal of Proteome Research. 2008 Mar;7(3):897-907.
130. Al-Rawashdeh FY, Scriven P, Cameron IC, Vergani PV, Wyld L. Unfolded protein response activation contributes to chemoresistance in hepatocellular carcinoma. European Journal of Gastroenterology & Hepatology. Sep;22(9):1099-105.
131. Bayley J-P, Devilee P. Warburg tumours and the mechanisms of mitochondrial tumour suppressor genes. Barking up the right tree? Current Opinion in Genetics & Development. Jun;20(3):324-9.
132. Djidja M-C, Claude E, Snel MF, Scriven P, Francese S, Carolan V, et al. MALDI-ion mobility separation-mass spectrometry imaging of glucose-regulated protein 78 kDa (Grp78) in human formalin-fixed, paraffin-embedded pancreatic adenocarcinoma tissue sections. Journal of Proteome Research. 2009 Oct;8(10):4876-84.
133. Zhuang L, Scolyer RA, Lee CS, McCarthy SW, Cooper WA, Zhang XD, et al. Expression of glucose-regulated stress protein GRP78 is related to progression of melanoma. Histopathology. 2009 Mar;54(4):462-70.
134. Wang Q, He Z, Zhang J, Wang Y, Wang T, Tong S, et al. Overexpression of endoplasmic reticulum molecular chaperone GRP94 and GRP78 in human lung cancer tissues and its significance. Cancer Detection & Prevention. 2005;29(6):544-51.
135. Woodhead AJ, Angove H, Carr MG, Chessari G, Congreve M, Coyle JE, et al. Discovery of (2,4-dihydroxy-5-isopropylphenyl)-[5-(4-methylpiperazin-1-ylmethyl)-1,3-

dihydroisoindol-2-yl]methanone (AT13387), a novel inhibitor of the molecular chaperone Hsp90 by fragment based drug design. Journal of Medicinal Chemistry. Aug 26;53(16):5956-69.
136. Bagatell R, Whitesell L. Altered Hsp90 function in cancer: a unique therapeutic opportunity. Molecular Cancer Therapeutics. 2004 Aug;3(8):1021-30.
137. Pearl LH, Prodromou C, Workman P. The Hsp90 molecular chaperone: an open and shut case for treatment. Biochemical Journal. 2008 Mar 15;410(3):439-53.
138. Ruan K, Song G, Ouyang G. Role of hypoxia in the hallmarks of human cancer. Journal of Cellular Biochemistry. 2009 Aug 15;107(6):1053-62.
139. Mote PL, Tillman JB, Spindler SR. Glucose regulation of GRP78 gene expression. Mechanisms of Ageing & Development. 1998 Aug 14;104(2):149-58.
140. Koumenis C, Bi M, Ye J, Feldman D, Koong AC, Helmut S, et al. Hypoxia and the Unfolded Protein Response. Methods in Enzymology: Academic Press; 2007. p. 275-93.
141. Rischin D, Fisher R, Peters L, Corry J, Hicks R. Hypoxia in head and neck cancer: studies with hypoxic positron emission tomography imaging and hypoxic cytotoxins. International Journal of Radiation Oncology, Biology, Physics. 2007;69(2 Suppl):S61-3.
142. Sorensen BS, Horsman MR, Vorum H, Honor B, Overgaard J, Alsner J. Proteins upregulated by mild and severe hypoxia in squamous cell carcinomas in vitro identified by proteomics. Radiotherapy & Oncology. 2009 Sep;92(3):443-9.
143. Shah JP. Patterns of cervical lymph node metastasis from squamous carcinomas of the upper aerodigestive tract. American Journal of Surgery. 1990 Oct;160(4):405-9.
144. Elkablawy MA, Maxwell P, Williamson K, Anderson N, Hamilton PW. Apoptosis and cell-cycle regulatory proteins in colorectal carcinoma: relationship to tumour stage and patient survival. Journal of Pathology. 2001 Aug;194(4):436-43.
145. Bewick V, Cheek L, Ball J. Statistics review 12: survival analysis. Critical Care. Oct;8(5):389-94.
146. Sawyers CL. The cancer biomarker problem. Nature. 2008 Apr 3;452(7187):548-52.
147. Yahiro K, Morinaga N, Moss J, Noda M. Subtilase cytotoxin induces apoptosis in HeLa cells by mitochondrial permeabilization via activation of Bax/Bak, independent of C/EBF-homologue protein (CHOP), Ire1alpha or JNK signaling. Microbial Pathogenesis. Oct;49(4):153-63.
148. Morinaga N, Yahiro K, Matsuura G, Moss J, Noda M. Subtilase cytotoxin, produced by Shiga-toxigenic Escherichia coli, transiently inhibits protein synthesis of Vero cells via degradation of BiP and induces cell cycle arrest at G1 by downregulation of cyclin D1. Cellular Microbiology. 2008 Apr;10(4):921-9.
149. Giono LE, Manfredi JJ. The p53 tumor suppressor participates in multiple cell cycle checkpoints. Journal of Cellular Physiology. 2006 Oct;209(1):13-20.
150. Pawlik TM, Keyomarsi K. Role of cell cycle in mediating sensitivity to radiotherapy. International Journal of Radiation Oncology, Biology, Physics. 2004 Jul 15;59(4):928-42.

151. Bonner JA, Harari PM, Giralt J, Azarnia N, Shin DM, Cohen RB, et al. Radiotherapy plus cetuximab for squamous-cell carcinoma of the head and neck. New England Journal of Medicine. 2006 Feb 9;354(6):567-78.
152. Benavente S, Huang S, Armstrong EA, Chi A, Hsu K-T, Wheeler DL, et al. Establishment and characterization of a model of acquired resistance to epidermal growth factor receptor targeting agents in human cancer cells. Clinical Cancer Research. 2009 Mar 1;15(5):1585-92.
153. Cuddihy AR, Bristow RG. The p53 protein family and radiation sensitivity: Yes or no? Cancer & Metastasis Reviews. 2004 Aug-Dec;23(3-4):237-57.
154. Crul M, van Waardenburg RCAM, Beijnen JH, Schellens JHM. DNA-based drug interactions of cisplatin. Cancer Treatment Reviews. 2002 Dec;28(6):291-303.
155. Bosch ME, Sanchez AJR, Rojas FS, Ojeda CB. Analytical methodologies for the determination of cisplatin. Journal of Pharmaceutical & Biomedical Analysis. 2008 Jul 15;47(3):451-9.
156. Chou T-C. Theoretical basis, experimental design, and computerized simulation of synergism and antagonism in drug combination studies. Pharmacological Reviews. 2006 Sep;58(3):621-81.
157. Siddik ZH, Hagopian GS, Thai G, Tomisaki S, Toyomasu T, Khokhar AR. Role of p53 in the ability of 1,2-diaminocyclohexane-diacetato-dichloro-Pt(IV) to circumvent cisplatin resistance. Journal of Inorganic Biochemistry. 1999 Oct;77(1-2):65-70.
158. Peyrou M, Hanna PE, Cribb AE. Cisplatin, gentamicin, and p-aminophenol induce markers of endoplasmic reticulum stress in the rat kidneys. Toxicological Sciences. 2007 Sep;99(1):346-53.
159. Mandic A, Hansson J, Linder S, Shoshan MC. Cisplatin induces endoplasmic reticulum stress and nucleus-independent apoptotic signaling. Journal of Biological Chemistry. 2003 Mar 14;278(11):9100-6.
160. Coling DE, Ding D, Young R, Lis M, Stofko E, Blumenthal KM, et al. Proteomic analysis of cisplatin-induced cochlear damage: methods and early changes in protein expression. Hearing Research. 2007 Apr;226(1-2):140-56.
161. McCollum AK, Lukasiewicz KB, Teneyck CJ, Lingle WL, Toft DO, Erlichman C. Cisplatin abrogates the geldanamycin-induced heat shock response. Molecular Cancer Therapeutics. 2008 Oct;7(10):3256-64.
162. Tao L, Zhou L, Zheng L, Yao M. Elemene displays anti-cancer ability on laryngeal cancer cells in vitro and in vivo. Cancer Chemotherapy & Pharmacology. 2006 Jul;58(1):24-34.
163. Fritschy J-M. Is my antibody-staining specific? How to deal with pitfalls of immunohistochemistry. European Journal of Neuroscience. 2008 Dec;28(12):2365-70.
164. Abcam. KDEL antibody- ER Marker (ab12223). 2011 [updated 2011; cited]; Available from: http://www.abcam.com/KDEL-antibody-10C3-ER-Marker-ab12223.html.
165. Daneshmand S, Quek ML, Lin E, Lee C, Cote RJ, Hawes D, et al. Glucose-regulated protein GRP78 is up-regulated in prostate cancer and correlates with recurrence and survival. Human Pathology. 2007 Oct;38(10):1547-52.

166. Arya AK, El-Fert A, Devling T, Eccles RM, Aslam MA, Rubbi CP, et al. Nutlin-3, the small-molecule inhibitor of MDM2, promotes senescence and radiosensitises laryngeal carcinoma cells harbouring wild-type p53. British Journal of Cancer. Jul 13;103(2):186-95.
167. Wang H, Paton JC, Paton AW. Pathologic changes in mice induced by subtilase cytotoxin, a potent new Escherichia coli AB5 toxin that targets the endoplasmic reticulum. Journal of Infectious Diseases. 2007 Oct 1;196(7):1093-101.
168. Maver PJ, Poljak M, Seme K, Kocjan BJ. Detection and typing of low-risk human papillomavirus genotypes HPV 6, HPV 11, HPV 42, HPV 43 and HPV 44 by polymerase chain reaction and restriction fragment length polymorphism. Journal of Virological Methods.169(1):215-8.
169. Mahalingam D, Swords R, Carew JS, Nawrocki ST, Bhalla K, Giles FJ. Targeting HSP90 for cancer therapy. British Journal of Cancer. 2009 May 19;100(10):1523-9.
170. Porter JR, Fritz CC, Depew KM. Discovery and development of Hsp90 inhibitors: a promising pathway for cancer therapy. Current Opinion in Chemical Biology. Jun;14(3):412-20.
171. Camphausen K, Tofilon PJ. Inhibition of Hsp90: a multitarget approach to radiosensitization. Clinical Cancer Research. 2007 Aug 1;13(15 Pt 1):4326-30.
172. Richter K, Buchner J. Hsp90: chaperoning signal transduction. Journal of Cellular Physiology. 2001 Sep;188(3):281-90.
173. Grbovic OM, Basso AD, Sawai A, Ye Q, Friedlander P, Solit D, et al. V600E B-Raf requires the Hsp90 chaperone for stability and is degraded in response to Hsp90 inhibitors. Proceedings of the National Academy of Sciences of the United States of America. 2006 Jan 3;103(1):57-62.
174. Bagatell R, Beliakoff J, David CL, Marron MT, Whitesell L. Hsp90 inhibitors deplete key anti-apoptotic proteins in pediatric solid tumor cells and demonstrate synergistic anticancer activity with cisplatin. International Journal of Cancer. 2005 Jan 10;113(2):179-88.
175. Russell JS, Burgan W, Oswald KA, Camphausen K, Tofilon PJ. Enhanced cell killing induced by the combination of radiation and the heat shock protein 90 inhibitor 17-allylamino-17- demethoxygeldanamycin: a multitarget approach to radiosensitization. Clinical Cancer Research. 2003 Sep 1;9(10 Pt 1):3749-55.
176. Bisht KS, Bradbury CM, Mattson D, Kaushal A, Sowers A, Markovina S, et al. Geldanamycin and 17-allylamino-17-demethoxygeldanamycin potentiate the in vitro and in vivo radiation response of cervical tumor cells via the heat shock protein 90-mediated intracellular signaling and cytotoxicity. Cancer Research. 2003 Dec 15;63(24):8984-95.
177. Stingl L, Stuhmer T, Chatterjee M, Jensen MR, Flentje M, Djuzenova CS. Novel HSP90 inhibitors, NVP-AUY922 and NVP-BEP800, radiosensitise tumour cells through cell-cycle impairment, increased DNA damage and repair protraction. British Journal of Cancer. May 25;102(11):1578-91.
178. Curry J, Angove H, Fazal L, Graham B, Harada I, Lyons J, et al. Significance of long term pharmacodynamic actions of the hsp90 inhibitor AT13387. 2009 [updated

2009; cited]; Available from: http://www.astex-therapeutics.com/event_pdfs/AT13387%20AACR%202009%20Poster%20Final.pdf.
179. Bull EEA, Dote H, Brady KJ, Burgan WE, Carter DJ, Cerra MA, et al. Enhanced tumor cell radiosensitivity and abrogation of G2 and S phase arrest by the Hsp90 inhibitor 17-(dimethylaminoethylamino)-17-demethoxygeldanamycin. Clinical Cancer Research. 2004 Dec 1;10(23):8077-84.
180. Stewart DJ. Mechanisms of resistance to cisplatin and carboplatin. Critical Reviews in Oncology-Hematology. 2007 Jul;63(1):12-31.
181. Liang K, Lu Y, Jin W, Ang KK, Milas L, Fan Z. Sensitization of breast cancer cells to radiation by trastuzumab. Molecular Cancer Therapeutics. 2003 Nov;2(11):1113-20.
182. Kawaguchi Y, Kono K, Mimura K, Mitsui F, Sugai H, Akaike H, et al. Targeting EGFR and HER-2 with cetuximab- and trastuzumab-mediated immunotherapy in oesophageal squamous cell carcinoma. British Journal of Cancer. 2007 Aug 20;97(4):494-501.